Pathophysiological and Pharmacological Relevance of NO/cGMP Signaling in Atherosclerosis

Dissertation

der Mathematisch-Naturwissenschaftlichen Fakultät

der Eberhard Karls Universität Tübingen

zur Erlangung des Grades eines

Doktors der Naturwissenschaften

(Dr. rer. nat.)

vorgelegt von

Malte Roeßing

aus Willich

Tübingen

2024

Gedruckt mit Genehmigung der Mathematisch-Naturwissenschaftlichen Fakultät der Eberhard Karls Universität Tübingen.

Tag der mündlichen Qualifikation:	11.04.2024
Dekan:	Prof. Dr. Thilo Stehle
1. Berichterstatterin:	Dr. Susanne Feil
2. Berichterstatter:	Prof. Dr. Robert Lukowski

Zusammenfassung

Atherosklerose führt zu Herzinfarkt und Schlaganfall, den weltweit häufigsten Todesursachen. Diese Erkrankung ist gekennzeichnet durch eine chronische Entzündung der Blutgefäßwand, die mit der Bildung atherosklerotischer Plaques einhergeht. Dabei kommt den glatten Gefäßmuskelzellen (VSMCs) eine zentrale Rolle zu. VSMCs tragen durch Migration, klonale Expansion und phänotypische Modulation erheblich zur Plaquebildung bei. Die molekularen Mechanismen, die zur Veränderung des VSMC-Verhaltens bei der Atherogenese führen, sind noch nicht vollständig geklärt. Das intrazelluläre Signalmolekül zyklisches Guanosinmonophosphat (cGMP), das durch die Stickstoffmonoxid (NO)-empfindliche Guanylylcyclase (NO-GC) synthetisiert wird, ist zentral für die (Patho-)Physiologie von VSMCs. Es wird vermutetet, dass sich eine Störung des NO/cGMP-Signalwegs in VSMCs auf die phänotypische Modulation der VSMCs und das Plaque-Wachstum auswirkt. Unklar ist allerdings, ob eine pharmakologische Stimulation/Aktivierung des NO/cGMP-Signalwegs in VSMCs pro- oder anti-atherogen wirkt.

Die vorliegende Studie hatte zum Ziel, die pathophysiologische und pharmakologische Relevanz des NO/cGMP-Signalwegs in VSMCs in einem Mausmodell der Atherosklerose weiter aufzuklären und seinen potenziellen Einfluss auf das Wachstum und die Zusammensetzung der atherosklerotischen Plaques zu untersuchen. Um die Aktivität des NO/cGMP-Signalwegs *in vivo* zu modulieren, wurden NO-GC modulierende Pharmaka oder die gezielte genetische Inaktivierung der NO-GC in VSMCs (NO-GC^{smko}) verwendet. Ein neuartiger Aspekt dieser Studie war der Vergleich der Wirkungen eines NO-GC Aktivators (BAY Aktivator) und eines NO-GC Stimulators (Vericiguat). Beide Substanzen induzieren die Bildung von cGMP durch Bindung an die NO-GC, unterscheiden sich aber in ihrer Wirkungsweise. NO-GC-Stimulatoren verstärken die Aktivität der NO-GC unabhängig oder synergistisch mit endogenem NO. Dem hingegen aktivieren NO-GC-Aktivatoren die dysfunktionale Häm-oxidierte NO-GC. Insbesondere unter pathophysiologischen Zuständen mit erhöhtem oxidativem Stress, wie bei Atherosklerose, wird für NO-GC Aktivatoren ein hohes therapeutisches Potential vermutet.

Zur Analyse wurden verschiedene biochemische, immunologische und histochemische Analyse-Methoden kombiniert. Zunächst wurde die Expression von NO-GC als potenzielle pharmakologische Zielstruktur durch *in situ* Immunfluoreszenzfärbung in VSMCs und Makrophagenantigen-2 (MAC2)-positiven Zellen in atherosklerotischen Plaques nachgewiesen, was auch auf die Möglichkeit einer pharmakologischen Modulation des Enzyms hinwies. MAC2 wurde als zellulärer Marker für aus VSMCs abgleiten transdifferenzierten Makrophagen-ähnlichen Zellen oder Makrophagen eingesetzt. Interessanterweise zeigte die *en face* Analyse von atherosklerotischen Aorten, dass die Behandlung mit dem BAY Aktivator zu einer signifikanten Zunahme der atherosklerotischen Läsionsfläche führte, während Vericiguat diesen pro-

atherosklerotischen Effekt nicht zeigte. Umfassende Analysen zeigten, dass die verabreichten Pharmaka im Blutplasma nachweisbar waren und verschiedene Parameter, die die Atherosklerose beeinflussen könnten, wie Blutdruck, Lipidprofil und Blutbild, durch die BAY Aktivator Behandlung nicht signifikant verändert wurden. Um die funktionelle Relevanz des NO/cGMP-Signalwegs in VSMCs für den pro-atherosklerotischen Effekt des BAY-Aktivators zu untersuchen, wurden *in vitro* Experimente mit isolierten primären VSMCs aus Mausaorten durchgeführt. Zunächst wurden die Effekte der NO-GC-Modulatoren auf die intrazelluläre cGMP-Konzentration in Echtzeit unter normalen und oxidativen Bedingungen mithilfe eines Förster-/Fluoreszenz-Resonanzenergietransfer (FRET)-basierten cGMP-Biosensors visualisiert. Zusätzlich wurden die Effekte auf das Wachstum von VSMCs mithilfe des xCELLigence-Systems überprüft. Diese Experimente zeigten, dass sowohl der BAY Aktivator als auch Vericiguat die cGMP-Konzentration erhöhten und das Wachstum der VSMCs förderten. Wie erwartet, zeigte der BAY Aktivator unter Bedingungen mit oxidativem Stress eine höhere Wirksamkeit auf das intrazelluläre cGMP Level, was auch eine erhöhte Wirksamkeit unter atherosklerotischen Bedingungen implizieren könnte. Basierend auf den Ergebnissen der vorliegenden Studie sowie der vorhandenen Literatur postulieren wir, dass die wachstumsfördernden Effekte der NO-GC Modulatoren wahrscheinlich mit der Rolle der NO-GC bei der phänotypischen Modulation von VSMCs zusammenhängen. Interessanterweise ergab unsere *in vivo* Studie, dass die durch BAY Aktivator Behandlung hervorgerufene Vergrößerung der atherosklerotischen Läsionsfläche mit einer Akkumulation von MAC2-positiven Zellen einherging. Dies deutet darauf hin, dass die Aktivierung des NO/cGMP-Signalwegs zu einer Anreicherung von VSMCs abgeleiteten transdifferenzierten Makrophagen-ähnlichen Zellen oder Makrophagen führte.

Es war außerdem geplant, die Zielstruktur-Spezifität der Wirkungen der NO-GC Modulatoren sowie die pathophysiologische Rolle der NO/cGMP-Signalkaskade in VSMCs mittels eines NO-GC^{smko}-Mausmodell zu validieren. Obwohl wir erfolgreich das NO-GC^{smko}-Mausmodell generierten, wiesen die vorläufigen Daten darauf hin, dass die Induktion von NO-GC^{smko} zu einem hypertensiven Phänotyp und erhöhten Plasmalipidwerten führte, was die Interpretation der Daten hinsichtlich der Effekte auf die Atherosklerose erschwerte. Es wurde zum jetzigen Zeitpunkt von weiteren Rückschlüssen aus diesen Daten abgesehen.

Zusammenfassend deuten unsere Ergebnisse auf einen pro-atherosklerotischen Effekt der Aktivierung des NO/cGMP-Signalwegs durch die Behandlung mit BAY Aktivator hin. Dabei vermuten wir, dass dies eng mit einer erhöhten Wirksamkeit des BAY Aktivators unter den in atherosklerotischen Plaques vorherrschenden oxidativen Bedingungen und der Wirkung auf die phänotypische Modulation der VSMCs im Plaque verbunden ist. Diese Ergebnisse bilden die Grundlage für weitere Forschung, um das Verständnis der pathophysiologischen und pharmakologischen Relevanz des NO/cGMP-Signalwegs in der Atherosklerose zu vertiefen.

Summary

Atherosclerosis leads to heart attack and stroke, the most common causes of death worldwide. This disease is characterized by chronic inflammation of the blood vessel walls, accompanied by the formation of atherosclerotic plaques. Vascular smooth muscle cells (VSMCs) play a crucial role in this process. VSMCs significantly contribute to the plaque formation through migration, clonal expansion, and phenotypic modulation. The molecular mechanisms leading to the alteration of VSMC behavior in atherogenesis are not fully understood. The cyclic guanosine monophosphate (cGMP) signaling pathway, synthesized by the nitric oxide (NO)-sensitive guanylyl cyclase (NO-GC) is a key factor in the (patho-)physiology of VSMCs. It is assumed that a disruption of the NO/cGMP signaling pathway in VSMCs impact phenotypic modulation and plaque growth. However, it remains unclear whether pharmacological stimulation/activation of the NO/cGMP pathway in VSMCs exerts pro- or anti-atherogenic effects.

This study aimed to further elucidate the pathophysiological and pharmacological relevance of the NO/cGMP pathway in VSMCs in a mouse model of atherosclerosis and investigate its potential effects on atherosclerotic plaque growth and composition. To modulate the activity of the NO/cGMP signaling pathway *in vivo*, NO-GC modulating drugs or cell specific genetic inactivation of NO-GC in VSMCs (NO-GC^{smko}) were used. A novel aspect of this study was the comparison of the effects of a NO-GC activator (BAY Activator) and a NO-GC stimulator (Vericiguat). Both compounds induce cGMP generation by binding to NO-GC but differ in their mode of action. NO-GC stimulators enhance NO-GC activity independently or synergistically with endogenous NO. In contrast, NO-GC activators activate the dysfunctional heme-oxidized NO-GC. Particularly under conditions of increased oxidative stress, as observed in atherosclerosis, NO-GC activators are assumed to have high therapeutic potential.

Various biochemical, immunological, and histochemical methods were combined for analysis. Initially, the expression of NO-GC as a potential drug target was demonstrated by *in situ* immunofluorescence staining in VSMCs and macrophage antigen-2 (MAC2)-positive cells in atherosclerotic plaques, indicating the possibility of pharmacological modulation of the enzyme. MAC2 was used as a cellular marker for VSMC-derived transdifferentiated macrophage-like cells or macrophages. Interestingly, *en face* analysis of atherosclerotic aortas showed that BAY Activator treatment led to a significant increase in the atherosclerotic lesion area, while Vericiguat did not exhibit this pro-atherosclerotic effect. Comprehensive analyses revealed that the administered drugs were detectable in the blood plasma and that various parameters that could influence atherosclerosis, such as blood pressure, plasma lipid profile and complete blood count, were not significantly changed by the BAY Activator treatment. To investigate the functional relevance of the NO/cGMP signaling pathway in VSMCs for the pro-atherosclerotic

effect of the BAY Activator, *in vitro* experiments were performed with primary VSMCs isolated from mouse aortas. First, the effects of NO-GC modulators on intracellular cGMP concentration were visualized in real-time under normal and oxidative conditions using a Förster/fluorescence resonance energy transfer (FRET)-based cGMP biosensor. Additionally, the effects on VSMC growth were examined using the xCELLigence system. These experiments demonstrated that both the BAY Activator and Vericiguat increased cGMP levels and promoted VSMC growth. As expected, the BAY Activator showed higher efficacy in increasing intracellular cGMP levels under conditions of oxidative stress, which may also imply an enhanced efficacy under atherosclerotic conditions. Based on the results of the present study and the existing literature, we postulate that the growth-promoting effects of NO-GC modulators are likely associated with the role of NO-GC in the phenotypic modulation of VSMCs. Interestingly, our *in vivo* study revealed that the increased atherosclerotic lesion area caused by the BAY Activator treatment was accompanied by an accumulation of MAC2-positive cells. This indicates that activation of the NO/cGMP signaling pathway led to an enrichment of VSMC-derived transdifferentiated macrophage-like cells or macrophages.

It was also planned to validate the target specificity of the effects of NO-GC modulators and the pathophysiological role of the NO/cGMP signaling cascade in VSMCs using an NO-GC^{smko} mouse model. Although we successfully generated the NO-GC^{smko} mouse model, the preliminary data suggested that the induction of NO-GC^{smko} led to a hypertensive phenotype and elevated plasma lipid levels, which complicated the interpretation of the data regarding the effects on atherosclerosis. Thus, no further conclusions were drawn from these data at this time.

In summary, our results suggest a pro-atherosclerotic effect of activation of the NO/cGMP signaling pathway by BAY Activator treatment. We hypothesize that this is closely related to the increased efficacy of BAY Activator under the oxidative conditions prevalent in atherosclerotic plaques and the impact on the phenotypic modulation of VSMCs in the plaque. These findings provide the basis for further research to deepen our understanding of the pathophysiological and pharmacological relevance of the NO/cGMP signaling pathway in atherosclerosis.

Table of contents

List of figures

List of tables

List of abbreviations

Abbreviation	Meaning
ANP	Atrial natriuretic peptide
ApoE	Apolipoprotein E
$ApoE^{ko}$	Apolipoprotein E knockout
BNP	Brain natriuretic peptide
CAG	Cytomegalovirus early enhancer / chicken β-actin / rabbit β-globin promoter
cAMP	Cyclic adenosine monophosphate
CAT domain	C-terminal catalytic
CC domain	Coiled-coil domain
CFP	Cyan fluorescent protein
cGi500	cGMP indicator with an EC50 of 500 nM
cGK	cGMP-dependent protein kinase
cGMP	3',5'-cyclic guanosine monophosphate
CIH	Chromogenic immunohistochemistry
CNG	Cyclic nucleotide-gated
CNP	C-type natriuretic peptide
Cre	Cyclisation recombination
Ctrl	Control
CYB5R3	Cytochrome b5 reductase 3
DEA/NO	Diethylamine NONOate
DETA/NO	Diethylenetriamine NONOate
DMSO	Dimethyl sulfoxide
ECM	Extracellular matrix
eNOS	endothelial NOS
FC	Fibrous cap
FRET	Förster/fluorescence resonance energy transfer
GAPDH	Glyceraldehyde 3-phosphate dehydrogenase
GC	Guanylyl cyclase
GFP	Green fluorescent protein
GTP	Guanosine triphosphate
HDL	High-density lipoprotein
H-NOX domain	Heme Nitric oxide/Oxygen binding domain
HSP 90	Heat shock protein 90
IF	Immunofluorescence
iNOS	Inducible NOS
LDL	Low-density lipoprotein
LDLr	Low-density lipoprotein receptor

MAC2	Galectin-3
MMP	Matrix metalloproteinase
MSC-like	Mesenchymal stem cell-like
nNOS	Neuronal NOS
NO	Nitric oxide
NO-GC	Nitric oxide (NO)-sensitive guanylyl cyclase
$NO\text{-}GC^{smko}$	VSMC-specific NO-GC knockout
NOS	Nitric oxide synthase
NP	Natriuretic peptides
NPR-C	NP receptor C
O/N	Over night
ODQ	1H-[1,2,4]oxadiazolo[4,3-a]quinoxalin-1-one
$ONOO^-$	Peroxynitrite
PAS domain	Per/Arnt/Sim domain
PDE	Phosphodiesterase
pGC	Transmembrane particulate GC
PSR	Picrosirius red
pVSMCs	Primary vascular smooth muscle cell
ROS	Reactive oxygen species
RT	Room temperature
SM22α	Smooth muscle protein 22-α
SM-MHC	Smooth muscle myosin heavy chain
SRF	Serum free medium
VASP	Vasodilator-stimulated phosphoprotein
VLDL	Very-low-density lipoprotein
VSMC	Vascular smooth muscle cell
YFP	Yellow fluorescent protein
αSMA	α-smooth muscle actin

1. Introduction

1.1 Atherosclerosis

1.1.1 Atherosclerosis, a general overview

Atherosclerosis is a chronic inflammatory disease of the arterial vessel wall that ultimately leads to heart attack and stroke [1]. Therefore, atherosclerosis is the leading cause of death and disability worldwide [2]. Depending on genetic predisposition and lifestyle, all humans are affected by atherosclerosis to varying degrees throughout their lifetime [3]. This silent disease develops slowly and without symptoms, starting in young adulthood and progressing to severe consequences later in life [3, 4].

The pathophysiology of atherosclerosis is characterized by the formation of atherosclerotic lesions, so-called plaques, in medium and large-sized arteries. This complex process is primarily initiated by endothelial dysfunction and the accumulation of certain plasma lipoproteins, including low-density lipoproteins (LDL) and remnants of triglyceride-rich lipoproteins, within the arterial wall. This triggers an inflammatory response involving various cells, such as monocytes/macrophages and lymphocytes [1, 5]. As the inflammatory reaction progresses, fundamental structural changes occur in the vessel wall, leading to plaque formation. The development of atherosclerotic plaques involves complex interactions among different cell types, including endothelial cells, macrophages, and vascular smooth muscle cells (VSMCs) [1, 5, 6].

The most significant complication of atherosclerosis is thrombus formation caused by plaque rupture or erosion [3]. In the context of heart attacks and strokes, this means that the formed thrombus can occlude coronary or cerebral arteries, resulting in myocardial or cerebral focal ischemia [1]. This ischemic event can cause severe damage to the heart or brain, or even lead to death. The severity of ischemia determines the extent of damage and the patient's prognosis. However, clinical impact of atherosclerosis extends beyond these acute events, as disease progression can lead to arterial narrowing and chronic ischemic conditions, such as stable angina pectoris and peripheral arterial occlusive disease [3].

The development and progression of atherosclerosis are influenced by a combination of non-modifiable and modifiable risk factors. Non-modifiable factors include age, sex, and genetic predisposition. In contrast, modifiable risk factors include dyslipidemia, hypertension, smoking, diabetes mellitus, obesity, stress, sedentary lifestyle, and unhealthy diet [1, 3]. Controlling these risk factors can reduce the probability of atherosclerosis development and progression as well as associated cardiovascular events [3]. In addition to adopting a healthier lifestyle, pharmacotherapeutic interventions play a significant role to control atherosclerosis. These interventions include the use of statins to lower LDL cholesterol levels, antihypertensive drugs

to control blood pressure, and antiplatelet drugs to reduce the risk of blood clots [1, 3]. In an advanced and acute stage of the disease, which is associated with chronic ischemia, nitrates (nitric oxide donors) can be used to dilate the blood vessels and reduce vascular resistance [7]. Invasive procedures such as percutaneous coronary intervention and coronary artery bypass grafting may also be considered for patients with severe symptomatic atherosclerotic disease, particularly when medical therapy alone is insufficient. These procedures aim to eliminate arterial stenosis and restore normal blood flow [3, 8]. However, it is important to consider that the use of these therapeutic options can often be associated with significant side effects or have other limitations [9, 10].

Despite the availability of therapy approaches targeting various aspects of the disease, atherosclerosis continues to have a significant impact on global health [5, 11]. The increasing number of severely affected individuals and the rising mortality rate highlight the urgent need for improved treatment options. However, the multifactorial nature of the disease presents a major challenge in the development of more effective therapies. It is crucial to further investigate the pathogenesis of atherosclerosis to enhance our understanding and identify novel therapeutic targets and strategies. Ultimately, these efforts aim to reduce the long-term burden of morbidity and mortality associated with atherosclerosis.

1.1.2 ApoE-knockout mouse: a model for atherosclerosis

Atherosclerosis is a multifactorial disease whose complexity and chronicity complicate the study of the underlying molecular and cellular mechanisms [12]. Animal models are essential tools for mimicking the key aspects of the disease to better understand these pathogenic mechanisms and develop effective therapeutic strategies [13]. Although *in vitro* approaches are valuable for studying isolated cellular processes, they often fail to capture the dynamic interactions between different cell types, tissues, and organ systems. In contrast, animal models offer a more comprehensive approach that encompasses not only dynamic interactions but also the interplay of genetic, environmental, and physiological factors involved in the development and progression of atherosclerosis. Thus, animal models have significantly contributed to expanding our knowledge of atherosclerosis and its associated pathophysiology [13, 14]. Commonly used animal models in atherosclerosis research include rabbits, pigs, and mice [13].

Among these, mice are most frequently used as an atherosclerotic animal model. The main advantages of mouse models are their low cost and fast breeding, genetic manipulability, and rapid development of atherosclerosis [12, 14]. However, unlike humans, mice primarily transport cholesterol through high-density lipoprotein (HDL) particles and have low levels of pro-atherogenic LDL and very-low-density lipoprotein (VLDL) particles. As a result, mice do not naturally develop atherosclerosis [15]. This limitation can be overcome by genetically manipulating lipid metabolism and adjusting the diet of the mice [14].

One of the most commonly used mouse models for atherosclerosis is the Apolipoprotein E (ApoE)-knockout ($ApoE^{ko}$) mouse model [13, 16, 17]. ApoE is a glycoprotein involved in lipid metabolism and cholesterol transport. It serves as a structural component of VLDL, HDL and chylomicrons, acting as a ligand for the LDL receptor (LDLr), the VLDL receptor, and the LDL receptor-related protein in the liver and thus facilitates the clearance of chylomicrons and VLDL remnants from the plasma [18]. Consequently, the functional knockout of ApoE in mice leads to spontaneous hypercholesterolemia. $ApoE^{ko}$ mice develop atherosclerotic lesions within a few months on a standard chow diet [13, 18]. Feeding these mice with a cholesterol- and fat-rich diet further accelerates this process and results in the formation of more advanced plaques [14]. Atherosclerotic lesions in $ApoE^{ko}$ mice form at similar sites as in humans, predominantly in the aortic root, aortic arch, carotid arteries, and major branches of the aorta. However, in contrast to humans, no plaques develop in the coronary arteries of $ApoE^{ko}$ mice [14, 18, 19].

Essentially, an animal model is chosen based on its ability to best mimic the pathophysiological condition in humans, which allows the translation of the results [13]. However, there are limitations due to interspecies differences [18]. It is crucial to consider the limitations of the described $ApoE^{ko}$ mouse model when interpreting research results. As mentioned, there are differences in lipid profiles between mice and humans. $ApoE^{ko}$ mice have a prevalence of VLDL rather than LDL, whereas in humans, an elevated plasma level of LDL cholesterol represents a major risk factor that promotes the development and progression of atherosclerosis [1, 17, 18]. Furthermore, ApoE has multifunctional roles in addition to its effects on lipoprotein metabolism [13]. Thus, $ApoE^{ko}$ also affects inflammation, oxidation, macrophage biology, and smooth muscle cell proliferation and migration. These factors may potentially affect plaque development [13, 14]. Another limiting factor is that the lesions rarely rupture despite the accelerated development of atherosclerosis. As a result, they do not lead to thrombosis, subsequent vessel occlusion, and ischemia. In contrast, this acute complication is common in humans [14, 18]. Despite these limitations, the $ApoE^{ko}$ mouse model represents a valuable tool for the elucidation of fundamental disease mechanisms and the evaluation of potential therapeutic interventions in atherosclerosis.

1.1.3 Atherogenesis

Atherogenesis describes the pathobiological process of atherosclerosis, involving the initiation and progression of atherosclerotic plaque formation within the walls of blood vessels. Atherosclerotic plaques mainly form in large to medium-sized arteries, such as the aorta and carotid arteries, in both humans and mice [14, 20]. Blood vessels are complex tissues consisting of several distinct layers. In large to medium-sized arteries, the vessel wall comprises three layers: the tunica intima, tunica media, and tunica externa (adventitia) (**Figure 1, left side**) [1]. The tunica intima, the innermost layer, is in direct contact with the circulating blood [1, 21]. It

consists of a monolayer of endothelial cells, which act as a barrier and regulate the exchange of nutrients, gases, and waste products between the blood and surrounding tissues. In addition to this barrier function, the endothelium plays a crucial role in regulating the vascular tone [22]. Dysfunction or damage of endothelial cells contribute significantly to the initiation and progression of atherosclerosis [1, 3]. Below the endothelium lies the subendothelial layer, primarily composed of glycosaminoglycans and collagen, which provides structural support [1, 21]. There are significant differences between humans and mice in the complexity and spatial extent of the subendothelial layer, which are also reflected in the development of atherosclerosis. In human arteries, prominent diffuse intimal thickening (DIT) occurs before the formation of atherosclerotic plaques [23]. The tunica media is mainly composed of vascular smooth muscle cells (VSMCs) and extracellular matrix (ECM), which contains elastin, collagen, and other macromolecules. This structural organizations enables the vasoconstriction and vasodilation to control blood pressure and distribution [21, 24]. Despite being composed of a single cell type, the tunica media exhibits a certain level of heterogeneity. VSMCs from different vessels or also of the same vessel can have distinct embryonic origins, leading to variations in their gene expression profiles or function, such as their reaction to growth factors [6, 25-27]. The tunica externa (adventitia), the outermost layer, primarily consists of connective tissue containing collagen fibers, (myo-)fibroblasts, various immune cells, adipocytes, and nerve endings. In larger vessels, the tunica externa may contain vasa vasorum, tiny blood vessels that supply oxygen and nutrients to the outer vessel layers [28]. Overall, the complex structure of the vessel wall ensures the stability, functionality, and adaptability of the blood vessels, especially in response to the dynamic demands of the cardiovascular system. The integrity of this structure is of immense importance for maintaining the overall health and performance of the entire organism.

This is particularly evident in pathophysiological processes, such as atherogenesis. Thus, the development of atherosclerotic plaques is accompanied by a fundamental structural change in the vessel wall [1]. These processes can be divided into different stages: initiation (**Figure 1**), progression, and complications (**Figure 2**) [3]. This is not about self-contained stages but rather about overlapping and slowly developing phases. The sites at which plaques develop in the vessel are influenced by various systemic and local factors, with differences in the hemodynamic forces exerted on the vessel wall playing an important role. Areas in the vessel exposed to disturbed blood flow, such as arterial branches or curvatures, are particularly prone to plaque formation [20, 29]. In these vascular areas, long-term exposure to a disturbed flow might lead to increased endothelial activation. This process is characterized by reduced NO production and increased oxidative stress, endothelial turnover, permeability, and proinflammatory activation [20]. As a result of the compromised barrier function, lipoproteins accumulate in the intimal layer, partly due to interactions with the intimal extracellular matrix macromolecules [1, 30]. The retained LDL and triglyceride-rich remnant lipoproteins can aggregate and

undergo chemical modifications, triggering a stronger inflammatory response [1, 3]. This leads to a significant upregulation in the expression of adhesion molecules (P-selectin, E-selectin, VCAM1, and ICAM1) and chemotactic factors (CCL2, CCL5) by endothelial cells, which results in the recruitment of blood monocytes [1, 31]. These monocytes enter the intima and differentiate into macrophages that play a crucial role in the progression of plaque formation. While during the initiation phase of plaque formation, macrophages primarily contribute through recruitment, their presence in more advanced plaques is mainly due to macrophage proliferation [1, 32]. Macrophages take up aggregated and modified intimal lipoproteins through scavenger receptors or phagocytosis, leading to the formation of foam cells [1]. VSMCs also significantly contribute to the amount of foam cells in the plaque core region [6]. During the initiation phase, medial VSMCs are stimulated to transform from a contractile to a proliferative state and begin to migrate into the intima [1]. These modulated VSMCs exhibit a high phenotypic plasticity and can transdifferentiate to resemble other cell types, such as macrophage-like cells, and/or can develop into foam cells through the uptake of lipoproteins [6, 27, 33]. Additionally, modulated VSMCs migrate into the region below the endothelium, where they secrete ECM (mostly consisting of collagen) and form the so-called "fibrous cap" (FC) [1, 34]. The FC is considered to have protective properties against plaque rupture. It serves as a structural support to prevent the exposure of prothrombotic material of the plaque core [35]. Details on the significant role of VSMCs in plaque formation and how they contribute to the cellular heterogeneity of plaques due to their high phenotypic plasticity can be found in **Section 1.2**. As the plaque formation progresses, lipids, modulated/transdifferentiated VSMCs, macrophages, and foam cells continue to accumulate in the intima. Due to the progressively proinflammatory environment within the plaque, adaptive immune cells, such as T cells and B cells, are also attracted. The involvement of these cell types in plaque formation is complex and opposing. Different T and B cell subtypes have been associated with both anti-atherosclerotic and pro-atherosclerotic effects [36]. Given the complexity of this topic, a more detailed description would exceed the scope of this thesis.

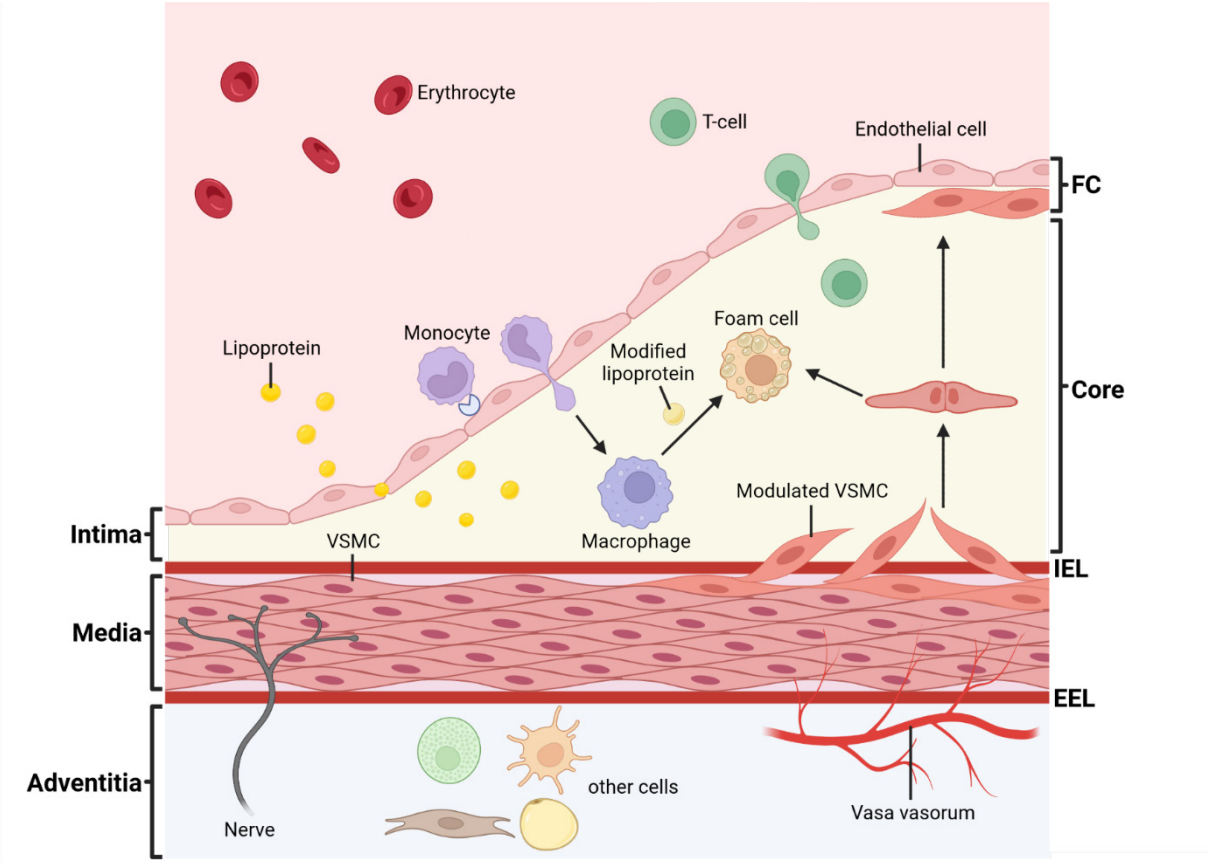

Figure 1. Initiation of atherosclerotic plaque formation.
The vessel wall of a healthy artery consists of three distinct layers: the tunica intima, tunica media, and adventitia. The tunica intima is composed of a single layer of endothelial cells that border the luminal blood flow, along with an underlying thin layer of connective tissue. The tunica media is composed of VSMCs and elastic fibers. The adventitia, also known as the tunica externa, is the outermost layer of a blood vessel and composed of connective tissue, various cells, and nerve endings. In larger vessels, the adventitia can contain vasa vasorum, tiny blood vessels that provide nutrients to the outer layer of the media. The formation of atherosclerotic plaques lead to a fundamental change in the vessel wall structure. During the initiation phase of plaque formation, lipoproteins enter the intima at sites of enhanced disturbed flow. The lipoproteins then aggregate and undergo chemical modification, rendering them pro-inflammatory and immunogenic. Monocytes bind to adhesion molecules on the activated endothelium and supported by chemoattractant chemokines, invade the intima. In the intima, monocytes mature into macrophages and take up the modified lipoproteins to form foam cells. Due to the pro-inflammatory milieu, T cells also invade the intima and regulate the functions of innate immune cells. Medial VSMCs are stimulated to migrate into the intima, where they expand clonally and undergo phenotypic modulation and transdifferentiation. VSMCs not only form the plaque-stabilizing fibrous cap but also contribute to the core region of the plaque, for example as foam cells. For more details see the text. VSMC, vascular smooth muscle cell; FC, fibrous cap; IEL, internal elastic lamina; EEL, external elastic lamina. Adapted from Libby et al., 2019 [3]. Image created using BioRender.com.

With further plaque development, intimal macrophages and modulated VSMCs in the plaque core and FC may undergo increased programmed (apoptosis) or another form of cell death [3]. Normally, the dead cells are cleared by macrophages through efferocytosis [37]. However, at later stages of plaque development, impaired clearance of dead cells, known as defective efferocytosis, leads to the formation of a necrotic core [3, 37]. Foam cells also significantly contribute to necrotic core formation. Although they can efflux cholesterol through transporters ABCA1 and ABCG1, they frequently undergo apoptosis, resulting in the growth of the necrotic core composed of cholesterol and cell debris [1]. As the plaque development progresses, a stable atherosclerotic plaque can grow large enough to obstruct blood flow, leading to chronic ischemia. However, the most clinically significant events are myocardial infarction or stroke [1,

3]. These acute events are triggered by the formation of a thrombus resulting from the rupture of a "vulnerable" plaque. The vulnerability of a plaque is more related to its composition than its size [1]. Fibrous plaques with thick FCs are considered to be more stable compared to fatty, inflammatory, and necrotic plaques [1, 3]. Therefore, in the advanced stage of plaque development, increased inflammation and cell death play a significant role in plaque stability. Activated inflammatory cells, such as macrophages, contribute to plaque destabilization by amplifying inflammation and producing proteases or collagenases that degrade the ECM in the plaque [1, 3, 38]. As a result of the inflammatory processes, the synthesis of interstitial collagen by VSMCs is inhibited, and at the same time, the expression of matrix metalloproteinases (MMPs) by VSMCs is likely increased [3, 35]. Additionally, due to increased death of VSMCs, ECM production decreases [35]. Overall, this eventually leads to a thinner and weaker FC that may rupture under increased hemodynamic forces, releasing thrombotic material. As part of the wound-healing process, platelets bind to subendothelial collagen and become activated [3, 35]. The initiated coagulation cascade leads to thrombin-mediated fibrin generation and the formation of a thrombus [35]. Along with a locally disturbed homoeostatic function of the endothelium, this can result in the formation of a persistent and occlusive thrombus or, if the thrombus detaches, to a circulating embolus within the cardiovascular system [3, 35]. In both cases, the obstruction of blood flow can trigger an ischemic insult, such as a myocardial infarction and stroke [3]. However, it is important to note that especially in animal models, such as the atherosclerotic $ApoE^{ko}$ mouse model, plaque ruptures and thrombus formation are very rare events and thus do not have the same significance as in humans [14].

For completeness, it should be mentioned that in addition to plaque rupture, plaque erosion can also lead to acute thrombotic complications [39]. Plaque erosion is not associated with the rupture of the FC but rather with the sloughing or desquamation of the endothelial layer [5]. Eroded plaques differ morphologically from the typical ruptured plaque. These plaques are usually rich in extracellular matrix and VSMCs, have low amounts of lipids, and are less inflammatory [3, 27]. The process of plaque erosion involves endothelial damage with the involvement of neutrophils, which likely promote endothelial erosion through neutrophil extracellular traps (NETs) and thus favor thrombus formation [5, 39].

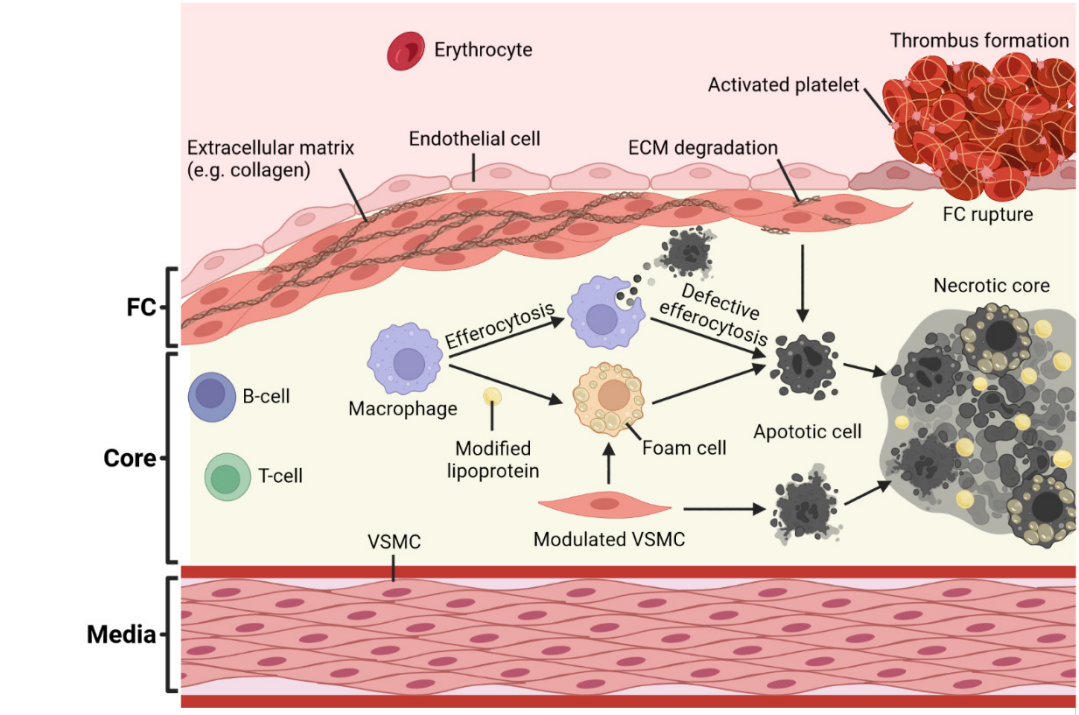

Figure 2. Progression of atherosclerotic plaque formation and complications.
During the progression of atherosclerotic plaque formation, VSMCs, macrophages, and other cells proliferate. Modulated VSMCs contribute to the formation of the fibrous cap by secreting extracellular matrix (e.g., collagen). As the plaque advances, plaque cells undergo increased programmed (apoptosis) or other forms of cell death. The debris from dead and dying cells accumulates, giving rise to a lipid-rich necrotic core. Defective efferocytosis (impaired clearance of dead cells) also contributes to the formation of the necrotic core. Increasing necrosis and inflammation lead to thinning and structural weakening of the fibrous cap, which increases the susceptibility to plaque rupture. Rupture of the plaque exposes thrombogenic material, stimulating the formation of a thrombus, possibly resulting in a myocardial infarction or stroke. For more details see the text. VSMC, vascular smooth muscle cell, FC, fibrous cap. Adapted from Libby et al., 2019 [3] Image created using BioRender.com.

1.2 Role of VSMCs in atherosclerosis

The development of atherosclerotic plaques involves complex interactions among various cell types, including endothelial cells, inflammatory cells (such as macrophages and lymphocytes), and VSMCs. VSMCs are mainly located in the tunica media layer of the blood vessel wall and are responsible for maintaining the vascular tone and regulating blood pressure due to their unique contractile properties [27]. Within the tunica media, VSMCs exhibit a spindle-like shape and secrete ECM macromolecules like elastin, collagen, and proteoglycans [6, 27]. They are characterized by the expression of essential proteins necessary for their contractile function. These proteins include α-smooth muscle actin (αSMA), smooth muscle protein 22-α (SM22α), and smooth muscle myosin heavy chain (SM-MHC) [27, 40-44]. In their healthy vascular state, known as the contractile phenotype, VSMCs are primarily quiescent and highly differentiated, with limited migration and proliferation potential. However, they possess a considerable phenotypic plasticity, which is highly relevant for the development and composition of atherosclerotic plaques [45].

As described in **Section 1.1.3**, VSMCs are a crucial cell type present at all stages of atherogenesis [6]. During the initial phase of plaque formation, inflammatory mediators and cytokines stimulate VSMCs to migrate from the medial to the intimal layer of arteries and undergo clonal expansion. Only a few VSMC clones in the media are likely to give rise to the entire VSMC population within the plaque [27, 46-48]. The invaded VSMCs not only contribute to the formation of the beneficial plaque-stabilizing FC beneath the endothelium but also play a significant role in the core region of the atherosclerotic plaque [27]. Depending on the plaque stage, 30 - 70% of all cells within the atherosclerotic plaque are VSMC-derived [6, 27]. The behavior of VSMCs during plaque growth is accompanied by significant cellular adaptations. In response to environmental influences such as growth factors/inhibitors, mechanical factors, cell-cell and cell-matrix interactions, extracellular lipids and lipoproteins, and various inflammatory mediators, VSMCs can alter their phenotypes [40, 45]. This phenomenon is referred to as VSMC phenotypic modulation or switching [45]. Phenotypic modulation involves enhanced proliferation, increased migration, loss of contractility, elevated ECM synthesis, and reduced expression of VSMC-specific markers, such as αSMA [6, 45]. Studies have shown that over 80% of VSMC-derived cells in murine plaques and the majority in human plaques are negative for αSMA [27, 46]. Interestingly, it has also been observed that medial VSMCs beneath the atherosclerotic lesion can lose contractile markers, suggesting that phenotypic modulation may occur before migration and proliferation and independently of clonal expansion [27, 49].

The phenotypic plasticity of VSMCs has been described for decades in cell culture [50]. When isolated from a healthy aorta, VSMCs tend to shift from their contractile phenotype to a synthetic or modulated phenotype during cell cultivation. This modulated phenotype is characterized by a rhomboid morphology, reduced contractile filaments, and increased proliferation potential [44, 45, 51]. The conditions and duration of cultivation, as well as the passaging of isolated primary cells can significantly influence the process of phenotypic modulation [51-56]. However, the initially implied binary nature of phenotypic modulation is a misconception and does not reflect the complexity and diversity of this phenomenon in atherogenesis [6]. Phenotypic modulation is more specifically described as a continuous, non-terminal, and likely (at least partially) reversible process through which VSMCs in atherosclerotic plaques can adopt a modulated phenotype and alter their gene expression profiles to resemble other cell types [6, 27, 34, 44]. The extent of phenotypic modulation achieved is often referred to as "transdifferentiation" [27].

Numerous *in vitro* studies, along with lineage tracing and single-cell transcriptomic studies (scRNAseq), have demonstrated that modulated VSMCs within atherosclerotic plaques can adopt different phenotypes, leading to a complex plaque composition (**Figure 3**) [27]. For example, Feil et al. impressively demonstrated that medial VSMCs significantly contribute to

plaque formation through clonal expansion and transdifferentiation into macrophage-like cells [33]. These macrophage-like cells are characterized by high expression of "macrophage markers" such as macrophage antigen 2 (MAC2), CD68, and pro-inflammatory cytokines [27, 33, 57, 58]. However, the presence of these macrophage markers does not necessarily imply that VSMC-derived cells obtain complete macrophage functionality or cell specificity [27]. Nonetheless, there are indications that these transdifferentiated VSMCs could exert functions like conventional macrophages [33]. Furthermore, studies have shown that VSMC-derived cells, similar to macrophages, can transdifferentiate into foam cells through the uptake of modified lipids via scavenger receptors or other processes [27, 45]. VSMC-derived cells account for up to 70% of macrophage marker-positive cells and foam cells in mouse atherosclerotic plaques and in similar proportions in humans [6, 33, 59, 60]. In addition to transdifferentiation into macrophage-like or foam cells, VSMCs also potentially transdifferentiate into osteochondrogenic, mesenchymal stem cell-like (MSC-like), or myofibroblast-like/fibromyocyte cells, as supported by multiple studies [27, 58, 61-63].

The various transdifferentiated cells not only contribute to a highly heterogeneous plaque composition but may also influence processes underlying plaque stability, such as plaque growth, lipid retention, inflammation, and ECM composition [34]. Historically, VSMCs have been regarded as plaque stabilizing. This assumption is based on the concept that the thickness of the FC and the number of VSMCs it contains correlate directly with plaque stability, considering that VSMCs are the main source of collagen and proteoglycans in the fibrous matrix [34, 45]. This is believed to result in higher mechanical tensile strength and enhanced resistance against rupture [34]. The FC is mainly formed by modulated VSMCs and myofibroblast-like/fibromyocytic cells and is the region where most αSMA-positive cells are located within the plaque [27, 47, 48]. Of note, not all αSMA-positive cells in the fibrous cap are derived from medial VSMCs [27, 64]. On the other hand, foam cells and macrophage-like cells could potentially have a destabilizing effect on the plaque due to pro-inflammatory properties and their contribution to the expansion of the necrotic core [27, 34]. However, further research is needed to solidify/corroborate these assumptions and accurately assess the contribution of the different transdifferentiated VSMCs to plaque stability. In principle, the phenomenon of phenotypic modulation of VSMCs in atherosclerosis and its potential reversibility offer opportunities for therapeutic intervention. New therapeutic strategies could be used to stimulate the accumulation of plaque-stabilizing VSMC phenotypes, eliminate harmful ones, or transform them into beneficial VSMC phenotypes to enhance plaque stability [27, 34, 65].

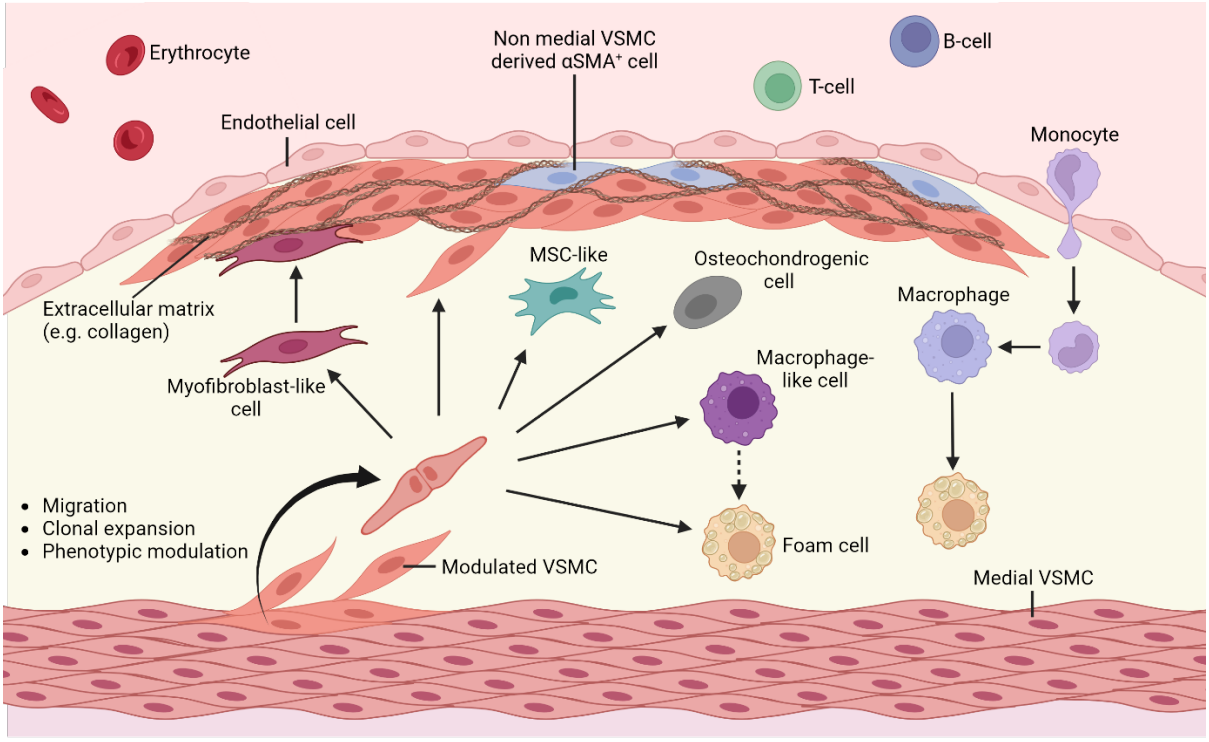

Figure 3. The role of VSMCs in the formation of atherosclerotic plaques.
During atherogenesis, inflammatory mediators and cytokines stimulate medial vascular smooth muscle cells (VSMCs) to migrate toward the intimal arterial layer and expand clonally. Thereby, VSMCs undergo structural and functional changes, a phenomenon known as phenotypic modulation and transdifferentiation. This leads to a loss in the expression of markers associated with contractile VSMCs (e.g., αSMA) and a shift in their gene expression profiles, which make them resemble other cell types. These modulated VSMCs adopt various phenotypes such as macrophage-like cells, foam cells, osteochondrogenic cells, mesenchymal stem cell-like (MSC-like) cells, or myofibroblast-like/fibromyocyte cells. They contribute to the formation of the fibrous cap (FC) and the core region of the atherosclerotic plaque. Notably, the phenotypes contribute to FC formation, including modulated VSMCs and myofibroblast-like/fibromyocyte cells, are assumed to be important for plaque stabilization. While foam cells and macrophage-like cells in the core are associated with a potentially plaque-destabilizing effect. Endothelial cells, inflammatory cells (e.g.: macrophages, B cells, and T cells) and other cells that are not derived from medial VSMCs are also involved in plaque formation. For more details see the text. αSMA: α-smooth muscle actin. Adapted from Bennet et al., 2016 [66]. Image created using BioRender.com.

1.3 cGMP signaling pathway

1.3.1 The cGMP signaling pathway and its therapeutic potential

The cyclic guanosine monophosphate (cGMP) signaling pathway plays a pivotal role in regulating diverse physiological and pathophysiological processes [67]. These include cardiovascular homeostasis, inflammation, sensory transduction, cellular growth, differentiation, survival, and more [68]. Noteworthy in the context of this work is its outstanding importance for the cardiovascular system, especially for vasodilation, blood pressure control, thrombus formation, and atherosclerosis. Most of these processes are influenced by activation of the cGMP signaling pathway within VSMCs [67, 69, 70]. Nevertheless, the functions of the cGMP signaling pathway extend beyond VSMCs and exert their effects across different cell types, such as platelets, neurons, and fibroblasts [67]. At the center of this signaling cascade is the intracellular secondary messenger cGMP [68, 71]. cGMP is formed from guanosine triphosphate (GTP) through two distinct families of guanylyl cyclases (GCs): transmembrane particulate

GCs (pGCs), mainly activated by natriuretic peptides (NP), and cytosolic NO-sensitive ("soluble") GCs (NO-GC), stimulated by nitric oxide (NO) produced by NO synthase (NOS) [67, 68, 72-74] (**Figure 4**). The physiological effects of cGMP are mediated by three classes of effector proteins: cyclic nucleotide-gated (CNG) cation channels, cGMP-dependent protein kinases (cGKs), and phosphodiesterases (PDEs) that hydrolyze cyclic nucleotides. While the latter two are found in various mammalian tissues, the question of whether CNG channels have a function outside the sensory system in mammals remains controversial [67, 75-77].

The therapeutic potential of the cGMP signaling pathway is highlighted by a multitude of clinically employed drugs targeting different components [78]. In **Figure 4**, the major drug classes and their target components are indicated. These drugs are used primarily in cardiovascular disease, but not exclusively. For instance, angina pectoris, characterized by chest pain due to occluded cardiac blood vessels, is treated with NO-releasing organic nitrates (NO donors), such as isosorbide mononitrate, dinitrate, sodium nitroprusside, and molsidomine. The stimulation of NO-GC by NO leads to elevated cGMP levels in vessel walls, causing vessel relaxation and restoring blood supply to the myocardium [7, 79]. Additionally, other therapeutic strategies involve NO-GC modulators such as Riociguat (Adempas®) and Vericiguat (Verquvo®), used in cases of pulmonary hypertension and heart failure [79-82]. The mode of action of the different NO-GC modulators is explained in **Section 1.4** in detail. Apart from targeting the NO-GC, PDE inhibitors, such as sildenafil (Viagra®), offer an alternative approach by inhibiting intracellular cGMP degradation. Assuming that endogenous cGMP generation is effective, inhibition of degradation leads to enhancement of cGMP signaling. The PDE5 inhibitor sildenafil is applied to treat erectile dysfunction and pulmonary hypertension [83]. Moreover, drugs targeting the NP/pGC/cGMP pathway are clinically approved. The compound sacubitril, in combination with the angiotensin II receptor blocker valsartan (Entresto®), is used for the treatment of heart failure [84, 85]. Sacubitril inhibits the NP-degrading enzyme neprilysin, leading to increased NP concentrations and subsequently elevated cGMP levels [84, 86]. This combined approach has a protective impact on the myocardium, affecting blood pressure, natriuresis, diuresis, and preventing fibrotic remodeling [84, 85]. Beyond cardiovascular applications, Vasoritide (Voxzogo®), a CNP analog, holds promise for addressing congenital short stature (achondroplasia) [87-89].

In summary, the cGMP signaling pathway plays an important role in numerous (patho-) physiological processes and is a popular therapeutic target for the treatment of a wide range of diseases. This suggests that future studies may uncover further therapeutic applications in this field.

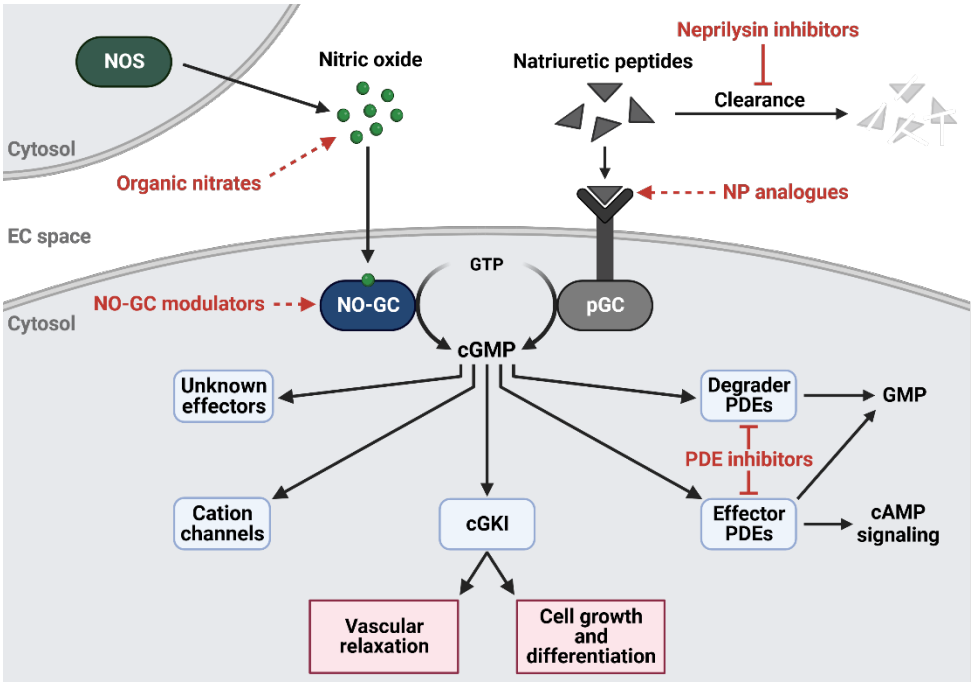

Figure 4. The cGMP signaling pathway.
The cyclic guanosine monophosphate (cGMP) signaling pathway regulates various physiological processes, such as vascular relaxation, cell growth, and differentiation. Stimulation of the guanylyl cyclases (NO-GC and pGC) with their respective ligands, nitric oxide or natriuretic peptides, leads to the generation of cGMP by converting guanosine triphosphate (GTP). Nitric oxide is generated by NO synthase (NOS). The physiological effects of cGMP are mediated by three classes of effector proteins, including cyclic nucleotide-gated (CNG) cation channels, cGMP-dependent protein kinases (cGKs), and bispecific phosphodiesterases (PDEs). The different PDEs can hydrolyze cGMP to GMP and/or modulate the cyclic adenosine monophosphate (cAMP) concentration. The major drug classes targeting different components of the cGMP signaling pathway are indicated (red). For more details see the text. NP, natriuretic peptide; NO-GC, NO-sensitive guanylyl cyclase; pGC, particulate guanylyl cyclase. Adapted from Feil and Kemp-Harper, 2006 [90]. Image created using BioRender.com.

1.3.2 cGMP signaling in VSMCs

In the course of the past decades the role of cGMP in vascular biology has been extensively studied in the context of vascular tone regulation. It is now well-established that the activation of the cGMP signaling pathway by NO or atrial natriuretic peptide (ANP) results in elevated intracellular cGMP levels in VSMCs, ultimately causing vasodilation [69, 90, 91]. Beyond its function in VSMC contractility, the cGMP signaling pathway is also involved in the regulation of VSMC growth, differentiation, and survival [92, 93]. Consequently, VSMCs express various components of the cGMP signaling pathway at both generator and effector levels [94-98]. However, the exact expression profile of these components likely varies temporally and spatially among individual VSMCs [99].

cGMP is generated by two types of guanylyl cyclases (pGC and NO-GC), which differ in their subcellular localization and are activated by different ligands [67, 68, 72, 73]. In mammals, the pGC enzyme family consists of 7 members of transmembrane GCs, referred to as GC-A to GC-G. These receptors can be stimulated by various intra- and extracellular cues, mediating a variety of physiological effects ranging from blood pressure control to endochondral ossification [72, 100]. In general, pGCs consist of an extracellular ligand-binding domain, a single

transmembrane region, and an intracellular region containing a catalytic GC domain [72]. The two most important pGCs in the cardiovascular system and especially in VSMCs are GC-A and GC-B. The generation of cGMP by these two homodimeric receptors is selectively activated by peptide hormones. GC-A is preferentially activated by ANP and brain natriuretic peptide (BNP), while GC-B selectively binds C-type natriuretic peptide (CNP) [72, 100]. Although the two receptors exhibit high selectivity for their respective NPs, they can also bind the other NPs with lower affinity [101, 102]. ANP, BNP, and CNP are synthesized as preprohormones and are processed to their biologically active mature form through the transmembrane ectoenzyme corin (ANP and BNP) or the intracellular peptidase furin (CNP) [72, 103, 104]. These mature forms consist of a 17-amino acid disulfide ring structure extended by short N- and C-terminal tails [100]. ANP and BNP are mainly synthesized under physiological conditions in the atrium and act on their target tissues in an endocrine manner [72, 105]. CNP, on the other hand, probably acts in a paracrine or autocrine manner following its local synthesis, for instance by endothelial cells and VSMCs [106, 107]. The inactivation of extracellular NPs can occur through degradation by the extracellular peptidase neprilysin or by binding to the NP receptor C (NPR-C or clearance receptor). NPR-C binds all NPs with high affinity but lacks an intracellular catalytic GC domain, leading to internalization and subsequent degradation of NPs [108]. In addition to this function, there is evidence that NPR-C may also have cGMP-independent signaling effects [109].

In addition to pGCs, cGMP in VSMCs can be generated by cytosolic NO-GC. NO-GC is a heterodimeric heme protein consisting of an α-subunit and a β-subunit. In mammals, the enzyme exists in two functional isoforms: NO-GC1 (α1β1) and NO-GC2 (α2β1). While NO-GC1 is predominantly expressed in most peripheral tissues, particularly in blood vessels, NO-GC2 is mainly detected in the nervous system. However, both isoforms coexist in the tissues, except in platelets, which exclusively express NO-GC1 [110, 111]. Due to the central significance of NO-GC in this study, a detailed description of its structure and function is provided in **Section 1.3.3**. The catalytic function of NO-GC is stimulated by the binding of the endogenous ligand NO to the heme group of the β-subunit [67, 110]. Endogenous NO is synthesized from L-arginine by three types of NOS: neuronal NOS (nNOS), inducible NOS (iNOS), and endothelial NOS (eNOS) [74]. These three isoforms differ in their expression patterns, regulation, catalytic activity, and (associated) NO output [74, 112, 113]. eNOS is expressed in endothelial cells, while nNOS is primarily found in neurons, but can also be detected in some non-neuronal tissues. The activity of these two constitutively expressed NOS isoforms is regulated in a calcium/calmodulin-dependent manner. Under inflammatory conditions, iNOS is expressed in various cell types, including VSMCs, macrophages, and leukocytes. The regulation of this isoform occurs through expression and is not dependent on calcium [74]. The physiologically effective concentration of NO most likely ranges between 100 pM and 5 nM [114]. Through the

NO/cGMP signaling axis, NO can influence various physiological processes, including vasodilation (through VSMC contractility), gastrointestinal motility, and platelet reactivity [110, 115, 116]. However, it is important to note that NO can also exert cGMP-independent effects, such as S-nitrosylation of metal centers and cysteine residues in intracellular proteins [117].

In VSMCs, the transduction of cGMP signals occurs mainly on the effector protein level through cGKs and PDEs [76, 77, 118]. cGKs are homodimeric serine/threonine kinases that mediate cGMP effects by phosphorylation of target proteins. In mammals, the expression of two isoforms of cGK is observed: cGKI (comprising cGKIα and cGKIβ) and cGKII. The cytosolic cGKI, similar to NO-GC, plays an important role in the gastrointestinal tract, platelets, brain, and especially in the cardiovascular system [76]. However, evidence for the functional expression of cGKII in the cardiovascular system is still lacking. Instead, cGKII is described to have functions in the kidney, bones, and brain. The two isoforms of cGKI, cGKIα and cGKIβ, are prominently expressed in VSMCs [118]. Although encoded by the same gene (Prkg1), they differ in the N-terminal leucine zipper domain transcribed from two alternative exons. The N-terminus mediates crucial functions such as homodimerization, localization, substrate specificity, and cGMP affinity [76]. Of note, cGKIβ is activated at approximately 10-fold higher cGMP concentrations compared with cGKIα [118]. Interestingly, in VSMCs, the two isoforms can compensate for each other at the functional level [98]. Furthermore, cGKI consists of a tandem cGMP-binding domain and a C-terminal catalytic domain. In the absence of cGMP, cGKI is inhibited by an autoinhibitory/pseudo-substrate domain located at the N-terminus. Activation occurs when two cGMP molecules bind to each subunit, thereby enhancing catalytic activity. This enables cGKI to impact various physiological processes [76]. One of the best-studied cGKI-cGMP-dependent regulatory effects is the effect on acute VSMC relaxation in vessels [76, 98, 118]. This vasodilatory effect is primarily based on the cGKI-mediated reduction of the intracellular calcium concentration and regulation of myosin light chain (MLC) phosphorylation status [76].

cGMP signals are terminated by the activity of PDEs, which hydrolyze cGMP to GMP. The PDE superfamily consists of 11 subgroups, most of which include multiple isoforms [77, 119]. These subgroups vary in terms of expression patterns, ligand selectivity, and substrate specificity [119]. The regulation of cGMP signaling occurs through cGMP-specific “degrader” PDEs (PDE5, 6, 9) as well as bispecific PDEs capable of hydrolyzing both cGMP and cyclic adenosine monophosphate (cAMP) (PDE1, 2, 3, 10, 11) [77, 83]. In addition to their role in the degradation of cyclic nucleotides, bispecific PDEs are also involved in downstream signal transduction. They provide mechanisms for crosstalk, allowing cGMP to modulate cAMP-dependent signaling. For instance, elevated cGMP concentrations can competitively inhibit PDE3, leading to increased cAMP levels in VSMCs. Consequently, these bispecific PDEs are sometimes

referred to as “effector” PDEs [119]. Other PDEs (PDE 4, 7, 8) specifically degrade cAMP [77, 83]. In VSMCs, PDE1, 3, 4, 5, 9, and 10 are likely expressed, with PDE5 probably being the most important cGMP-hydrolyzing PDE [78, 83, 120, 121]. In this context, PDE5 is involved in regulating VSMC tone through cGMP degradation. It is noteworthy that PDEs seem to play a crucial role in compartmentalizing of cGMP within the cell. The activity of PDEs regulates the subcellular distribution of cGMP generated by different GCs, leading to the formation of local cGMP pools [78, 122].

1.3.3 Structure and function of the NO-GC

As previously outlined, NO-GC is a central component of the NO/cGMP signaling axis and acts as a receptor for NO produced by NOS. Upon NO binding, it triggers an increase in the production rate of cGMP, leading to modifications in cellular functions mediated by a diverse range of effector proteins [110]. Consequently, these modifications affect various physiological processes, particularly within the cardiovascular, nervous, and gastrointestinal systems. Such effects encompass vascular relaxation, platelet aggregation, and synaptic transmission [110, 115, 116]. Moreover, the dysregulation of this signaling axis plays a significant role in various diseases, including hypertension, cardiac hypertrophy, metabolic syndrome, and neurodegenerative disorders [67, 116].

NO-GC is a heterodimer consisting of an α- and a β-subunit. Based on the identity of their α subunit, there exist two heterodimeric isoforms known as NO-GC1 (α1β1) and NO-GC2 (α2β1) [110]. In mice, the distinct subunits are encoded by the genes Gucy1a1 (α1-subunit) and Gucy1b1 (β1-subunit) on chromosome 3, and Gucy1a2 (α2-subunit) on chromosome 9 [73]. Although a β2-subunit has been identified through homology analysis, there is no evidence regarding its physiological function or *in vivo* protein expression, classifying it as a pseudogene. Both NO-GC isoforms coexist in most tissues except in platelets. In blood vessels and most peripheral tissues, NO-GC1 predominates, whereas in the brain, both isoforms are equally expressed [110]. Nonetheless, the biological significance of these isoforms’ coexistence remains incompletely understood. Physiological analyses and biochemical/kinetic characterization of the two isoforms have not revealed significant differences in their enzymatic function [73]. Instead, studies involving genetically modified mouse strains lacking one of the α subunits suggested that the loss of one isoform can be partially compensated by the presence of the other [67, 111]. In contrast, global or VSMC-specific deletion of the β1-subunit in mice led to a functional knockout of NO-GC. This was associated, for example, with loss of vascular relaxation capacity after stimulation by NO as well as with hypertension [94, 123]. However, differences in the C-terminal ends of the α-subunits are assumed to result in potential variations in the subcellular localization of the two isoforms [110].

Both α- and β-subunits share some sequence homology and are divided into four domains: an N-terminal H-NOX (Heme Nitric oxide/Oxygen binding) domain, a Per/Arnt/Sim (PAS) domain, a Coiled-Coil (CC) domain, and a C-terminal catalytic (CAT) domain. The PAS and CC domains facilitate protein-protein interactions and likely form a structured assembly upon dimerization [124, 125]. These domains also contribute to the transfer of conformational changes caused by NO binding to the CAT domain. [116]. The CAT domain is responsible for the enzymatic conversion of GTP to cGMP, requiring Mg^{2+} as a cofactor. Both the α- and the β-subunit contribute to the formation of the catalytic center and thus to catalysis [110]. Consequently, the dimerization of the α- and β-subunits is essential for the formation of a stable and functional enzyme [111, 123]. The H-NOX domain contains a ferrous b-type heme prosthetic group, crucial for high-affinity NO binding [124]. Notably, despite both subunits containing an H-NOX domain, only the H-NOX domain of the β1-subunit can bind the prosthetic heme-cofactor [125]. The prosthetic heme-cofactor binds by forming a complex with the conserved histidine 105 and the heme-binding motif Y-x-S-x-R (tyrosine 135, serine 137, and arginine 139) of the β1-subunit [125-127]. Thus, mutation of histidine 105 in the β1-subunit results in loss of NO sensitivity of NO-GC [128].

In its NO-sensitive heme-containing state, NO-GC displays low basal activity that can be stimulated by NO binding [125]. The binding of NO to the Fe ion of the heme-cofactor disrupts the proximal histidine 105-iron bond, forming a distal five-coordinated ferrous nitrosyl enzyme. [124, 125]. This initiates a conformational change in the H-NOX and PAS domains, conveyed through the stretching of the CC domain to the catalytic domain [124, 129]. These conformational changes involve a comprehensive structural reconfiguration of the entire enzyme, ultimately enabling the opening of the GTP binding site and activating the catalytic domain [124, 130]. The inactive state of NO-GC is characterized by a bent conformation, while activation results in an elongated, dumbbell-shaped structure [124]. The enzymatic activity of NO-GC can be increased 200-fold upon activation with NO [110]. Interestingly, a two-step model for NO-dependent activation of NO-GC has been proposed based on various studies. According to this model, treating NO-GC with a stoichiometric equivalent of NO and its binding to the heme-cofactor results in partial activation. Complete activation only occurs with the introduction of excess NO and binding to a second non-heme-dependent NO binding site [116, 125, 130, 131]. As the NO concentration decreases, NO dissociates from the second binding site, reducing the catalytic activity of the enzyme [125]. Although this model is consistent with the findings of biochemical and structural studies, further clarification is still required.

Given the significance of NO-GC in cGMP generation and maintenance of numerous physiological functions, there is considerable scientific interest in understanding its regulation. In addition to regulation through NO availability, the redox status of the prosthetic heme-cofactor

within the H-NOX domain plays a central role [116, 132]. The reduced state of the heme Fe ion (Fe^{2+}) is necessary for NO binding and the subsequent activation of NO-GC. However, this Fe^{2+} ion in the heme group is prone to oxidation to Fe^{3+} which renders the heme group insensitive to NO binding. Furthermore, oxidation can also weaken the heme-histidine 105 complex, leading to the loss of the heme cofactor and resulting in a heme-free state of NO-GC (apo-NO-GC) [132]. The apo-NO-GC is rapidly degraded by the cells [133]. Notably, in both the heme-oxidized and heme-free states, NO-GC cannot be activated in a NO-dependent manner, subsequently impairing the enzymatic function. Structural analyses have demonstrated that these states adopt a bent conformation similar to the inactive heme-unliganded state of NO-GC [124]. However, it is assumed that a sensitively controlled redox equilibrium exists between the different states of NO-GC within the cell (**Figure 5**) [79, 132]. Two proteins are likely involved in restoring functional NO-GC and thereby maintaining intracellular redox equilibrium: Heat shock protein 90 (HSP90) and cytochrome b5 reductase 3 (CYB5R3) [132]. HSP90 is responsible for heme insertion by forming a complex with apo-NO-GC and stabilizing it [132, 134]. CYB5R3, a heme iron reductase that is ubiquitously expressed in VSMCs, reduces the NO-GC heme iron and thereby re-sensitizes NO-GC to NO [132, 135, 136]. Further details on how the redox equilibrium is established and how it contributes to the regulation of NO-GC activity are the subjects of ongoing research. However, in the context of pathophysiological scenarios, it's speculated that in diseases associated with increased inflammation and oxidative stress (e.g., atherosclerosis), the intracellular redox equilibrium plays a pivotal role in the respective pathogenesis [136, 137]. Oxidative stress is accompanied by the increased formation of reactive oxygen species (ROS). Particularly, peroxynitrite ($ONOO^-$) alters the redox state of NO-GC. This may cause a shift of the equilibrium from the NO-sensitive heme-containing NO-GC form toward the oxidized, dysfunctional, heme-free form, thereby impairing the NO/cGMP signaling [132, 136]. Interestingly, a class of drugs has been developed that binds to the oxidized and heme-free NO-GC, thereby restoring cGMP generation (**Section 1.4**) [136]. These drugs, called NO-GC activators, hold significant promise for their therapeutic potential, especially in diseases characterized by elevated oxidative stress.

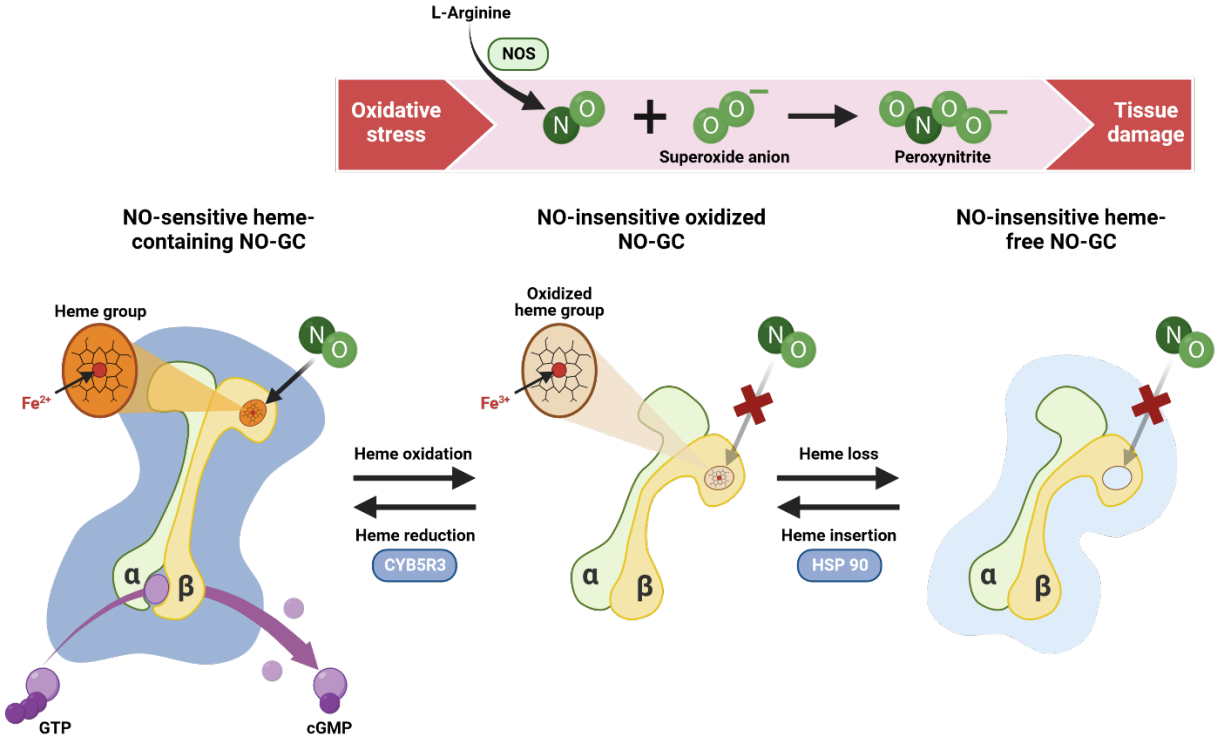

Figure 5. Intracellular redox equilibrium of different NO-GC states.
NO-GC is a heterodimeric protein composed of an α-subunit and a heme group-containing β-subunit. The catalytic function of NO-GC, which converts guanosine triphosphate (GTP) to cyclic guanosine monophosphate (cGMP), is activated by the binding of the endogenous ligand nitric oxide (NO) to the heme group. NO is synthesized from L-arginine by NO synthase (NOS). The Fe^{2+} ion of the heme group is prone to oxidation which renders NO-GC insensitive to NO binding and may result in the complete loss of the heme group. In both the NO-insensitive oxidized and heme-free states, NO-GC adopts an inactive bent conformation devoid of enzymatic function. The different stages of NO-GC exist in a sensitively controlled redox equilibrium in the cell. Heat shock protein 90 (HSP 90) and cytochrome b5 reductase 3 (CYB5R3) are likely involved in preserving the redox equilibrium with heme insertion and reduction, respectively. Under pathological conditions characterized by increased oxidative stress, a shift in the redox equilibrium to the NO-insensitive heme-free state is believed to compromise NO/cGMP signaling. Oxidative stress is associated with an increased formation of reactive oxygen species (ROS), known to oxidize and deactivate various biomolecules, thereby contributing to tissue damage. Peroxynitrite ($ONOO^-$), formed by the reaction of NO and superoxide anion (O_2^-), is hypothesized to alter the redox state of NO-GC. For more details see the text. Adapted from Sandner et al. 2021 [79]. Image created using BioRender.com.

1.3.4 Real-time imaging of cGMP using the FRET-based biosensor cGi500

The molecular and cellular mechanisms underlying the multifaceted role of cGMP in (patho)physiological processes and pharmacological therapy effects are still not completely understood [78]. To gain a deeper understanding, it is highly valuable to determine the concentration of cGMP under specific conditions. Although commercially available antibody-based assays enable the quantification of cGMP levels at specific time points, they lack temporal and spatial resolution due to the requirement of total cell and tissue lysis. Additionally, these assays do not allow real-time visualization of dynamic changes in cGMP levels, including its formation by GCs and degradation by PDEs [78]. To overcome these limitations, genetically encoded fluorescent cGMP indicator proteins have been developed. These cGMP biosensors are powerful tools for analyzing dynamic changes in cGMP levels in real-time within native cells, thus providing insights into the spatiotemporal dynamics of endogenous cGMP signaling and the effects of drugs [78].

The working principles of most cGMP biosensors are based on Förster/fluorescence resonance energy transfer (FRET). FRET describes the radiation-less energy transfer between an excited donor fluorophore to an acceptor fluorophore, with its efficiency depending on the distance between them (decreasing with increasing distance) [138]. Therefore, cGMP biosensors typically consist of two fluorophores connected by a cGMP binding domain. The binding of cGMP induces a conformational change, thereby altering the FRET efficiency. The extent of the cGMP-induced change in FRET efficiency can be used to determine the intracellular cGMP concentration.

Different cGMP biosensors vary in their cGMP affinity and thus also in their sensitivity to measure intracellular cGMP concentrations. Therefore, the choice of a specific biosensor depends strongly on the biological question and experimental requirements [78]. One frequently used cGMP biosensor is cGi500 (with an EC50 of 500 nM), which enables the detection of cGMP concentrations in cGi500 transgenic cells in the presumably physiological range of approximately 100 nM to 3 µM [78, 139]. cGi500 consists of a tandem cGMP binding domain derived from bovine cGKI, flanked by cyan fluorescent protein (CFP) and yellow fluorescent protein (YFP). In the absence of cGMP, the fluorophores are in proximity, leading to maximal energy transfer (maximum FRET efficiency) from CFP to YFP upon excitation. When cGMP binds, a conformational change occurs, resulting in a measurable decrease in energy transfer. Consequently, the emission of YFP at 535 nm decreases, while the emission of CFP at 480 nm increases. The change in FRET efficiency, indicated by the CFP/YFP ratio (R), correlates with the intracellular cGMP concentration (R ~ [cGMP]) [78].

Furthermore, the availability of the cGi500 sensor mouse line offers significant advantages. These mice contain a cGi500 construct inserted into the Rosa26 gene locus and express cGi500 under the control of a Cytomegalovirus early enhancer/chicken β-actin/β-globin (CAG) promoter. The cGi500 sensor can be stably expressed either globally in all tissues or in a cell type-specific manner by crossing the "floxed" sensor mice with Cre mice [78, 140]. This enables real-time FRET-based cGMP imaging in sensor-expressing isolated primary cells, tissues, and *in vivo* under native conditions. Importantly, the expression of the biosensor does not result in noticeable side effects or toxicity, allowing its use in these various experimental setups [78, 140].

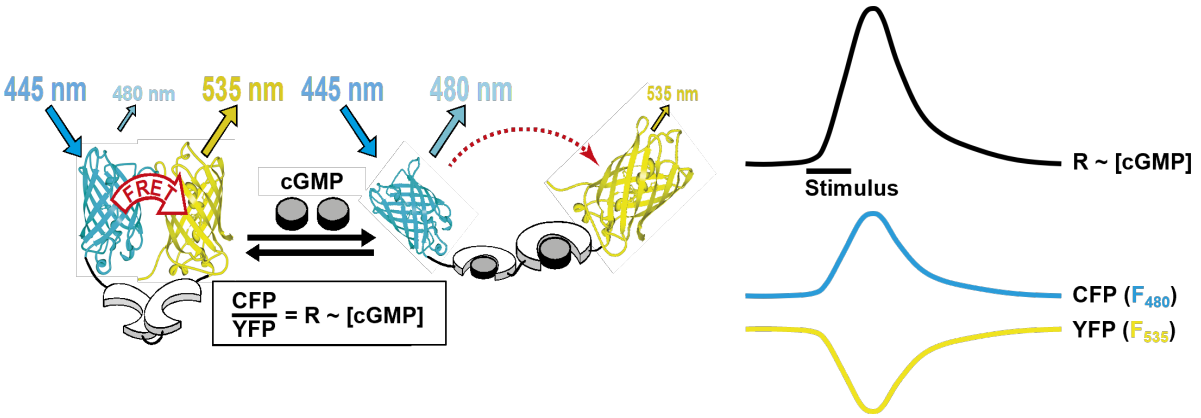

Figure 6. Schematic structure and working principle of the FRET-based cGMP biosensor cGi500.
The FRET-based cGMP biosensor cGi500 consists of a tandem cGMP-binding domain of bovine cGKI (shown in white) flanked by two fluorophores: CFP (FRET donor, cyan) and YFP (FRET acceptor, yellow). In the cGMP-free state, FRET occurs at maximum efficiency from CFP to YFP upon excitation with light at 445 nm. The binding of two cGMP molecules (shown in grey) induces a conformational change, resulting in a reduction of energy transfer. This leads to a decrease in light emission of YFP at 535 nm, while the emission of CFP at 480 nm increases. Thus, the change in the FRET efficiency, represented by the CFP/YFP ratio (R), correlates with the cGMP concentration ([cGMP]). This process enables real-time analysis of cGMP concentration (CFP/YFP ratio (R), black trace) following any stimulation (stimulus, black line). The simultaneous and antiparallel changes in CFP (F_{480}, cyan trace) and YFP (F_{535}, yellow trace) fluorescence intensity over time are used to validate the authenticity of cGMP-dependent FRET signals. For more details see the text. cGMP: 3',5'-cyclic guanosine monophosphate; CFP, cyan fluorescent protein; YFP, yellow fluorescent protein. Adapted from Thunemann et al. 2014 [141].

1.4 NO-GC as a pharmacological target

As mentioned in previous chapters, the NO/cGMP signaling cascade plays a critical role in regulating various cardiovascular functions. Accordingly, disruptions in this pathway are closely associated with pathological processes, underscoring its substantial therapeutic potential. This potential is exemplified by a wide range of clinically validated and approved drugs that target this pathway. Many of these drugs focus on modulating the activity of NO-GC, directly influencing cGMP production.

In the nineteenth century, the first treatments using NO-releasing substances like amyl nitrite or nitroglycerin were conducted to address angina pectoris, even before the chemical and physiological processes involved were fully understood [142, 143]. Angina pectoris arises from myocardial ischemia due to an imbalance in oxygen supply. The released NO from these NO donors binds to NO-GC, resulting in cGMP generation and subsequent vasodilation of blood vessels and coronary arteries, thereby restoring myocardial oxygen supply [7]. Nowadays, NO donors such as isosorbide mononitrate, dinitrate, sodium nitroprusside, and molsidomine, which offer sustained NO release, have received approval for the treatment of angina pectoris [7, 79]. However, the clinical significance of NO donors in the treatment of myocardial and vascular dysfunctions is rapidly declining [79]. This decline can be attributed to their strong disadvantages, including pronounced side effects, a narrow therapeutic window, and the development of drug tolerance (tachyphylaxis), which severely limits their utility [79, 144].

To overcome the limitations associated with NO donors and expand the therapeutic potential of the NO/cGMP signaling pathway, two categories of small pharmaceutical molecules have been developed: NO-GC stimulators and activators. Both types of compounds function as NO-independent modulators of NO-GC, inducing cGMP generation through allosteric binding. However, NO-GC stimulators and activators primarily differ in terms of their binding sites and modes of action (**Figure 7**) [136, 145, 146]. NO-GC stimulators such as YC-1 and Riociguat probably bind to a cleft between the H-NOX and CC domains of the β subunit, inducing a conformational change and stabilizing the NO-GC in an active form [130]. The activation of NO-GC strictly depends on the presence of the prosthetic ferrous heme (Fe^{2+}) moiety [145]. NO-GC stimulators can stimulate NO-GC activity in the absence or presence of NO and exhibit a strong synergistic effect when combined with NO [136]. NO-GC stimulators have already received clinical approval and are successfully used in the treatment of various cardiovascular diseases. The first NO-GC stimulator of its class, Riociguat, is clinically employed for pulmonary arterial hypertension and chronic thromboembolic pulmonary hypertension [79, 80]. Another NO-GC stimulator, Vericiguat (VERQUVO®), with improved pharmacokinetic and pharmacodynamic properties, has recently been approved for the treatment of symptomatic chronic heart failure with reduced ejection fraction [81, 82]. Further preclinical and clinical studies are ongoing to explore new therapeutic applications in different diseases [136].

On the other hand, NO-GC activators bind to both the heme-oxidized (Fe^{3+}) and heme-free forms of NO-GC. By occupying the heme pocket within the H-NOX domain of the β-subunit, they mimic the NO-heme-bound state, consequently activating cGMP formation independent of heme and NO [79, 130]. This heme-oxidized or heme-free form of NO-GC is primarily associated with disease conditions characterized by oxidative stress and does not respond to endogenous NO or NO-GC stimulators. Therefore, the binding mode of NO-GC activators is of particular interest for the clinical use of NO-GC activators in pathophysiological situations burdened by high oxidative stress [147]. In contrast to the NO-GC stimulator class, there are currently no clinically approved NO-GC activators. Nevertheless, several preclinical studies support their potential for the treatment of portal hypertension and chronic kidney disease (CKD) [136, 148-151]. Indeed, promising clinical trials are already investigating the use of NO-GC activator Runcaciguat in CKD patients with severe cardiovascular comorbidities (CONCORD; NCT04507061) and in patients with non-proliferative diabetic retinopathy (NEON-NPDR; NCT04722991).

In conclusion, NO-GC stimulators and activators represent effective strategies for modulating the NO/cGMP signaling pathway under pathological conditions characterized by reduced NO bioavailability and oxidative stress. Furthermore, the successful market approvals and the numerous preclinical and clinical approaches targeting various indications highlight the immense

therapeutic potential embodied by the NO/cGMP signaling cascade for the treatment of a variety of diseases.

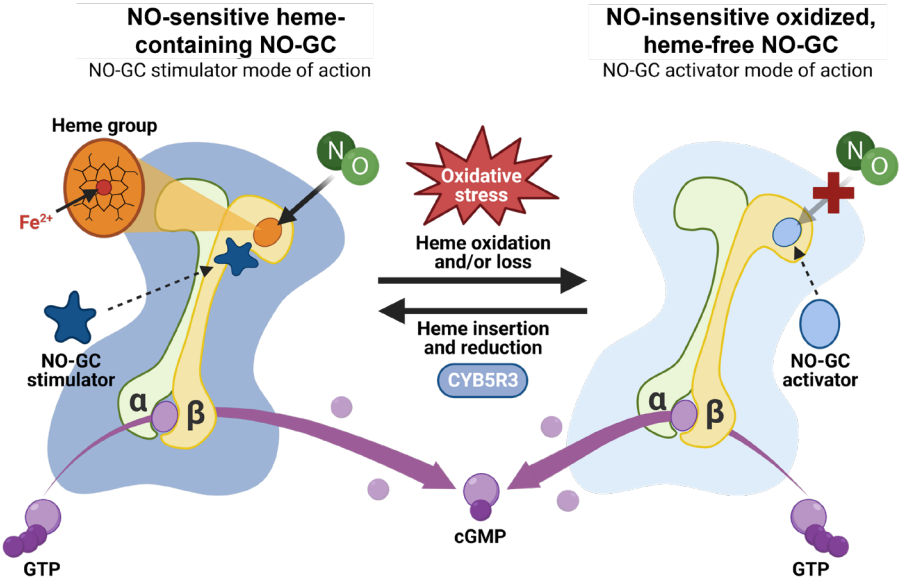

Figure 7. NO-GC modulators mode of action.
Schematic representation of the mechanisms by which NO-GC stimulators and NO-GC activators modulate the NO/cGMP signaling pathway. Both types of compounds induce guanosine monophosphate (cGMP) generation from guanosine triphosphate (GTP) by allosteric binding to NO-GC but differ in binding site and mode of action. NO-GC stimulators bind directly to the β-subunit of the NO-sensitive heme-containing NO-GC and exhibit a dual mode of action. They can stimulate NO-GC activity in the absence or presence of NO, increasing its sensitivity to endogenous NO. Oxidative stress could lead to the oxidation of the heme cofactor of NO-GC, possibly resulting in the loss of the heme group and subsequently impairing the enzymatic function. Enzymatic dysfunction can be remedied through the binding of NO-GC activators to the heme pocket within the β-subunit of both the oxidized and heme-free forms of NO-GC. The replacement of the heme group results in an NO and heme-independent activation of NO-GC. The NO-sensitive heme-containing and NO-insensitive oxidized, heme-free forms of NO-GC exist in a redox equilibrium with each other, in which the oxidized heme group can be reduced by cytochrome b5 reductase 3 (CYB5R3). For more details see the text. Adapted from Sandner et al. 2021 [79]. Image created using BioRender.com.

1.5 NO/cGMP signaling pathway in VSMCs and atherosclerosis

Nowadays, there is scientific consensus on the central role of the NO/cGMP signaling axis in VSMCs as a critical regulator of many physiological functions and the immense relevance of phenotypic plasticity of VSMCs in atherosclerosis (see **Section 1.1.3** and **Section 1.3.2**). However, the role of the NO/cGMP signaling pathway in the phenotypic modulation of VSMCs and its importance in atherogenesis is still controversially discussed.

A frequently used *in vitro* model to investigate the role of the NO/cGMP signaling pathway in phenotypic modulation is cultured VSMCs. Most studies agree that the NO/cGMP signaling pathway likely has an impact on phenotypic modulation. However, it is still controversial whether the NO/cGMP pathway promotes or inhibits phenotypic modulation [70]. Many studies have been conducted with passaged VSMCs. These studies indicated that the stimulation of the NO/cGMP signaling axis likely inhibits VSMC modulation while simultaneously promoting the contractile phenotype, leading to reduced cell growth [152-154]. In contrast, studies with

isolated primary VSMCs (pVSMCs) suggest that the generation of cGMP through NO-GC promotes the modulated phenotype. It has been shown that the genetic deletion of NO-GC1 leads to reduced growth and migration of pVSMCs [155]. This result is supported by multiple studies demonstrating that the stimulation of the axis with NO donors like DETA/NO or the cGMP analog 8-Br-cGMP promotes the growth of pVSMCs [92, 93, 155-159]. Moreover, it has been shown that the growth-promoting effect of the generated cGMP in pVSMCs primarily depends on the stimulation of cell adhesion mediated by the expression of β1 and β3 integrins [92]. It's worth noting that low concentrations of DETA/NO led to cGMP-dependent growth stimulation, while high concentrations inhibited growth independently of the NO/cGMP/cGKI signaling axis [93, 155, 158, 159]. Essentially, the controversial results regarding the effect of the NO/cGMP signaling pathway on the phenotypic modulation of cultured VSMCs seem to significantly depend on the cell model (primary or passaged VSMCs) used. As previously described, cultivation can influence the phenotype of VSMCs, with a modulated phenotype being favored by passaging [51-56]. Thus, depending on the cell model, the initial state of VSMCs may vary between contractile (primary) or modulated (passaged) cells, which consequently leads to a different influence of the NO/cGMP signaling axis [159]. Interestingly, the controversial effect has also been described in various studies where the effect of DETA/NO and 8-Br-cGMP on both primary and passaged VSMCs was parallelly investigated [92, 156]. The growth-promoting effect of cGMP in pVSMCs has been shown to be lost in early cell passages and even slightly reversed in later cell passages [92]. It was hypothesized that the passaging of VSMCs leads to a functional change in the endogenous NO/cGMP signaling axis, thus resulting in a change in the growth response [92, 93]. However, the exact cause of these controversial results is still to be clarified.

A similar discrepancy exists in the results of various *in vivo* studies analyzing the role of the NO/cGMP signaling axis in atherogenesis in animal models of atherosclerosis. Systemic and chronic treatment with NO-GC modulators was reported in few studies, with limited information, to be atheroprotective [160-163]. Furthermore, in a study conducted under conditions of pre-existing atherosclerosis, the PDE5 inhibitor Sildenafil demonstrated also an anti-atherosclerotic effect [164]. Across all these studies, treatment with drugs that elevate cGMP levels resulted in a reduction of lesion area [160, 161, 164]. However, global genetic knockout of NO-GC1 suggested a pro-atherosclerotic role of the NO/cGMP signaling pathway, as the atherosclerotic lesion area was also significantly reduced in knockout mice in this study. [155]. The interpretation of results of such studies involving global manipulation of the NO/cGMP signaling axis by systemic pharmacological treatments or conventional knockouts is challenging. In addition to compound-specific effects, the observed effects could be based on a complex interplay of different cell types or the influence on physiological processes (e.g., blood pressure, inflammation), which in turn have effects on atherogenesis. A more precise approach is

provided by a cell-type-specific and inducible conditional knockout, which allows postnatal ablation of genes and attributing the effects to a specific cell type. Such a genetic ablation model combined with genetic tracking of VSMC fate during plaque development has already been used to investigate the role of cGKI in VSMCs for atherosclerosis at the level of effector proteins [93]. The results of this study were in line with those of the study of the global NO-GC1 knockout and suggested that the NO/cGMP/cGKI signaling axis in VSMCs promotes the progression of atherosclerosis [93, 155]. Moreover, it was even shown that VSMCs lacking cGKI were almost exclusively located in the media and did not significantly contribute to plaque development [93]. In both mouse studies, it was suggested that the observed effects of the NO-GC1 and cGKI knockouts on the atherosclerotic lesion area could be based on altered phenotypic modulation of VSMCs [93, 155]. However, whether this is the case remains to be clarified and requires further investigation.

In summary, there is solid evidence for the functional relevance of the VSMC-specific NO/cGMP signaling axis in atherogenesis. However, further studies are needed to clarify the specific role of the signaling axis in the phenotypic modulation of VSMCs and whether its function in atherogenesis is beneficial or detrimental. Of particular interest are the reasons for the controversial results between genetic and pharmacological manipulation of the NO/cGMP axis *in vivo* and the role of VSMCs in this process. In this context, it will also be interesting to determine whether the modulation of the NO/cGMP signaling pathway represents a suitable therapeutic strategy in the treatment of atherosclerosis.

1.6 Aim of the work

Atherosclerosis can result in myocardial infarction and stroke, which are the leading causes of death in the world [1, 2]. Due to the high lethality, there is an enormous need for suitable therapeutic options. However, the development of novel therapeutic strategies requires a better understanding of atherogenesis.

The NO/cGMP signaling pathway in VSMCs plays a key role in many vascular functions. The activation of NO-GC in VSMCs by NO leads to an intracellular increase in cGMP. This subsequently triggers downstream cGMP effector proteins and finally influences vascular relaxation, VSMC growth, and differentiation (**Figure 8**). Previous studies have indicated that the dysfunction of the NO/cGMP siganling pathway might be involved in the development and growth of atherosclerotic plaques [93, 155]. This effect might be associated with an altered phenotypic modulation/transdifferentiation behavior of VSMCs and may therefore affect plaque composition [155]. Therefore, **this study aimed to elucidate the pathophysiological and pharmacological relevance of the NO/cGMP signaling pathway in VSMCs in atherosclerosis.** The study analyzed the potential link between the NO/cGMP signaling and

VSMC phenotypic modulation with a special focus on its effect on atherosclerosis (**Figure 8**). NO-GC modulating drugs (BAY Activator tool compound and Vericiguat) or genetic alterations via SMC-specific NO-GC knockout were used to modulate the NO/cGMP pathway and analyze its impact on the formation of atherosclerotic plaques. **We hypothesize that the modulation of the NO/cGMP signaling pathway affects the phenotypic modulation of VSMCs, potentially leading to fundamental changes in plaque composition and size.**

The combination of the pharmacological and genetic approaches could provide a comprehensive overview of how the NO/cGMP signaling pathway in VSMCs affects atherogenesis and whether its pharmacological modulation with NO-GC stimulators and/or activators represents a novel therapeutic option to favorably modulate atherogenesis.

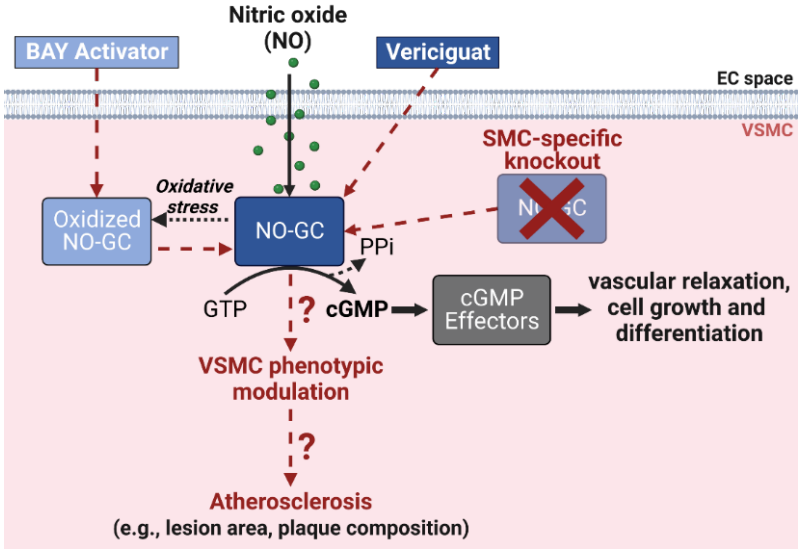

Figure 8. Overview of the project aim.
Activation of NO-sensitive guanylyl cyclase (NO-GC) in vascular smooth muscle cells (VSMCs) by nitric oxide (NO) leads to the generation of second messenger cyclic guanosine monophosphate (cGMP) by converting guanosine triphosphate (GTP). This subsequently triggers downstream cGMP effector proteins and finally influences vascular relaxation, VSMC growth, and differentiation. NO-GC modulating drugs (such as BAY Activator tool compound and Vericiguat) and/or genetic alterations via smooth muscle cell (SMC)-specific knockout can be used to modulate the NO/cGMP signaling axis (in VSMCs). Vericiguat (NO-GC stimulator) binds directly to NO-sensitive heme-containing NO-GC, whereas the BAY Activator (NO-GC Activator) acts on the NO-insensitive oxidized, heme-free form. Both interactions result in increased intracellular cGMP levels. The study aimed to elucidate the pathophysiological and pharmacological relevance of the NO/cGMP signaling pathway in VSMCs in atherosclerosis. Here, the link between the NO/cGMP signaling axis and VSMC phenotypic modulation regarding its effect on atherosclerosis was analyzed. Red dashed arrows indicate the pharmacological and genetic manipulation of NO-GC activity. EC space, extracellular space; PPi, pyrophosphate. Image created using BioRender.com.

2. Materials and Methods

The Materials and Methods section is based on protocols of the Feil working group (AG Feil, Institute of Biochemistry, University Tubingen). Among other references, the protocols from the doctoral thesis of Dobrowinski, H. [159], Lehners, M. [99], and Stehle, D. [165] were used and modified. Each protocol contains both background information and detailed instructions for performing each method. The required materials, including solutions and buffers, are indicated in the protocols, and more comprehensive details can be found in **Section 2.1**.

2.1 Materials

2.1.1 Chemicals and reagents

Table 1. Overview of common chemicals and reagents.

Reagent/Chemical	Company	Reagent/ Chemical	Company
2-ß-Mercaptoethanol	Roth	KCl	Sigma-Aldrich
Acetic acid	Sigma-Aldrich	KH_2PO_4	Merck
Ammonium persulfate (APS)	Roth	LE agarose	Biozym
Bovin serum albumin	Roth	Methanol	Sigma-Aldrich
Bromophenol blue	Roth	$MgCl_2$ [50 mM]	Invitrogen
$CaCl_2$, anhydrous	Roth	Milk powder	Roth
Citric acid	Roth	Na_2HPO_4	Roth
DAB	Sigma-Aldrich	NaCl	Roth
D-Glucose	Fisher	NaOH pellets	Roth
Direct Red 80	Sigma-Aldrich	Normal goat serum	Millipore
DMEM medium -Glutamax™	Gibco	Paraformaldehyde	Roth
Dimethyl sulfoxide (DMSO)	Roth	Phenylmethylsulfonylfluoride (PMSF)	Roth
D-Sucrose	Roth	Rotiphorese Gel 30	Roth
DTT	Roth	Sodium dodecyl sulfate (SDS)	Roth
EDTA	Roth	Tamoxifen	Sigma-Aldrich
Ethanol	Sigma-Aldrich	TEMED	Roth
FCS	Gibco	Toluene	Sigma-Aldrich
Glycerol	Roth	Tris (Trizma base)	Sigma-Aldrich
Glycine	Sigma-Aldrich	Triton X-100	Roth
HCl (37 %), fuming	Roth	Trypan blue (0.4 %)	Gibco
HEPES	Roth	Tween-20	Roth
Hydrogen peroxide (30 %)	Roth	Xylene cyanol	Roth
Isopropanol	Sigma-Aldrich		

2.1.2 Buffer and Solutions

Unless otherwise specified, all buffers and solutions were prepared with demineralized water and stored at room temperature (RT). Where indicated, the pH of the buffers and solutions was adjusted with 10 M and 1 M aqueous NaOH and HCl solutions. The percentages of chemicals and liquids used for the preparation of buffers and solutions are expressed as weight/volume (% w/v) for solid chemicals or as volume/volume (% v/v) for liquids.

Phosphate-buffered saline (PBS) (pH 7.4)

135 mM NaCl (7.9 g/L), 3 mM KCl (0.2 g/L), 8 mM Na_2HPO_4 (1.42 g/L), 2 mM KH_2PO_4 (0.24 g/L), add up to 1 L H_2O, adjust to pH 7.4 with NaOH or HCl, autoclave

Tris-Cl [1 M] (pH 8.0)

121.1 g Tris in 800 mL H_2O, add 42 mL HCl, adjust pH to 8.0, add up to 1 L H_2O

NaOH [10 mM] (pH)

40 g NaOH in 100 mL H_2O

10x Tris-buffered saline (TBS) (pH 8.0)

1.5 M NaCl (87.7 g/L), 100 mM Tris (12.11 g/L), add up to 1 L H_2O, adjust pH to 8.0

TBS-Tween (TBS-T)

1x TBS (100 mL 10x TBS), 0.1 % Tween-20 (1 mL), add up to 1 L H2O

2.1.2.1 Genotyping

DNA extraction buffer

1 µL proteinase K (1 g/L) (Genaxxon), 1 x Reaction buffer (5 µL 10x Reaction buffer (Complete II KCl, Bioron), add 44 µl H_2O, prepare freshly

DNA loading dye

30 % glycerol (30 mL glycerol [100%]), 0.05 % bromophenol blue (2 mL bromophenol blue [25 g/L] in H_2O), 0.05 % xylene cyanol (2 mL xylene cyanol [25 mg/mL] in H2O), 66 mL 10x TBE, store at -20 °C

10x RT buffer

500 mM KCl (5 mL KCl [1 M]), 100 mM Tris-Cl pH 8.0 (1 mL Tris-Cl [1 M] pH 8.0), 15 mM MgCl2 (0.15 mL $MgCl_2$ [1 M]), 2 mM of each dNTP (0.2 mL dATP/dCTP/dTTP/ dGTP [100 mM]), add 3.05 mL H_2O, store at -20 °C

2.1.2.2 Cell isolation and cultivation

100x Pen/Strep

10 000 U/mL penicillin (Gibco), 10 000 µg/mL streptomycin (Gibco), store at -20 °C

Serum-free medium (SRF)

500 mL DMEM medium with GlutaMAX™ (Gibco), 4.5 g/L D-glucose, and 1 % Pen/Strep, store at 4°C

Culture medium (full medium)

500 mL serum free medium, 10 % BSA and 1 % Pen/Strep, store at 4°C

Ca^{2+}-free medium (pH 7.4)

85 mM Na L-glutamate (15.91 g/L), 60 mM NaCl (3.5 g/L), 10 mM HEPES (2.38 g/L), 5.6 mM KCl (0.42 g/L), 1 mM $MgCl_2$ (0.2 g/L), add up to 1 L H_2O, adjust pH to 7.4 with HCl, autoclave, store at 4 °C

Collagenase stock [10 mg/ml]

100 mg Collagenase (Sigma-Aldrich) in 10 mL Ca^{2+}-free medium, store at -20°C

Hyaluronidase stock [10 mg/ml]

100 mg Hyaluronidase (Sigma-Aldrich) in 10 mL Ca^{2+}-free medium, store at -20°C

Papain stock [7 mg/ml]

100 mg Papain (Sigma-Aldrich) in 14.29 mL Ca^{2+}-free medium, store at -20°C

BSA stock [100 mg/ml]

0.5 g BSA in 5 mL Ca^{2+}-free medium, sterilize by filtration, store at -20°C

DTT stock [100 mg/ml]

0.5 g DTT in 5 mL Ca^{2+}-free medium, sterilize by filtration, store at -20°C

2.1.2.3 Protein extraction

PMSF [100 mM]

174 g PMSF in 10 mL ethanol [100 %]

SDS [20 %]

200 g SDS in 800 ml H_2O at 60 °C, finally add up to 1 L H_2O

EDTA [0.5 M] (pH 8.0)

1 g EDTA to 800 mL H_2O, add NaOH pellets (~20 g) to adjust pH to 8.0, add up to 1 L H_2O, autoclave

Cell lysis buffer

21 mM Tris-Cl (210 µL Tris-Cl (pH 8.0) [1 M]), 0.67 % SDS (335 µL SDS [20 %]), 0.2 mM PMSF (20 µL PMSF [100 mM]), add up to 10 mL H_2O, add 1 tablet PhosStop (Roche) and 1 tablet cOmplete (Protease inhibitor cocktail, Roche), prepare freshly

Tissue lysis buffer

50 mM Tris-Cl (500 µL Tris-Cl (pH 8.0) [1 M]), 100 mM NaCl (1 mL NaCl), 5 mM EDTA (100 µL EDTA [0.5 M]), 2 % SDS (1 mL SDS [20 %]), 2.5 mM PMSF (250 µL PMSF [100 mM]), add up to 10 mL H_2O, add 1 tablet PhosStop (Roche) and 1 tablet cOmplete (Protease inhibitor cocktail, Roche), prepare freshly

2.1.2.4 SDS-PAGE and Western blot analysis

APS [20 %]

20 % APS (200 g/L), add 10 mL H_2O, store at -20 °C

4x Tris/SDS pH 6.8

0.5 M Tris (60 g/L Tris), 0.4 % SDS (40 g/L), add 100 mL H_2O, adjust pH to 6.8, store at 4 °C

4x Tris/SDS pH 8.8

1.5 M Tris (182 g/L Tris), 0.4 % SDS (40 g/L), add 100 mL H_2O, adjust pH to 8.8, store at 4 °C

10x SDS running buffer

0.25 M Tris (32.2 g/L), 1.9 M glycine (144 g/L), 0.1 % SDS (10 g/L), add 500 mL H_2O

5x SDS loading dye

0.32 M Tris-Cl (3.2 mL Tris-Cl (pH 6.8) [1 M]), 40 % glycerol (4 mL glycerol), 15 % SDS (150 g/L), 25 % β-mercaptoethanol (2.5 mL β-mercaptoethanol), 0.1 % bromophenol blue (1 g/L), add up to 10 mL H_2O, store at -20 °C

Anode solution I

300 mM Tris (36.3 g/L), 20 % methanol (200 mL methanol [100 %]), add up to 1 L H_2O, adjust pH to 10.4

Anode solution II

25 mM Tris (3 g/L Tris), 20 % methanol (200 mL methanol [100 %]), add up to 1 L H_2O, adjust pH to 10.4

Cathode solution

40 mM 6-amino hexanoic acid (5.2 g/L), 25 mM Tris (3 g/L), 20 % methanol (200 mL methanol [100 %]), add up to 1 L H2O, adjust pH to 7.6

Blocking solution

5 % milk powder (50 g/L), add up to 100 mL TBS-T, store at 4 °C

Primary Ab solution

5 % BSA (50 g/L), 0.05 % NaN3 (50 mg/L), add up to 50 mL TBS-T, store at 4 °C

TBS-T/milk

1 % milk powder (10 g/L), add up to 100 mL TBS-T, store at 4 °C

2.1.2.5 FRET-based cGMP measurement in cultured VSMCs

D-glucose [2.5 M]

18 g D-glucose in 30 mL H_2O, dissolve in an ultrasound water bath at 37 °C, add up to 40 ml H_20, sterilize by filtration, store as 2 mL aliquots at RT

NaOH [10 mM]

40 mg NaOH in 100 mL H_2O

Imaging Buffer (IB) pH 7.4

140 mM NaCl (8.2 g/L), 5 mM KCl (0.37 g/L), 1.2 mM MgCl2 (0.24 g/L), 2 mM CaCl2 (0.22 g/L), 5 mM HEPES (1,19 g/L), add 5 L H_2O, adjust pH to 7.4 with NaOH, autoclave and store at RT, add 2 mL 2.5 M D-Glucose (10 mM final concentration) to 500 mL buffer before use

2.1.2.6 Fixation of tissue

Fixation solution

4 % PFA (40 g/L) in PBS, prepare 100 mL, store as 20 mL aliquots at -20 °C

2.1.2.7 Complete blood count

ACD-Buffer

12.5 g Na_3-Citrate (25 g/L), 6.82 g citric acid (13.64 g/L), 10 g Glucose (20 g/L), add 500 mL H_2O, adjust pH to 4.69 with NaOH, sterilize by filtration, store at -20 °C

2.1.2.8 Oil Red O staining

Methanol [78 %]

78 ml technical methanol [100 %], add up to 100 mL H_2O

NaOH [1 M]

20 g sodium hydroxide (40 g/L), add 500 mL H_2O

Oil Red O stock [0.5 %]

0.5 g Direct Red 80 (5 g/L), add 100 mL technical methanol [100 %], protect the bottle from light

Oil Red O staining solution

35 mL Oil Red O stock (0.5 % in technical methanol), add 10 mL NaOH [1 M], filter the solution (0.45 PTFE membrane filter, 20 ml BD Luer-Lok™ syringe), prepare freshly

2.1.2.9 Chromogenic immunohistochemistry (CIH)

Peroxidase blocking solution

6.3 % H2O2 (300 µL H_2O_2 [30 %]), 0.9 % methanol (130 µL methanol [10 %]), 1 mL PBS, prepare freshly.

Antigen retrieval solution

10 mM sodium citrate (2.94 g/L), add 1 L H_2O, adjust pH to 6.0 with citric acid

CIH blocking solution

10 % normal goat serum in TBS-T, store at 4 °C.

Ab solution (CIH)

5 % normal goat serum in TBS-T

ABC solution

12 µl reagent A and 12 µl reagent B, add 600 µl PBS and incubate 30 min, add 600 µl TBS-T directly before use

DAB stock solution [0.1 %]

40 mg DAB (1 g/L) in 40 mL PBS, store at -20°C

DAB staining solution

0.05 % DAB (800 µl DAB [0.1 %]), 0.02 % H_2O_2 (1 µL H_2O_2 [30 %]), add 800 µl PBS, prepare directly before use

2.1.2.10 Picrosirius red (PSR) staining

Sirius red staining solution

0.5 g Direct Red 80 (1 g/L) in 500 mL picric acid solution [1.3 %]

Acidified water

2.5 ml acetic acid in 500 ml H_2O

2.1.2.11 Immunofluorescence (IF) staining

Sucrose solution [30%]

30 % sucrose (300 g/L), add 100 mL PBS, store at 4 °C

PBS-T

0.1% Triton-X (1 mL), add 1 L PBS

IF block solution

1 % normal goat serum in PBS-T, store at 4 °C

2.1.3 Animal diet

Standard diet

Standard diet for mice (1324) containing 11 % fat, 24 % protein, and 65 % carbohydrates from Altromin (Altromin Spezialfutter GmbH & Co.KG, Germany).

Breeding diet

Breeding diet for mice (1314) containing 14 % fat, 27 % protein, and 59 % carbohydrates from Altromin (Altromin Spezialfutter GmbH & Co.KG, Germany).

Atherogenic diet

Western diet (E15723-34, TD88137) containing 21 % butter fat and 1.25 % cholesterol (42 kj% fat, 15 kJ% protein, 43 kJ% carbohydrates) from Ssniff (ssniff Spezialdiäten GmbH, Germany). The chow was delivered in a vacuum-sealed 5 kg package and was stored at 4°C. The Western diet was supplemented with the NO-GC modulators (Vericiguat and BAY Activator) at a concentration of 150 ppm (150 mg/kg diet).

2.1.4 cGMP signaling pathway modulating compounds and drugs

Table 2. Overview of the cGMP signaling pathway modulating compounds and drugs.
Listed are the NO-GC modulating drugs used in this work. The NO-GC activator tool compound BR11707 was provided by Prof. Dr. P. Sandner, BAYER AG.

Compound	In-text name	Stock concentration	Order number	Company
8-Bromoguanosine 3′,5′-cyclic monophosphate	8-Br-cGMP	100 mM in H_2O	B004-250E	BioLog
Diethylamine NONOate	DEA/NO	100 mM in 10 mM NaoH	372965-00-9	Axxora
Diethylenetriamine NONOate	DETA/NO	100 mM in 10 mM NaoH	Cay82100-100	Biomol
Verquvo	Vericiguat	10 mM in DMSO	ADV465750353	Sigma-Aldrich
BR11707	BAY Activator	10 mM in DMSO	internal	BAYER AG (GER)
1H-[1,2,4]oxadiazolo[4,3-a]quinoxalin-1-one	ODQ	20 mM in DMSO	41443-28-1	Axxora

2.1.5 Antibodies

Table 3. Used primary antibodies.
Listed are the primary antibodies used in the present study. The working dilution is indicated depending on the approach. Antibodies were diluted in primary Ab solution (TBS-T +5 % BSA +0.05 % NaN3) for Western blot (WB), in Ab solution (5 % normal goat serum in TBS-T) for Chromogenic immunohistochemistry (CIH) and in IF blocking solution (1% normal goat serum, 0.1% Triton X-100 in PBS) for immunofluorescence (IF) staining.

Antibody	Source	Dilution	Approach	Order number	Company/Manufacturer
αSMA	Rabbit	1:10000 1:1000 1:2000	WB IF CIH	ab124964	Abcam
αSMA-cy3 conjugated	Mouse	1:100	IF	C6198	Sigma-Aldrich
cGKIc	Rabbit	1:5000	WB	-	Prof. Dr. R. Feil
GAPDH	Rabbit	1:1000	WB	#2118	Cell Signaling
GFP	Chicken	1:2000	IF	#13970	Abcam
MAC2	Rat	1:5000 1:200 1:200	WB IF CIH	CI8942	Cederlane
NO-GC β1	Rabbit	1:1000	IF	ab124964	Abcam
NO-GC β1 2A	Rabbit	1:1000	WB	-	Prof. Dr. A. Friebe
p-VASP (Ser239)	Rabbit	1:1000	WB	#3114	Cell Signaling
VASP	Rabbit	1:1000	WB	#3132	Cell Signaling

Table 4. Used secondary antibodies.
Listed are the secondary antibodies used in the present study. The dilution factor is indicated depending on the approach. Antibodies were diluted in TBST/milk (1 % milk powder in TBST) for Western blot (WB), in Ab solution (5 % normal goat serum in TBS-T) for Chromogenic immunohistochemistry (CIH) and in IF blocking solution (1% normal goat serum, 0.1% Triton X-100 in PBS) for immunofluorescence (IF) staining. HRP: Horseradish peroxidase.

Antibody	Source	Dilution	Approach	Order number	Company
α-rabbit-HRP	Goat	1:5000	WB	70749	Cell Signaling
α-rabbit-AlexaFluor488	Goat	1:1000	IF	A11008	Life Technologies
α-rabbit-AlexaFluor594	Goat	1:1000	IF	A-11012	Life Technologies
α-rabbit-biotinylated	Goat	1:250	CIH	VEC-BA-1000-MC15	Biozol
α-chicken-AlexaFluor488	Goat	1:1000	IF	A11039	Invitrogen
α-rat-HRP	Goat	1:5000	WB	31470	Invitrogen
α-rat-AlexaFluor488	Goat	1:1000	IF	112-545-167	Jackson Immu-noResearch
α-rat-biotinylated	Rabbit	1:250	CIH	VEC-BA-4001-MC05	Biozol

2.1.6 Software

In the present study, the following software tools were used for data acquisition, analysis, and presentation: FIJI (ImageJ) was used along with the relevant plugins for image analysis [166,

167]. Origin2023b (OriginLab) and Excel365 (Microsoft) were used for data analysis. Figures and illustrations were created using BioRender.com and Microsoft PowerPoint. Additionally, EndNote 20 (Clarivate) was employed to generate the bibliography. Any additional software applications are explicitly indicated in the respective sections of the methods.

2.2 Transgenic mice

2.2.1 Animal ethics statement

All animal experiments were conducted in strict accordance with Directive 2010/63/EU of the European Parliament and received approval from local authorities (Regierungspräsidium Tübingen, IB 7/18G and IB 1/22G). Mice used for the isolation of aortas, both with and without subsequent cultivation of pVSMCs, were reported to the University of Tübingen's animal welfare officer (IB 1/20M and IB 2/22M). Throughout the planning and execution of the experiments, the ethical principles of "3-Rs" (Replace, Reduce and Refine) and animal welfare were considered as the highest priority.

2.2.2 Mouse husbandry and breeding

Mice were housed in the animal facility of the Interfaculty Institute of Biochemistry at Eberhard Karls University Tubingen. Standard housing conditions included a temperature of 22°C, relative humidity of 50-60%, and a 12-hour light/12-hour dark cycle. Mice had *ad libitum* access to a standard maintenance diet and tap water. Pregnant mice and the litters (up to weaning) received a special breeding diet. Depending on the experimental requirements, the diet was switched to an atherogenic diet for 15-18 weeks. For details about the composition of the used diets see **Section 2.1.3**. Mice were housed in type II long cages, accommodating a maximum of 5 mice, with shredded wood bedding. Each cage was supplemented with wooden tunnels or plastic houses and cellulose. For breeding purposes, one or two female mice were paired with a male. Once pregnancy was visually confirmed, pregnant female mice were transferred together to a type III cage, and their diet was adjusted accordingly. Litters were weaned at 3 weeks of age, separated by sex, and marked with ear tags. Ear biopsies were collected for genotyping (**Section 2.2.4**).

2.2.3 Mouse lines

Animal models are indispensable tools for mimicking the key aspects of diseases to better understand these mechanisms and develop effective therapeutic strategies. In contrast to *in vitro* approaches, animal models provide a comprehensive approach that captures the dynamic interactions between cells and organs and the impact of the interplay between genetic, environmental, and physiological factors [13, 14]. In the present study, transgenic mice with knocked-in reporter genes and knocked-out genes related to lipid metabolism and the cGMP signaling pathway were used. These transgenic mice enabled *in vitro* real-time FRET analysis

of intracellular cGMP levels (Global-cGi500), the emulation of atherosclerosis in mice (ApoE^{ko}), and the functional characterization of the role of the NO/cGMP signaling pathway in atherogenesis (NO-GC^{smko}) (**Table 1**, **Table 6**). The transgenic mouse lines used to generate the experimental mouse lines in this study are described in **Table 5**. All transgenic mice used in this study were bred on the C57BL/6NCrl background.

Table 5. Overview of transgenic mouse lines used in the present study.
Listed are the various transgenic mouse lines used in the present study. The nomenclature for the genotypes is as follows: "wt" refers to the wildtype allele, "L2" refers to a flanked targeted sequence/gen by two loxP sites, "L1" refers to an excised target sequence/gen after Cre recombination (only one loxP remains), "ko" refers to gene knockout. If not otherwise indicated, all mice used in the present study were bred on a C57BL/6NCrl background.

Internal name	Systematic name	Description	Ref.
Bl6	C57BL/6NCrl	Wildtyp mice; if not otherwise indicated, all mice used in the present study were bred on a C57BL/6NCrl background.	[168]
ApoE^{ko}	B6.129P2-Apoe^{tm1Unc}	Global knock out of the Apolipoprotein E. Frequently used mouse model of atherosclerosis.	[16]
cGi500-L1	B6;129-Gt(ROSA)26Sor$^{tm4.1(ACTB-tdTomato,-cGi-500)Feil}$	Global expression of the cGMP biosensor cGi500 under the control of CAG promoter.	[140]
mT/cGi500-L2	B6;129-Gt(ROSA)26Sor$^{tm4(ACTB-tdTomato,-cGi-500)Feil}$	Cre inducible expression of the cGMP biosensor cGi500 under the control of CAG promoter. The mTomato gene stop cassette is flanked by loxP sites, which allows the Cre-mediated recombination (switch from mTomato to cGi500 expression).	[140]
SMA-CreER^{T2}	B6-Tg(Acta2-cre/ERT2)51Pcn	Expression of the tamoxifen-dependent CreER^{T2} under the control of the mouse SMA promoter.	[169]
NO-GC$^{L2/L2}$	B6;129-Gucy1b3$^{tm1.2Frb}$	The exon 10 of the NO-GC β1 subunit gene is flanked by loxP sites, which allows the Cre-mediated inducible ablation of the NO-GC β1 subunit.	[123]

Detailed information on the experimental mouse lines investigated in the present study is given in **Table 6**. In the present study, FRET-based cGMP measurements were performed with pVSMCs isolated from mice globally expressing the cGMP biosensor cGi500. For further information about the cGMP biosensor and the Global-cGi500 mouse line, see **Section 1.3.4**. The ApoE knockout mouse model in combination with an atherogenic diet was used as a model of atherosclerosis (see also **Section 1.1.2**). Using ApoE^{ko} mice, the effects of various NO-GC modulators on atherogenesis were examined. Additionally, a mouse line on the ApoE^{ko} background was generated that allowed the characterization of VSMC-specific conditional knockout of NO-GC in atherosclerosis. For this purpose, mice expressing the inducible Cre-ER^{T2} recombinase under the control of the αSMA promoter were crossed with mice carrying a floxed NO-GC β1-subunit gene (NO-GC^{smko}: SMA-CreER^{T2} x NO-GC$^{L2/L2}$ x mT/cGi500-L2). The cell-specific knockout was induced by intraperitoneal injection of tamoxifen (5 x 1 mg/mouse/day) at 8 and 10 weeks of age. Specifically, the experimental animals received two cycles of tamoxifen

injection for five consecutive days, with a break of nine days in between. The corresponding mouse lines for the control of VSMC-specific NO-GC knockout (Ctrl) and the effects of SMA-CreER^{T2} (Cre-Ctrl) were also generated. The cell type specificity of Cre-mediated recombination and the efficiency of NO-GC^{smko} in experimental animals were validated through immunofluorescence staining and Western blot analysis (**Section 3.3.1**). Please note that these mouse lines also carry the reporter gene for cell-specific expression of the cGMP biosensor cGi500 (mT/cGi500-L2). This provides future studies the opportunity to conduct VSMC-specific FRET-based cGMP measurements and lineage tracing studies in atherosclerosis. The experimental mice were comparatively examined for supposed side effects caused by the biosensor expression. No effect of homozygous or heterozygous expression of the biosensor could be detected. In this work, experiments were conducted with litter-matched animals.

Table 6. Experimental mouse lines investigated in the present study.
Listed are the various experimental mouse lines investigated in the present study. The nomenclature for the genotypes is as follows: ”wt” refers to the wildtype allele, “L2” refers to a flanked targeted sequence/gen by two loxP sites, “L1” refers to a excised target sequence/gen after Cre recombination (only one loxP remains), “ko” refers to gene knockout. If not otherwise indicated, all mice used in the present study were bred on a C57BL/6NCrl background. Please note, that recombined cells in Ctrl mice carry one functional and one defective NO-GC allele.

In-text name	Full genotype	Approach
Wildtyp	C57BL/6NCrl	Analysis of the effects of NO-GC modulators on growth of isolated pVSMCs (*in vitro*).
ApoE^{ko}	ApoE^{ko}	Analysis of NO-GC modulators effects on atherosclerosis (*in vivo*).
Global-cGi500	cGi500-L1	FRET-analysis of the effects of NO-GC modulators on cGMP signaling in isolated pVSMCs (*in vitro*).
NO-GC^{smko}	ApoE^{ko} x NO-GC$^{L2/L2}$ x mT/cGi500-L2 x SMA-CreER^{T2}	Analysis of αSMA-specific NO-GC knock-out.
Ctrl	ApoE^{ko} x NO-GC$^{L2/wt}$ x mT/cGi500-L2 x SMA-CreERT2	Control for NO-GC^{smko} effects.
Cre-Ctrl	ApoE^{ko} x NO-GC$^{L2/L2}$ x mT/cGi500-L2	Control for SMA-CreER^{T2} effects, lack of the αSMA-CreERT2 transgene.

2.2.4 Genotyping

Controlling the genetic status is essential when working with transgenic mice. Therefore, the genotyping of experimental mice was conducted at three weeks of age and re-verified after the experiment, if applicable. The DNA was isolated from ear biopsies. Consequently, polymerase chain reaction (PCR) was employed to distinguish between wildtype and transgenic genotypes. PCR products were separated by agarose gel electrophoresis, and their lengths were compared to a DNA ladder for genotype assignment. **Table 7** provides an overview of the target genes, the corresponding specific primer combinations, and the expected fragment lengths for genotyping.

Table 7. PCR primer and programs for genotyping.
The generated PCR products and the predicted size in base pair (bp) are given for each potential genotype (wildtype (wt), transgenic (tg), floxed (L1, L2) or knock-out (ko) allele). Primers were obtained from Eurofins and stored as 25 µM stocks in HPLC-grade H2O at – 20 °C.

Target	Primer	Sequence (5'–3')	Volume [µl]	Product size		PCR Programm		
ApoE	RF115	GCCTAGCCGAGGGAGAGCCG	0.3	ko	245 bp	95 °C	3 min	
	RF117	GCCGCCCCGACTGCATCT	0.3			94 °C	10 sec	
				+	163 bp	57°C	30 sec	35x
	RF151	AGTTCTTGTGTGACTTGGGAG	0.3			72 °C	30 sec	
						72 °C	10 min	
Cre	Cre800	GCTGCCACGACCAAGTGACAG-CAATG	0.3	tg	402 bp	95 °C	5 min	
						95 °C	10 sec	
						58 °C	30 sec	35x
	Cre1200	GTAGTTATTCGGATCATCAGC-TACAC	0.3	+	none	72 °C	30 sec	
						72 °C	5 min	
cGi(L1) **cGi(L2)**	BB01	CTCTGCTGCCTCCTGGCTTCT	0.3	+	330 bp	95 °C	5 min	
						95 °C	10 sec	
	BB02	CGAGGCGGATCACAAGCAATA	0.3	L1	250 bp	61 °C	30 sec	35x
						72 °C	30 sec	
	BB03	TCAATGGGCGGGGGTCGTT	0.3	L2	250 bp	72 °C	5 min	
NO-GC	BB19	AAGATGCTGAAGGGAAGGATGC	0.3	L1	830 bp	95 °C	3 min	
						95 °C	60 sec	
	BB20	CAGCCCAAAGAAACAAGAA-GAAAG	0.3	L2	720 bp	63 °C	45 sec	37x
						72°C	60 sec	
	BB21	GATGTGGGATTGTTTCTGAGG A	0.3	+	680 bp	72 °C	7 min	

To genotype the experimental mice:

1. Extract DNA by incubating ear biopsies in 50 µL DNA extraction buffer overnight at 55 °C.
2. Vortex samples and centrifuge for 5 min at 18000 rcf. Transfer the DNA-containing supernatants into new tubes.
3. Heat-inactivate proteinase K (Genaxxon) for 15 min at 95 °C in a thermocycler and store DNA samples at -20 °C or continue with PCR.
4. Prepare master mixes:
    a. All PCRs (except NO-GC): 2.5 µL 10x RT buffer, 0.2 µL DFS-Taq DNA polymerase (Bioron), 0.3 µl each primer according to **Table 7**, add 19-20 µL H_2O
    b. NO-GC PCR: 2.5 µL 10x PCR Rxn buffer (Invitrogen), 0.75 µL MgCl2 [50 mM], 0.5 µL dNTPs [10mM] (Gennaxxon), 0.25 µL Taq DNA polymerase (Invitrogen), 0.3 µL each primer according to **Table 7**, add 18.25 µL H_2O
5. Transfer 23 µL master mix to a PCR reaction tube and add 2 µl DNA sample. Vortex and spin down briefly.
6. Place the PCR reaction tube in the thermocycler and run the appropriate PCR program (**Table 7**). After the PCR, add 5 µL of 6x DNA loading dye to the samples.

7. For analysis of the PCR products, prepare a 2 % agarose gel:
    a. Dissolve 2 g agarose in 1x TAE buffer and heat the solution in a microwave until agarose is solved (~2 min).
    b. Let the solution cool down for 15 min at RT while stirring, then add 3 µL Midori green (Nippon Genetics).
    c. Pour the gel into a chamber, place combs, and let the gel solidify for at least 30 min.
    d. Place gel in an electrophoresis chamber filled with 1x TAE buffer, remove combs.
8. Load approximately 12 µL of PCR sample or 8 µL of 1 kb Plus DNA Ladder (Invitrogen) per well on the agarose gel and run the gel at 120 V for approximately 30 min.
9. Visualize and document the separated PCR products under UV light with ChemiDoc Imaging System (Bio-Rad).

2.3 Vascular smooth muscle cell culture

To analyze the effects of NO-GC modulators *in vitro*, VSMCs were isolated from the aorta of transgenic and wildtype mice with an age of 8-16 weeks. In this work, only isolated and cultured primary cells (cell passage 0) were used. The buffers and solution used for VSMC isolation and cultivation are described in **Section 2.1.2.1**. Cells were grown in full medium at 37°C with 6% CO2. Depending on the approach (**Table 8**), the cells were cultured in full medium for approximately 4-7 days. The medium was then replaced with serum-free medium (SRF) to ensure defined conditions for the experiment if required.

Table 8. Overview of the used cell culture conditions depending on the approach.

Approach	Culture format	Seeded cell number	Full medium	Serum starvation
VASP phosphorylation assay	6 well plate	$2*10^5$ cells/well	7 days (~90 % confluency)	YES; for 48 h
cGMP measurement	24 well plate (glass cover slip)	$5*10^4$ cells/well	4-5 days	YES; O/N
xCELLLigence	xCELLigence well plate	$2*10^4$ cells/well	7 days	NO

2.3.1 Cell isolation

To isolate VSMCs from mice aorta:

1. Euthanize the mouse with CO_2 and confirm its death by checking the inter-toe reflex, followed by cervical dislocation. If re-genotyping is needed, cut off an earpiece and follow the instructions in **Section 2.2.4**.
2. Spray the abdominal fur of the mouse with 70% ethanol and open the abdominal cavity with a midline incision along the *linea alba*. Cut through the peritoneum and ribs to open

the thoracic cavity, and then bend the chest to expose the heart. Move the liver and gastrointestinal tract aside and remove the spleen and lung. To isolate the aorta, grab the heart with forceps and carefully pull it upwards so that the aorta is slightly tensed. Cut along the spine until the kidneys are passed. Remove the aorta and store it in PBS. Repeat this step until all mice are processed.

3. Transfer the aorta to a 10 cm petri dish with PBS. Remove the surrounding adipose tissue under a stereo microscope using two fine forceps. To remove the kidneys, pull them aside with forceps, and cut the renal vessel close to the kidney. Separate the aorta from the heart at the aortic root. Carefully remove any remaining blood in the aorta by gently squeezing it with forceps.
4. Transfer the cleaned aorta into a Ca2+-free medium and place it in a 3.5 cm dish on ice. If multiple aortas are isolated at the same time, repeat step 3 for each aorta until all aortas are cleaned.
5. Cut the cleaned aorta into pieces that are 2-3 mm in size.

To achieve sterile conditions, all subsequent steps should be performed in a cell culture hood.

6. Prepare the lysis buffer A (0.25 mL/aorta, but at least 0.5 mL) in a 15 mL tube and transfer the pieces into the solution.

   Lysis buffer A

   10 % papain stock, 1 % BSA stock, and 1 % DTT stock in Ca2+-free medium, prepared freshly

7. Incubate the solution for 1 h at 37°C in the water bath and mix the aorta pieces every 15-20 minutes.
8. Stop the digestion by centrifuging at 200 rcf for 3 minutes.
9. In the meantime, prepare lysis buffer B in an appropriate tube (same volume as lysis buffer A).

   Lysis buffer B

   10 % collagenase stock, 10 % hyaluronidase stock and 1 % BSA stock in Ca2+-free medium, prepared freshly

10. Carefully remove the supernatant with a pipette and add lysis buffer B to resuspend the aorta pieces.
11. Incubate the solution for a maximum of 12 minutes at 37°C in a water bath. During the first 5 minutes of digestion, mix the solution every minute. For the following 7 minutes of incubation, suspend the mixture occasionally by pipetting several times up and down each minute.

12. To stop the digestion, add full medium (3-4x the volume of lysis buffer B) to the resuspension.
13. Centrifuge the resuspension at 200 rcf for 8 minutes.
14. Carefully aspirate the supernatant and resuspend the cell pellet in an appropriate volume of full medium (1 mL for up to 4 aortas).
15. Count viable cells in a Neubauer counting chamber by mixing 18 µL of the cell suspension with 2 µL trypan blue.
16. Depending on the approach, dilute the cell suspension in full medium and plate the appropriate cell number on the desired format (**Table 8**.).
17. Culture the cells at 37°C and 6% CO_2 in a cell culture incubator.

2.3.2 FRET-based cGMP measurement

The working principle of the FRET-based cGMP biosensor cGi500 is described in **Section 1.3.4**. This biosensor has proven to be a valuable tool in various *in vitro*, *ex vivo*, and *in vivo* experiments, allowing for real-time measurement of changes in intracellular cGMP levels [78, 139, 170]. In this study, we used the cGi500 biosensor to investigate the effects of different substances modulating the NO/cGMP signaling pathway on intracellular cGMP generation in pVSMCs.

2.3.2.1 FRET-based cGMP measurements in isolated pVSMCs.

FRET-based cGMP measurements were conducted following the protocol described by Thunemann et al., 2013 [170]. An inverted epifluorescence microscope (Axiovert 200, Zeiss) equipped with a fluorescence-grade air objective (Plan-NeoFluar 10x/0.3; Zeiss) and a 1.0/1.6x Optovar lens was utilized. The light source consisted of a computer-controlled xenon short-arc lamp (Oligochrome, TILL Photonics) with an electronic shutter. Simultaneous acquisition of CFP and YFP fluorescence signals was achieved using a Dual-View beam splitter (Photometrics) equipped with a 516 nm dichroic mirror and two emission filters (BP 480/50 nm for CFP and BP 535/40 nm for YFP). For FRET-based cGMP measurements, the CFP donor fluorophore was excited at 445/20 nm, and the emitted signals were collected and separated using the Dual-View beam splitter and appropriate emission filters. All signals were recorded using an electron-multiplying charge-coupled device (EM-CCD) camera (Retiga R1, QImaging). To visualize the expression of the cGi500 sensor in VSMCs, an additional set of excitation (BP 497/16) and emission (BP 535/22 nm) filters, in combination with the 516 nm dichroic mirror, was used for direct recording of YFP fluorescence.

This microscope setup was combined with a custom-built superfusion system, which allowed for the time-controlled application of different drugs and the investigation of cGMP signaling dynamics in the same cell during a single measurement. The system included a FPLC pump (Pharmacia P-500, GE Healthcare), FPLC injection valves (Pharmacia V-7, GE Healthcare),

and a superfusion chamber (RC-26, Warner Instruments) for continuous superfusion of the cells with imaging buffer (IB). A vacuum pump (Laboport N86, KNF Neuberger) was also connected to the system to remove excess buffer Sample loops of varying sizes were included in the system for drug application, with the 2 mL loop primarily used for drug application and the 7 mL loop for ODQ application.

Figure 9 shows the workflow to measure real-time changes in cGMP levels in isolated pVSMCs. Aortic VSMCs were isolated from mice globally expressing the FRET biosensor cGi500 (global-cGi500), as described in **Section 2.3.1**. Transgenic pVSMCs were seeded on 12 mm glass coverslips and cultured in full medium for 4-5 days at 37°C and 6% CO2 in a cell culture incubator (**Table 8**). One day prior to FRET-based cGMP measurements, the cells were serum starved. For the FRET-based cGMP measurements, the cover slip with attached cells was placed in the superfusion flow chamber and the drug effects on cGMP generation were monitored. The following setup was used: 4x4 binning, 300 ms exposure, 5-second cycle time, a flow rate of 1 mL/min, and a 10x magnification objective.

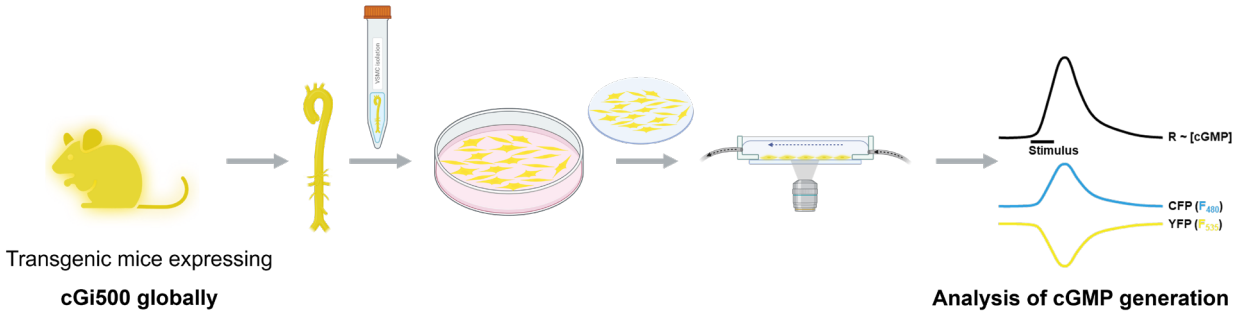

Figure 9. FRET-based cGMP measurements in isolated pVSMCs.
Schematic representation of the workflow for measuring intracellular cGMP levels in isolated pVSMCs. Aortic VSMCs are enzymatically isolated from transgenic mice globally expressing the FRET biosensor cGi500 and cultured on a glass coverslip for 5-6 days. The glass coverslip with attached VSMCs is transferred to the superfusion flow chamber, and the VSMCs are continuously perfused with imaging buffer during the measurement. The connected superfusion system enables time-controlled treatment of the cells with various drugs. The cGi500 biosensor allows for real-time FRET-based visualization of intracellular cGMP concentration. The CFP/YFP ratio (R, black curve) correlates with intracellular cGMP concentration ([cGMP]). Changes in FRET efficiency after any stimulus are documented and subsequently analyzed, with cGMP generation being attributed to each stimulus with single-cell resolution. cGMP: 3',5'-cyclic guanosine monophosphate, CFP, cyan fluorescent protein; YFP, yellow fluorescent protein Image created using BioRender.com.

To measure cGMP-levels in pVSMCs:

1. Calibrate the beam splitter using a calibration grid (Photometrics) for optimal CFP-YFP alignment before the first measurement of the day.
2. Replace the solvent within the perfusion system and sample loops (injection valves in load mode) with imaging buffer (IB)
3. Assemble the superfusion chamber with a coverslip and promptly cover the cells with IB to prevent drying.

4. Place the chamber on the microscope stage and connect it to the superfusion system. Initiate the superfusion and adjust the liquid level in the chamber using the outlet needle to ensure continuous flooding of the cells with IB.
5. Use the YFP-direct filter set to identify a representative field of view, taking into account cell density and morphology. Make sure there is a cell-free area available for background correction.
6. Capture a high-resolution image of the representative region (1x1 binning and 1-second exposure time, YFP-direct filter set). This image will be used to mark the cell outlines as regions of interest (ROIs) during data evaluation.
7. Switch to the FRET filter set and adjust the settings for the measurement (4x4 binning, 300 ms exposure, 5-second cycle time). Begin the measurement and mark cells that account for cellular heterogeneity and the background for online analysis.
8. Record the baseline of CFP and YFP intensities for at least 30 frames at the start of each individual experiment. This baseline information is crucial for later baseline correction.
9. Dilute the drugs of interest to their final concentration in IB immediately before use. Load the solution into the sample loop and apply the drug to the cells via the injection valve (switch to load mode). Note that there may be a delay in the drugs reaching the samples due to the system's dead volumes when evaluating FRET/cGMP signals.
10. Between individual drug applications, use online analysis to confirm that the CFP/YFP ratio returns to the baseline. Before loading the next drug into the sample loop, flush the loop twice with IB.
11. After the measurement, turn off the superfusion and disassemble the superfusion flow chamber. Clean the superfusion system by flushing it with 20% ethanol.

2.3.2.2 Data analysis and quantification of FRET/cGMP signals

The VisiView software (Visitron) was used for online image acquisition during FRET measurement. Afterwards, offline processing and analysis of the time-lapse image was carried out by Fiji (ImageJ) to extract the fluorescence data followed by further evaluation of the FRET/cGMP signals using Microsoft Excel (Office365; Microsoft) and Origin 2023b (OriginLab).

The FRET traces for individual cells were extracted from the time-lapse images using Fiji. Therefore, regions of interest (ROIs)/ cells were marked based on the high resolution (1x1 binning) picture recorded at the beginning of the experiment. For the background correction an additional ROI in a cell-free region was defined. Since the FRET measurements were recorded with a 4x4 binning, a Python script was used to downscale the ROIs from the 1x1 binning image. Mean fluorescence intensities for CFP (F_{480}) and YFP (F_{535}) were then determined from the time-lapse images of each channel.

Subsequently, Microsoft Excel was used to calculate the normalized FRET/cGMP signals. First, mean fluorescence intensities of F_{480} and F_{535} are corrected for background signals of the respective channel. These values were used to calculate the F_{480}/ F_{535} ratio. Then, the F_{480} and F_{535} values as well as the F_{480}/ F_{535} ratio were normalized to the baseline (first 30 frames). This normalized ratio value represents the measured cGMP concentration (R ~ [cGMP]; shown as grey traces in the representative graphs). Note that in the present work the abbreviations "R ~ [cGMP]", "F_{480}" and "F_{535}" refers to the background corrected and normalized values.

Finally, the normalized ratio trace and single traces were evaluated in the Origin Pro software. Traces were examined regarding signal quality and anti-parallel development of the F_{480} and F_{535} individual signals. Subsequently, the ratio trace was subjected to smoothing using the Savitzky-Golay filtering method (smoothing windows size of 15-20 data points) to prepare it for further signal analysis. Additionally, baseline correction was applied to account for changes in the baseline, such as those caused by photobleaching. The Peak Analyzer tool in Origin Pro was employed to calculate the area under the curve (AUC) and peak height (relative R (cGMP) change) for each FRET/cGMP signal. Please note that the peaks were defined manually.

2.3.3 Real-time cell growth assay (xCELLigence)

xCELLigence Real-Time Cell Analysis system (Roche Diagnostics GmbH) is a non-invasive, label-free method for continuously monitoring cell growth. The system uses microtiter well plates embedded with gold microelectrodes on the bottom of each well (E-Plates®). The microelectrodes cover approximately 80% of the well bottom and enable measurement of the electron flow through the solution (**Figure 10**). The impedance (Z) of the electron flow is reported using a unitless parameter called cell index (CI). The CI is calculated by the impedance of the background subtracted from the impedance at individual time point n and normalized to the nominal impedance value ($CI = (Z_{tn} – Z_{t0}) / Z_{nom}$). The dynamic change of impedance caused by the cells can be correlated to processes such as cell adhesion, proliferation, or death. The xCELLigence system can be used for different applications, including drug testing [171].

Figure 10 provides an example of a real-time impedance trace of the growth of pVSMCs on xCELLigence microtiter well plates. pVSMCs started to adhere after 30-50 hours. This is followed by a gradual yet steady increase in CI, which may indicate the transition state to the cell proliferation phase (undefined mix phase). The VSMCs grow exponentially (proliferation) until they reach confluence. The CI value cannot further increase and plateaus. The plateau demonstrates that the microelectrodes surface area is fully covered [171]. Based on previous studies, the time point after 72 hours was used to analyze cell growth of VSMCs and NO-GC modulator effects [159]. Since in the present study, drugs were added to the cell suspension from the

beginning, this time point includes both the effects on adhesion and proliferation. Thus, we do not differentiate between the two phases and analyze the effects on cell growth.

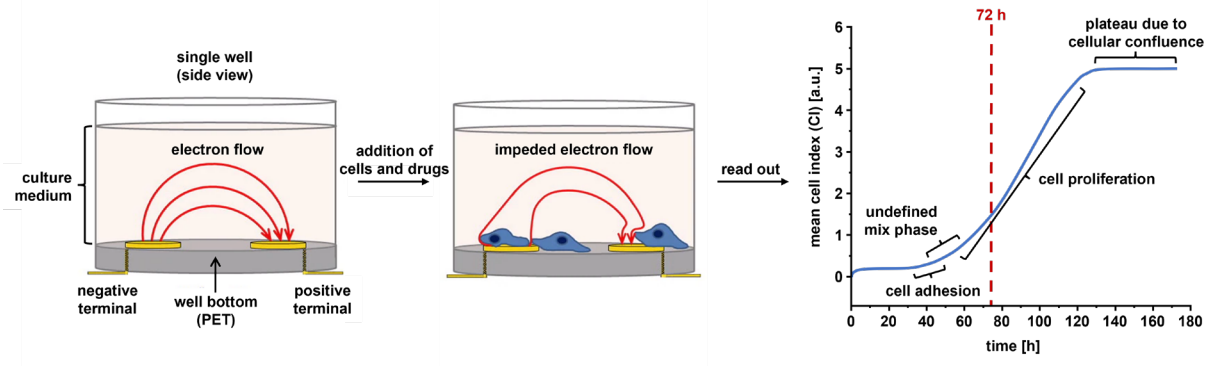

Figure 10. Schematic representation of the working principle of the xCELLLigence system for measuring cell growth.
The xCELLigence RTCA DP system is used to analyze cell growth in real time. The bottom of each well of microtiter plates (E-Plates®) is covered by gold microelectrodes, which enable the measurement of electron flow through the culture medium. Cell adhesion and proliferation lead to a measurable increase in impedance. The change in the impedance is reported using a unitless parameter called cell index (CI). The analysis at the 72-hour time point (72 h) includes the effects of cell adhesion, an undefined mix phase, and cell proliferation. Image adapted from www.agilent.com [171].

To analyze the cell growth via xCELLigence:

1. Isolate pVSMCs (as described in **Section 2.3.1**.) and adjust the cell number to seed $2*10^4$ cells / 100 µl.
2. Add 100 µL pre-warmed (37 °C) full medium to each well of the E-Plate.
3. Open the RTCA software and create the layout. At least 4 wells per condition should be prepared. Set an appropriate schedule for the experiment. In the present study the following two-step schedule was used:

   1st step. One sweep as a background measurement.

   2nd step. 700 sweeps with 15-minute intervals to follow cell growth over 7 days.
4. Insert the E-Plate into the RTCA DP analyzer and make sure it is properly aligned.
5. Begin 1st step to measure the background cell index of each well.
6. Remove the E-Plate and add 100 µL of the prepared cell suspension. If drugs should be used, add the desired drugs to the cell suspension before adding the cell suspension to the well.
7. Place the E-Plate back into the analyzer.
8. Start the experiment after 30 minutes of incubation (start 2nd step).

For more detailed information, read the RTCA DP Instrument Short Guide.

2.4 Analysis of protein expression

In the present study, western blotting was used to analyze the (phosphor-)protein expression of cultured VSMCs and tissue samples. The protein lysates were prepared, and their concentrations were determined with the Lowry assay. The proteins were then separated through

SDS-PAGE, blotted onto a polyvinylidene difluoride (PVDF) membrane, and immunologically detected to determine differences in protein expression and phosphorylation state between experimental groups.

2.4.1 Protein extraction from VSMCs

VSMCs were isolated from the aorta as described in **Section 2.3.1** and cultured until they reached a confluence of ≥ 80% in the cell culture dish. Prior to lysis, the cells were serum-starved (**Table 8**). The lysis buffer was supplemented with PMSF and cOmplete protease inhibitor cocktail to inhibit cellular proteases. If required, PhosStop was added to prevent the dephosphorylation of phosphoproteins by cellular phosphatases.

To extract protein from cells:

1. Isolate pVSMCs and let grow to ≥ 80 % confluency at 37°C and 6% CO2.
2. Wash the cells twice with PBS (RT).
3. Serum starve the cells for 24 h by incubating them in SRF.
4. Aspirate the SRF and add an appropriate volume of cell lysis buffer (approx. 100-150 µl for one well of a six-well plate). Use a cell scraper to detach and lyse the cells by scratching the culture dish. If a high protein concentration is required, transfer the lysis buffer to the next well and pool the wells to increase protein concentration.
5. Transfer the suspension to a 1.5 mL Eppendorf tube.
6. Denature the proteins for 10 min at 95 °C.
7. Centrifuge for 5 min at 18,000 rcf at 4 °C and transfer the supernatant into a new tube.
8. Store the samples at -20°C or proceed to protein quantification and SDS-PAGE.

2.4.2 Protein extraction from tissue

Tissues from experimental animals (aorta, heart, brain) were isolated following the procedure described in **Section 2.3.1 (steps 2-3)**. The tissues were carefully cleaned of any surrounding tissue, then quickly frozen in liquid nitrogen and stored at -20 °C. To extract the protein, the tissues were homogenized using the FastPrep-24 system (MP Biomedicals).

To extract protein from tissue:

1. Prepare one FastPrep 2 ml Lysing Matrix Tube per sample and add a spatula of Garnet Lysing Matrix A and one ceramic sphere (MP Biomedicals) to each tube.
2. Transfer tissues into the prepared Lysing Matrix Tubes.
3. Add an appropriate volume of tissue lysis buffer (200 µL/aorta or 7.5 µl/mg other tissues) into the Lysing Matrix Tube. The volume of tissue lysis buffer should not be less than 200 µL.

4. Place the tubes in the FastPrep device and run two cycles for 30 s at 6.5 M/s (speed). Centrifuge 1 min at 18,000 rcf at 4 °C and place tubes on ice between cycles.
5. Centrifuge samples for 1 min at 18,000 rcf at 4 °C and transfer the supernatant into a 1.5 mL Eppendorf tube.
6. Denature the proteins by heating the samples for 10 min at 95 °C.
7. Centrifuge samples for 5 min at 18,000 rcf at 4 °C and transfer the supernatant into a 1.5 mL Eppendorf tube.
8. Store the samples at -20°C or proceed to protein quantification and SDS-PAGE.

2.4.3 Quantification of protein concentration with Lowry assay

The quantification of protein concentration is an essential step in protein analysis, enabling the use of known protein concentrations as standards for accurate comparison of experimental samples. In this study, Peterson's modification of the Lowry method (Total protein Kit, micro lowry, Peterson's modification, Sigma-Aldrich) was used to quantify the protein concentration [172, 173]. The assay was performed in a 96-well plate format in duplicates. The protein concentration was measured by determining the absorbance at 660 nm and comparing the values with a calibration curve prepared using a BSA dilution series.

To quantify the protein concentration:

1. Add 100 µL of each concentration from the BSA dilution series (12.5 µg/mL, 25 µg/mL, 50 µg/mL, 100 µg/mL, 200 µg/mL BSA in H_2O) as duplicates into the wells of a 96-well plate. As reference use 100 µL H_2O.
2. Fill 95 µl into two wells and add 5 µl of the protein lysate to each. As reference use 5 µl lysis buffer filled up to 100 µL with H_2O. If a high protein concentration is expected, a pre-dilution of the protein lysate should be prepared.
3. Add 100 µL Lowry Reagent Solution, use a multi-channel pipette to mix the samples, and incubate for 20 min at RT.
4. Add 50 µL Folin-Ciocalteau use a multi-channel pipette to mix the samples and incubate for 30 min at RT in the dark.
5. Determine the absorbance at 660 nm with the multi-well plate reader (Multiskan EX, Thermo) and calculate the average of duplicates.
6. Prepare a calibration curve using the measured values of the BSA dilution series. Calculate the protein concentration of the samples based on the calibration curve.

2.4.4 SDS-PAGE and Western blot

SDS-PAGE followed by Western blot is a widely used method for the analysis of denatured proteins. It involves the separation of proteins based on their molecular weight and charge using SDS-PAGE and the subsequent detection of specific proteins

through Western blot using antibodies [174, 175]. This method provides a reliable and sensitive means of detecting specific proteins in complex samples and enables the visualization of even small differences in protein levels between samples. For the detection of the specific proteins, primary antibodies (**Table 3**) were used in combination with HRP-linked secondary antibodies (**Table 4**).

To analyze the protein expression by SDS-PAGE and Western blot:

1. Prepare the 1.5 mm, 10 % SDS gels with the desired comb (**Table 9**). In the present work, 15-pocket comb was used, which allowed to load up to 30 µl sample.

Table 9. Composition of 1.5 mm, 10 % SDS gel.
The given volumes are sufficient for two 1.5 mm, 10 % SDS gels using the mini-PROTEAN Tetra Cell System (Bio-Rad).

For two gels (1.5 mm)	Rotiphorese	4x Tris/SDS pH 6.8	4x Tris/SDS pH 8.8	H_2O	TEMED	APS
Separating gel (10 %)	3.30 mL	-	2.5 mL	3.05 mL	10 µL	25 µL
Stacking gel (4 %)	0.65 mL	1.25 mL	-	4.10 mL	10 µL	50 µL

2. Place the gels in the running chamber and fill up the inner and outer parts with 1x SDS running buffer. Remove combs and rinse pockets with running buffer.
3. Dilute the protein samples to a desired protein amount (10-15 µg/well) with 1 x SDS loading dye. Denature the protein lysate for 10 min at 95 °C and centrifuge for 1 min at 18,000 rcf at RT.
4. Load the samples into the pockets. Use 5 µL protein ladder (PageRuler™ Prestained Protein Ladder, 10-180 kDa, Thermo scientific) as a size reference.
5. Run the gel for 10 min with 100 V until the samples passed the stacking gel and then apply up to 150 V for approx. 1 h (Standard Power Pack P25, Biometra).
6. Assemble the “blotting sandwich” on the semi-dry western blot device (Trans-Blot® SD semi-dry transfer cell, Bio-Rad). Place the Whatman blotting papers in the respective buffers and arrange them as demonstrated below. Prior to using the PVDF membrane, activate it by immersing it in 100 % methanol for 1 min at RT and then wash with anode solution II.

   Setup of the “blotting sandwich”:

   - Cathode (top)
   - 8 Whatman papers soaked with cathode buffer
   - SDS gel
   - PVDF membrane (activated with 100 % methanol)
   - 4 Whatman papers soaked with anode buffer II
   - 4 Whatman papers soaked with anode buffer I
   + Anode (bottom)

7. Remove potential air bubbles by gently rolling a plastic pipette over the blotting sandwich.
8. Blot the membrane for 90 min with a current of 50 mA/gel.
9. Disassemble the blotting sandwich and block the membrane for 1 h with blocking solution (5% milk powder in TBS-T) at RT.
10. If needed, cut the membrane approx. at the height corresponding to the protein of interest. Use the protein ladder as orientation.
11. Wash the membrane 2x 5 min with TBS-T before immunostaining.
12. Incubate the membrane in the primary Ab solution overnight at 4°C in a 50 mL falcon on a rolling shaker.
13. Wash the membrane 3x 5 min with TBS-T/milk (1% milk powder in TBS-T) at RT.
14. Incubate the membrane with the HRP-coupled secondary antibody (secondary antibody in TBS-T/milk) for 1 hour at RT.
15. Wash the membrane 3x 5 min with TBS-T at RT.
16. Develop the western blot by the addition of ECL substrate (mix 1:1 solution A and solution B of WesternBright Sirius ECL substrate (Biozym)) and use the ChemiDoc imaging system to detect the chemiluminescence.
17. To assign the protein size, visualize and document the protein ladder with a colorimetric image.
18. In case of studying proteins with similar size, either prepare two Western blots in parallel or reuse the membrane. To reuse the membrane, soak it in TBS-T for 1 h and then repeat the steps from step 9.

2.4.5 NO/cGMP stimulation and VASP phosphorylation assay

The NO/cGMP signaling pathway-specific effects of the NO-GC modulators were analyzed on effector protein level by examining the phosphorylation status of VASP. VASP is a well-known target of both cGKI and cAMP-dependent kinase (cAK), and it can be phosphorylated at multiple sites, including Ser157, Ser239, and Thr278 [176]. In the present study, SDS-PAGE followed by Western blot was performed to analyze the VASP phosphorylation status in pVSMCs and isolated aorta (**Section 2.4.4**). It is important to note that the phosphorylation status of VASP affects its migration in SDS-PAGE, with unphosphorylated VASP migrating at 46 kDa, while VASP phosphorylated by cGKI or cAK at Ser157 migrates at 50 kDa [177]. Since cGKI has a higher preference for phosphorylating VASP at Ser239, a phospho-VASP (Ser239)-specific antibody (**Table 3**) was used to measure cGKI-specific activation and signaling [178].

VASP phosphorylation assay in isolated VSMCs:

1. Isolate pVSMCs according to the protocol in **Section 2.3.1 (steps 2-3)**. Seed $2*10^5$ cells/well in a 6-well plate and let grow till 80 % confluency (**Table 8**).

2. Wash the cells twice with PBS (RT).
3. Serum starve the cells for 48 h by incubating them in SRF.
4. Aspirate the serum-free medium and add the stimulation medium (SRF containing PhosStop ± desired drugs).
5. Incubate the cells for 30 min at 37°C and 6% CO2.
6. Wash the cells twice with ice-cold PBS.
7. Prepare protein lysates (Cell lysis buffer containing PhosStop) (**Section 2.4.1**).
8. Analyze the VASP phosphorylation by SDS-PAGE and Western blot.

VASP phosphorylation assay in isolated aorta:

1. Isolate the aorta and clean it properly from surrounding tissue in PBS (**Section 2.3.1; steps 2-3**). Each aorta should stay 30 min in PBS.
2. Cut the aorta into approx. 2-3 mm pieces.
3. Incubate the aorta for 30 min in stimulation medium (SRF containing PhosStop ± desired drugs) at 37°C on a shaker.
4. To stop the stimulation centrifuge for 3 min at 200 rcf at 4 °C.
5. Aspirate the stimulation medium and wash the aorta once with ice-cold PBS and vortex shortly.
6. Centrifuge for 3 min at 200 rcf at 4 °C.
7. Aspirate the supernatant and snap freeze the aorta in liquid nitrogen.
8. Prepare protein lysates (Tissue lysis buffer + PhosStop) (**Section 2.4.2**).
9. Analyze the VASP phosphorylation by SDS-PAGE and Western blot.

2.5 Analysis of atherosclerosis

2.5.1 Experimental setup

Different experimental setups were chosen based on the study objectives. One setup was utilized to investigate and compare the effects and therapeutical potential of different NO-GC modulating drugs (BAY Activator and Vericiguat) on atherosclerosis in mice (**Figure 11**). The second experimental setup was designed to analyze and characterize the SMC-specific NO-GC knockout on atherogenesis (**Figure 12**). Furthermore, this experimental setup was used to assess the suitability of the αSMA-specific NO-GC knockout mouse model for validating the specificity of the NO-GC modulators. Since atherosclerosis does not naturally occur in mice, mice with an $ApoE^{ko}$ background were used in all experiments. $ApoE^{ko}$ mice are a common choice for atherosclerosis research because they spontaneously develop hypercholesterolemia due to genetically impaired lipid metabolism. This condition leads to the formation of atherosclerotic lesions, which can be accelerated when combined with an atherogenic diet (high-

fat diet, HFD) [13]. For further details about the ApoE^{ko} mouse model of atherosclerosis, please see **Section 1.1.2**.

To investigate and compare the effects of different NO-GC modulating drugs (BAY Activator and Vericiguat), the drugs were mixed with a concentration of 150 ppm into the HFD and fed to ~10 weeks old mice for 16 weeks (BAY Activator) or 18 weeks (Vericiguat). Assuming an average daily food intake of 5 g and an average body weight of 30 g per mouse, this corresponded to a daily dose of 25 mg/kg [179]. The experimental groups were formed litter and body weight matching and were randomly assigned to male and female control or treatment groups (**Supplementary table 1**). As NO-GC modulators have an antihypertensive effect and blood pressure may has an impact on atherosclerotic outcome, blood pressure was studied using a tail-cuff blood pressure system (**Section 2.5.2**) [80, 81, 136, 180-182]. Blood pressure was measured in BAY Activator-treated and matched control mice on four consecutive days before the initiation of the high-fat diet (HFD) and then regularly throughout the 16-week study period. During the final phase, blood pressure measurements were performed in all experimental groups (BAY Activator and Vericiguat) over three consecutive days. Additionally, blood samples and other physiological parameters of the experimental mice were analyzed to get an overview of systemic drug effects and to exclude indirect effects on atherosclerosis. The food intake was monitored by measuring the weight gain (body weight start and end of HFD) and plasma lipid levels (final blood sampling). The drug plasma concentration was determined to ensure the successful absorption of the drugs in a sufficient concentration. The unbound fraction was of particular interest, as it indicates the free, pharmacologically active drug concentration in the blood [183]. The overall health of the experimental mice was assessed by measuring complete blood counts and determining organ weights (liver, spleen, kidneys, and heart). In another project, the livers of the experimental mice were further investigated to assess the therapeutic potential of NO-GC modulators in non-alcoholic steatohepatitis (NASH) (unpublished data; Rajeeth, K., Roessing M., et al.). To analyze the effects of the drugs on atherosclerotic lesion areas, the aortas were examined using Oil Red O staining (**Section 2.5.5**). To obtain a general overview of potential changes in plaque composition, the protein expression levels in atherosclerotic aorta lysates were analyzed using Western blot (**Section 2.4.4**). For a more specific insight into plaque composition at the cellular level, cell-specific marker proteins and tissue components were identified in tissue sections from various regions of the aorta (aortic root and arch) using in-situ staining techniques, including chromogenic (**Section 2.5.6.1**), picrosirius red (**Section 2.5.6.2**) and immunofluorescence (**Section 2.5.6.3**) staining. Please note that, for the examination of the aortic arch via immunofluorescence staining, the aortas that had already been stained and analyzed with Oil Red O were used.

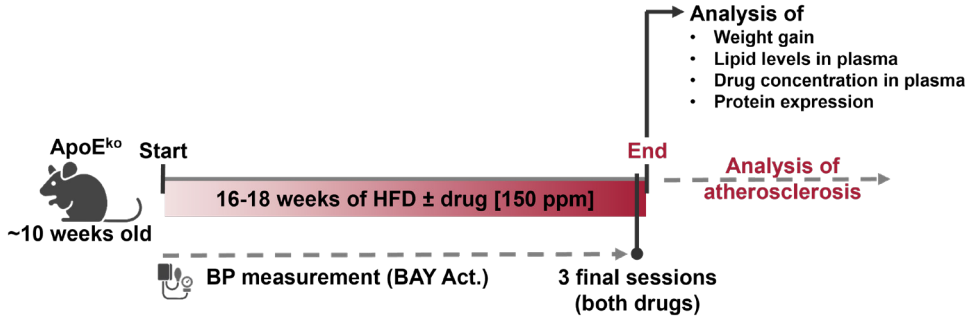

Figure 11. Experimental setup to analyze the effects of NO-GC modulators on atherosclerosis.
Graphical outline of the experimental setup for analyzing the effects of BAY Activator and Vericiguat on atherosclerosis. To induce atherosclerosis, ApoE knockout (ApoE^{ko}) mice were fed a high-fat diet (HFD) for 16 weeks (BAY Activator) or 18 weeks (Vericiguat). The drugs were supplemented at a concentration of 150 ppm into the HFD. Food intake was monitored by tracking weight gain and measuring plasma lipid levels. Blood pressure was regularly monitored (BP measurement) in BAY Activator-treated mice and their matched controls throughout the 16-week study period. During the final phase, blood pressure measurements were conducted in all experimental groups (both drugs: BAY Activator and Vericiguat) over three consecutive days. Subsequently, mice were euthanized, and the aorta, along with other organs and blood, was isolated for further analysis. For instance, the drug plasma concentration was determined to ensure the successful absorption of the drugs. For more details see the text. Image created using BioRender.com.

To analyze the impact of SMC-specific ablation of NO-GC on atherogenesis, the Cre/loxP-system was used to generate a temporally and spatially controlled NO-GC knockout (NO-GC^{smko}). For this purpose, ApoE^{ko} mice expressing the inducible CreER^{T2} recombinase under the control of the αSMA promoter were crossbred with ApoE^{ko} mice carrying a NO-GC β1-subunit gene, in which exon 10 flanked by two loxP-sites (**Section 2.2.3**). The resulting genotypes in subsequent generations of littermates allowed for Cre-mediated inducible ablation of the NO-GC β1 subunit in VSMCs following tamoxifen treatment. Tamoxifen injections (5 x 1 mg/mouse/day) were administered intraperitoneally to all groups of mice at 8 and 10 weeks of age to induce the knockout. Specifically, the experimental animals received two cycles of tamoxifen injection for five consecutive days, with a break of nine days in between. Subsequently, the mice were divided into three different groups based on their genotype and litter (**Supplementary table 1**):

1. **NO-GC^{smko}** (SMC-specific NO-GC knockout)
2. **Ctrl** (heterozygous NO-GC knockout)
3. **Cre-Ctrl** (Cre control)

At 12 weeks of age, the standard diet was replaced with an atherogenic diet for 18 weeks. Verification of the SMC-specific ablation of NO-GC was conducted through Western blot analysis. The efficiency of SMA-CreER^{T2}-mediated recombination in the aorta was validated using IF-staining. Given the well-known role of the NO/cGMP signaling pathway in vessel relaxation and blood pressure regulation, blood pressure was monitored to account for alterations resulting from VSMC-specific NO-GC ablation (NO-GC^{smko} mice compared to control mice). Consequently, blood pressure measurements were performed using the tail-cuff blood pressure system during the final phase over three consecutive days. The same physiological parameters

were studied, and identical experiments were conducted as previously described. Lastly, we evaluated the impact of SMC-specific NO-GC ablation on plaque atherosclerotic lesion area through oil red O staining.

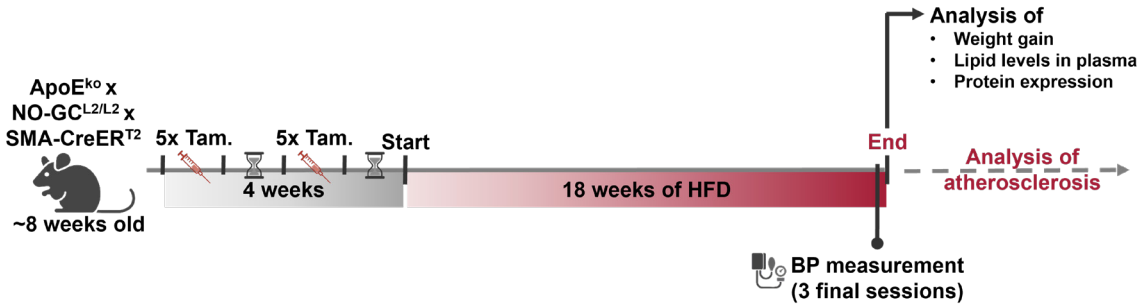

Figure 12. Experimental setup to analyze the effects of the SMC-specific NO-GC knockout on atherogenesis. Graphical outline of the experimental setup for characterizing smooth muscle cell (SMC)-specific NO-GC knockout (NO-GC^{smko}) in an ApoE knockout (ApoE^{ko}) mouse model of atherosclerosis. To generate the NO-GC^{smko} mice, mice expressing the inducible Cre-ER^{T2} recombinase under the control of the αSMA promoter were crossed with mice carrying a floxed NO-GC β1-subunit gene (NO-GCsmko: ApoE^{ko} x NO-GC$^{L2/L2}$ x SMA-CreER^{T2}). Mice were divided into NO-GC^{smko} and control groups based on their genotype and litter matching. Intraperitoneal tamoxifen injections occurred in two cycles, each for five consecutive days (5 x 1 mg/mouse/day) at 8 and 10 weeks of age, with a nine-day break in between cycles and before switching to a high-fat diet (HFD). Mice were fed the HFD for 18 weeks, and food intake was monitored by tracking weight gain and measuring plasma lipid levels. Blood pressure was measured (BP measurement) during the final phase over three consecutive days. Subsequently, mice were euthanized, and the aorta, along with other organs and blood, was isolated for further analysis. For more details see the text. Image created using BioRender.com.

2.5.2 Non-invasive blood pressure measurement

The CODA® tail-cuff system from Kent Scientific is a high-throughput, non-invasive method for measuring blood pressure in up to four mice simultaneously. This system uses volume pressure recording (VPR) sensor technology to measure blood pressure in the tail of the mouse. The validity of this technology has been confirmed through comparison to the gold standard method, radiotelemetry [184]. The tail-cuff system utilizes two cuffs: an occlusion cuff (O-cuff) and a volume pressure recording cuff (VPR-cuff) (**Figure 13., A**). The inflation of the O-cuff occludes the blood flow in the tail. During the slow deflation of the O-cuff, the VPR-cuff measures the physiological characteristics of the returning blood. Arterial pulsations from the blood flow cause tail swelling, which is measured by the VPR-cuff to determine the systolic blood pressure. The diastolic blood pressure is automatically measured when the rate of swelling in the tail stops increasing [185]. In addition to blood pressure, the CODA system can record other parameters including heart rate, tail blood volume, and tail blood flow (**Figure 13, B**).

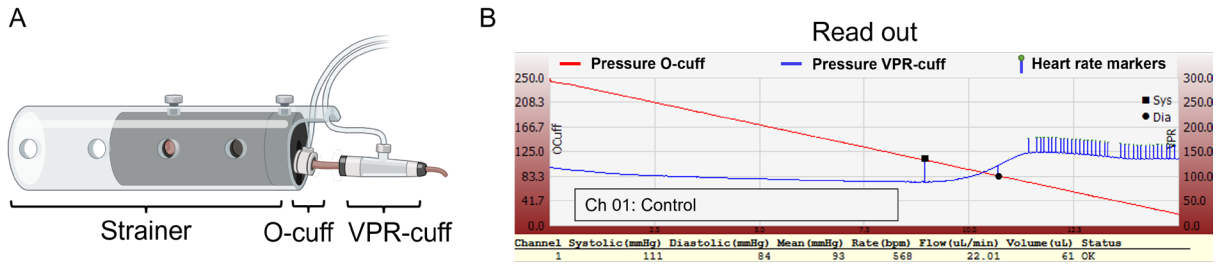

Figure 13. Schematic representation of the working principle of CODA non-invasive blood pressure system. **(A)** The tail-cuff system consists of an animal holder (strainer), an occlusion cuff (O-cuff), and a volume pressure recording cuff (VPR-cuff), which allows to measure the blood pressure in the tail. **(B)** Representation of the read-out of a blood pressure measurement. The CODA system measures six parameters: systolic blood pressure (mmHg), diastolic blood pressure (mmHg), heart rate (bpm), tail blood flow (µL/min), and tail blood volume (µL). Image created using BioRender.com.

Given the diurnal variability in blood pressure, it is essential to schedule repeated measurements at consistent times of the day. Training sessions are necessary to acclimate mice to the CODA tail-cuff system, thereby enhancing the accuracy and reliability of the measurements. We recommend conducting three to four training sessions in the days preceding the experiment. Prior to initiating a new experiment, the bladders of all required cuffs should be replaced to ensure comparable experimental conditions across all channels throughout the study. In the experimental design, it should be noted that depending on the respective channel, there may be a different influence of the hardware on the measured values. Therefore, mice of each experimental group should be measured in pairs in the same channel to equally weight the hardware influence in the groups (**Table 10**).

Table 10. Example of an experimental design to measure blood pressure in mice.
Experimental setup to prevent unequal influence of hardware on the measured blood pressure values. Mice of each experimental group (Ctrl. and Exp.) should be measured in pairs in the same channel after each other (Session 1 and 2). Ctrl., Control; Exp., Experimental

Session	Channel 1	Channel 2	Channel 3	Channel 4
1	Ctrl. Mouse 1	Ctrl. mouse 2	Exp. Mouse 3	Exp. Mouse 4
2	Exp. Mouse 1	Exp. mouse 2	Ctrl. mouse 3	Ctrl. Mouse 4

To measure the blood pressure of mice:

1. Turn on and start the warming platform. Set it to level 5.
2. Pre-warm the empty animal holder by placing it on the warming platform.
3. Open the CODA Software and select “use all displayed devices”.
4. Use the “user and animal manager” to add the user and mice to the database.
5. Create a new experiment and assign the user and animals, which will also serve as a template for future sessions.
6. Start a new session and configurate the settings (Acclimation cycles: 5, Cycles per set: 15, others: default settings).

7. Restrain the mice by placing them gently in the animal holders. Ensure the nose is protruding through the hole in the nose cone during straining. The mouse tail extends through the rear hatch of the holder. Adjust the holder as necessary to secure comfortably, but limited movement.
8. Place the mice on the warming platform and cover the tails with the fleece blanket.
9. Use the provided non-contact infrared thermometer to measure the temperature at the base of the tail, which should be above 35°C before starting the experiment. It takes 3-5 min to reach the proper temperature.
10. Position the cuffs on the animal's tail, starting with the O-cuff near the base and sliding the VPR-cuff up the tail with the larger diameter end first, leaving a small gap between the cuffs. Fix the tubing of the cuffs to the animal holder. Cover the tails and cuffs with the fleece blanket.
11. Wait for 2 min for the animals to calm down and their blood pressure to normalize.
12. Start the measurement.
13. After each session, release the mice first and then clean the strainers and warming platform with soap and water.
14. Check the values of each cycle to ensure the software has set the systolic and diastolic values correctly and exclude any incorrect cycles from the session.

For more detailed information, read the CODA Non-Invasive Bood Pressure System manual for high throughput.

2.5.3 Preparation of atherosclerotic mice

1. Weigh all mice before starting the HFD feeding period, and periodically throughout the experiment if necessary. At the end of the experiment, record the mice's weight to determine weight gain throughout the study.
2. Anesthetize the mouse with 5% isoflurane in O_2, using the anesthesia unit-Research (Eickenmeyer). Place the mouse in the anesthesia chamber and remove it as soon as the anesthesia takes effect. Control the anesthesia status by checking the toe pinch reflex. Decapitate the mouse and collect the desired amount of blood in the designated tube and follow the protocol outlined in **Section 9.**
3. Cut off a piece of the ear and follow the instructions in **Section 2.2.4** to determine the genotype of the mouse.
4. To isolate the desired organs, follow the instructions in **Section 2.3.1** (**steps 2-3**). Weigh the organs including the liver, kidney, spleen, and heart. Clean the aorta superficially until all larger pieces of tissue are removed. This saves time before tissue fixation or protein extraction. Fine cleaning is done after fixation. During the cleaning procedure, avoid grabbing the vessels directly as it may damage the vessel wall. To minimize the

risk of such damage, it is recommended to grab the surrounding tissue or the heart instead.

5. Fix the aorta and heart for 20 min at RT in fixation solution (4 % PFA in PBS) to proceed with analysis of the lesion area. If the organs were isolated for protein analysis by Western blot, snap-freeze them in liquid nitrogen and follow the instructions in **Section 2.4**.
6. After fixation, wash the aorta and heart 2x with PBS for 10 min.
7. Repeat the steps 2-6 until all mice are processed.
8. Continue cleaning the aorta carefully from all remaining tissue. Cut the heart through a cross-section into two halves (heart tip and base).
9. Before further processing, store the aorta and heart in a 12-well plate in PBS at 4 °C. Seal the well plate with parafilm. Subsequently, the aorta was stained with Oil Red O (**Section 2.5.5**) and embedded in Tissue Tek O.C.T. for Immunofluorescence (IF) staining (**Section 2.5.6.4**). The heart was embedded in paraffin (Surgipath Paraplast X-tra, Leica) for CIH (**Section 2.5.6.1**) and PSR-staining (**Section 2.5.6.2)**.

2.5.4 Plasma sample analysis

The blood plasma of experimental mice was analyzed to gain insight into their physiological condition and to eliminate any extraneous factors that might affect the experimental outcomes, such as inadequate elevation of plasma lipid levels and/or drug absorption. Blood samples of all mice were obtained by final blood collection at the end of the HFD feeding period in the morning. To achieve an optimal determination of the blood drug concentration, the mice were not starved before sampling.

Determination of lipid levels:

1. Collect 500 µL – 1 mL blood in 1.3 mL Lithium-Heparin microtubes (Sarstedt) and gently invert the tube twice.
2. Store the blood sample at 4 °C until all mice are processed.
3. Centrifuge for 10 min at 2000 rcf at 4 °C.
4. Transfer the supernatant to a 1.5 mL tube and store the plasma sample at - 80 °C.

Determination of drug concentration:

1. Collect 500 µL – 1 mL blood in 1.3 ml EDTA microtubes (Sarstedt) and gently invert the tube twice.
2. Store the blood sample at 4 °C until all mice are processed.
3. Centrifuge for 10 min at 2000 rcf at 4 °C.
4. Transfer the supernatant to a 1.5 mL tube and store the plasma sample at - 80 °C.

Determination of complete blood count

1. Collect two drops of blood in a 1.5 mL tube containing 40 µL ACD buffer and gently invert the tube.
2. Store the blood sample at RT until all mice are processed.
3. Measure the samples with the automatic hematology analyzer (Sysmex KX-21N).

Prof. Dr. med. A. Peter (University Hospital Tubingen) and Prof. Dr. P. Sandner (BAYER AG) kindly analyzed multiple lipid parameters in plasma (**Table 11**, **Table 12**). The drug plasma concentration was kindly analyzed by Dr U. Hofmann (Dr. Margarete Fischer-Bosch Institute of Clinical Pharmacology (IKP)) and Prof. Dr. P. Sandner (BAYER AG) (**Supplementary table 2**). The complete blood count was measured in collaboration with the Department of Cardiology and Angiology of the University Hospital Tubingen (**Supplementary table 3**).

2.5.5 Oil Red O staining of atherosclerotic lesion area

Oil Red O staining is a well-established technique for quantifying lesion areas in atherosclerotic aortas. In this study, we used Oil Red O staining to analyze the effects of NO-GC modulators and NO-GC^{smko} on the atherosclerotic lesion area. When atherosclerotic aortas are incubated with Oil Red O, the dye selectively accumulates in atherosclerotic plaques due to its ability to stain neutral fats and cholesteryl esters [186]. In contrast, healthy tissue is only slightly stained, as it mainly contains phospholipids. This differential staining produces a strong contrast that allows easy visual distinction between the plaque areas and the healthy tissue.

1. Isolate and fix the aorta as described in **Section 2.5.3**.
2. Transfer the aorta in 78% methanol and incubate for 5 min at RT on a shaker.
3. Incubate the aorta for 90 min at RT in Oil Red O staining solution on a shaker.
4. Transfer the aorta back into 78% methanol and incubate for ~10 min at RT. Since this step destains the aorta to improve contrast, it is important to control the progress regularly. Finish the step early if there is sufficient destaining or extend it if necessary.
5. Put the aorta back into PBS and continue with the cleaning process. Carefully remove all the remaining surrounding tissue and Oil Red O drip. Store the aorta in PBS at 4°C until documentation and further embedding in tissue-tek for immunofluorescence staining (**Section 2.5.6.4**).

To document the atherosclerotic plaques, the Oil Red O stained aorta was placed in a 10 cm petri dish filled with PBS and a Polydimethylsiloxane (Sylgard® 184, Downcorning) bottom. The aorta was covered with a glass slide and evenly weighted down with two 10 g lead weights. Illumination was provided by an integrated LED ring light and vertical LED spots set to full luminosity. The aortas were photographed from both sides using a Canon EOS 750D digital

camera mounted with a 1.6x lens on a stereomicroscope (Stemi 508, ZEISS) (0.63x magnification). To ensure consistency, all aortas were documented with the same camera settings.

ImageJ was used to quantify the area of atherosclerotic plaques. Quantification was performed by an investigator who was blinded to the experimental groups. The aorta and all lesion areas were encircled using the freehand polygon selection tool. The lesion area was separately quantified for the full aorta, aortic arch, and thoracoabdominal aorta. Therefore, the aortic arch was defined as follows: 1 mm in front of the brachiocephalic artery, 1 mm behind the left subclavian artery, including the brachiocephalic artery and left subclavian artery up to their branching point, and 1 mm in length of the left common carotid artery. Based on this, the area for the full aorta and thoracoabdominal aorta was also defined. The relative plaque area was determined by normalizing the lesion area to the total area of the respective part. The front and back sites were averaged for calculation. Statistical analysis was performed with Origin Pro software.

2.5.6 Analysis of atherosclerotic plaque composition

The identification of cell-specific marker proteins (e.g., αSMA and Mac-2) can provide valuable information about the cellular composition of atherosclerotic plaques. IF- and CIH-staining are commonly used methods for in situ analysis of protein expression in tissue sections. Additionally, tissue components such as collagen can be visualized using further staining methods like PSR-staining, enabling the assessment of plaque stability. Since the plaque composition can vary in different regions of the aorta, in this study, we examined tissue sections from both the aortic root and the aortic arch [6]. The plaque composition of the aortic root was assessed using CIH- and PSR-staining in paraffin-embedded serial sections. The use of the aortic root offers the advantage of investigating identical regions within and between experimental groups due to its orientation toward the characteristic structures of the aortic root [187]. In contrast, plaque composition in the aortic arch was examined using IF-staining of frozen sections. This approach was used because it allowed for the examination of the same aortas previously stained with Oil Red O without the need for prior de-staining. Furthermore, by combining different methods, we can overcome some of the limitations of each method, leading to more accurate and reliable results. The primary antibodies used in this study are listed in **Table 3** and the secondary antibodies in **Table 4**.

2.5.6.1 Chromogenic immunohistochemistry of paraffin section

Chromogenic immunohistochemistry is a technique used for detecting and visualizing proteins in tissues through the enzymatic conversion of a substrate into a visible-colored product. CIH involves the use of primary antibodies that recognize the specific protein of interest, a secondary antibody, and a reporter enzyme such as horseradish peroxidase (HRP). In this study, the avidin-biotin-complex method (ABC method) was employed using HRP as the reporter enzyme

and 3,3'-diaminobenzidine (DAB) as the chromogen. The enzymatic reaction catalyzed by HRP leads to the conversion of DAB into a brown-colored product that can be observed under a standard light microscope [188]. CIH is highly sensitive due to the signal-amplifying properties of the ABC complex, making it ideal for detecting low-abundance proteins in tissues, particularly in archival paraffin-embedded tissues [189]. However, CIH can be affected by non-specific binding of antibodies, limited color options, and difficulty in distinguishing closely localized antigens. In this study, aortic roots were stained by CIH to analyze potential differences in plaque compositions caused by treatment with BAY Activator. The hearts were previously isolated and fixed as described in **Section 2.5.3**. Subsequently, they were dehydrated, embedded in paraffin, cut into 10-µm serial sections, and stained as described below:

Dehydration and paraffin embedding

1. Dehydrate hearts by an increasing ethanol concentration row in a 12-well plate at RT:
    a. 60% EtOH/H_2O for 1 h
    b. 70% EtOH/H_2O for 1 h
    c. 80% EtOH/H_2O for 1 h
    d. 90% EtOH/H_2O for 1 h
    e. 2x 100% EtOH/H_2O for 20 min
2. Transfer the heart to a 2 mL Eppi containing 100 % toluene for 2 min.
3. Place the heart into tissue cassettes and immerse it in molten paraffin (Surgipath Paraplast X-tra, Leica) at 57°C overnight. Repeat this step twice with fresh paraffin solutions.
4. Cut the heart transversely into two parts: the basal and apical halves, positioning the cut just below the auricle.
5. Embed both heart halves in clean liquid paraffin using an embedding system comprising a metal mold and a plastic embedding ring. Embed the basal half so that the cut edge faces the bottom of the metal mold. For preservation purposes, simply embed the apical part on the side of the paraffin block. Allow the paraffin to solidify overnight at -20°C.
6. Store the paraffin-embedded tissue at RT until further processing.

Sectioning

To prepare serial cross-sections of the aortic root, we used the protocol described by Centa et al. (2019) [187] with minor adjustments.

1. Prepare cross-sections of the aortic root using the microtome (HistoCore Biocut, Leica). Caution: Begin collecting all sections from the point at which one of the three aortic valve leaflets becomes visible in the section.

2. If necessary, adjust the cutting angle to ensure that all three aortic leaflets are visible simultaneously in the section.
3. Starting from this point, prepare 10 µm serial cross-sections until the entire aortic root has been sectioned. Document any lost sections to facilitate later reconstruction of the distances between them.
4. Transfer the sections to a preheated water bath (42 °C) and allow them to stretch.
5. Mount the serial sections on a series of 10 poly-D-lysine-coated object slides (Thermo Scientific). Arrange the sections as shown in **Figure 14** to enable staining for different cell-specific marker proteins in consecutive sections from various regions of the aortic root.
6. Allow the sections to dry completely overnight and store them at RT until further processing.

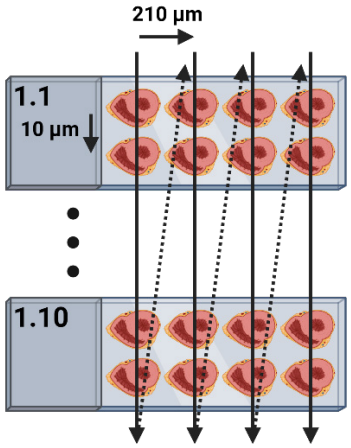

Figure 14. Order of paraffin serial sections on object slides.
Serial 10 µm-thick paraffin sections of the aortic root were prepared using a microtome. These sections were arranged on object slides to form a series organized in columns. The series starts with "1.1" and ends with "1.10." Arrows indicate the distance between sections on each slide, with each column containing 20 sections and each series consisting of 10 slides. Image created using BioRender.com.

Staining

1. For the staining of different marker proteins in serial sections and similar regions of the aortic root, first select the corresponding slides from the series.
2. Incubate the object slices right before use overnight at 37 °C to prevent the tissue sections from detaching.
3. Deparaffinize sections by immersing them twice with 100 % toluene for 2 min at RT.
4. Rehydrate the sections with decreasing ethanol concentration at RT:
    a. 2x EtOH 100% for 2 min
    b. 1x EtOH 90% for 2 min
    c. 1x EtOH 80% for 2 min
    d. 1x EtOH 70% for 2 min
    e. 1x EtOH 60% for 2 min

5. Immerse the slides in PBS for 5 min at RT.
6. Block endogenous peroxidase activity using peroxidase blocking solution. Place the slides in a humidified chamber at RT for 20 min to prevent drying out.
7. Wash the slides with PBS for 3 min at RT.
8. Incubate the slides with antigen retrieval solution for 15 min at RT. Place the slides into a water bath and boil them for 10 min at 92 °C to unmask the antigens.
9. Allow the slides to cool down before washing them with TBS-T for 5 min at RT.
10. To block unspecific antibody binding sites, incubate the sections with the CIH blocking solution for 2 h at RT in a humidified chamber. Remove CIH blocking solution and create a hydrophobic barrier around the sections using a Super Pap Pen Liquid Blocker (BIOZOL).
11. Incubate the sections with the primary antibody (diluted in Ab solution) overnight at 4°C in a humidified chamber.
12. Wash the slides with TBS-T three times for 5 min each at RT.
13. Incubate the sections with the secondary antibody (diluted in Ab solution) for 2 h in a humidified chamber at RT.
14. Remove the secondary antibody solution and wash sections with TBS-T three times for 10 min each at RT to remove nonspecifically bound antibodies.
15. In the meantime, prepare the ABC solution (Vectastain Elite ABC Kit Peroxidase, vector Labs) and incubate the sections in a humidified chamber for 30 min at RT in the dark.
16. Wash the slides with TBS-T three times for 5 min each at RT.
17. Incubate sections with DAB staining solution at RT until a brownish color develops. Check the color development under a microscope. Stop staining by immersing the slides in H_2O when the specific staining has the desired intensity in relation to the background.
18. Mount sections with several drops of Aquatex mounting medium (Merck) and cover them with a coverslip of an appropriate size.
19. Allow the mounting medium to solidify overnight before sealing the edges of the coverslip with clear nail polish.

Brightfield images of CIH-staining were captured using a digital camera (Canon EOS 750D) equipped with a 1.6x lens mounted on an upright epifluorescence microscope (Axioskop 20, ZEISS). The microscope was equipped with an A-Plan 5x/0.12 objective and an A-Plan 10x/0.5 objective (ZEISS) and used a tungsten halogen lamp with a condenser as the light source for brightfield imaging. EOS Utility software was employed to control the camera and set exposure times. The objectives were adjusted to meet the requirements of the specific staining processes. Before starting the documentation, the microscope was configured according to

Kohler's illumination settings. The ISO setting was set to "automatic". White balance and focus were adjusted for each section.

2.5.6.2 Picrosirius red staining of paraffin section

VSMCs are the primary source of collagen within the atherosclerotic plaque. The increased presence of collagen in atherosclerotic plaques is in turn strongly associated with enhanced plaque stability [34, 190]. A common method for detecting and visualizing collagen in tissues is PSR-staining. PSR is a linear anionic dye with six sulfonate groups that bind to cationic collagen fibers [191, 192]. This results in pronounced red staining of collagen structures in tissue sections, greatly facilitating the differentiation between collagen-rich plaques and the vessel wall in brightfield microscopy. When documented under polarized light, even different collagen fiber types can be specifically visualized. This is based on the fact that PSR enhances the natural birefringent properties of collagen upon binding, causing collagen Type I (thick) fibers to appear red-orange, while collagen Type III (thin) fibers appear green under polarized light. This allows for easy differentiation of collagen fibers from the background during quantification [191, 192]. To evaluate the effect of the BAY Activator on collagen content and its impact on plaque stability, 10 µm sections of the aortic root were stained with PSR. The procedure was the same as described for the CIH-staining protocol (**Section 2.5.6.1**). Deviating from protocol, the aortic root sections were subsequently stained with PSR as follows:

Staining

1. Deparaffinize and rehydrate the paraffin sections following the instructions in **Section 2.5.6.1**.
2. Wash the sections with H_2O.
3. Immerse the object slides with sections in the Sirius red staining solution and incubate them in the dark for 1 h.
4. Wash the sections twice with acidified water for 5 min each time at R. Then, immerse the sections in 100% ethanol for 3 minutes. Before mounting cover sections with 100 % toluene.
5. Mount the sections using a 1:1 dilution of 100 % toluene and DPX mounting medium. Use a coverslip of an appropriate size to fully cover the sections, taking care to avoid trapping air bubbles. If air bubbles do occur, gently move them to the edge of the coverslip.
6. Allow the mounting medium to solidify overnight, and capture images no later than five days after staining.

For documentation, the setup described in **Section 2.5.6.1** was used. Additionally, a filter system consisting of two polarizing filters was installed to capture PSR-staining under polarized

light. The first filter was positioned between the objective and the camera, while the second filter was placed between the light source and the specimen. Both filters were oriented at a 90° angle to each other, creating the darkest possible background and allowing only the light whose plane of polarization was altered by the PSR-stained collagen fibers to pass.

2.5.6.3 Assessment of plaque composition (Image analysis)

In this study, the plaque composition was assessed with respect to the expression of marker proteins αSMA and MAC2 and the collagen content. For this purpose, serial sections of the aortic roots from BAY Activator-treated and control mice were stained using CIH and PSR. To ensure comparability within and between experimental groups, serial sections from identical regions within the aortic root were selected, with the characteristic structure of the aortic root serving as a reference. The acquired images of CIH (brightfield) and PSR (brightfield and under polarized light) staining were analyzed using the image analysis software Fiji (ImageJ). The vessel (external vessel wall), individual atherosclerotic lesions, and the vessel lumen (internal vessel wall without lesions) were marked using the freehand polygon selection tool. As the border between plaque and vessel wall, the first elastic lamina below the plaque that was not disrupted was chosen. Due to the pronounced red staining of collagen structures in tissue sections by PSR binding, which facilitated the distinction between the individual compartments (e.g.: myocardium, aortic leaflets, vessel wall, and plaques) in brightfield microscopy, the brightfield images of the PSR-staining were used for quantifying the total vessel area. The atherosclerotic lesion areas were determined separately for each staining.

For the quantification of positively stained areas within the lesion areas, the protocol described in the doctoral thesis by M. Lehners (2022) [99] was used. Quantification was performed by an investigator who was blinded to the experimental groups. The parameters used for semi-automatic quantification were defined based on all images of the respective staining and applied consistently to all stainings. Deviating from the descriptive protocol, images taken under polarized light were used for quantifying the collagen content in the plaque. Due to the altered natural birefringent properties caused by PSR binding to collagen fibers, collagen Type I (thick) fibers appear red-orange, and collagen Type III (thin) fibers appear green under polarized light. By using the red color channel (not brown as in the CIH protocol), applying a strict threshold (excluding weak signals), and selecting the "dark background" setting, the areas within the lesions that exhibit an abundance of thick collagen fibers were identified. Conversely, weak signals indicated the absence or low presence of collagen, enabling the identification of collagen-rich areas within the lesion. By calculating the relative collagen-rich area, the size and developmental stage of individual plaques at the time of analysis were also considered. Therefore, the collagen-rich area of individual lesions was normalized to their respective lesion areas

(**Equation 1**). The same quantification and calculation method was applied to determine the αSMA- or MAC2-positive area.

Equation 1. Calculation method for relative collagen-rich area.

$$\text{Relative collagen-rich area [\%]} = \frac{\text{Collagen-rich area of individual lesion } [\mu m^2]}{\text{Individual lesion area } [\mu m^2]} \times 100\ [\%]$$

2.5.6.4 Immunofluorescence staining of frozen section

Immunofluorescence staining is a commonly used technique to study protein expression and localization in tissues at the single-cell level. This technique involves the use of a primary antibody to recognize a specific protein of interest and a secondary antibody conjugated with fluorescent dyes to detect the antigen-antibody complex. However, the accuracy and reliability of IF can be compromised by factors such as background autofluorescence, non-specific binding of antibodies, and photobleaching of fluorescent dyes. Despite these challenges, IF is particularly useful for co-staining multiple proteins and can provide valuable insights into the heterogeneity of cell populations in tissues with single-cell resolution. In this study, the nuclear stain DAPI was combined with green (Alexa Fluor 488) and red (Alexa Fluor 594/Cy3) fluorescence to investigate the colocalization of cell-specific marker proteins in the aortic arch. The aortas were previously isolated and fixed as described in **Section 2.5.3**. Note that the aortas have also been previously stained with Oil Red O (**Section 2.5.5**). IF-staining of the aortic arch was performed as follows:

Embedding

1. Incubate the aorta O/N in sucrose solution at 4 °C.
2. Cut the aorta into four pieces in the sucrose solution immediately before the embedding procedure. Embed all pieces, with the aortic arch embedded separately from the thoracic and abdominal aortic sections, in Tissue-Tek O.C.T. Compound (Sakura) on dry ice (**Figure 15**).
3. When Tissue-Tek O.C.T was completely solidified, store the embedded tissue at -80 °C.

Sectioning

1. Prepare 10 µm serial sections with the cryostat (Cryostat MNT, Slee Medical GmbH).
2. Allow tissue sections to adhere to the object slide (SuperFrost Plus, ThermoFisher Scientific) for 30 min at RT.
3. Store sections at – 80 °C until the start of IF-staining.

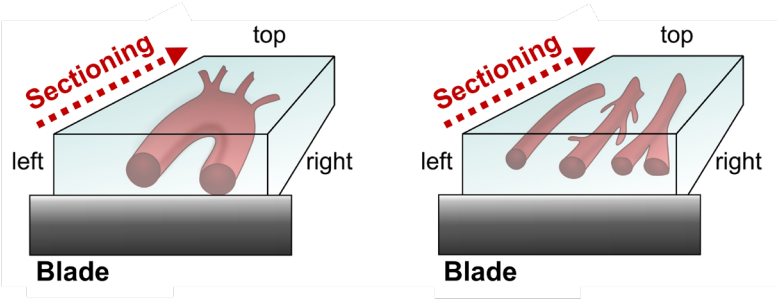

Figure 15. Embedding of aortic tissue for preparation of frozen sections.
The aorta was divided into four pieces, with the aortic arch embedded separately from the thoracic and abdominal aortic sections in Tissue-Tek. All pieces were embedded horizontally. Serial sections, each 10 µm thick, were prepared using a cryostat. The blade designates the cutting plane (sections cut from bottom to top). This allows the aorta to be sliced into rings and then mounted onto glass slides for subsequent staining.

Staining

1. Allow frozen sections on the object slide to equilibrate to room temperature (RT) for approximately 30 min.
2. Remove Tissue-Tek O.C.T. by washing the sections with PBS for 10 min.
3. To block unspecific antibody binding sites, incubate the sections with IF blocking solution for 1 h at RT. Remove the IF blocking solution and create a hydrophobic barrier around the sections using a Super Pap Pen Liquid Blocker (BIOZOL).
4. Incubate the sections with the primary antibody (diluted in blocking solution) overnight at 4°C in a humidified chamber to prevent drying out. For co-staining, mix all primary antibodies in blocking solution, ensuring antibodies of the same species of origin are avoided. Additionally, implement appropriate single-staining controls.
5. Remove the primary antibody solution and wash the sections with PBS-T three times for 10 min each at RT.
6. Incubate the sections with the secondary antibody (diluted in blocking solution) for 2 h in a humidified chamber at RT. Keep sections in the dark. If necessary, add fluorescent dye-conjugated primary antibodies along with secondary antibodies at this step.
7. Remove the secondary antibody solution and wash sections with PBS-T three times for 10 min each at RT.
8. Immerse the object slides with sections in H_2O, then remove the liquid before proceeding to the next step. Work quickly from this point on to prevent the tissue sections from completely drying out.
9. Add 1-2 drops of ROTI®Mount FluorCare DAPI (Roth) per object slide to mount the sections and stain with DAPI. Use a coverslip of an appropriate size to cover the sections, avoiding air bubble entrapment. If air bubbles occur, carefully push them to the edge of the coverslip.
10. Before capturing images using the laser scanning microscope (LSM) 710 setup, allow the mounting medium to solidify overnight.

For documentation of fluorescence staining, we used the LSM 710 setup. This setup comprises an inverted Axio Observer.Z1 stand (ZEISS) microscope platform. Furthermore, this comprehensive system incorporates multiple lasers, allowing simultaneous excitation of various fluorophores. This includes a diode laser (405 nm) for DAPI acquisition, a multiline Argon laser (458 nm, 488 nm, and 514 nm) for AlexaFluor (AF) 488 acquisition, a diode-pumped solid-state laser (561 nm) for AF594 acquisition, and a He/Ne laser (633 nm) for AF647 acquisition. Additionally, we enhanced imaging capabilities with either a C-APOCHROMAT 10x/0.45 water objective lens (ZEISS) or a Plan-APOCHROMAT 20x/0.8 air objective lens (ZEISS). Image acquisition was controlled using the ZEN Black software (ZEISS).

2.6 Statistical analysis

The statistical analysis was performed using Origin2023b (OriginLab). Initially, the data were assessed for normal distribution through the Shapiro-Wilk test. Depending on the sample size, a decision was made between employing a parametric or nonparametric test. When the sample size was less than ~20, even with confirmed normal distribution following homoscedasticity testing, a nonparametric test was conducted. For pairwise comparisons, either a standard Student's t-test (parametric) or Mann-Whitney U test (nonparametric) was used. In the case of comparisons of more than two groups, a One-Way ANOVA with subsequent *post-hoc* Bonferroni test (parametric) or Kruskal-Wallis ANOVA followed by *post-hoc* Dunn's test (nonparametric) was performed. Alternatively, when dealing with repeated measures (dependent variables), a choice was made between One-Way repeated measures ANOVA followed by *post-hoc* Bonferroni test (parametric) or Friedman ANOVA with subsequent *post-hoc* Dunn's test (nonparametric). Statistical significance was considered at $p < 0.05$ and indicated with varying levels of significance (n.s.: not significant, *$p \leq 0.05$, **$p \leq 0.01$, ***$p \leq 0.001$).

3. Results

3.1 Pharmacological modulation of the NO/cGMP signaling pathway in atherosclerosis

Over the past decades, there has been an increased interest in the pathophysiological relevance of the NO/cGMP signaling axis in VSMCs for atherosclerosis. Previous studies have indicated that the NO/cGMP signaling pathway is involved in the development of atherosclerotic plaques, which may be associated with altered phenotypic modulation or transdifferentiation of VSMCs [93, 155]. However, several aspects of the role of the NO/cGMP signaling axis in the altered behavior of VSMCs during atherogenesis are still unresolved. The approach of the pharmacological modulation of this pathway has also already been used to gain further insights into its pathophysiological and pharmacological relevance [160-163]. In the meantime, the pharmaceutical industry has developed new drugs with improved pharmacokinetic and pharmacodynamic profiles [81, 136, 181]. Thus, this study employed these next-generation NO-GC modulators to investigate the pathophysiological and pharmacological relevance of the NO-GC signaling pathway in VSMCs in atherosclerosis. To my knowledge, this is the first study comparing the effects of a NO-GC stimulator with those of a NO-GC activator on atherosclerosis. This may not only provide general insights into the pathophysiological and pharmacological relevance of the NO/cGMP pathway but also elucidate the therapeutic potential of different NO-GC modulator categories. Therefore, ApoE^{ko} mice were fed an atherosclerotic diet, which was supplemented with Vericiguat or a NO-GC Activator tool compound (BAY Activator). Subsequently, the effects on atherogenesis, physiological parameters, and plaque composition were analyzed (**Figure 11**). For further details on the experimental setup, see **Section 2.5.1**.

3.1.1 Localization of NO-GC in healthy and atherosclerotic aorta

Both classes of NO-GC modulating drugs, NO-GC activators and stimulators, target the NO/cGMP signaling pathway by directly binding to NO-GC, which triggers the generation of cGMP [136, 145, 146]. For these drugs to have a modulatory effect on the NO/cGMP signaling axis in VSMCs, NO-GC must be expressed in VSMCs under the respective health condition. It is well established that NO-GC is highly expressed in medial VSMCs under healthy condition [73, 94]. In this study, this was confirmed by IF-staining of wildtype aortic sections that revealed co-expression of NO-GC and the VSMC marker αSMA in the cells of aortic media (**Figure 16, A)**. However, it is not yet examined in detail if VSMCs express NO-GC under atherosclerotic conditions. To investigate the expression status of NO-GC, IF-staining of aortic sections from ApoE^{ko} mice with advanced plaques was performed (**Figure 16, B**). The expression of NO-GC was examined using a NO-GC ß1 subunit-specific antibody. Co-staining of NO-GC and αSMA

was used to identify VSMCs and to assign the characteristic plaque regions, such as the fibrous cap, core, and media. NO-GC-positive cells were detected in all three regions of the atherosclerotic plaque (**Figure 16 B, Zoom**). Cells co-expressing αSMA and NO-GC were identified in the fibrous cap and media (**Figure 16 B, Zoom, FC and media**), while cells in the plaque core showed only NO-GC but no αSMA expression (**Figure 16 B, Zoom, Core**). This raised the question about the cellular origin of these NO-GC-positive, αSMA-negative cells in the plaque core.

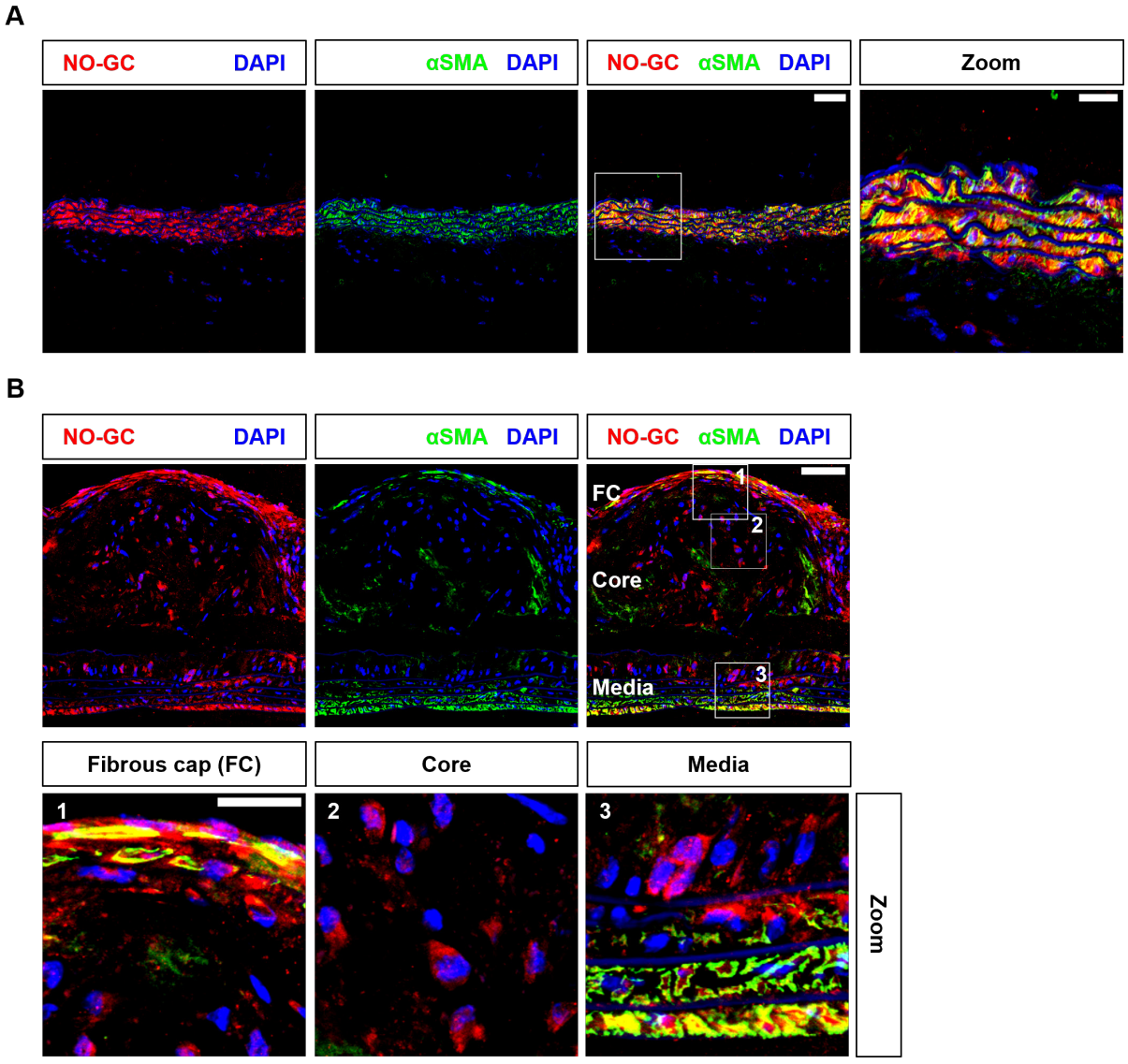

Figure 16. NO-GC expression in healthy and atherosclerotic aorta.
Analysis of NO-GC and αSMA expression in sections (10 µm) of **(A)** a healthy aorta from a wildtype mouse and **(B)** an atherosclerotic aorta from ApoE^{ko} mouse by immunofluorescence staining. The panels show (from left to right) immunofluorescence staining of NO-GC (red), αSMA (green) and an overlay image. Nuclei are counterstained with DAPI (blue). Scale bar is 50 µm. The characteristic plaque regions fibrous cap (FC), core and media are highlighted in the overlay image. Scale bar is 50 µm. The boxed regions in the overlay images are magnified (Zoom) to demonstrate the NO-GC localization in wildtype and atherosclerotic aorta. Scale bar is 20 µm.

During the development of atherosclerotic plaques, VSMCs can migrate, undergo clonal expansion, and transdifferentiate. These processes are accompanied by fundamental structural and functional changes, resulting in the loss of traditional VSMC marker proteins like αSMA [6,

45]. Consequently, the complex composition of the plaque complicates the determination of the cell type of the NO-GC-positive cells found in the plaque core. Nonetheless, studies have demonstrated that VSMCs can undergo transdifferentiation into macrophage-like cells, which contribute to the formation of the plaque core. These macrophage-like cells are derived from medial VSMCs that lose expression of traditional VSMC markers and rather express MAC2, a marker for macrophages and/or macrophage-like cells [33, 70]. To further investigate the cell type of NO-GC-positive cells in the plaque core, atherosclerotic plaque sections from ApoE^{ko} mice were subjected to IF-staining. A MAC2 antibody was used to identify macrophage-like cells within the atherosclerotic plaque. While NO-GC expression was again detected in the fibrous cap, core, and media (**Figure 17, 1st panel**), MAC2-positive cells were localized only in the fibrous cap and core regions of the atherosclerotic plaque (**Figure 17**, **2nd panel**). In the plaque core region, some cells co-expressing NO-GC and MAC2 were identified (**Figure 17**, **Zoom, yellow**). These findings suggest that the cell type of NO-GC-positive cells in the core that lack aSMA expression may be only partially macrophage-like cells. The cell type of NO-GC-positive and αSMA/MAC2-negative cells remains uncertain. However, it should be noted that further fate mapping approaches are necessary to reach a definitive conclusion regarding the cellular origin of the NO-GC/MAC2-positive cells found in the plaque core region.

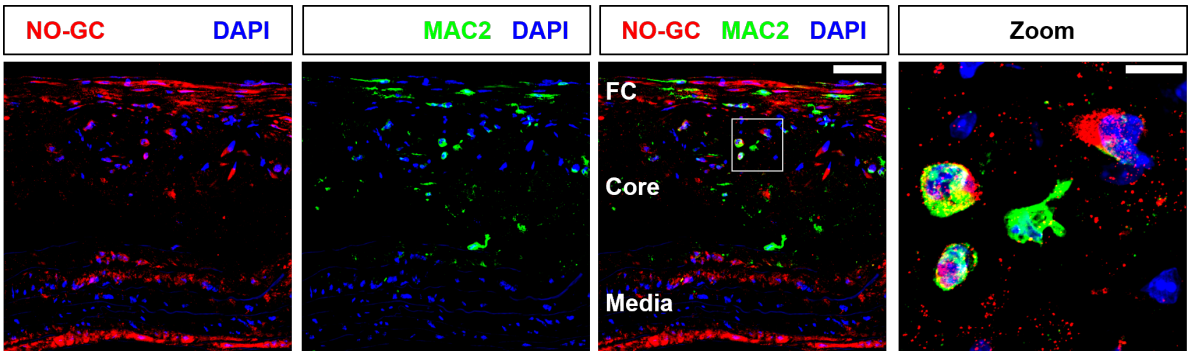

Figure 17. MAC2 expression in NO-GC-positive cells in the plaque core.
Immunofluorescence staining of frozen aortic section (10 µm) for NO-GC and MAC2 in the atherosclerotic plaque of an ApoE^{ko} mouse. The panels show (from left to right) immunostaining of NO-GC (red), MAC2 (green) and an overlay image. Nuclei are counter-stained with DAPI (blue). Scale bar is 50 µm. The characteristic plaque regions fibrous cap (FC), core and media are highlighted in the overlay image. The boxed region in the overlay image is magnified (Zoom) to demonstrate the co-localization of NO-GC and MAC2 (yellow). Scale bar is 10 µm.

In summary, it has been shown that NO-GC is expressed by VSMCs under both healthy and atherosclerotic conditions. NO-GC-expressing cells in the atherosclerotic plaque were detected in the media, core, and fibrous cap. Furthermore, these results indicate that some of the NO-GC expressing cells may be modulated/transdifferentiated, macrophage-like cells in the plaque core.

3.1.2 Effect of BAY Activator and Vericiguat on atherosclerotic lesion area

The detection of the drug target in VSMCs under both healthy and atherosclerotic conditions provides the basis for pharmacological modulation of the NO/cGMP pathway in VSMCs during

different stages of atherogenesis. To investigate the effects of the NO-GC modulators on atherosclerosis, ApoE^{ko} mice were fed an atherogenic diet which was supplemented with BAY Activator or Vericiguat at a concentration of 150 ppm for 16 weeks (BAY Activator) or 18 weeks (Vericiguat) (**Section 2.5.1**). Assuming an average daily food intake of 5 g and an average body weight of 30 g per mouse, this corresponded to a daily dose of 25 mg/kg [179]. Subsequently, aortas were isolated and stained with Oil Red O to visualize atherosclerotic plaques and compare the lesion area of atherosclerotic aortas of treated (atherogenic diet + BAY Activator or Vericiguat) and control mice (atherogenic diet). The lesion area was determined from images of both sides of the aorta, averaged, and quantified for the total aorta, the aortic arch, and the thoracic/abdominal aorta separately. The relative lesion area was calculated by normalizing it to the total area of the respective part of the aorta. Since sex-specific drug effects could not be excluded at this point, the lesion area was assessed separately for both sexes (**Figure 18 (male), Supplementary figure 1 (female)**). Lesion areas could be clearly identified by the red color after Oil Red O staining (**Figure 18 A, C (male); Supplementary figure 1 A, C (female))**. In all experimental groups, typical atherosclerotic plaque development was observed in the aortic arch and at branching vessels.

The treatment with the BAY Activator resulted in a significant increase in the lesion area (**Figure 18 B (male); Supplementary figure 1 B (female)**). This effect was particularly clear in the thoracic/abdominal aorta in male mice, in which treatment led to an approx. 12-fold increase in lesion area (Male, Ctrl: 2.0 ± 0.1 % vs. BAY Act.: 24.8 ± 3.9 %). In the aortic arch, the BAY Activator treatment also led to a doubling of the lesion area (Male, Ctrl: 26.7 ± 1.0 % vs. BAY Act. 50.8 ± 3.5 %). Similarly, in the female mice, a significant increase (approx. 6-fold) in the lesion area was observed in the thoracic/abdominal aorta in response to the treatment with the BAY Activator (Female, Ctrl: 1.7 ± 0.2 % vs. BAY Act.: 10.7 ± 1.9 %) (**Supplementary figure 1 B**). The increase in the size of the lesion area observed in the aortic arch of female mice after BAY Activator treatment (Female, Ctrl: 29.7 ± 4.4 % vs. BAY Act.: 44.7 ± 5.6 %) did not reach statistical significance. In general, no difference in lesion area was identified between control groups of both sexes (**Supplementary figure 2**). However, the observed effect of BAY Activator treatment was weaker in female mice, suggesting a potential sex-specific difference in the manifestation of the drug effect. For meaningful conclusions regarding a sex-specific difference, the number of mice in this experiment was not sufficient.

To confirm the observed effects of BAY Activator treatment on the atherosclerotic lesion area and assess reproducibility another independent experiment was conducted. This experiment used a similar setup but involved a new batch of an atherogenic diet supplemented with 150 ppm of BAY Activator. In principle, the described results of BAY Activator treatment on the atherosclerotic lesion area could be validated with this additional experiment (**Figure 32 D**).

Specifically, treatment with BAY Activator in male mice resulted in a significant increase in the atherosclerotic lesion area in the total aorta, whereas a similar trend was evident in female mice that did not reach statistical significance. In general, the observed effect was less pronounced in both sexes compared to the first experiment. Similar to the first experiment, no difference in lesion area between the control groups of both sexes was observed (**Supplementary figure 2**). In summary, both independent experiments showed that treatment with BAY Activator leads to an increase in atherosclerotic lesion area in mice. Please note that all results shown in the present work refer to BAY Activator experiment 1, unless otherwise stated.

In contrast to the BAY Activator, the NO-GC stimulator Vericiguat did not lead to significant differences in lesion area following the 18 weeks treatment period (**Figure 18 D** (male) **Supplementary figure 1 D** (female)). Additionally, no significant difference in lesion area was found between the sexes among the control mice (**Supplementary figure 2**).

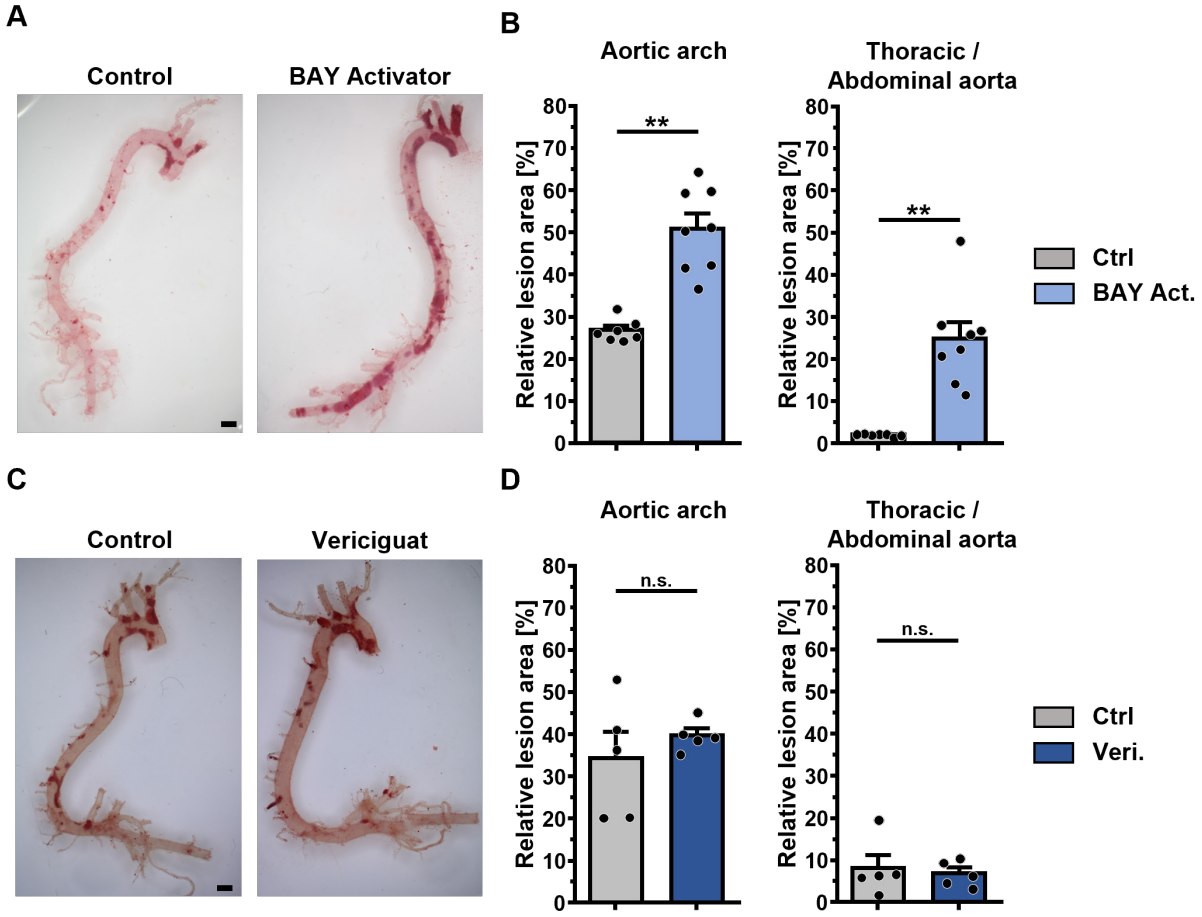

Figure 18. Atherosclerotic lesion area in male mice after treatment with BAY Activator or Vericiguat. Analysis of atherosclerotic lesion area in aortas from ApoE^{ko} mice by Oil Red O staining after 16 weeks (Ctrl/BAY Act.) or 18 weeks (Ctrl/Veri.) treatment with BAY Activator (BAY Act.) or Vericiguat (Veri.). The drugs were supplemented at a concentration of 150 ppm into the atherosclerotic diet. **(A, C)** Representative images of Oil Red O-stained atherosclerotic aortas of control (Ctrl) and BAY Act. **(A)** or Veri. **(C)** treated male mice. Atherosclerotic lesions appear red. Scale bars are 1 mm. (**B, D)** Relative lesion area of the aortic arch or thoracic/abdominal aorta of Ctrl and BAY Act. **(B)** or Veri. **(D)** treated male mice. The atherosclerotic lesion area was determined from both sides of the aorta, averaged, and normalized to the total area of the respective part. Data are represented as mean + SEM (Ctrl BAY Act.: 7 mice, BAY Act.: 8 mice, Ctrl Veri.: 5 mice, Veri.: 5 mice). Statistical significance is indicated by asterisk (*p ≤ 0.05; **p ≤ 0.01; n.s.: not significant, Mann-Whitney U test). Ctrl, Control, BAY Act., BAY Activator, Veri., Vericiguat.

Overall, treatment with the BAY Activator resulted in a marked increase in lesion area, particularly in the thoracic/abdominal aorta, while Vericiguat treatment showed no significant difference compared to the control group. It is worth noting that the lesion area in the control groups may be different in each experiment (**Supplementary figure 2**), which is why litter matched mice are always used and compared in the control and treated groups in each experiment.

3.1.3 Impact of NO-GC modulator treatment on the physiological parameters

The effectiveness of drugs primarily depends on their pharmacodynamic and pharmacokinetic properties. The chosen method of drug administration can play a crucial role. In the present study, the drugs were administered orally through the diet. Consequently, successful absorption by the gastrointestinal tract is a prerequisite for the drugs to reach the intended site of action in a sufficient concentration [193]. The extent of absorption was evaluated by measuring the plasma concentration of BAY Activator and Vericiguat. As drugs bind reversibly to proteins in the plasma, it becomes important to distinguish between the total drug concentration and the unbound fraction, which represents the free and pharmacologically active concentration of the drug in the plasma [183, 194]. It is important to note that the proportion of drug absorption and plasma protein binding can significantly vary among different compounds and relies on their physiochemical properties [183, 193].

Blood samples were collected from the mice at the end of the feeding period and the plasma was subsequently isolated. In collaboration with BAYER AG and the Dr. Margarete Fischer-Bosch Institute of Clinical Pharmacology, total plasma concentrations of the drugs were quantified. In order to determine the unbound fraction, the equilibrium dialysis method was additionally employed [194]. Due to the limited number of mice, the results for both sexes had to be pooled. Both drugs were detected in the plasma (BAY Act.: 2073 ± 249 nM; Veri.: 2752.7 ± 304.4 nM) (**Figure 19 A, C**). In the Vericiguat control group, minor contamination of 21.2 nM (total drug concentration) with Vericiguat was detected in one mouse (**Supplementary table 2**). This contamination has been considered negligible due to the relatively low amount in the total plasma concentration. With a significantly lower concentration, both drugs were detected in the unbound fraction (BAY Act.: 16.6 ± 2 nM; Veri.: 56.1 ± 8.4 nM) (**Figure 19 A, C)**.

The oral administration of drugs can result in systemic effects that potentially exert an indirect influence on atherosclerosis. To evaluate these systemic effects, various physiological parameters of the experimental mice were examined. One notable factor to consider is the concentration-dependent antihypertensive effect of NO-GC modulators [81, 136, 150, 181, 182]. Due to the well-established connection between blood pressure and the development of atherosclerosis, it is essential to investigate the impact of drug treatment on blood pressure [1]. Therefore, blood pressure was measured for all experimental groups at the end of the feeding period using a tail-cuff blood pressure system. Treatment with the BAY Activator had no effect on

either systolic or diastolic blood pressure in both sexes (**Figure 19 B** (male); **Supplementary figure 4 A** (female)). Since, no significant difference in blood pressure was found between the sexes of the control and treatment groups, we pooled data of female and male mice to increase the sample size. Even with the increased sample size, no statistically significant effect of BAY Activator treatment on mean blood pressure was observed (Ctrl: 85.5 mmHg vs. BAY Act.: 88.1 mmHg) (**Figure 32 B**). Additionally, the blood pressure of BAY Activator-treated male mice was determined at four days prior to the start of the treatment and then regularly throughout the 16-week study period (**Supplementary figure 3**). Similarly, the atherogenic diet or BAY Activator treatment did not cause blood pressure changes at any time point.

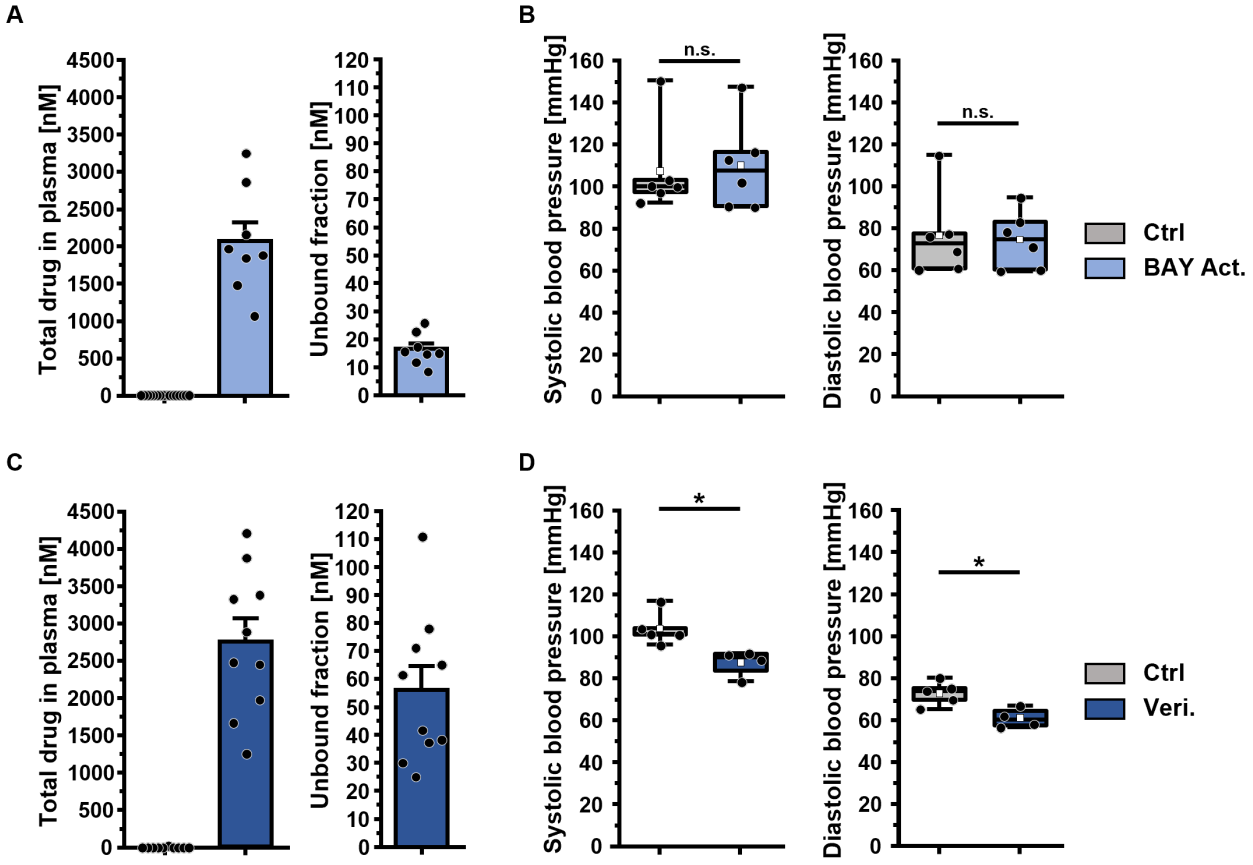

Figure 19. Drug plasma concentration and blood pressure in BAY Activator or Vericiguat treated mice. ApoEko mice were fed with an atherogenic diet supplemented with 150 ppm BAY Activator for 16 weeks (Ctrl/BAY Act.) or 150 ppm Vericiguat for 18 weeks (Ctrl/Veri.). **(A, C)** Total concentration and unbound fraction of BAY Activator (BAY Act.) **(A)** or Vericiguat (Veri.) **(C)** in plasma of control (Ctrl) or treated mice. Blood samples were collected from the mice at the end of the feeding period and the plasma was subsequently isolated. The mice were not starved before sampling. The drug concentration in plasma was measured in collaboration with Dr. U. Hofmann (Dr. Margarete Fischer-Bosch Institute of Clinical Pharmacology) and Prof. Dr. P. Sandner (BAYER AG). For the analysis, the results of both sexes were pooled. Data are represented as mean + SEM (Ctrl BAY Act.: 8 mice, BAY Act.: 16 mice, Ctrl Veri.: 10 mice, Veri.: 10 mice). **(B, D)** Systolic and diastolic blood pressure of Ctrl and BAY Act. **(B)** or Veri. **(D)** treated male mice. Blood pressure measurements were performed using a tail-cuff blood pressure system at the end of the feeding period for three consecutive days. The data from three consecutive days were averaged for each animal. Data are represented as median (horizontal line), 25% - 75% interquartile range (box), 5% - 95% range percentile (whiskers) and mean (white square) (Ctrl BAY Act.: 6 mice, BAY Act.: 6 mice, Ctrl Veri.: 5 mice, Veri.: 4 mice). Statistical significance is indicated by asterisk (*p ≤ 0.05; n.s.: not significant, Mann-Whitney U test). Ctrl, Control, BAY Act., BAY Activator, Veri., Vericiguat.

For the Vericiguat experimental setup, only a final blood pressure measurement was conducted. It was observed that treatment with Vericiguat moderately reduced systolic blood

pressure (Male, Ctrl: 103.9 mmHg vs. Veri. 87.8 mmHg) and diastolic (Ctrl: 72.8 mmHg vs. Veri. 61.0 mmHg) blood pressure in male mice. It was observed that treatment with Vericiguat moderately reduced systolic blood pressure (Ctrl: 103.9 mmHg vs. Veri. 87.8 mmHg) and diastolic blood pressure (Ctrl: 72.8 mmHg vs. Veri. 61.0 mmHg) in male mice (**Figure 19 D**). A similar trend of blood pressure reduction was observed in female mice (systolic, Ctrl: 110.2 mmHg vs. Veri.: 97.3 mmHg and diastolic, Ctrl: 80.5 mmHg vs. Veri.: 66.5 mmHg) (**Supplementary figure 4 B**). Since there were no significant differences in systolic and diastolic blood pressure between male and female mice, the data were pooled to validate the effects of Vericiguat on blood pressure with a larger sample size. This revealed a statistically significant decrease in mean blood pressure in the Vericiguat-treated mice compared to the respective control mice (Ctrl: 86.5 mmHg vs. Veri.: 73.0 mmHg) (**Figure 32 F**). However, the physiological relevance of this moderate blood pressure-lowering effect of Vericiguat on the development of atherosclerosis has not been further investigated and, therefore remains unclear.

Increased plasma lipid levels are strongly associated with the development of atherosclerosis [5, 195]. Since increased cholesterol, LDL and triglyceride levels represent well-accepted risk factors for atherosclerosis, the analysis focused on determining the lipid plasma levels in the experimental mice (**Table 11**) [5, 196-198]. Blood samples were collected from the mice at the end of the feeding period. Due to a small sample size, the data from BAY Activator Experiment 1 and 2 had to be pooled for the determination of the lipid values. The plasma obtained was analyzed in collaboration with the "Zentrallabor" of the University Hospital of Tübingen. All mice fed an atherogenic diet exhibited elevated plasma lipid levels compared to the control group fed with normal diet (n.d.) (**Table 11**, n.d. vs. atherogenic diet). In contrast, none of the analyzed lipids showed significant differences in plasma levels between the treatment groups and sexes. The pooled data from male and female mice validated this result e.g., for total Cholesterol (Ctrl: 1611.1 ± 109.8 vs. BAY Act.: 1697.8 ± 116.5; Ctrl: 1961.5 ± 126.3 vs. Veri.: 1586 ± 134.7) (**Figure 32 C, G**). Additionally, other physiological parameters such as body weight and organ weight were examined. No significant differences were found between the control and treatment groups (**Table 11**). However, a clear weight gain was observed in each experimental group over the feeding period with the atherogenic (**Table 11**, body weight start vs. end).

Due to the significant impact of BAY Activator treatment on the size of the lesion area, the general health condition of both the control and BAY Activator-treated mice was determined by complete blood count analysis. Blood samples were analyzed using an automatic hematology analyzer. Given the limited sample number, the data of both sexes were combined. No changes were observed in the numbers of white blood cells, red blood cells, or platelets. Additionally, all other parameters were comparable to the control group. (**Supplementary table 3**). This may indicate the absence of systemic inflammation or hemolysis.

Table 11. Physiological parameters of mice after atherogenic diet ± NO-GC modulators.
Listed are the plasma lipid parameters of mice fed a normal diet (Ctrl n.d.), atherogenic diet (Ctrl.) or atherogenic diet supplemented with 150 ppm BAY Act. or Veri. Blood was collected from mice at the end of the atherogenic diet (± 150ppm NO-GC modulator) feeding period (BAY Activator: 16 weeks, Vericiguat: 18 weeks) in the morning. The experimental mice were not starved before sampling. The lipid parameters were measured in collaboration with Prof. Dr. med. A. Peter (University Hospital Tubingen). All data are represented as mean ± SEM. Ctrl, Control; n.d., normal diet; BAY Act., BAY Activator; Veri., Vericiguat; LDL, low-density lipoprotein.

Parameter	n.d.	Atherogenic diet							
	Both	Male		Female		Male		Female	
	Ctrl n.d.	Ctrl	BAY Act.	Ctrl	BAY Act.	Ctrl	Veri.	Ctrl	Veri.
Number of mice	7	5	5	4	4	5	5	5	5
Total Cholesterol [mg/dL]	85.0 ± 13.5	1598.0 ± 207.6	1944.0 ± 78.8	1627.5 ± 18.0	1390 ± 119.5	2019.0 ± 195.6	1714.0 ± 198.5	1904.0 ± 178.5	1458.0 ± 184.4
Triglycerides [mg/dL]	115.7 ± 8.6	213.0 ± 40.4	367.0 ± 65.0	120.0 ± 15.1	86.3 ± 5.5	368.0 ± 33.5	192 ± 29.9	170 ± 18.1	201.0 ± 25.5
LDL [mg/dL]	10.7 ± 2.5	227.0 ± 29.4	268.0 ± 17.4	258.8 ± 8.8	196.3 ± 18.1	274.0 ± 36.9	262.0 ± 34.5	302.0 ± 27.6	208.0 ± 34.5
Number of mice	-	7	8	5	4	5	5	5	5
Body weight start [g]	-	25.9 ± 0.7	26.3 ± 0.6	23.0 ± 0.4	23.6 ± 0.5	26.84 ± 1.2	26.5 ± 1.3	22.2 ± 1.0	22.4 ± 0.6
Body weight end [g]	-	34.5 ± 1.7	30.6 ± 1.1	30.1 ± 0.9	27.0 ± 0.4	40.9 ± 1.9	38.4 ± 1.9	34.7 ± 1.9	35.0 ± 2.1
Liver-to- body weight [mg/g]	-	67.2 ± 7.5	68.3 ± 1.2	64.8 ± 1.1	57.5 ± 3.2	70.7 ± 5.8	70.7 ± 3.2	65.6 ± 3.5	60.9 ± 4.1
Heart-to-body weight [mg/g]	-	4.5 ± 0.5	4.0 ± 0.2	3.9 ± 0.4	4.3 ± 0.4	4.5 ± 0.3	4.3 ± 0.3	5.2 ± 0.4	5.3 ± 0.5
Kidney-to-body weight [mg/g]	-	6.5 ± 0.7	6.0 ± 0.9	5.4 ± 0.4	5.7 ± 0.5	5.3 ± 0.5	5.8 ± 0.2	5.0 ± 0.2	4.7 ± 0.4

Collectively, both NO-GC modulators, BAY Activator, and Vericiguat, were successfully detected in the plasma of the respective treatment groups. At the detected concentration, Vericiguat moderately lowered blood pressure, while the BAY Activator treatment did not influence the blood pressure. No significant systemic effects on physiological parameters, such as plasma lipid levels, body weight, organ weight, and blood cell count, were observed as a result of treatment with the NO-GC modulators.

3.1.4 Influence of the BAY Activator on the composition of atherosclerotic plaques

Atherosclerotic plaques are complex structures that consist of multiple cell types, like macrophages, or VSMCs. VSMCs contribute fundamentally to the formation of the fibrous cap as well as the core region of the atherosclerotic plaque. Thereby they can change their phenotypes and transdifferentiate into other cell types, such as MAC2-positive macrophage-like cells (**Section 1.2**). To investigate whether the increased plaque area observed in BAY Activator-treated mice is associated with changes in VSMC or macrophage content during plaque development, the cellular composition of the plaques was analyzed.

To obtain a general overview of potential changes in the plaque composition, the protein expression level in atherosclerotic aortas of control mice as well as of those treated with BAY Activator or Vericiguat were analyzed using Western blot. $ApoE^{ko}$ mice were fed an atherosclerotic diet supplemented with either BAY Activator or Vericiguat for 15 weeks. Subsequently, total protein was isolated from the atherosclerotic aortas. Due to the limited number of mice, the sexes had to be pooled. The analysis focused on the protein expression of MAC2 as a marker for modulated/transdifferentiated VSMCs or macrophages (**Figure 20 A**). Additionally, the expression of αSMA, as a classical marker for VSMCs, and of NO-GC, as the drug target, were investigated (**Supplementary figure 5 A**). The expression levels of NO-GC and αSMA showed no differences between the control group and any of the groups treated with NO-GC modulators (**Supplementary figure 5 B, C**). Also, treatment with Vericiguat did not exhibit an effect on MAC2 expression levels (**Supplementary figure 5 D**). However, Western blot analysis revealed that treatment with BAY Activator led to a statistically significant increase in MAC2 expression in the total aorta when compared to the control group (**Figure 20 B**). These significant changes in MAC2 expression levels throughout the entire aorta may indicate alterations in plaque composition induced by BAY Activator treatment.

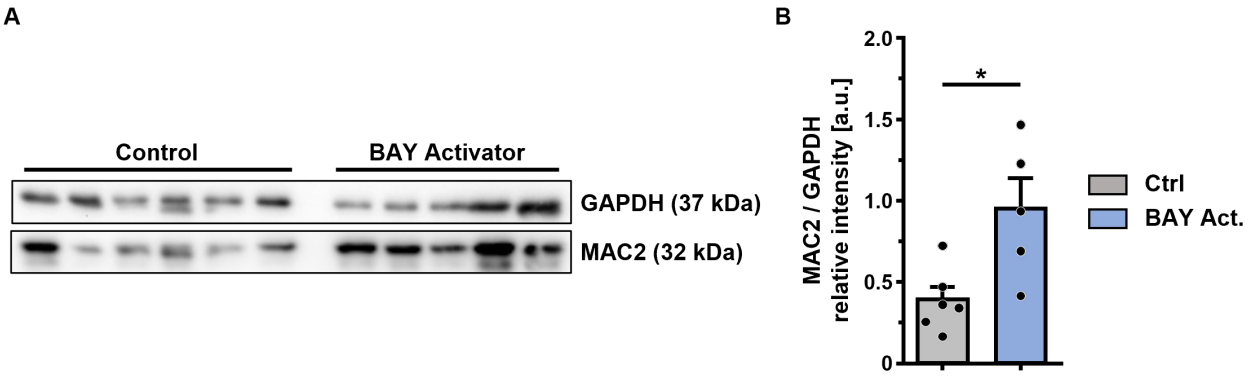

Figure 20. MAC2 expression in atherosclerotic aortas of BAY Activator treated mice.
Western blot analysis of protein expression in atherosclerotic aortas from ApoE^{ko} mice after 15 weeks of atherogenic diet. BAY Activator was supplemented at a concentration of 150 ppm into the diet. **(A)** Image of Western blot analysis of MAC2 expression. GAPDH was used as loading control. **(B)** Quantification of relative band intensity of MAC2 by densitometric analysis. The band intensity was normalized to the band intensity of the loading control. Data are represented as mean + SEM (Ctrl: 6 mice, BAY Act.: 5 mice). The expected molecular weights of the respective target proteins are indicated. Statistical significance is indicated by asterisk (*p ≤ 0.05; n.s.: not significant, Mann-Whitney U test). Ctrl, Control, BAY Act., BAY Activator.

Due to the significant increase in lesion area in the different groups of BAY Activator-treated mice and the observed increased in MAC2 expression levels throughout the aorta, the subsequent analysis of plaque composition focused on a representative experimental group of four control mice compared to four BAY Activator-treated male mice of experiment 1. In mouse models of atherosclerosis, the aortic root is commonly characterized by prominent lesions. Additionally, it provides an opportunity to compare the plaque composition between different groups in a defined region within the aorta. These factors make the aortic root an ideal region for conducting a comprehensive histological examination. Thus, 10 µm paraffin cross-sections of the aortic root were prepared to investigate the plaque composition at the cellular level. Subsequently, consecutive sections were analyzed using PSR-staining to detect collagen, as well as CIH to identify the cell-specific marker proteins αSMA and MAC2. These approaches can provide valuable information about the cellular composition and stability of the plaque following the BAY Activator treatment. To ensure comparability within and between the experimental groups, similar sections within the aortic root were selected, with the characteristic structure of the aortic valve with its three leaflets serving as a reference.

First, the aortic root cross sections were examined for differences in the atherosclerotic lesion area between the control and BAY Activator mice. For this purpose, brightfield images of the PSR-stained sections were used. PSR specifically binds collagen fibers in the tissue, resulting in the formation of distinct, red-colored collagen structures [192]. This allowed the red-stained collagen-rich lesions to be easily distinguished from the vessel wall (**Figure 21 A**). Upon visual inspection of the brightfield images of PSR-stained aortic root, it was already apparent that BAY Activator-treated mice exhibited a significantly increased lesion area. This observation was further confirmed by quantification and statistical analysis of the lesion area covering the vessel wall (Ctrl: 56458.2 ± 10399.5 µm^2 vs. BAY Act.: 101175.9 ± 14668.9 µm^2) (**Figure 21**

B, left). Thus, treatment with the BAY Activator resulted in a significant increased the lesion area in the aortic root, consistent with the comprehensive analysis of the total aorta as described in **Section 3.1.2**.

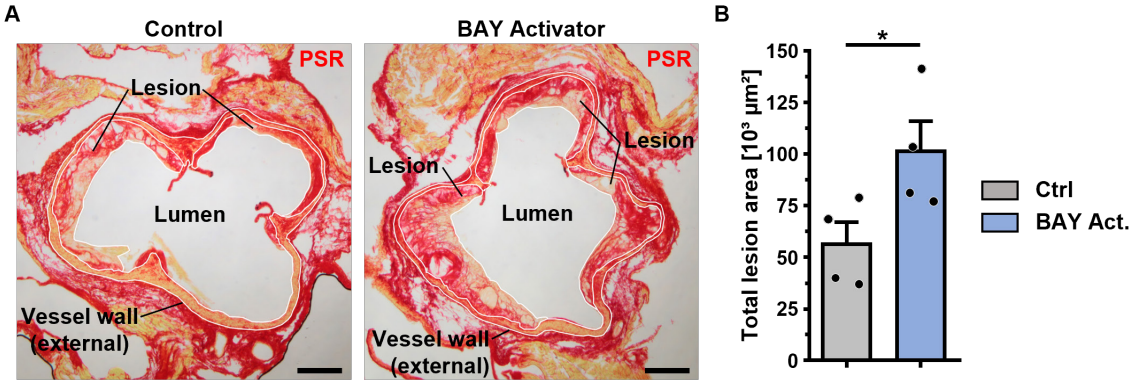

Figure 21. Atherosclerotic lesion area in aortic root after BAY Activator treatment.
Analysis of atherosclerotic lesion area in aortic root cross sections (10 µm) from ApoE^{ko} mice by Picrosirius Red (PSR) staining after 16 weeks of atherogenic diet. BAY Activator was supplemented at a concentration of 150 ppm into the diet. (**A**) Representative brightfield images of PSR stained aortic root cross sections of control (Ctrl) and BAY Activator (BAY Act.) treated male mice. The white lines outline the total vessel area (external vessel wall), lumen area and atherosclerotic lesions. Scale bars are 200 µm. (**B**) Quantification of atherosclerotic lesion in aortic root cross sections of Ctrl and BAY Act. treated male mice. To ensure comparability, similar regions within the aortic root were selected, using aortic valves as a reference. Data are represented as mean + SEM (Ctrl: 4 mice, BAY Act.: 4 mice). Statistical significance is indicated by asterisk (*p ≤ 0.05; n.s.: not significant, Mann-Whitney U test). ctrl, Control, BAY Act., BAY Activator, PSR, Picrosirius red.

Next, plaque composition was examined regarding the impact of BAY Activator treatment on the expression of the classical VSMC marker αSMA, the macrophage-like cell or macrophage marker MAC2 and the collagen content within the lesion area in the aortic root. Plaque composition was individually assessed for each plaque of the different sections. This analysis considers that the developmental stage of individual plaques at the time of analysis may have an impact on their composition.

The αSMA staining of plaques in both the control and BAY Activator-treated groups exhibited the expected characteristics of atherosclerotic plaques. Most plaques were covered by an αSMA-rich fibrous cap, while a low amount of αSMA was observed in the core region (**Figure 22 A**). Only a small level of αSMA expression was detected in the vessel wall below the plaques, whereas strong expression was observed in regions of the vessel wall that were free of plaques. When comparing the total αSMA-positive area in the aortic root between the experimental groups, only a small but not statistically significant difference in αSMA-positive area in the lesion area was detected (Ctrl: 4290.5 ± 1487.4 µm^2 vs. BAY Act.: 5486.7 ± 1079.2 µm^2) (**Figure 22 B**).

Furthermore, we evaluate the effect of the BAY Activator on collagen content. Therefore, we additionally analyzed the PSR-stained sections under polarized light (**Supplementary figure 6**). Under polarized light type I (thick) fibers are shown red-orange and type III (thin) fibers green (**Figure 22 D**) [191, 192]. In the present study, the analysis focused on identifying and

quantifying the accumulation of thick collagen fibers, which is why they are referred to as collagen-rich regions. For further details about the analysis, see **Section 2.5.6.2**. No statistically significant differences were observed in the total collagen-rich area (Ctrl: 8141.2 ± 3234.9 µm^2 vs. BAY Act.: 8663.1 ± 1238.0 µm^2) between control and BAY Activator-treated mice (**Figure 22 E**).

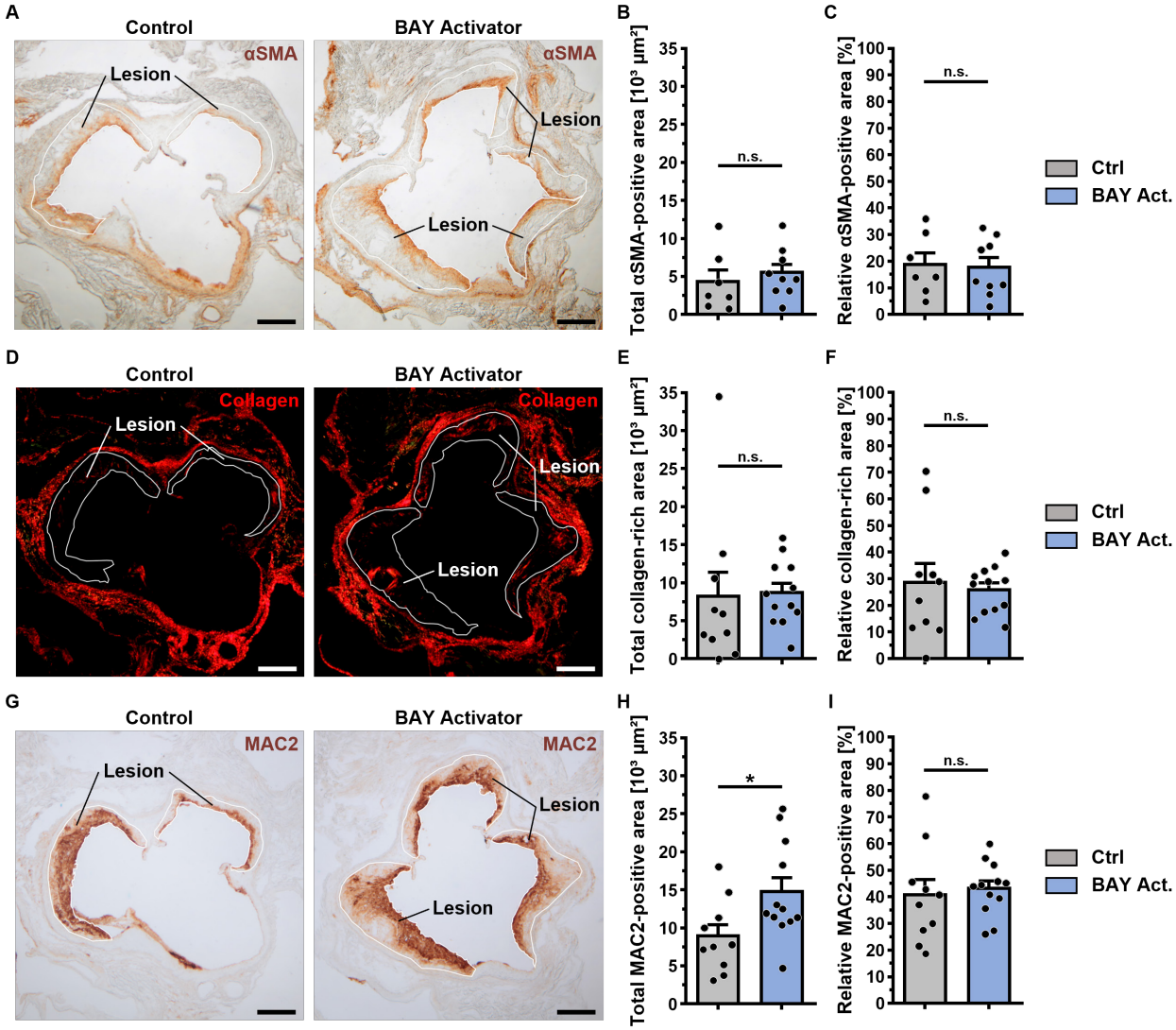

Figure 22. Effect of BAY Activator treatment on plaque composition in the aortic root.
Analysis of the plaque composition in aortic root consecutive cross sections (10 µm) from ApoE^{ko} mice by chromogenic immunohistochemistry (CIH) and Picrosirius red (PSR) staining after 16 weeks of atherogenic diet. BAY Activator (BAY Act.) was supplemented at a concentration of 150 ppm into the diet. (**A, C, G**) Representative brightfield images of CIH-staining for αSMA **(A)** and MAC2 **(D)** and polarized images of PSR-staining for collagen **(G)** in aortic root sections of control (Ctrl) and BAY Act. treated male mice. αSMA-positive and MAC2-positive areas appear brown. Under polarized light thick collagen fibers are displayed in red-orange and thin collagen fibers in green. The white lines outline the atherosclerotic lesions. Scale bars are 200 µm. (**B, D, H**) Quantification of total αSMA- or MAC2-positive and collagen-rich area within atherosclerotic lesions (**C, F, I**) Quantification of relative αSMA- or MAC2-positive and collagen-rich area within atherosclerotic. To account for the variation in size and composition of individual plaques, the respective stained area was set relative to the individual lesion area. To ensure comparability, similar regions within the aortic root were selected, using aortic valves as a reference. Each dot represents an individual plaque. Data are represented as mean + SEM (αSMA-staining: Ctrl: 7 plaques from 3 mice, BAY Act.: 9 plaques from 3 mice; MAC2-staining: Ctrl: 10 plaques of 4 mice, BAY Act.: 12 plaques from 4 mice; PSR-staining: Ctrl: 10 plaques from 4 mice, BAY Act.: 12 plaques from 4 mice). Statistical significance is indicated by asterisk (*p ≤ 0.05; n.s.: not significant, Mann-Whitney U test). ctrl, Control, BAY Act., BAY Activator.

The effect of BAY Activator treatment on content of macrophage-like cells or macrophages was investigated by analyzing the expression level of MAC2 within the atherosclerotic plaque. In general, a high MAC2 expression level could be detected in the fibrous cap and core regions in the atherosclerotic plaques of both groups (**Figure 22 G**). Nevertheless, consistent with the Western blot analysis of the whole aorta (**Figure 20**), the MAC2 expression in lesions of the aortic root was significantly increased in the BAY Activator-treated mice compared to the control mice (Ctrl: 8890.9 ± 1509.7 µm2 vs. BAY Act.: 14719.1 ± 1836.0 µm2) (**Figure 22**. **H**). This finding might initially indicate an accumulation of transdifferentiated VSMCs and/or macrophages due to BAY activator treatment in the aortic root lesions and thus a change in plaque composition. However, this significant change in total MAC2-positive area expression might be related to the increased lesion area in BAY Activator-treated mice. To investigate the relationship, the MAC2-positive area of each plaque was normalized in relation to the respective lesion area. It was shown that the significant increase in MAC2-positive area resulting from BAY Activator treatment was normalized by accounting for individual lesion areas (Ctrl: 40.7 % ± 5.8 % vs. BAY Act.: 43.1 %± 2.9 %) (**Figure 22 I**). Consequently, the treatment with BAY Activator led to an increase in MAC2 expression directly proportional to the increased lesion area in the aortic root. Overall, this suggests that the elevated presence of transdifferentiated macrophage-like cells or macrophages in the plaques was associated with individual plaque size. Similarly, αSMA expression (Ctrl: 18.7 % ± 4.3 % vs. BAY Act.: 17.7 %± 3.6 %) and collagen content (Ctrl: 28.6 % ± 7.1 % vs. BAY Act.: 25.8 %± 2.5 %) did not show relative changes based on the lesion area (**Figure 22 C, F**).

An increased presence of αSMA-positive VMSCs, particularly in the fibrous cap region, along with elevated collagen content within the atherosclerotic plaque, is strongly associated with enhanced plaque stability [6, 34, 190, 199]. Conversely, an augmented presence of macrophage-like cells or macrophages may potentially exert a destabilizing effect on the plaque, leading to a higher risk of adverse events such as plaque rupture and subsequent thrombosis [27, 34, 199]. Thus, any alterations in plaque composition concerning αSMA expression, collagen content, or MAC2 expression due to BAY Activator treatment may potentially indicate an influence on plaque stability. Therefore, we assessed plaque stability by establishing the αSMA expression or collagen content in relation to MAC2 expression (total αSMA-positive area or total collagen-rich area over the total MAC2-positive area). A smaller ratio indicates reduced plaque stability. Plaques from the aortic roots of BAY Activator-treated mice did not exhibit a significant difference in the αSMA/MAC2 or Collagen/MAC2 ratio compared to the respective control mice (**Figure 23**). This finding suggests that BAY Activator treatment had no significant effect on plaque stability. However, it should be noted that there is a high degree of variance in individual plaque stability within the experimental groups, and only a selected and limited

number of mice have been examined at present. To gain meaningful insights into the effect of the BAY Activator on plaque stability, it is essential to increase the sample size.

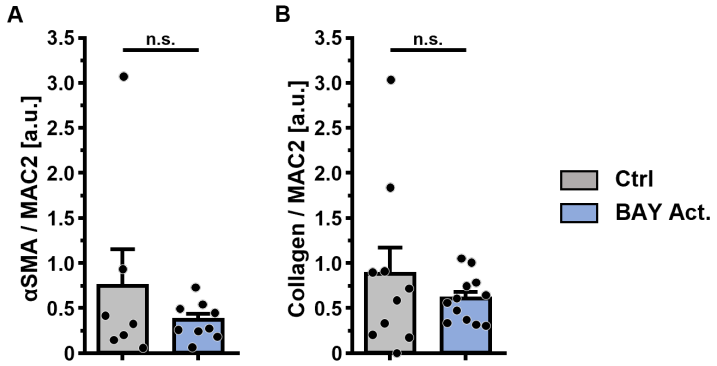

Figure 23. Effect of BAY Activator treatment on plaque stability.
Analysis of the plaque stability in aortic root consecutive cross sections (10 µm) from ApoEko mice by chromo-genic immunohistochemistry (CIH) and Picrosirius red (PSR) staining after 16 weeks of atherogenic diet. BAY Activator (BAY Act.) was supplemented at a concentration of 150 ppm into the diet. The Plaque stability was assessed by the ratio of **(A)** the αSMA-positive area or **(B)** the collagen-rich area to the MAC2-positive area of the atherosclerotic lesions. Each dot represents an individual plaque. Data are represented as mean + SEM (αSMA / MAC2: Ctrl: 7 plaques from 3 mice, BAY Act.: 9 plaques from 3 mice; Collagen / MAC2: Ctrl: 10 plaques of 4 mice, BAY Act.: 12 plaques from 4 mice). No statistically significant differences were found (n.s.: not significant, Mann-Whitney U test). ctrl, Control, BAY Act., BAY Activator.

The composition of atherosclerotic plaques can indeed vary in different areas of the aorta, including the aortic root, aortic arch, and the abdominal/thoracic part of the aorta. Regional differences in multiple factors, including variations in hemodynamic forces and the embryonic origin of distinct aortic segments, may influence the plaque composition [6, 20, 25]. Consequently, it is crucial to examine plaque composition in lesions from various regions. Regions exposed to disturbed flow, such as arterial bifurcations or curvatures, are particularly more prone to plaque formation [20, 29]. Therefore, the aortic arch is another area where prominent atherosclerotic lesions tend to develop (**Section 3.1.2**). To investigate the effects of BAY Activator treatment on the plaque composition in the aortic arch, 10 µm cryosections were prepared and subjected to examination through immunofluorescence staining. It should be noted that due to the lack of reference points, no statement can be made about the comparability of the sections regarding their exact localization in the aortic arch, but an attempt was made to compare morphologically similar regions.

In this case as well, the focus was placed on the expression levels of the VSMC marker αSMA and the marker for macrophage-like cells or macrophages MAC2 in co-staining. To evaluate the protein expression and localization at the single-cell level, cell nuclei were stained with DAPI (4′,6-diamidino-2-phenylindole). Consistent with the results described in the previous paragraphs, a noticeably larger lesion area was observed in the aortic arch of mice treated with the BAY Activator compared to the control group (**Figure 24**). In both experimental groups, αSMA-positive cells were detected in the fibrous cap region of the atherosclerotic plaques, as well as throughout the entire media (**Figure 24 , 1st panel**). MAC2-positive cells were localized in both the fibrous cap and core regions of the atherosclerotic plaque (**Figure 24, 2nd panel**).

A substantial increase in MAC2-positive cells and a lower increase in αSMA-positive cells within the atherosclerotic plaque due to BAY Activator treatment was observed. Essentially, the plaques in the control and BAY Activator groups had similar relations in sizes and compositions in terms of αSMA and MAC2 expression as observed in the aortic root. Thus, it can be assumed that the observed increase in MAC2 in BAY Activator-treated mice is also in relation to the enlarged plaque size. A more detailed analysis and statistical evaluation of the advanced plaques in the aortic arch is still pending.

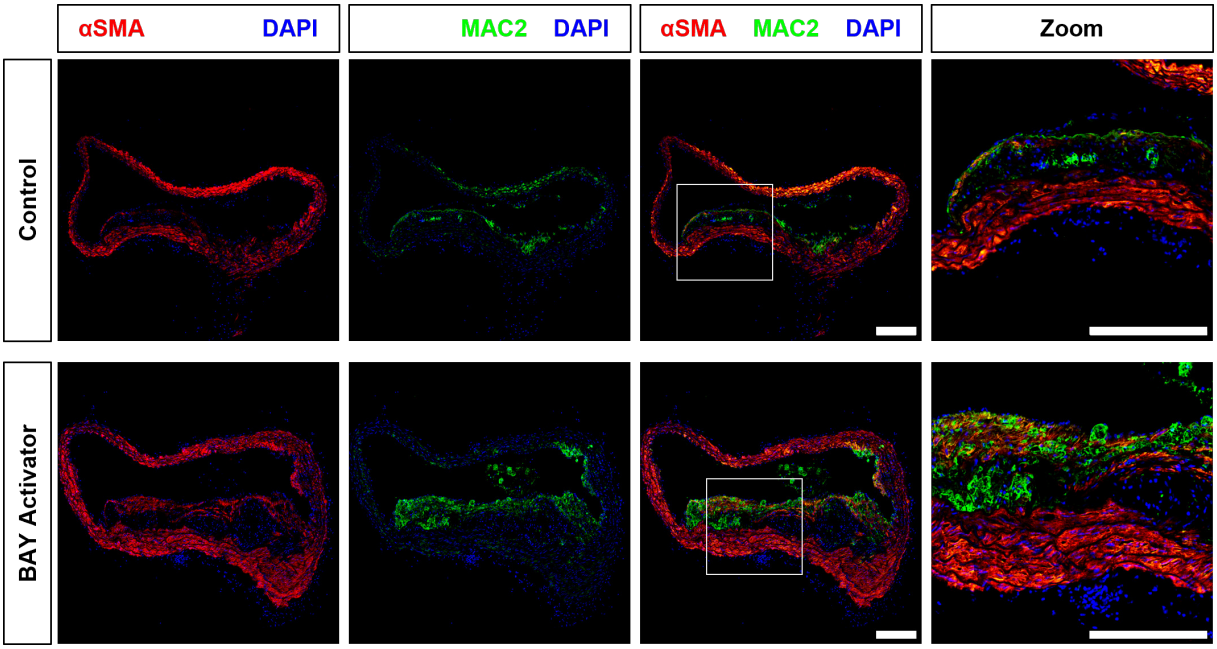

Figure 24. Effect of BAY Activator treatment on plaque composition in the aortic arch.
Analysis of αSMA and MAC2 expression in aortic arch cross sections (10 µm) from ApoE^{ko} mice by immunofluorescence staining after 16 weeks of atherogenic diet. BAY Activator was supplemented at a concentration of 150 ppm into the diet. The panels show (from left to right) immunostaining of αSMA (red), MAC2 (green), and an overlay image. Nuclei are counterstained with DAPI (blue). Boxed regions in overlay images are magnified (Zoom). One representative image of four biological replicates for each experimental group is shown. Scale bars are 200 µm.

In summary, treatment with the BAY Activator resulted in a significant increase in plaque size and MAC2 expression in various examined regions of the aorta, while αSMA expression and collagen content did not show significant changes compared to the control group. However, this MAC2 enrichment correlated with the impact of the BAY Activator on lesion area, prompting questions about the relationship between the two. Could this increased amount of MAC2-positive macrophage-like cells or macrophages be responsible for the enlarged plaque area? The potential influence of BAY Activator treatment on the stability of atherosclerotic plaques in the aortic root has not yet been conclusively clarified. However, the data suggest that there is no significant effect on plaque stability.

3.2 Functional effects of the NO-GC modulators on primary VSMC

The previous results demonstrated a significant increase in the plaque area and a relative enrichment of MAC2 within atherosclerotic plaques following the administration of the BAY

Activator. However, the reasons behind these effects and the relevance of the NO/cGMP signaling pathway in VSMCs in this context remain unclear. To delve deeper into these aspects, isolated pVSMCs were used as an *in vitro* model to analyze the mechanistic aspects in detail. The focus of the study was specifically directed towards investigating the impact of the different NO-GC modulators on intracellular cGMP generation, signal transduction, and VSMC growth.

The FRET-based biosensor cGi500 represents a powerful tool for visualizing and quantifying changes in intracellular cGMP levels in native cells. This biosensor binds cGMP reversibly within the physiological range, allowing the monitoring of drug effects on intracellular cGMP levels in real-time with single-cell resolution [78]. For example, using the cGi500 biosensor, it has already been demonstrated that the natural ligand NO induces cGMP generation in pVSMCs in a concentration-dependent manner [159]. The effect of NO on intracellular cGMP levels in VSMCs was also validated in this study by titrating the NO derivative DEA/NO (**Supplementary figure 7**). This demonstrates the sensitivity and suitability of the cGi500 biosensor for investigating the efficacy of drugs in affecting cGMP levels.

First, the efficacy of BAY Activator and Vericiguat in modulating NO-GC activity in VSMCs was assessed. VSMCs were isolated from transgenic mice ubiquitously expressing the cGi500 biosensor. The cells were cultured for four to five days and serum-starved overnight before FRET/cGMP measurement. Subsequently, cGMP was visualized in VSMCs by analyzing CFP/YFP-FRET changes in response to increasing concentrations (0.001 µM to 10 µM) of the NO-GC modulators. Of note, the quantitative analysis only includes cells that exhibited consistent cGMP generation upon treatment with the specific drug. However, it is important to mention that during the measurement not all cells showed cGMP generation after drug treatment. This observation was not further investigated in detail in this study.

The inflammatory environment within the atherosclerotic plaque is assumed to generate a high degree of oxidative stress [137, 200]. Moreover, it is described that NO-GC activators predominantly act on the NO-insensitive, oxidized or heme-free form of NO-GC [136, 146]. To investigate the impact of oxidative stress on drug efficacy, increasing concentrations (ranging from 0.001 µM to 10 µM) of the BAY Activator were tested under normal conditions (absence of ODQ) or in the presence of the NO-GC-oxidizing agent ODQ to mimic oxidative stress (**Figure 25**). The oxidation status of NO-GC was verified by treating the cells with DEA/NO (50 nM) before and after ODQ preincubation. To ensure comparability, cells under normal conditions were treated also with DEA/NO (50 nM), DMSO (0.1 %, vehicle control) and DEA/NO (50 nM). Indeed, the observed reduction in NO-Induced cGMP generation demonstrated the successful oxidation of the system. However, ODQ treatment was not sufficient to eliminate cGMP generation in response to DEA/NO completely (**Supplementary figure 8 B**). It should be noted that DMSO treatment under normal conditions already slightly decreased the NO signal

compared to the initial DEA/NO application (**Supplementary figure 8 A**). Subsequent application of increasing concentrations of the BAY Activator demonstrated a concentration-dependent increase in intracellular cGMP levels in both native and ODQ-treated VSMCs (**Figure 25 A, C**). Under normal conditions, the BAY Activator led to significant cGMP generation at a concentration of 0.1 µM compared to the DMSO control stimulus (0.1 % DMSO: 0.04 ± 0.01 a.u. versus 0.1 µM BAY Activator: 0.35 ± 0.03 a.u.) (**Figure 25 B**). In contrast, in presence of ODQ, only a concentration of 0.01 µM of BAY Activator was required to achieve a significant cGMP generation (0.1 % DMSO: 0.21 ± 0.02 a.u. versus 0.01 µM BAY Activator: 0.44 ± 0.03 a.u.) (**Figure 25 D**). However, when evaluating the effects of the BAY Activator in the presence of ODQ, it is important to note that the vehicle control (0.1% DMSO) already induced a minor cGMP signal. A calculation of the EC_{50} value was not possible because saturating concentrations of BAY Activator could not be achieved under both conditions.

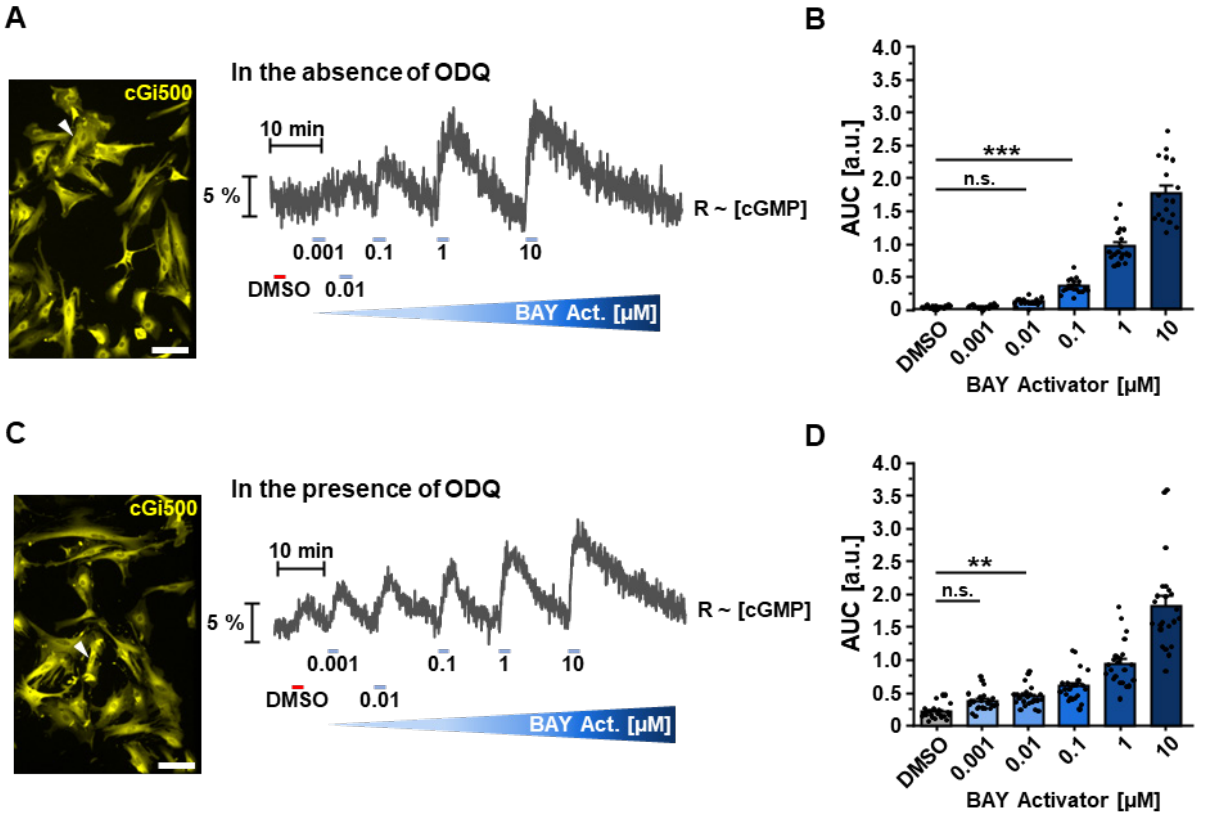

Figure 25. Effect of BAY Activator treatment on intracellular cGMP levels in primary VSMCs.
FRET-based cGMP imaging was performed in aortic pVSMCs. VSMCs were isolated from cGi-L1 mice (expressing the cGi500 biosensor globally) and cultured on coverslips for 5-6 days. **(A, C)** Representative cGMP measurement of VSMCs to analyze the concentration dependent effect of BAY Activator (BAY Act.) in the absence **(A)** or presence **(C)** of ODQ. VSMCs were visualized by the YFP fluorescence (yellow) of cGi500 (left). The change of intracellular cGMP levels over time (grey, ratio trace "R" ~ [cGMP]) following BAY Activator treatment was detected (right, cGMP response pattern of one representative VSMC). The percent change of the ratio trace compared to the baseline ("ΔR/R") is indicated. White arrowheads indicate the VSMC represented by the ratio trace in the right panel. During the measurement, cells were treated with DMSO (0.1 %, vehicle control) and increasing concentrations of BAY Act. (0.001 µM to 10 µM) for 2 min each. Cells were preincubated with ODQ (20 µM, 7min) or DMSO (0.1 %, 7 min) beforehand. **(B, D)** Statistical analysis was performed using the area under the curve (AUC) of the signals. Each dot represents an individual VSMC. Data are represented as mean + SEM (absence of ODQ: 18 cells; presence of ODQ: 23 cells). Statistical significance is indicated by asterisk (*p ≤ 0.05; **p ≤ 0.01; ***p ≤ 0.001; n.s.: not significant, One-Way repeated measures ANOVA followed by post-hoc Bonferroni test). One representative measurement of three biological replicates is shown. Scale bars are 100 µm. BAY Act., BAY Activator; AUC, area under the curve.

Similar to the investigation of the BAY Activator, the efficacy of Vericiguat in modulating NO-GC activity in VSMCs was examined. To evaluate this, VSMCs were exposed to increasing concentrations of Vericiguat after an initial DMSO application. Since NO-GC stimulators are assumed to act exclusively on NO-sensitive, heme-containing NO-GC, the efficacy of Vericiguat was analyzed only under normal conditions [145]. As with the BAY Activator, a concentration-dependent effect on intracellular cGMP levels was observed also for Vericiguat (**Figure 26 A**). At a concentration of 1 µM Vericiguat, a significant effect on intracellular cGMP levels was observed (0.1 % DMSO: 0.04 ± 0.01 a.u. versus 1 µM Vericiguat: 0.44 ± 0.03 a.u.) (**Figure 26 B**). Note that in these experiments, saturating concentrations of vericiguat were not reached, making the calculation of the EC_{50} impossible.

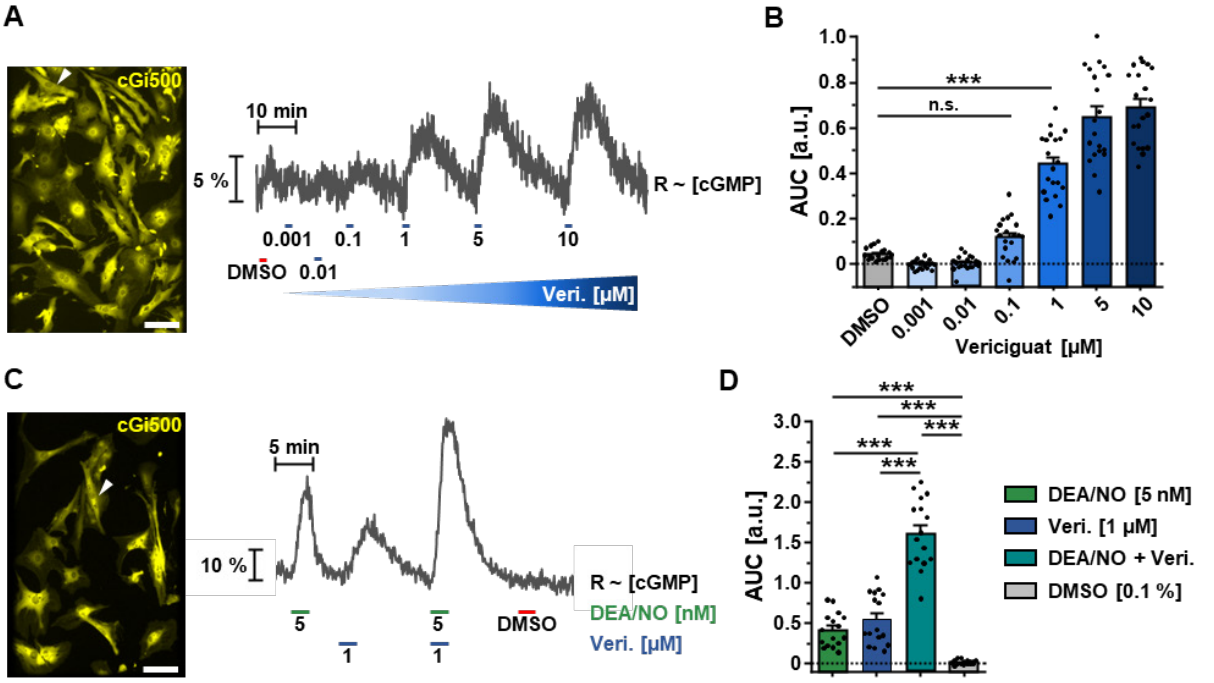

Figure 26. Effect of Vericiguat treatment on intracellular cGMP levels in primary VSMCs.
FRET-based cGMP imaging was performed in aortic pVSMCs. VSMCs were isolated from cGi-L1 mice (expressing the cGi500 biosensor globally) and cultured on coverslips for 5-6 days. **(A, C)** Representative cGMP measurement of VSMCs to analyze the concentration dependent **(A)** and synergistic **(C)** effect of Vericiguat (Veri.). VSMCs were visualized by the YFP fluorescence (yellow) of cGi500 (left). The change of intracellular cGMP levels over time (grey, ratio trace "R" ~ [cGMP]) following treatment was detected (right, cGMP response pattern of one representative VSMC). The percent change of the ratio trace compared to the baseline ("ΔR/R") is indicated. White arrowheads indicate the VSMC represented by the ratio trace in the right panel. To analyze the concentration-dependent effect of Vericiguat, cells were treated with DMSO (0.1 %, vehicle control) and increasing concentrations of Veri. (0.001 µM to 10 µM) for 2 min each. To analyze the synergistic effect of Veri. cells were treated with DEA/NO (5 nM), Veri (1 µM), the combination of both and DMSO (0.1 %, vehicle control) for 2 min each. **(B, D)** Statistical analysis was performed using the area under the curve (AUC) of the signals. Each dot represents an individual VSMC. Data are represented as mean + SEM (Veri. titration: 20 cells; Synergism analysis: 23 cells). Statistical significance is indicated by asterisk (*p ≤ 0.05; **p ≤ 0.01; ***p ≤ 0.001; n.s.: not significant, One-Way repeated measures ANOVA followed by post-hoc Bonferroni test). One representative measurement of at least three biological replicates is shown. Scale bars are 100 µm. Veri., Vericiguat; AUC, area under the curve.

NO-GC stimulators, such as Vericiguat, exhibit a dual mechanism of action. They can stimulate NO-GC activity both independently and synergistically with the natural ligand NO [136, 201]. To analyze the synergistic effects of Vericiguat and NO, both substances (Vericiguat and DEA/NO) were applied individually or in combination, and cGMP levels in VSMCs were

monitored. The concentrations used were selected based on the titrations of DEA/NO and Vericiguat (**Figure 26 B**, **Supplementary figure 7 B**). To prevent system saturation, for each substance a concentration within the dynamic range of the drug efficacy, and thus close to the presumed EC50 concentration, was used to investigate the potentiating effect of the combination. In line with the previous experiments, DEA/NO (5 nM) and Vericiguat (1 µM) alone induced robust, but non-saturated cGMP generation (AUC of 0.1 % DMSO: 0.014 ± 0.01 a.u. versus DEA/NO: 0.41 ± 0.05 a.u. or Veri.: 0.55 ± 0.08 a.u.) (**Figure 26 C, D**). Combined treatment of VSMCs with both substances, however, induced significantly stronger cGMP generation than compared to the single applications (AUC of control: 0.014 ± 0.01 a.u. versus DEA/NO + Veri.: 1.61 ± 0.11 a.u.). This result is further supported by an additional control measurement, which demonstrated the absence of the potentiating effect when DEA/NO is combined with DMSO (0.1 %, drug vehicle) (**Supplementary figure 9**).

Taken together, FRET microscopy of pVSMCs showed a concentration dependent cGMP generation in response to Vericiguat treatment. In addition, the data indicated the capacity of Vericiguat to potentiate endogenous NO-induced cGMP signaling.

Both NO-GC modulators induced concentration-dependent cGMP generation in pVSMCs. Subsequently, the signal transduction of the cGMP signals generated by the NO-GC modulator treatment was examined on the effector level. The VASP phosphorylation assay was used to monitor the activity of the effector protein cGKI. The working principle of this assay is shown in **Figure 27 A**. The assay is based on the premise that modulation of NO-GC activity, either through NO or NO-GC modulators, leads to cGMP generation, which subsequently activates cGKI to phosphorylate VASP. Moreover, cGKI activity can be directly stimulated with the cell-permeable cGMP analog 8-Br-cGMP. The changes in the phosphorylation status of VASP were then analyzed using Western blot analysis. It is important to note, that migration of VASP in SDS-PAGE is influenced by its phosphorylation status, with unphosphorylated VASP migrating at 45 kDa, while VASP phosphorylated by cGKI migrates at 50 kDa.

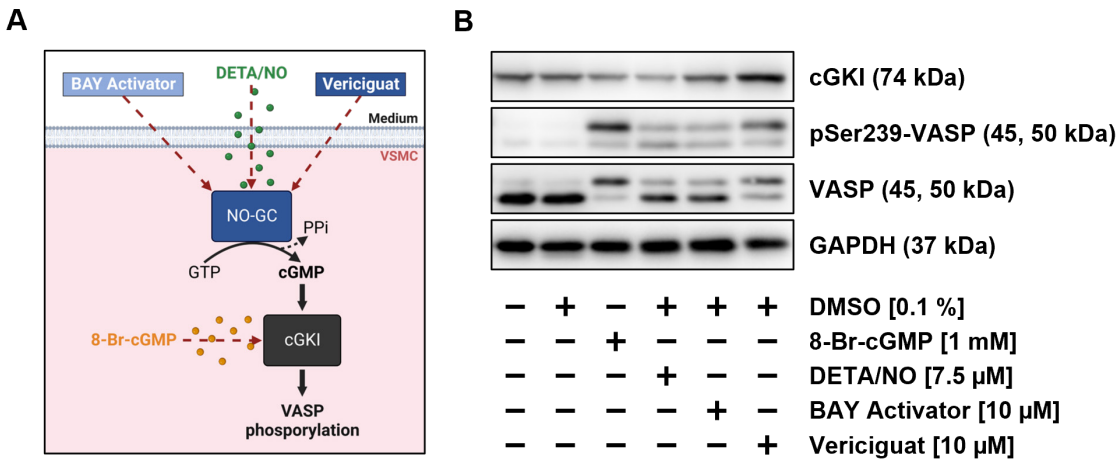

Figure 27. Analysis of VASP phosphorylation in primary VSMCs following BAY Activator and Vericiguat treatment.
VASP phosphorylation assay to analyze transduction of the cGMP signals generated by BAY Activator and Vericiguat treatment. **(A)** Schematic representation of the working principle of the VASP phosphorylation assay. Activation of NO-sensitive guanylyl cyclase (NO-GC) in vascular smooth muscle cells (VSMCs) by the NO-derivative DETA/NO or NO-GC modulators (Vericiguat and BAY Activator) leads to generation of the second messenger cyclic guanosine monophosphate (cGMP) by converting guanosine triphosphate (GTP). Subsequently, cGMP triggers downstream cGMP-dependent protein kinase (cGKI) to phosphorylate the vasodilator-stimulated phosphoprotein (VASP). cGKI activity can also be directly stimulated with the cell-permeable cGMP analog 8-Br-cGMP. Red dashed arrows indicate the different options to modulate cGKI activity. Image created using BioRender.com. **(B)** Western blot analysis of VASP phosphorylation status after modulation of the NO/cGMP signaling axis. VSMCs were isolated from wildtype mice. VSMCs were incubated with vehicle DMSO (0.1 %), cell-permeable cGMP analog 8-Br-cGMP (1 mM), NO donor DETA/NO (7.5 µM), BAY Activator (10 µM) or Vericiguat (10 µM) prior to protein extraction. Levels of cGKI, VASP and pSer239-VASP, and GAPDH (loading control) expression were analyzed by Western blot (n = 1 Western Blot). The expected molecular weights of the respective target proteins are indicated. PPi, pyrophosphate.

pVSMCs from wildtype mice were cultured for seven days and subjected to an additional two days of serum starvation. Then, VSMCs were stimulated with DETA/NO (7.5 µM), BAY Activator (10 µM), and Vericiguat (10 µM) prior to Western blot analysis. Control conditions involved treatment with DMSO (0.1 %) or 8-Br-cGMP (1 mM). Since cGKI preferentially phosphorylate VASP at Ser239, a phospho-VASP (Ser239)-specific antibody was used in addition to a total VASP antibody. Treatment with DMSO did not result in increased VASP phosphorylation compared to the unstimulated condition. In contrast, treatment with 8-Br cGMP led to phosphorylation of almost the complete VASP protein pool. Also, treatment with DETA/NO and the NO-GC modulators (BAY Activator and Vericiguat) increased VASP phosphorylation compared to the control condition (**Figure 27 B**). These results demonstrated that the modulatory effect of BAY Activator and Vericiguat on NO-GC activity in pVSMCs was transmitted to the effector protein level.

Previous studies have demonstrated that the activation of the NO/cGMP signaling pathway promotes the growth of pVSMCs in culture. Moreover, this growth-promoting effect has been attributed to the activation of the NO-GC/cGMP/cGKI signaling axis [92, 93, 159]. As our study has already confirmed that BAY Activator and Vericiguat activate the NO-GC/cGMP/cGKI signaling axis, we aimed to investigate the impact of these NO-GC modulators on VSMC growth. The effects of the NO-GC modulators were evaluated using the xCELLigence system, which

allowed the real-time monitoring of cell growth. The typical growth behavior of cultured pVSMCs on xCELLigence microtiter well plates is described in **Section 2.3.2**. This essentially includes adhesion after approx. 30 hours, transition to the proliferation phase via undefined mix phase, followed by exponential growth until confluence is reached (plateauing). Based on previous studies, the time point after 72 hours was defined for analyzing the effects of the NO-GC modulators on pVSMC growth [159]. Since the drugs were added to the cell suspension from the beginning, this time point encompasses the effects on both adhesion and proliferation. Therefore, the overall effect on cell growth was investigated, without considering the two phases separately.

pVSMCs were isolated from wildtype mice and seeded into an xCELLigence plate in the absence (Ctrl) or presence of BAY Activator (0.1 µM), Vericiguat (1 µM), and/or DETA/NO (2.5 µM). The concentration of DETA/NO was chosen based on previous research [93, 159]. The concentration-dependent biphasic effect of DETA/NO, which promotes growth at low concentrations and suppresses growth at high concentrations, was also confirmed in this study (**Supplementary figure 10 A, B**). Based on these findings, a concentration of 2.5 µM DETA/NO was selected as the test concentration for stimulating growth. Note that all tested conditions included DMSO (0.1 %), which did not affect VSMC growth behavior (**Supplementary figure 10 C**). As expected from previous data, DETA/NO treatment demonstrated a growth-promoting effect on pVSMCs. Both the BAY Activator and Vericiguat significantly stimulated growth compared to the control (**Figure 28**). Upon comparing the effects of BAY Activator and Vericiguat treatments relative to their respective controls after 72 hours, it was observed that treatment with the BAY Activator exhibited a twofold promoting effect on VSMC growth, whereas Vericiguat demonstrated a 1.5-fold promoting effect (**Figure 28 A, B (right)**). To analyze the synergistic effect of Vericiguat and DETA/NO on VSMC growth, cells were also treated with the combination of both substances. Compared to the single treatments, the combination exhibited a strong effect on VSMC growth behavior after 72 hours (**Figure 28 B**). Additionally, the real-time measurement indicated that stimulation with the combination may lead to earlier cell attachment and consequently an earlier start of VSMC growth (**Figure 28, B (left)**). These data showed that modulation of the NO/cGMP signaling axis using BAY Activator and Vericiguat promoted pVSMC growth. The combination of Vericiguat with DETA/NO further enhanced this effect.

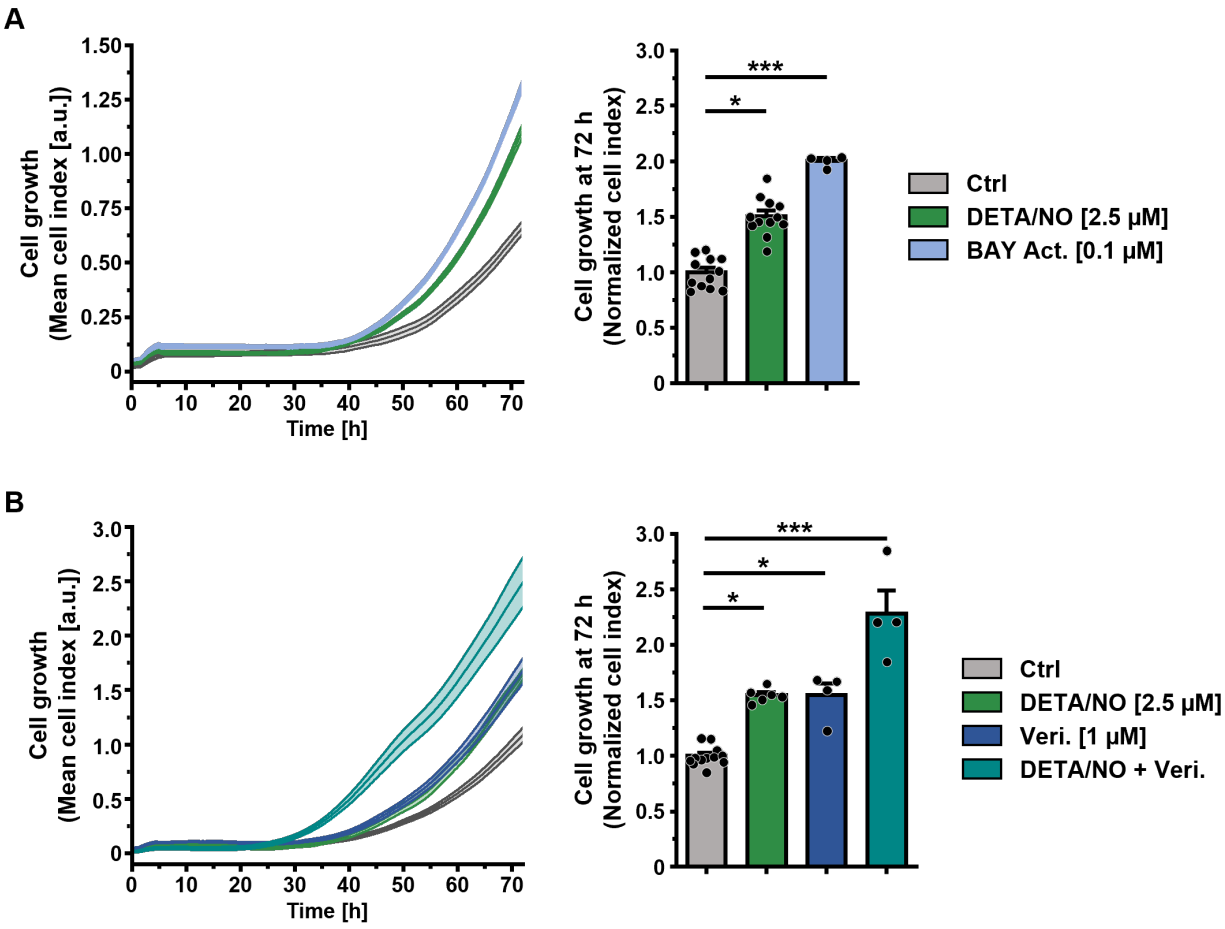

Figure 28. Effects of BAY Activator or Vericiguat on primary VSMC growth.
Real-time measurement of VSMC growth was performed using the xCELLigence system. pVSMCs isolated from wildtype mice were seeded in the absence (Ctrl) or presence of the NO donor DETA/NO (2.5 µM) and/or NO-GC modulators (BAY Act. or Veri., 1 µM). All conditions included 0.1 % DMSO (drug vehicle). The cell growth was analyzed in real-time (A-B, left panels) and after 72 h (A-B, right panels). Based on previous studies, the 72 h time point was used to analyze the effects on both cell adhesion and proliferation [159]. **(A)** Analysis of the VSMC growth behavior after BAY Act. treatment (Ctrl: 12 wells, DETA/NO: 12 wells, BAY Act.: 4 wells). **(B)** Analysis of the VSMC growth behavior after Veri. treatment. VSMCs were treated with a combination of DETA/NO (2.5 µM) and Veri (1 µM) (Ctrl: 12 wells, DETA/NO: 6 wells, Veri.: 4 wells; DETA/NO + Veri.: 4 wells). Data are represented as mean ± SEM for the real-time growth curves and as mean + SEM for the bar graph. Statistical significance is indicated by asterisks (*p ≤ 0.05; **p ≤ 0.01; ***p ≤ 0.001; n.s.: not significant, Kruskal-Wallis ANOVA with Dunn's post hoc test). One representative measurement of three biological replicates is shown. Ctrl, Control, BAY Act., BAY Activator, Veri., Vericiguat.

In summary, the combination of FRET/cGMP measurements, VASP phosphorylation assay and VSMC growth analysis suggests that the increase in cGMP generation induced by BAY Activator or Vericiguat treatment may lead to altered VSMC growth behavior.

3.3 Smooth muscle cell specific genetic modulation of the NO/cGMP signaling pathway in a mouse model of atherosclerosis

Up to this point, the present study has shown that the pharmacological modulation of the NO/cGMP signaling pathway with the BAY Activator has a strong impact on atherosclerosis. However, this systemic approach complicates the interpretation of the results, specifically regarding the involvement of VSMCs in this effect. To address this issue, a genetic mouse model can be employed, that allows the time- and tissue-specific inactivation of the functional NO-

GC (conditional knockout). Such a genetic ablation model has already been used to study the role of NO/cGMP signaling axis in VSMCs for atherosclerosis on effector protein level [93, 118]. To gain further insights into the relevance of the NO/cGMP signaling axis in VSMCs for atherosclerosis, the present study used a conditional VSMC-specific knockout of the NO-GC β1 subunit leading to the destruction of a functional NO-GC enzyme. This genetic mouse model also provides an opportunity to evaluate the specificity of the BAY Activator-mediated effects on the modulation of the NO/cGMP pathway in VSMCs.

For conditional knockout of NO-GC specifically in VSMCs a tamoxifen-inducible Cre/loxP recombination system was used. ApoE^{ko} mice expressing the inducible CreER^{T2} recombinase under the control of the αSMA promoter were crossbred with ApoE^{ko} mice carrying floxed NO-GC alleles. The cell-specific knockout was induced by intraperitoneal injection of tamoxifen (5 x 1 mg/mouse/day) at 8 and 10 weeks of age. To eliminate potential confounding factors, all experimental mice, including the controls, were treated with tamoxifen. Subsequently, SMC-specific NO-GC knockout (NO-GC^{smko}) and control (Ctrl) mice were fed an atherogenic diet for 18 weeks (**Figure 12**). After the development of atherosclerotic plaques, the effects of the SMC-specific deletion of NO-GC on atherogenesis and physiological parameters were analyzed. All experimental groups, genotypes, and performed analyses are listed in **Supplementary table 1**. For further details on the experimental setup, see **Section 2.5.1**.

3.3.1 Analysis of the efficiency and SMC-specific deletion of NO-GC

Before analyzing the effects of the SMC-specific NO-GC knockout on atherosclerosis, we initially characterized the recombination efficiency and tissue specificity of the SMA-CreER^{T2}-mediated NO-GC knockout. The working principle of SMA-CreER^{T2}, which generates SMC-specific deletion of NO-GC, is illustrated in **Figure 29 A** (left panel). The expression of CreER^{T2} is controlled by the αSMA promoter to ensure cell type specificity. Following two rounds of tamoxifen injection, the metabolized 4-hydroxytamoxifen (4-OHT) binds to CreER^{T2}, enabling the recombinase to translocate from the cytosol into the nucleus. In the case of SMC-specific NO-GC knockout, the exon 10 of Gucy1b1 flanked by two loxP-sites is then excised by recombinase activity, resulting in the disruption of the expression of the NO-GC in VSMCs.

The efficiency of the recombinase activity was validated by immunofluorescence staining of frozen aortic sections from control and NO-GC^{smko} mice, isolated five weeks post-tamoxifen injection (fed with normal diet). The expression of NO-GC in the aortic media was examined using a ß1 subunit-specific antibody. In the control aorta (Ctrl), high NO-GC expression was detected in the media, as previously described for healthy/wildtype conditions (**Section 3.1.1**). In contrast, the expression of NO-GC was almost completely abolished in the aorta of the NO-GC^{smko} mouse (**Figure 29 A**). These results indicate a remarkably efficient recombination mediated by SMA-CreER^{T2} in the experimental mice.

In addition, the tissue specificity of the Cre-mediated recombination in the experimental mice was examined using Western blot analysis. Atherosclerotic aortas, brains and hearts were isolated from control (Ctrl, Cre-Ctrl) and NO-GC^{smko} mice at the end of the 18 weeks feeding period of the atherogenic diet. The expression of NO-GC in protein lysates was subsequently analyzed. In all three tissues, no differences in NO-GC expression were observed between the control groups (**Figure 29 B**). The NO-GC expression in the brain and heart lysates of the NO-GC^{smko} mouse was identical to that of the control. However, a significant reduction in NO-GC expression was observed in the lysate of the atherosclerotic aorta from the NO-GC^{smko} mouse compared to the lysates of the brain and heart. This suggests a tissue-specific reduction in NO-GC expression. Additionally, a comparison between control and NO-GC^{smko} mice confirmed the strong efficiency of SMA-CreER^{T2} in deleting NO-GC in atherosclerotic aortas.

Altogether, the results verified a highly efficient deletion of the NO-GC expression in the aortas of NO-GC^{smko} experimental mice.

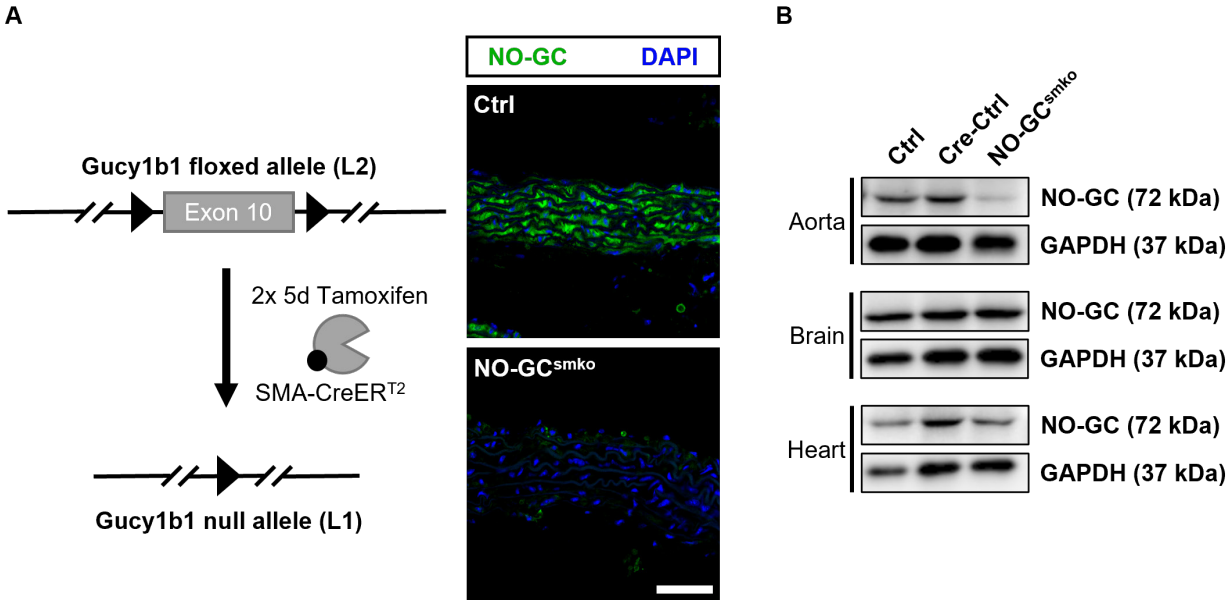

Figure 29. Efficiency of SMC-specific NO-GC deletion in NO-GC^{smko} mice.
SMC-specific NO-GC knockout (NO-GC^{smko}) and control mice (Ctrl, Cre-Ctrl) were bred on an ApoE-deficient background. The mice were treated with tamoxifen to induce the SMC-specific NO-GC knockout. Intraperitoneal tamoxifen injections occurred in two cycles, each for five consecutive days (5 x 1 mg/mouse/day) with a nine-day break in between. The efficiency of the SMC-specific knockout was evaluated by immunofluorescence staining and Western blot. **(A)** Left panel: Schematic representation of the Gucy1b1 allele before (top) and after (bottom) SMA-CreER^{T2}-dependent recombination. Before Cre-mediated recombination, Exon 10 of both alleles is flanked by loxP sites (triangle) ("L2"). After Cre recombination, Exon 10 is excised ("L1", only one loxP remains), which finally leads to a disruption of the β1 subunit of NO-GC. Right panels: Representative images of the immunofluorescence staining of frozen aortic sections (10 µm) of Ctrl and NO-GC^{smko} mice. Immunofluorescence staining was performed 5 weeks after tamoxifen treatment. The panels show immunostaining of NO-GC (green) and nuclei (DAPI, blue). Scale bar, 50 µm. **(B)** Verification of SMC-specific NO-GC deletion in atherosclerotic aorta by Western blot analysis after 18 weeks of atherogenic diet. The two cycles of tamoxifen injection were applied at 8 and 10 weeks of age, with a nine-day break in between cycles and before switching to the atherogenic diet. NO-GC and GAPDH (loading control) expression were analyzed in protein lysates of the aorta, brain, and heart of NO-GC^{smko} and control mice (Ctrl, Cre-Ctrl) (n = 1 Western Blot). The expected molecular weights of the respective target proteins are indicated.

3.3.2 Impact of SMC-specific NO-GC deletion on atherosclerotic lesions formation

To assess the impact of SMC-specific ablation of NO-GC expression on the progression of atherosclerosis, atherosclerotic aortas from NO-GC^{smko} and control mice were isolated after 18 weeks of atherogenic diet, and the size of the lesion areas were compared. To visualize atherosclerotic lesions, the aortas were stained with Oil Red O. As already described in **Section 3.1.2**, lesion areas were documented from both sides of the aortas and then quantified separately for the aortic arch and thoracic/abdominal aorta to account for potential differences in plaque development. The plaque area was normalized to the total area of each respective part. Since sex-specific differences cannot be ruled out, lesion areas were analyzed separately for both sexes. Due to the limited number of mice and high variation within the experimental groups, the two control groups (Ctrl, Cre-Ctrl) were pooled from this point after statistical verification. Oil Red O staining resulted in a distinct red coloring, thus allowing easy identification of atherosclerotic plaques within the aortas (**Figure 30 A (male)**; **Supplementary figure 11 A (Female)**). Atherosclerotic plaques were consistently observed in the aortic arch and at branching vessels across all experimental groups. Notably, large parts of the vessel wall within the aortic arch (male, Ctrl: 41.6 ± 5.3 % vs. NO-GC^{smko}: 52.3 ± 6.6 %) were covered by atherosclerotic lesions in control and NO-GC^{smko} male mice (**Figure 30 B).** In comparison, a relatively smaller but still distinct lesion area was detected in the thoracic/abdominal aorta of these mice (male, Ctrl: 15.1 ± 3.1 % vs. NO-GC^{smko}: 28.2 ± 4.5 %). Similar results were observed in female mice for both the aortic arch (female: Ctrl: 46.5 ± 7.4 % vs. NO-GC^{smko}: 54.6 ± 3.8 %) and the thoracic/abdominal aorta (female: Ctrl: 11.2 ± 4.5 % vs. NO-GC^{smko}: 19.2 ± 4.0 %) (**Supplementary figure 11 B**). However, the slight differences in the size of the lesion area between the control and NO-GC^{smko} mice of both sexes in either the aortic arch or the thoracic/abdominal aorta were not statistically significant (**Figure 30 B**; **Supplementary figure 11 B**). But it should be noted that at least a trend toward an increased lesion area due to SMC-specific NO-GC knockout was observed in the aortic arch and thoracic/abdominal aorta for both sexes. This trend was more pronounced in male mice than in female mice, suggesting a potential sex-specific difference. Nevertheless, the sample size in this experiment was insufficient to further investigate this observation in detail and draw meaningful conclusions.

Overall, the data demonstrated that SMC-specific deletion of NO-GC did not significantly affect lesion areas size in atherosclerotic aortas. Although a trend towards increased lesion area was observed, the differences between control and NO-GC^{smko} mice of both sexes were not statistically significant. However, the absence of statistical significance might be caused by the limited number of experimental animals and the substantial variation within the experimental groups.

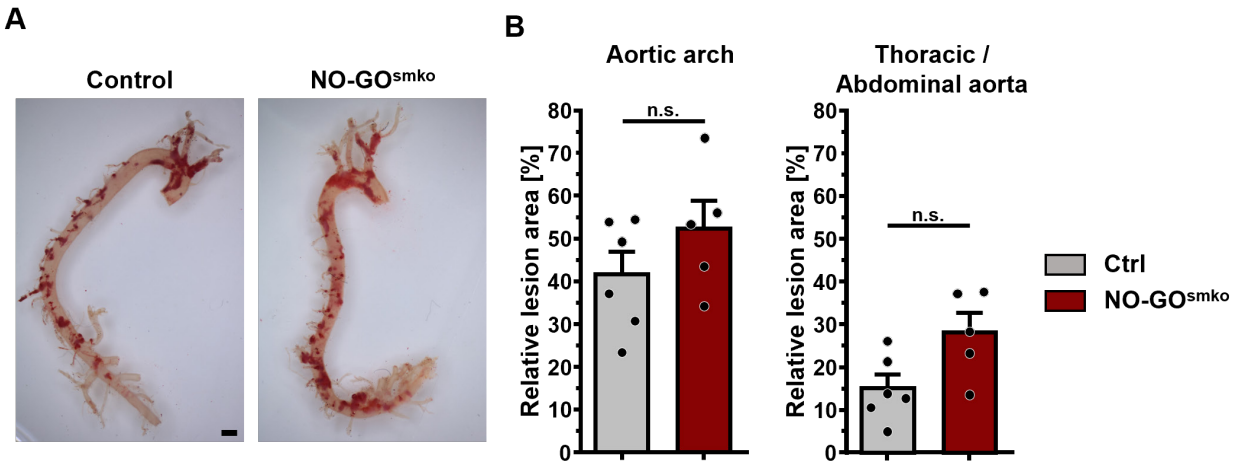

Figure 30. Effect of SMC-specific ablation of NO-GC on atherosclerotic lesion area in male mice.
Analysis of atherosclerotic lesion area in aortas from SMC-specific NO-GC knockout (NO-GC^{smko}) and control mice (Ctrl) mice by Oil Red O staining after 18 weeks feeding of an atherogenic diet. NO-GC^{smko} and Ctrl mice were bred on an ApoE-deficient background. The mice were treated with tamoxifen to induce the SMC-specific NO-GC knockout. Intraperitoneal tamoxifen injections occurred in two cycles, each for five consecutive days (5 x 1 mg/mouse/day) at 8 and 10 weeks of age with a nine-day break in between and before switching to atherogenic diet. **(A)** Representative images of Oil Red O-Stained atherosclerotic aortas of control (Ctrl; Cre-ctrl and Ctrl mice were pooled) and NO-GC^{smko} male mice. Atherosclerotic lesions appear red. Scale bars are 1 mm. **(B)** Relative lesion area of the aortic arch or thoracic/abdominal aorta of Ctrl and NO-GC^{smko} male mice. The atherosclerotic lesion area was determined from both sides of the aorta, averaged, and normalized to the total area of respective part. Data are represented as mean + SEM (Ctrl: 6 mice, NO-GC^{smko}: 5 mice). No statistically significant differences were found (n.s.: not significant, Mann-Whitney U test). Ctrl, Control, NO-GC^{smko}, SMC-specific NO-GC knockout.

3.3.3 Impact of SMC-specific NO-GC deletion on physiological parameters

The NO/cGMP signaling pathway in VSMCs is essential for maintaining vascular function, including vasorelaxation and the regulation of vascular tone. Disruption of this pathway by genetic ablation of the central enzyme potentially impacts these physiological functions, thereby influencing the progression of atherosclerosis. Consequently, various physiological parameters, such as blood pressure and plasma lipid levels were examined to assess the potential effects of VSMC-specific NO-GC deficiency.

Previous studies have already reported that both global and SMMHC-CreER^{T2}-mediated SMC-specific knockout of the NO-GC β1 subunit leads to an increase in systolic blood pressure in male mice [94, 123]. This knockout-induced increase in blood pressure could potentially promote atherosclerosis. Therefore, the blood pressure of control and NO-GC^{smko} mice was measured using a tail-cuff blood pressure system at the end of the feeding period.

Although not statistically significant, a noticeable trend towards increased systolic (male, Ctrl: 108.5 ± 7.2 mmHg vs. NO-GC^{smko}: 135.7 ± 3.0 mmHg) and diastolic (male, Ctrl: 82.2 ± 6.5 mmHg vs. NO-GC^{smko}: 99.5 ± 2.5 mmHg) blood pressure was observed in the NO-GC^{smko} mice compared to the control group (**Figure 31**). In female mice, a similar effect of the SMC-specific ablation of NO-GC on systolic (female, Ctrl: 117.0 ± 7.1 mmHg vs. NO-GC^{smko}: 142.9 ± 7.3 mmHg) and diastolic (female, Ctrl: 82.6 ± 4.5 mmHg vs. NO-GC^{smko}: 110.2 ± 5.7 mmHg) blood pressure was detected (**Supplementary figure 12**). In principle, the lack of statistical

significance could be due to the limited number of animals and the high variation within the experimental groups. To investigate the NO-GC^{smko} effects with an increased sample size, the data from male and female control or NO-GC^{smko} mice were pooled following a prior statistical verification. The trend of an elevated blood pressure in NO-GC^{smko} versus controls observed in both sexes became significant when the data of both sexes were pooled (**Figure 35 B**). This increase of around 22 mmHg in mean blood pressure (Ctrl: 92.3 ± 4.0 mmHg vs. NO-GC^{smko}: 114.8 ± 2.9 mmHg) should be considered, as it may affect atherosclerosis.

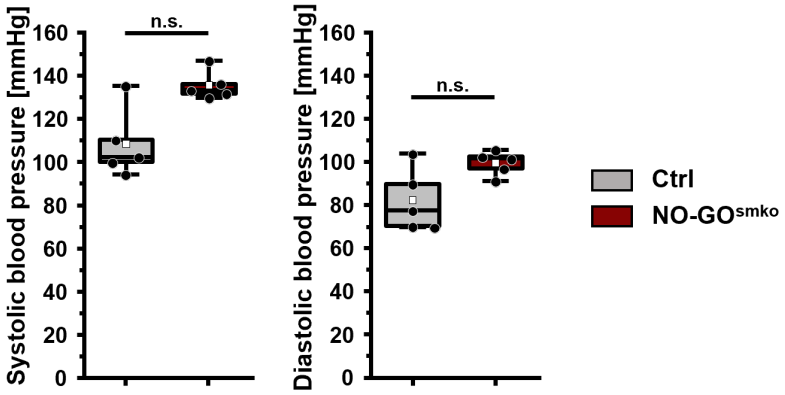

Figure 31. Impact of SMC-specific NO-GC knockout on blood pressure male mice.
Systolic and diastolic blood pressure in SMC-specific NO-GC knockout (NO-GC^{smko}) and control (Ctrl) male mice. The mice were bred on an ApoE-deficient background and fed with an atherogenic diet for 18 weeks. The mice were treated with tamoxifen to induce the SMC-specific NO-GC knockout. Intraperitoneal tamoxifen injections occurred in two cycles, each for five consecutive days (5 x 1 mg/mouse/day) at 8 and 10 weeks of age with a nine-day break in between and before switching to an atherogenic diet. The blood pressure was measured at the end of the feeding period over three consecutive days using a tail-cuff blood pressure system. The data of the three consecutive days were averaged for each animal. Data are represented as median (horizontal line), 25% - 75% interquartile range (box), 5% - 95% range percentile (whiskers) and mean (white square) (Ctrl: 6 mice, NO-GC^{smko}: 3 mice). No statistically significant differences were found (n.s.: not significant, Mann-Whitney U test). Ctrl, Control, NO-GC^{smko}, SMC-specific NO-GC knockout.

All additionally analyzed physiological parameters are listed in **Table 12**. The plasma lipid levels of the experimental mice were examined in collaboration with the “Zentrallabor” of the University of Tubingen. Blood samples were collected from the mice at the end of the 18-week feeding period. Mice on a high-fat diet exhibited elevated plasma cholesterol and LDL levels compared to the normal diet control group, indicating the intake of the atherogenic diet similar to the experimental mice shown in **Table 11**. None of the analyzed lipids showed significant differences between the control and NO-GC^{smko} mice between the sexes. A slight difference was observed in lipid levels after 18 weeks of atherogenic diet between NO-GC^{smko} mice and their respective controls of each sex. However, this difference was not statistically significant. After pooling data from male and female mice following prior statistical verification to increase the sample size, statistically significant differences in plasma lipid levels (e.g., total cholesterol) were observed between NO-GC^{smko} and control groups (**Figure 35 C**). Furthermore, body weight before and after the atherogenic diet feeding period, as well as organ weight, were examined. No significant differences were found between the control and NO-GC^{smko} mice of the same sex. However, sex had a notable impact on body weight, with female mice being

significantly lighter than male mice throughout the experiment. Moreover, weight gain was observed in all experimental groups over the 18-week feeding period. Nevertheless, the extent of weight gain varied between both sexes. On average, males gained approx. 15 g, while females only gained around 6 g.

Table 12. Physiological parameters of mice after atherogenic diet for 18 weeks.
Listed are the plasma lipid parameters of control and NO-GC^{smko} mice fed a normal diet (Ctrl n.d.) or atherogenic diet plus tamoxifen treatment (Ctrl and NO-GC^{smko}). Blood was collected from mice at the end of the atherogenic diet feeding period (18 weeks) in the morning. The experimental mice were not starved before sampling. Controls (Ctrl.): values from Ctrl and Cre-Ctrl mice were pooled. The lipid parameters were measured in collaboration with Prof. Dr. med. A. Peter (University Hospital Tubingen). All data are represented as mean ± SEM. Ctrl, Control; NO-GC^{smko}, SMC-specific NO-GC knock-out; n.d., normal diet; LDL, low-density lipoprotein.

Parameter	n.d.	Atherogenic diet			
	Male	Male		Female	
	Ctrl n.d.	Ctrl	NO-GC^{smko}	Ctrl.	NO-GC^{smko}
Number of mice	3	6	5	7	3
Total Cholesterol [mg/dL]	81.7 ± 6.7	1546.3 ± 294.4	2027.0 ± 142.0	1667.9 ± 116.9	2226.7 ± 63.3
Triglyceride [mg/dL]	125.0 ± 10.4	171.3 ± 47.2	223.0 ± 50.4	120 ± 13.0	163.3 ± 8.8
LDL [mg/dL]	8.3 ± 1.7	231.3 ± 52.1	329.0 ± 20.0	302.9 ± 27.6	391.7 ± 3.3
Number of mice	-	6	5	7	3
Body weight start [g]	-	30.7 ± 1.7	28.1 ± 1.1	22.7 ± 0.4	21.9 ± 0.3
Body weight end [g]	-	45.8 ± 1.4	44.3 ± 2.4	28.8 ± 1.0	27.7 ± 2.0
Liver-to-body weight [mg/g]	-	73.5 ± 4.9	67.1 ± 5.5	59.0 ± 4.0	63.0 ± 4.2
Heart-to-body weight [mg/g]	-	4.4 ± 0.2	4.7 ± 0.1	6.0 ± 0.3	5.4 ± 0.5
Kidney-to-body weight [mg/g]	-	5.1 ± 0.2	5.1 ± 0.3	5.7 ± 0.5	5.7 ± 0.5

Overall, similar to **Section 3.3.2**, the data indicate that the number of mice per sex in this experiment was not sufficient to clearly infer the effects of SMC-specific NO-GC deletion on physiological parameters. After pooling data from male and female mice, a significant increase in blood pressure by approximately 25 mmHg and an elevation in distinct plasma lipid levels in the SMC-specific NO-GC knockout compared to control mice were observed. This suggests that atherogenesis in this model is influenced by various parameters directly or indirectly associated with the deletion of NO-GC in smooth muscle cells. In order to gain meaningful insights, it is essential to increase the sample size.

4. Discussion

In VSMCs, the NO/cGMP signaling axis plays a central role in regulating several essential physiological functions, such as vascular relaxation, VSMC growth, and differentiation [90, 92, 93, 155]. This signaling axis has also been extensively studied in the context of atherosclerosis, providing solid evidence of its functional relevance in atherogenesis [70, 93, 155]. It has been suggested that the NO/cGMP signaling pathway might play a role in VSMC phenotypic modulation/transdifferentiation and has an effect on plaque composition [155]. However, many critical questions have remained unanswered in these previous studies. In particular, the discrepancy in results obtained by genetic or pharmacological modulation of the NO/cGMP signaling pathway *in vivo* has raised questions about its role in atherosclerosis and the involvement of phenotypic modulation of VSMCs in these effects [93, 155, 160, 161]. It is crucial to determine whether the modulation of the NO/cGMP signaling axis in VSMCs is beneficial or detrimental in atherosclerosis in order to assess the potential of the pathway as a pharmacological target.

Therefore, the aim of this study was to gain a deeper understanding of the pathophysiological and pharmacological relevance of the NO/cGMP signaling pathway in VSMCs in atherosclerosis. To achieve this, both a pharmacological and a genetic approach were used to modulate the activity of the NO/cGMP signaling axis. Therefore, the study comparatively examined in detail the effects and therapeutic potential of various next generation NO-GC-modulating drugs on atherosclerosis and plaque composition in $ApoE^{ko}$ mice. The genetic approach focused on the analysis and characterization of a SMC-specific NO-GC knockout in $ApoE^{ko}$ mice.

4.1 NO-GC expression in healthy and atherosclerotic aorta

The pharmacological approach chosen in this study aimed to modulate the activity of NO-GC by the use of NO-GC modulators, potentially influencing the behavior of VSMCs during atherogenesis in experimental mice. As described in **Section 1.4**, both categories of NO-GC modulators trigger cGMP generation by directly binding to the NO-GC β1 subunit (independent of the NO-GC isoform) [136, 145, 146]. Thus, it is of fundamental importance for the experimental approach that NO-GC is expressed in atherosclerotic vessels.

The expression of NO-GC in VSMCs under physiological conditions has been undisputed since the Nobel Prize-honored discovery of its central role in endothelium-dependent vascular relaxation [91, 202, 203]. However, VSMCs exhibit high phenotypic plasticity during plaque formation, which is associated with fundamental structural and functional changes [6, 45]. Additionally, Melichar et al. demonstrated that the expression level of NO-GC is reduced in atherosclerotic tissue [204]. This finding was supported by recent results from our group, which indicated a reduction in NO-GC expression in modulated VSMCs *in vitro* [99]. This raised the question of whether NO-GC is expressed in atherosclerotic plaques e.g., by VSMCs and/or

modulated VSMCs and therefore can be targeted by NO-GC modulators. While some studies have demonstrated a general NO-GC expression at the protein level in atherosclerotic murine aortas [161, 204], to our knowledge, NO-GC expression at the single-cell level within advanced murine atherosclerotic plaques has not been convincingly demonstrated in any study to date. Therefore, this study investigated NO-GC expression in both healthy and atherosclerotic murine aortas. It should be noted that the chosen approach did not distinguish between individual NO-GC isoforms. Thus, the expression of the β1 subunit may reflect the expression of a single isoform or the general expression of NO-GC [73].

In the present study, we demonstrated the expression of NO-GC in VSMCs within both healthy aortas and advanced atherosclerotic plaques. Notably, NO-GC-expressing VSMCs were specifically identified in the atherosclerotic plaque, including both the media and the fibrous cap, as evidenced by co-expression of αSMA. Interestingly, additional NO-GC-positive cells lacking αSMA expression were located in the plaque core. Further characterization of these cells revealed that some, though not all, of the NO-GC-positive cells in the plaque core co-expressed the macrophage marker MAC2. The expression of NO-GC in MAC2-positive cells suggests that these cells may represent transdifferentiated VSMCs or a distinct subset of macrophages [33, 57, 60, 205]. Indeed, it has been proposed that macrophages within atherosclerotic plaques may also express NO-GC [160]. Nevertheless, VSMC-derived cells constitute the majority of macrophage marker-positive cells and foam cells in atherosclerotic plaques [6, 33, 59, 60]. Therefore, the results may indicate that, in addition to VSMCs in the media and fibrous cap, specific modulated/transdifferentiated VSMCs within the plaque core may also express NO-GC. The identity of other NO-GC-positive cells lacking αSMA or MAC2 expression was not further investigated. It is important to note that the chosen experimental approach does not allow the determination of the cellular origin of the cells in the atherosclerotic plaque. In general, further studies, such as lineage tracing or the detection of additional marker proteins, are required to elucidate the cell types and cellular origin of the NO-GC-expressing cells in the core of the atherosclerotic plaque.

Nevertheless, based on the results, it can be confidently assumed that NO-GC is expressed in VSMCs under both healthy and advanced atherosclerotic conditions. This provides the basis for pharmacological modulation of the NO/cGMP signaling pathway in VSMCs with NO-GC modulators during atherogenesis in the selected atherosclerotic mouse model.

4.2 Impact of the NO-GC modulators on atherosclerosis

As mentioned in **Section 1.3**, the (patho-)physiological importance of the NO/cGMP signaling pathway is well-accepted, especially in the cardiovascular system. Over time, this has led to the development of numerous drugs that target this signaling cascade for the treatment of a

variety of diseases. Of particular interest is the category of NO-GC modulators due to their versatile therapeutic applications [136]. Recent studies have suggested that NO-GC modulators may have therapeutic applications in atherosclerosis [160-163]. On this basis, the present study used modern NO-GC modulators as tools to manipulate the NO/cGMP signaling pathway in a mouse model of atherosclerosis. This approach aimed to provide valuable insights into the pathophysiological and pharmacological relevance of the NO/cGMP signaling pathway in VSMCs in atherosclerosis and to evaluate its therapeutic potential. A novel aspect of this research was to compare the effects of a NO-GC activator tool-compound (BAY Activator) with those of a NO-GC stimulator (Vericiguat), which is already in clinical use. To achieve this, $ApoE^{ko}$ mice were chronically treated with BAY Activator for 16 weeks or with Vericiguat for 18 weeks starting at 10 weeks of age.

In the current study, chronic treatment with the BAY Activator resulted in a significant increase in the atherosclerotic lesion area. In contrast, treatment with the NO-GC stimulator Vericiguat did not affect atherosclerosis (**Figure 32 A, E**). This pronounced pro-atherosclerotic effect of the BAY Activator was observed in the aortic root, the aortic arch and particularly prominent in the thoracic/abdominal aorta (**Figure 18**, **Figure 21**). In general, these results are consistent with data from studies that have proposed a pro-atherosclerotic role of the NO/cGMP signaling pathway based on genetic manipulation [93, 155]. These studies have demonstrated that the reduction of cGMP signaling, either through a global knockout of NO-GC1 or the VSMC-specific knockout of cGKI, resulted in a decrease in lesion area. In contrast, some studies have shown that treatment with cGMP-elevating drugs also led to a reduction in lesion area [160-163]. Furthermore, no pro-atherogenic effects or increased mortality rates due to heart attacks and strokes have been reported from the clinical use of those drugs.

However, to our knowledge, this is the first time that the effects of a NO-GC activator on advanced atherosclerosis have been studied in detail in both male and female mice, making our study difficult to compare with previous work. To exclude the possibility that the effects on atherosclerosis were caused by adventitious factors independent of the BAY Activator, such as unknown contamination of the diet, a second group of mice was analyzed. Similar to the initial experiment, a new batch of the atherogenic diet enriched with 150 ppm BAY Activator was administered to the mice. In this second group, we again observed a significant increase in the lesion area between male mice treated with the BAY Activator versus control diet (**Figure 32 D**). Nevertheless, the differences were less pronounced, and there was greater variability in the results of each experimental group.

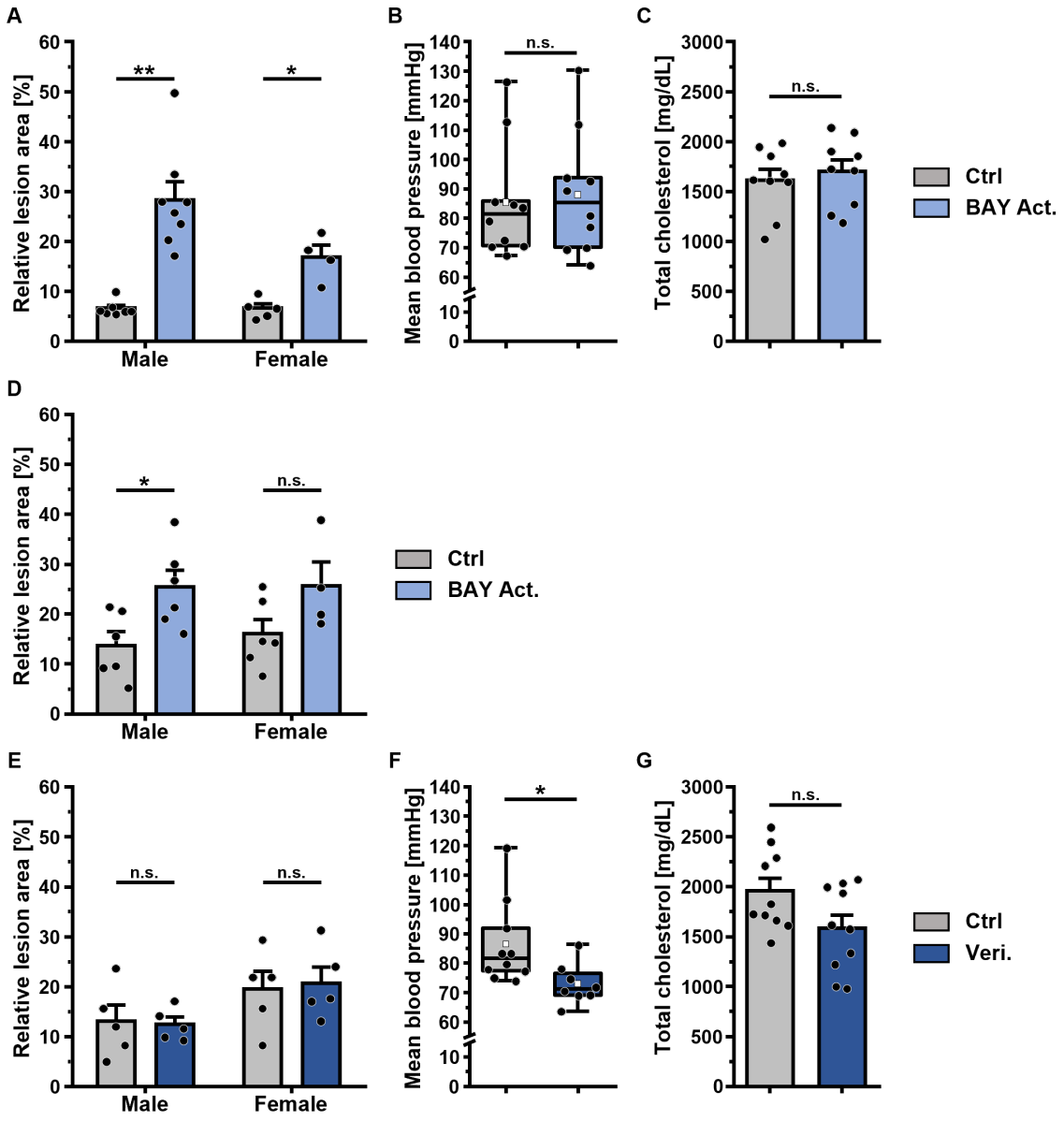

Figure 32. Overview of the main *in vivo* results of the pharmacological approach.
Overview of BAY Activator and Vericiguat effects on atherosclerotic lesion area in the total aortas, blood pressure and total cholesterol plasma level of ApoE^{ko} mice. ApoE^{ko} mice were fed with an atherogenic diet supplemented with 150 ppm BAY Activator for 16 weeks (Ctrl/BAY Act.) or 150 ppm Vericiguat for 18 weeks (Ctrl/Veri). **(A, D, E)** Analysis of relative lesion area in total aortas by Oil Red O staining of Ctrl and BAY Act. (experiment 1 **(A)** and. experiment 2 **(D)**), or Veri. **(C)** treated male and female mice. The atherosclerotic lesion area was determined from both sides of the aorta, averaged, and normalized to the total area of the respective part. Data are represented as mean + SEM. **(B, F)** Mean blood pressure of Ctrl and BAY Act. **(B)** or Veri. **(F)** treated mice (pooled sexes). Blood pressure measurements were performed using a tail-cuff blood pressure system at the end of the feeding period for three consecutive days. The data of the three consecutive days were averaged for each animal. Data are represented as median (horizontal line), 25% - 75% interquartile range (box), 5% - 95% range percentile (whiskers) and mean (white square). **(C, G)** Total cholesterol plasma level of Ctrl and BAY Act. **(B)** or Veri. **(D)** treated mice (pooled sexes). Data are represented as mean + SEM. Statistical significance is indicated by asterisk (*p ≤ 0.05; **p ≤ 0.01; n.s.: not significant, tested pairwise Mann-Whitney U test). Ctrl, Control, BAY Act., BAY Activator, Veri., Vericiguat.

A summary of the most important data from the various *in vivo* experiments in the present work is shown in **Figure 32**. Data from male and female mice were pooled when statistical analysis permitted this. Lesion area was increased in male mice of both BAY Activator-treated groups (Experiment 1 and Experiment 2). The less pronounced effect of BAY Activator treatment

observed in female mice in the first experiment were not significant in the female group of the second experiment (**Figure 32 A, D**). In Vericiguat-treated mice, no significant effects on atherosclerosis were observed compared to their litter-matched control mice (**Figure 32 E**). Blood pressure was not altered in the BAY Activator-treated mice, while it was slightly decreased in the Vericiguat-treated group versus controls (**Figure 32 B, F**). Plasma lipid levels was not affected in any of the groups (**Figure 32 C, G**).

Thus, the results of our study on the effect of NO-GC modulators on atherosclerosis differed from the results previously described in a small number of publications. Therefore, it is essential to elucidate the causes for these discrepancies in the current study, especially to understand the reasons for the lack of an effect of the NO-GC stimulator in contrast to the NO-GC activator, which demonstrated a pronounced impact on the atherosclerotic lesion area.

4.2.1 Potential secondary effects on atherogenesis

Especially with the chosen systemic approach of pharmacological treatment (feeding an atherogenic diet supplemented with BAY Activator or Vericiguat for 16-18 weeks), possible secondary effects, which may have an indirect influence on plaque development, play a significant role in the interpretation of the results. For instance, incorrect dosing, inadequate drug absorption, blood pressure effects, altered lipid metabolism, or increased inflammation could have had a secondary impact on the study's outcomes. To avoid potential secondary effects, the chosen experimental setup and the daily doses of approx. 25 mg/kg were based on previous studies. These studies evaluated the effects of various NO-GC modulators in similar or different disease models in mice and successfully detected therapeutic effects [161, 206, 207]. In our study, both Vericiguat (56.1 ± 8.4 nM) and the BAY Activator (16.6 ± 2 nM) were detected in the unbound fraction in plasma at concentrations comparable to the referenced studies (**Supplementary table 2**). Therefore, it is assumed that the drugs were administered in sufficient quantities and efficiently absorbed by the mice to achieve a corresponding therapeutic success while minimizing secondary effects. However, it should be noted that the present study used different NO-GC modulators with potentially varying pharmacokinetic properties. Even with similar plasma concentrations, this may result in a divergent effect size. Therefore, the effects of NO-GC modulators on physiological parameters in this study were also validated.

A notable factor is the concentration-dependent hypotensive effect of NO-GC modulators [80, 81, 136, 181, 182]. Given the established connection between blood pressure and atherosclerosis development, the study examined the blood pressure effects in all experimental groups [1, 208]. It was demonstrated that the 25 mg/kg dose of Vericiguat had a blood pressure-lowering effect of approx. 13.5 mmHg mean blood pressure, while the BAY Activator had no impact (**Figure 32 B, F**). It is possible that the chronic blood pressure-lowering effect of Vericiguat had an indirect anti-atherosclerotic effect that masked the effect of treatment on the lesion area.

However, Krishnan et al. used a comparable NO-GC stimulator at identical concentrations and demonstrated an antihypertensive effect that was classified as moderate [206]. Thus, in the present study, a moderate effect can be assumed. Therefore, the question arises whether such a moderate reduction in blood pressure can significantly influence the development of atherosclerosis [208]. Instead, the moderate antihypertensive effect of Vericiguat suggests successful target engagement in VSMCs in the vessel wall, confirming that Vericiguat was absorbed by the mice in sufficient concentrations.

Another significant factor that can influence the development of atherosclerosis is plasma lipids [5, 195]. However, in line with the literature, no alterations in lipid levels were detected in the plasma of the treatment groups compared to the respective control groups (**Table 11**, **Figure 32 C, G**) [161-164]. Whereas the expected increase in cholesterol and LDL levels in plasma due to the atherogenic diet was observed, indicating the successful intake of the diet [19].

In addition to dyslipidemia, inflammation mediated by immune cells, such as lymphocytes and macrophages, can play a substantial role in atherogenesis [5]. To exclude systemic inflammation as the cause of the significant effects of the BAY Activator on the lesion area, a complete blood count analysis was performed (**Supplementary table 3**). The results of this study provided no indications of systemic inflammation, as no changes in blood cell counts were detected following BAY Activator treatment. This is in line with a recent study by Mauersberger et al., in which treatment with a NO-GC stimulator also did not affect platelet and blood leukocyte counts [161]. However, it cannot be excluded that NO-GC modulators had a direct or indirect impact on the activity of immune cells, independent of cell count. Mauersberger et al. associated the anti-atherosclerotic effect of the tested NO-GC stimulator with reduced leukocyte recruitment mediated by the activation of NO-GC in platelets [161]. Furthermore, the cGMP signaling pathway has also been associated with anti-inflammatory effects in other studies [209, 210]. Based on these results, treatment with BAY Activator or Vericiguat would have been expected to improve atherosclerotic outcomes. Interestingly, liver analysis of the same mice used in the present study showed less fibrosis after BAY Activator treatment in comparison to controls, which most likely is mediated via the NO-GC-expressing hepatic stellate cells (unpublished data; Rajeeth, K., Roessing, M., et al.). Additionally, other studies have demonstrated a therapeutic effect of NO-GC modulators in diseases strongly associated with inflammatory processes [136, 142, 148-151, 211]. In line with this, the results in the current study also showed no effect of the BAY Activator on body weight and weight of the liver, kidney, and spleen. All of this argues against a systemic inflammation induced by the BAY Activator treatment, which could be the cause of the increased lesion area. In conclusion, there is no evidence of secondary effects of systemic pharmacological treatment that may have influenced atherogenesis.

4.2.2 Effects of timing and duration of treatment

The treatment effects observed in our study could have been influenced by the timing and duration of the BAY Activator and Vericiguat treatments. Atherosclerosis is a slowly progressing disease associated with complex structural changes at the cellular level (**Section 1.1.3**). These changes might result in a fundamental shift in the expression and functional significance of the NO/cGMP signaling pathway. Therefore, the pharmacological modulation of this pathway may yield different outcomes depending on the stage of the disease. Indeed, there is already evidence of changes in the NO/cGMP signaling pathway during the progression of the disease *in vivo* [212].

In the present study, ApoE^{ko} mice were chronically treated with the NO-GC modulators supplemented in an atherogenic diet starting at 10 weeks of age. It is well-established that the initial phase of plaque development in ApoE^{ko} mice on a standard chow typically begins around 12 weeks of age, and that this process can be accelerated by an atherogenic diet [15, 19, 213]. Therefore, it is assumed that the chosen treatment period of 16-18 weeks encompassed both the initial and advanced phases of atherogenesis. In contrast, in studies in which an anti-atherosclerotic effect was demonstrated, the duration of treatment was notably shorter. However, it is important to note that not all studies used identical mouse models, making direct comparisons between treatment durations challenging. For example, Vantler et al. observed an atheroprotective effect after 6 weeks of treatment in ApoE^{ko} mice and 12 weeks of treatment in LDL receptor-deficient (LDLr^{ko}) mice using the NO-GC stimulator 41-2272 [162]. This treatment period probably mainly addressed the initial phase of plaque development [14, 19]. In this context, it is also essential to consider that ApoE^{ko} mice on an atherosclerotic diet develop plaques with a more advanced phenotype and faster compared to LDLr^{ko} mice [14]. However, since the work from Vantler et al. was only published as an abstract, it was not possible to assess the disease stage. Recently, Mauersberger et al. provided support for these findings by observing an anti-atherosclerotic effect after 10 weeks of treatment with a Vericiguat-like NO-GC stimulator in LDLr^{ko} mice [161]. The discrepancy to the results of our study may potentially be attributed to the significantly longer treatment duration. It could be assumed that treatment in the early, initial phase of atherosclerosis has an anti-atherosclerotic effect, while at a later stage, the functional relevance of the NO/cGMP signaling pathway changes, and the therapeutic effect is either abolished (Vericiguat) or even reversed (NO-GC Activator). Therefore, it is of high interest to investigate the impact of NO-GC modulators treatment on the atherosclerotic lesion area exclusively in advanced stage of atherosclerosis.

4.2.3 Effects of NO-GC modulators on composition and plaque stability

While the assessment of lesion area provides a comprehensive overview of the impact of the BAY Activator on the progression of atherosclerosis, understanding plaque composition is

crucial for identifying potential causes behind changes in lesion size. VSMCs are present at all stages of atherosclerotic plaques, and their significant phenotypic plasticity plays a crucial role in both plaque growth and composition [6]. Consequently, in accordance with the study's focus, we analyzed the potential effects of pharmacological modulation of the NO/cGMP signaling axis on VSMCs in atherogenesis and its impact on plaque composition. As previously described by Feil et al., the presence of MAC2 in VSMC-derived cells within atherosclerotic plaques serves as an indicator of VSMC transdifferentiation into macrophage-like cells [33]. Therefore, in addition to αSMA (a classical marker for VSMCs) and collagen content, we examined changes in MAC2 expression as a marker for transdifferentiated VSMCs following drug treatment.

The Western blot analysis did not reveal any changes in αSMA expression in the entire aorta after BAY Activator or Vericiguat treatment. However, it indicated a significant increase in MAC2 expression in the whole aorta of mice treated with the BAY Activator. Conversely, treatment with Vericiguat did not exhibit this effect (**Figure 20**). Detailed *in situ* examination revealed an increase in total MAC2 expression in the core and fibrous cap of plaques in the aortic root of BAY Activator-treated mice, while total αSMA expression and collagen content remained unaffected (**Figure 22 B, E, H**). These findings were also validated in the aortic arch (**Figure 24**). Nevertheless, this increase in total MAC2 expression correlated with the significant effect of the BAY Activator on the lesion area (**Figure 22 I**).

However, the substantial increase in total MAC2 expression raises questions about the relationship between the increased lesion area and the presence of relatively more MAC2-expressing cells in plaques of BAY Activator-treated mice compared to control mice. One possible interpretation is that, as a result of BAY Activator treatment, larger plaques may also contain a higher proportion of migrated and clonally expanded VSMCs that have undergone transdifferentiation into macrophage-like cells. This corresponds with studies by Segura-Puimedon et al. and Wolfsgruber et al., collectively suggesting that the activation of the NO/cGMP/cGKI signaling axis promotes the phenotypic modulation of VSMCs and consequently, atherosclerosis [70, 93, 155]. Therefore, one conclusion could be that the BAY Activator promotes phenotypic modulation, leading to an accumulation of macrophage-like cells, which, in turn, results in larger plaques. However, since MAC2 is not an exclusive marker for macrophage-like cells, the data could also indicate an increased accumulation of macrophages [205]. Conversely, the increased presence of macrophages after treatment with BAY Activator may have promoted plaque growth. As described in **Section 1.1.3**, in addition to VSMCs, macrophages also play a crucial role in the progression of plaque formation. While macrophages primarily contribute to the initial stage of plaque formation through their recruitment, their presence in more advanced plaques is mainly attributed to macrophage proliferation [1, 32]. It would be interesting

to clarify whether increased monocyte recruitment in the initial stage or increased proliferation in the advanced stage is causative for potential macrophage accumulation. Furthermore, due to the diversity of macrophages and their associated different roles in atherosclerosis, it would be necessary to determine the potential macrophage phenotypes involved [214, 215]. It would also be interesting to investigate whether the numbers of other immune cells, such as lymphocytes, are increased in the plaques, which could indicate an increased local inflammation following BAY Activator treatment. Such an increased local inflammatory response in the vessel wall, which is associated with recruitment, adhesion, and, finally, migration of monocytes and lymphocytes could potentially also explain the significantly increased lesion area observed [216, 217].

In summary, the present results do not provide a definitive explanation for the increased MAC2 expression. Further investigations, such as inducible fate mapping experiments, are needed to clarify the cellular origin of the MAC2-positive cells, and whether they derive from medial VSMCs or monocytes/macrophages.

Moreover, as part of this study, we investigated whether potential alterations in plaque composition caused by BAY Activator treatment influenced individual plaque stability. As plaque stability is strongly associated with the content of collagen, αSMA-positive VSMCs, or MAC2-positive macrophage-like cells or macrophages, the αSMA/MAC2 or collagen/MAC2 ratio was used to assess plaque stability [6, 27, 34, 190, 199]. Surprisingly, despite a significantly increased presence of MAC2-expressing cells in the lesions of BAY Activator-treated mice, no noteworthy changes in plaque stability were observed compared to the control group. However, in the interpretation of these data, the substantial variance in individual plaque stability within the experimental groups and the limited number of animals must be considered. To obtain meaningful insights into the effect of the BAY Activator on plaque stability, the sample size must be increased.

4.2.4 Target specific and off-target effects of the NO-GC modulators

In this study, we examined the distinct effects of two compounds belonging to different categories, specifically NO-GC stimulators, and NO-GC activators, on atherosclerosis. The study results raised the question why these compounds exhibited pronounced differences in their impact on lesion area. One significant factor could be attributed to the differences in the mode of action between NO-GC stimulators and activators. Both types of compounds interact allosterically with NO-GC to induce cGMP generation, yet they diverge in terms of their binding partner and mode of action. NO-GC stimulators boost the activity of heme-containing NO-GC independently of NO and synergistically interact with endogenous NO. In contrast, NO-GC activators bind to and activate the oxidized, heme-free form of NO-GC [79]. Pathophysiological conditions associated with increased oxidative stress lead to a shift in the intracellular

concentration of the heme-containing NO-GC towards the oxidized, dysfunctional, heme-free form [79, 218, 219]. This altered form does not respond to endogenous NO or NO-GC stimulators. Furthermore, these pathophysiological conditions are linked to reduced NO availability [79]. Atherosclerosis, characterized as a chronic inflammatory disease of the vascular wall, is strongly associated with elevated oxidative stress and diminished NO bioavailability due to endothelial dysfunction [137, 200]. As the disease progresses, the increased inflammation promotes ROS production and thus oxidative stress, which is associated with reduced NO bioavailability. This suggests that an increase in oxidative stress in atherosclerotic plaques during the progression of atherosclerosis shifts the redox equilibrium of NO-GC. Consequently, this results in a higher efficacy of BAY Activator in comparison to Vericiguat. According to a target-specific effect, this implies that the BAY Activator leads to a more robust activation of the NO/cGMP signaling pathway in more advanced atherosclerotic plaques, thereby promoting plaque growth. A schematic representation of the hypothesis is given in **Figure 33**. This hypothesis is supported by studies that have demonstrated that NO-GC activators exhibit higher pharmacological activity *in vitro*, *ex vivo* within blood vessels, and *in vivo* under pathophysiological and oxidative stress conditions [79]. Moreover, it has already been established that the NO-GC activator 60-2770 leads to enhanced cGMP generation under atherosclerotic conditions in rabbits, while sensitivity to NO donors diminishes with advancing atherogenesis [212]. In our laboratory, while investigating the therapeutic potential of a NO-GC activator in chronic kidney disease, we found that NO-GC activators especially promote cGMP signaling and associated physiological effects under conditions of disease-related elevated oxidative stress [165, 220]. In contrast, within the same study, we observed that the NO-GC stimulator 41-2272 had a diminished impact on cGMP levels under similar oxidative conditions compared to the normal conditions in murine glomeruli [165]. Together these studies may suggest that the differences in the mode of action may have contributed to the differing effectiveness of the NO-GC modulators observed in the present study.

Furthermore, due to the systemic treatment, off-target effects may contribute to the observed effects of the BAY Activator. During the development of various NO-GC modulators, off-target effects have already been described for compounds such as YC-1. This particular compound not only stimulates NO-GC but also inhibits PDEs and has various effects independent of cGMP [79]. It is worth mentioning that the new generation of NO-GC modulators has made significant progress in addressing this concern. For NO-GC stimulators, such as Riociguat and Vericiguat, as well as NO-GC activators like Runcaciguat, a high specificity for NO-GC and drug safety has already been described [79, 81, 181, 182]. Since the BAY Activator is a tool compound, there is no data available regarding the specificity of the drug. Therefore, off-target effects, independent of its activation of NO-GC and the NO/cGMP signaling pathway, remain a potential factor, which could potentially contribute to an increase in lesion area. To validate

the specificity of the BAY Activator's effects on the NO/cGMP signaling pathway in VSMCs, this study included the characterization of an SMC-specific conditional NO-GC knockout mouse model (**Section 3.3**). Absence of the BAY Activator's effects on atherosclerosis in a NO-GC knockout model could confirm the specificity and exclude off-target effects. Additionally, it would be interesting to explore the effects of other NO-GC activators to determine whether there might be a class-wide effect associated with NO-GC activators. Notably, there has been an oral report of an anti-atherogenic effect for the NO-GC activator Ataciguat, which has not been published in a peer-reviewed journal [163]. Hence, a comparative study with Ataciguat performed under identical experimental conditions could provide valuable insights in comparison with the BAY Activator.

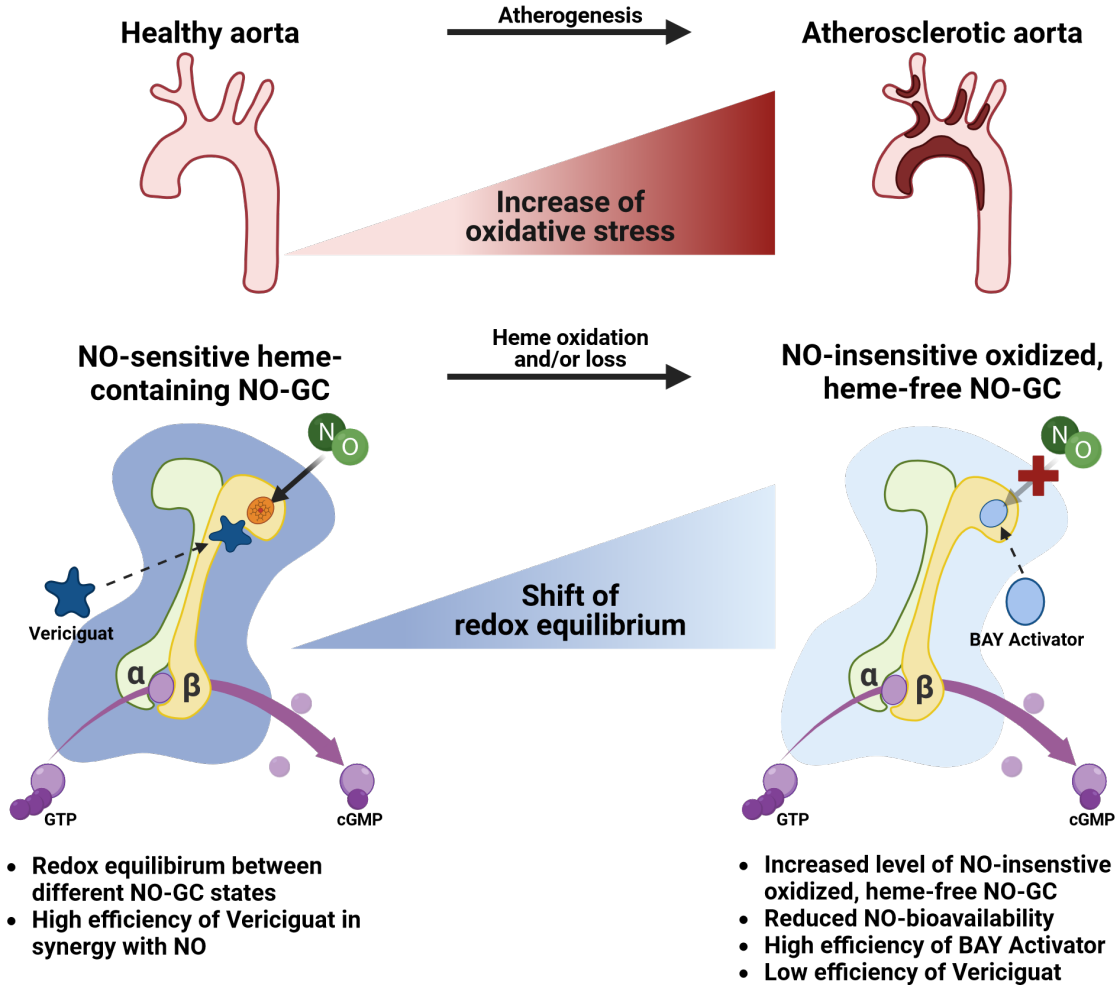

Figure 33. Increased oxidative conditions in the atherosclerotic aorta cause an enhanced efficiency of BAY Activator compared to Vericiguat.
Schematic representation of the hypothesis that increased oxidative conditions in the atherosclerotic aorta result in enhanced efficiency of the BAY Activator in comparison to Vericiguat. Both compounds induce the generation of cyclic guanosine monophosphate (cGMP) from guanosine triphosphate (GTP) through allosteric binding to nitric oxide-sensitive guanylate cyclase (NO-GC), but they differ in their binding site and mode of action. Vericiguat binds to the NO-sensitive heme-containing NO-GC and stimulates NO-GC independently and in synergy with nitric oxide (NO). BAY Activator binds to the NO-insensitive oxidized, heme-free NO-GC. In the healthy aorta, there exists a redox equilibrium between these two forms of NO-GC. As atherogenesis progresses, oxidative stress increases and leads to a shift in the equilibrium towards the dysfunctional oxidized, heme-free form of NO-GC. This form can only be activated by the binding of the BAY Activator to generate cGMP. Under oxidized conditions, the BAY Activator exhibits higher efficacy compared to Vericiguat. For more details see the text. Adapted from Sandner et al. 2021 [79]. Image created using BioRender.com.

4.2.5 Appropriate mouse model for the pharmaceutical approach

In scientific literature, it is not uncommon for animal experiments conducted by different research teams to yield controversial results, which limit the transferability of experimental findings to human diseases [13]. Consequently, this raises questions regarding the selection of the most appropriate animal model for a particular application. The ApoE^{ko} and LDLr^{ko} mouse models are among the most frequently used animal models for investigating the mechanisms underlying atherogenesis (**Figure 34**) [12, 14]. In the current study, we used the ApoE^{ko} model, which is described in detail in **Section 1.1.2**. However, despite its popularity, this mouse model has certain limitations. Notably, the lipid profile of ApoE^{ko} mice differs from that of humans [17, 18]. Furthermore, ApoE is a multifunctional protein with relevance in inflammation, macrophage biology, as well as in the proliferation and migration of VSMCs [13, 14, 221]. These multifaceted functions have the potential to influence the development of atherosclerotic plaques in ApoE^{ko} mice [14, 221]. In particular, regarding the observed increased presence of MAC2-positive cells in atherosclerotic plaques, the link between the use of the ApoE^{ko} model and the significant effect of BAY Activator treatment on lesion area is questioned. The LDLr^{ko} mouse model provides an alternative option to study atherogenesis and evaluate therapeutic interventions [14]. Similar to ApoE^{ko} mice, LDLr^{ko} mice have an impaired cholesterol metabolism, which leads to elevated plasma cholesterol and LDL levels and accelerated atherosclerosis development when fed an atherosclerotic diet (Western diet). In LDLr^{ko} mice, plasma cholesterol is primarily transported by LDL particles, resulting in a lipid profile more similar to that of humans. Moreover, unlike ApoE^{ko}, LDLr^{ko} does not affect inflammation [14, 222]. Indeed, some studies on the effect of NO-GC modulators in both ApoE^{ko} and LDLr^{ko} mice have already been described in the literature [161-163]. These studies have led to identical results in both mouse models. Consequently, this raises the question whether the observed effect of the BAY Activator is primarily attributable to the choice of the ApoE^{ko} model and whether different mouse models might yield different results. A logical next step could be a comparative study of the BAY Activator's effect in both ApoE^{ko} and LDLr^{ko} mice.

However, it is important to note that animal models generally cannot fully replicate the disease situation in humans. Determining which mouse model is most suitable to study the effects of the NO-GC modulators on atherosclerosis remains a complex matter and depends on the specific aspects under investigation [13, 18]. Furthermore, the extent to which the results in ApoE^{ko} or LDLr^{ko} mice can be extrapolated to the human situation remains an open question, which exceeds the scope of this study's discussion. Nevertheless, this consideration should be taken into account when interpreting the data and warrants further investigation into the clinical relevance of the effects of the NO-GC modulators in atherosclerosis.

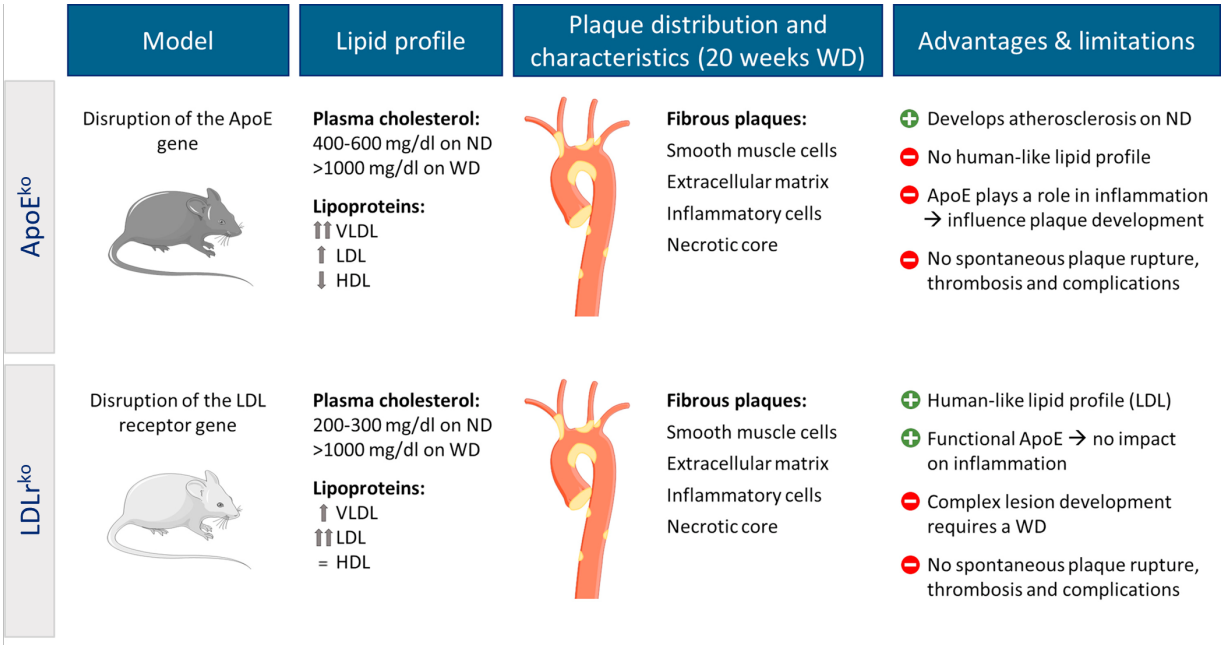

Figure 34. Comparison of ApoE^{ko} and LDLr^{ko} mouse models of atherosclerosis.
The ApoE^{ko} and LDLr^{ko} are the most frequently used mouse models to study atherosclerosis. The total plasma cholesterol levels on normal (ND) and Western diet (WD), changes in lipoprotein profile, specific plaque characteristics and advantages or limitations are indicated. Both mouse models demonstrate a similar distribution of plaques in the aorta after 20 weeks of WD. The composition of lesions in the aortic root and arch at this time point is also indicated. Adapted from Veseli et 2017 [14]. LDL, low-density lipoprotein; HDL, high-density lipoprotein; VLDL, very-low-density lipoprotein.

4.2.6 Impact of sex on the effect of NO-GC modulators

In the present study, the effects of two NO-GC modulators, BAY Activator and Vericiguat, on lesion area were independently examined in both sexes to account for sex-specific differences. It was observed that the effect of the BAY Activator was less pronounced in female mice, potentially indicating sex-specific differences (**Figure 32 A, D**). This hypothesis is supported by the fact that there were no differences in lesion area between the control groups of both sexes (**Supplementary figure 2**). Sex-specific differences in the impact on atherosclerosis have also been observed in other pharmacological approaches in mice [223, 224]. Moreover, accumulating evidence suggests that sex-specific differences in the manifestation and treatment outcomes of atherosclerosis have direct clinical relevance in humans [224]. While the underlying causes of these differences remain largely unexplored, factors, such as differences in sex hormone levels and certain genes located on the sex chromosomes, have been considered in the context of atherosclerosis pathogenesis [225-227].

Regarding the results of the present study, it will be interesting to clarify why the effect of the BAY Activator on the lesion area was less pronounced in female mice. The difference may primarily lie in the NO/cGMP signaling pathway itself. Interestingly, there are already hints indicating that sex-specific differences play a pivotal role in the pathophysiological significance of the NO/cGMP signaling axis within the cardiovascular system. For instance, it has been experimentally demonstrated that global deletion of the NO-GC1 isoform leads to the induction

of a hypertensive phenotype exclusively in male mice [228]. Further supporting this, Vermeersch et al. uncovered that the adaptive response to vascular injury is compromised in male NO-GC1 knockout mice. Notably, this study also revealed that male mice displayed significantly lower cGMP levels in the aortas, regardless of their genotype [229]. In summary, these studies underscore the presence of a possible sex-specific difference in the functional relevance of the NO/cGMP signaling pathway. It is worth noting that the difference in testosterone levels and the resulting testosterone-dependent cardiovascular effects have been implicated as a possible causal factor for the observed phenotype [228]. These findings provide insight into the intricate interplay between sex-specific factors and NO-GC modulation in atherosclerosis and open new avenues for further investigations.

4.3 Influence of the NO-GC modulators on primary VSMCs

The pharmaceutical approach in atherosclerotic mice provided valuable insights into the impact of NO-GC modulators on atherosclerosis. The results suggested a pro-atherosclerotic effect of the BAY Activator, which was associated with an increased accumulation of transdifferentiated macrophage-like cells or macrophages in the atherosclerotic plaque. However, a comprehensive explanation of the effects of the BAY Activator and why they differ from those of Vericiguat is still lacking. Moreover, the relevance of the NO/cGMP signaling pathway in VSMCs in this context remained unclear. To address this, we also examined the effects of NO-GC modulators on pVSMCs using *in vitro* methods (**Section 3.2**). Our focus was to evaluate the impact of the two compounds on intracellular cGMP generation by NO-GC under various conditions, effector protein-mediated signal transduction, and the growth of pVSMCs. This approach allowed us to study in detail the effects of NO-GC modulators on the cellular processes of VSMCs in a simplified setting, that facilitated the assessment of their role in atherosclerosis *in vivo*. **Table 13** offers a summary of the effects of BAY Activator and Vericiguat on pVSMCs, which will be discussed further in the subsequent sections.

Table 13. Summary of the effects of the NO-GC modulators on primary VSMCs.
Summary of the effects of NO-GC modulators (BAY Activator and Vericiguat) on intracellular cGMP levels, VASP phosphorylation, and growth of primary VSMCs. BAY Activator was tested under normal conditions and in the presence of the NO-GC oxidant ODQ (oxidized conditions). Vericiguat was tested both individually and in combination with nitric oxide (NO). (+) indicates a promoting effect compared to the control condition.

Parameter	BAY Activator		Vericiguat	
	Normal conditions	Oxidized conditions	Without NO	With NO
cGMP level	+	++	+	++
VASP-phosphorylation	+	Not tested	+	Not tested
pVSMC growth	+	Not tested	+	++

4.3.1 Impact of NO-GC modulators on NO/cGMP signaling in primary VSMCs

NO-GC stimulators and activators are known to modulate the activity of NO-GC independently of NO, thereby increasing intracellular cGMP levels [79]. In line with this, our study observed concentration-dependent cGMP formation in pVSMCs under normal conditions for both Vericiguat and the BAY Activator in the absence of exogenously added NO (**Figure 25**,**Figure 26**). Furthermore, this increase in intracellular cGMP levels also led to cGKI-mediated VASP phosphorylation, demonstrating the successful transduction of cGMP signals at the effector protein level (**Figure 27**). Therefore, it can be assumed that treatment with both NO-GC modulators stimulates the NO/cGMP/cGKI signaling axis in VSMCs under normal conditions. Additionally, assuming that NO-GC activators exclusively bind to the oxidized, heme-free form of NO-GC, the observation that the BAY Activator also led to an increase in cGMP under these normal conditions is highly interesting [79, 218]. This effect has already been described for other NO-GC activators that activated purified NO-GC and induced relaxation of healthy blood vessels [181, 220, 230, 231]. Based on this, it is concluded that the oxidized, heme-free form of NO-GC also exists under normal physiological conditions [79]. This significantly supports the assumption of an intracellular redox equilibrium between the different NO-GC forms, even under normal conditions, in VSMCs.

As discussed in **Section 4.2.4**, we hypothesized that a shift in this redox equilibrium of NO-GC forms and the different modes of action of NO-GC modulators might be a major factor in the observed divergence in the efficacy of BAY Activator and Vericiguat in atherosclerosis (**Figure 33**). Previous studies have suggested that NO-GC activators exhibit higher pharmacological activity, especially under disease conditions associated with high oxidative stress, such as atherosclerosis [79]. Therefore, our study also examined the effectiveness of the BAY Activator under oxidative stress conditions compared to normal conditions. In most studies (including the present one) aiming to analyze the importance of increased pathophysiological oxidative stress on NO-GC activity, ODQ was used as an oxidative stress mimic. It has been shown that ODQ effectively oxidizes NO-GC, reducing the enzyme's sensitivity to exogenously added NO [220, 232, 233]. In line with this, we demonstrated that treatment with ODQ significantly reduced NO-induced cGMP production in pVSMCs, thereby confirming the oxidative status of NO-GC (**Supplementary figure 8**). Therefore, it was assumed that ODQ treatment shifted the redox equilibrium in pVSMCs to the NO-insensitive oxidized, heme-free form of NO-GC, a condition that may resemble the pathophysiological situation in atherosclerosis. Subsequent treatment with BAY Activator under both native and oxidative stress conditions showed that the BAY Activator increased the cGMP levels in pVSMCs in a concentration-dependent manner independent of the oxidation status of NO-GC. Interestingly, the BAY Activator exhibited higher efficacy under oxidative stress conditions (**Figure 25**). These results primarily align with the

proposed mode of action of NO-GC activators [79, 218]. Furthermore, studies that compared the effects of NO-GC activators under native and oxidative stress conditions reported an increased efficacy following ODQ treatment [201, 220]. Thus, it is reasonable to assume that the BAY Activator also efficiently promotes the NO/cGMP signaling in VSMCs under atherosclerotic conditions.

Regarding the effect of NO-GC stimulators, it is assumed that they exclusively act on NO-sensitive, heme-containing NO-GC [79]. By binding to NO-GC, NO-GC stimulators stabilize the enzymatically active state (extended conformation), which, as shown in this study, leads to an increase in basal cGMP generation in the absence of NO (**Figure 26 A, B**) [130]. Additionally, it has been described in the literature that this binding also results in a strong synergistic effect with NO, increasing the sensitivity of NO-GC to NO [136]. The synergistic action of Vericiguat with NO on cGMP levels in pVSMCs was successfully demonstrated in our study (**Figure 26 C, D**). The effect of Vericiguat and NO alone on cGMP generation was significantly potentiated by the combination of the two substances, demonstrating that Vericiguat, as a NO-GC stimulator, also enhanced endogenous NO-induced cGMP signaling in VSMCs. This mode of action is particularly relevant in pathophysiological conditions of reduced NO bioavailability. For example, NO-GC stimulators have pharmacological implications in cardiovascular diseases such as pulmonary hypertension, which is associated with reduced endogenous NO bioavailability, which in turn impairs downstream cGMP signaling [79]. Atherosclerosis is also a disease associated with endothelial dysfunction and reduced NO bioavailability [137]. However, in contrast to other studies, the results of this study question the efficacy of NO-GC stimulators such as Vericiguat in atherosclerosis (**Section 4.2**). Possible reasons for this have been extensively discussed in the previous chapter. However, it is important to highlight again the differences in the mode of action of the NO-GC modulator categories and the demonstrated increased efficacy of the BAY Activator on cGMP signaling in pVSMCs under oxidative stress conditions and its significant impact on atherosclerosis. Since Vericiguat was only investigated under normal conditions in this study, it remains unclear which effect Vericiguat has on cGMP levels in VSMCs under oxidative conditions. However, we have already shown that the NO-GC stimulator BAY41-2272 had no effect on cGMP signaling in renal glomeruli in the presence of the NO-GC oxidant ODQ, while the NO-GC activator BAY-543 was effective [165]. Additionally, other studies have shown that NO-GC activators, such as Cinaciguat, have a higher potency than NO-GC stimulators under pathophysiological and oxidative conditions [79]. This may be due to the shift in the redox equilibrium between the NO-GC forms under these oxidative stress conditions, reducing the heme-containing form and causing NO-GC stimulators to simply lose their efficacy. Such a scenario is also conceivable under the highly inflammatory and oxidative conditions in the atherosclerotic plaque. Thus, evaluating the effect of Vericiguat on cGMP signaling in VSMCs under ODQ-induced oxidative stress conditions is an important

experiment that should be conducted to further investigate this hypothesis. It would also be interesting to compare the effects of the BAY Activator and Vericiguat on cGMP signaling in VSMCs in an *ex vivo* setup in isolated healthy and atherosclerotic aortas. The use of healthy and atherosclerotic mice selectively expressing the cGMP biosensor cGI500 in VSMCs would be suitable for real-time FRET-based cGMP imaging at the single-cell level in isolated aortas [78]. A similar approach has already been successfully established and conducted by Lehners et al. in our laboratory [99].

4.3.2 Impact of NO-GC modulators on primary VSMC growth

The previous results of our study suggest that NO-GC modulators affect the NO/cGMP signaling pathway in VSMCs according to their respective mode of action. However, it is unclear what functional relevance the increase in cGMP levels and subsequent activation of effector proteins in VSMCs have and what this means for the observed effects on atherosclerosis. Previous studies have shown that the NO/cGMP signaling pathway plays a significant role in the growth of VSMCs, although the exact impact is still discussed controversially [70]. Therefore, we analyzed the growth behavior of pVSMCs following stimulation of the NO/cGMP signaling pathway.

Before assessing the impact of NO-GC modulators on pVSMC growth, we first validated the effect of exogenous NO addition. In our study, we observed not only a growth-promoting effect when treating pVSMCs with 1.25 µM – 20 µM DETA/NO but also noticed that this effect was reversed by higher concentrations (25 µM – 100 µM) (**Supplementary figure 10**). This concentration-dependent ambivalent effect of NO on pVSMC growth has already been documented in various studies [93, 155, 158, 159]. For instance, similar to our study, Wolfsgruber et al. demonstrated that low concentrations (0.5 µM) of DETA-NO promoted VSMC growth, while high concentrations (100 µM) had inhibitory effects [93]. Furthermore, these studies revealed that the growth-promoting effects were mediated by the NO/cGMP/cGKI signaling axis, whereas the inhibitory effects were independent of this pathway [93, 155, 159]. Several studies have supported these findings by showing that treating pVSMCs with the cGMP analog 8-Br-cGMP enhanced growth through cGKI [92, 159]. Thus, it is generally assumed that the NO/cGMP/cGKI signaling axis plays a growth-promoting role in pVSMCs. Consistent with these findings, our study showed that both NO-GC modulators, Vericiguat and BAY Activator, had a strong growth-promoting effect on pVMCS (**Figure 28**). Additionally, it was demonstrated that the combination of NO and Vericiguat exhibited a strong synergistic effect, potentiating the growth-promoting effect as expected, based on the mode of action of NO-GC stimulators (**Figure 28 B**). These results align with the increases in intracellular cGMP levels in pVSMCs following treatment with NO-GC modulators and thus confirming the functional relevance of the NO/cGMP signaling pathway in the growth of VSMCs.

For a more comprehensive interpretation of these results, it is important to note that we evaluated the growth effects of NO-GC modulators 72 hours after treatment. However, since the VSMCs were treated from the time of cell seeding, the observed growth effect could have been caused by several mechanisms. The NO-GC modulators could potentially have anti-apoptotic, proliferative, and/or adhesive effects on pVSMCs. Previous studies have highlighted the primary role of cGMP-mediated increased adhesion efficiency in VSMC growth, whereas the effects on cell proliferation and apoptosis are secondary [92, 159]. It has been shown that the activation of cGKI through 8-Br-cGMP suppresses the RhoA/Rho-kinase signaling pathway, resulting in an increased expression of β1 and β3 integrins and, consequently, enhanced adhesion of pVSMCs [92]. Our real-time analysis of VSMC growth behavior also indicated that at least the synergistic effect of Vericiguat with NO led to significantly earlier cell adhesion and, consequently, an earlier onset of VSMC growth (**Figure 28 B**). The extent to which NO-GC modulators influenced proliferation remains unclear with the current approach. One possible way to investigate this further would be to treat VSMCs with NO-GC modulators after the initial adhesion phase, specifically investigating their effect on the proliferation phase.

The results of the present study underscore the functional relevance of the NO/cGMP signaling in VSMC growth and is in accordance with previously published studies. However, some conflicting studies indicate that both NO and the NO-GC stimulator YC-1 inhibit cell growth [152, 153, 156]. As described in **Section 1.5**, the differences in results are likely due to the choice of cell model. Many studies demonstrating an inhibitory effect on growth used cultured (repeatedly passaged) VSMCs, whereas our study employed primary isolated aortic VSMCs. Primary VSMCs are considered a model for contractile VSMCs, whereas passaged VSMCs represent phenotypically modulated VSMCs. Consequently, it is assumed that the relevance of the NO/cGMP signaling axis differs in these *in vitro* models [159]. In contrast to contractile VSMCs, characterized by abundant expression of contractile proteins and a low proliferation rate, phenotypically modulated VSMCs exhibit low contractility and are highly proliferative. Interestingly, NO-GC1-deficient pVSMCs showed reduced growth but increased expression of contractile markers [155]. In contrast, cGKI activation with 8-Br-cGMP increased growth and expression of markers for modulated VSMCs [93]. Taken together, these *in vitro* studies support a model in which enhanced NO/cGMP/cGKI signaling promotes the phenotypic modulation of contractile VSMCs toward a modulated phenotype [70, 93, 155]. Accordingly, the growth effects of the NO-GC modulators observed in this study can also be attributed to their role in promoting phenotypic modulation. Therefore, it would be valuable to investigate whether the treatment with NO-GC modulators influences the expression of marker proteins associated with contractile or phenotypically modulated VSMCs, in addition to the growth-promoting effect.

The extent to which such *in vitro* findings can be translated to a significantly more complex *in vivo* situation is questionable. Nevertheless, phenotypic modulation of VSMCs plays a crucial role in plaque formation (**Section 1.2**) [6, 45]. Consequently, the model presented for the relevance of the NO/cGMP/cGKI signaling axis in phenotypic modulation of VSMCs may also have implications in the context of atherosclerosis. Our *in vivo* results revealed that BAY Activator treatment results in larger atherosclerotic lesions, accompanied by an increased accumulation of potentially transdifferentiated macrophage-like cells. Combining our *in vitro* and *in vivo* findings, we conclude that activation of the NO/cGMP signaling in contractile medial VSMCs promotes their phenotypic modulation, leading to larger plaques with more transdifferentiated VSMCs.

It is essential to consider that *in vitro*, we observed effects on cGMP levels and the growth of pVSMCs for both NO-GC modulators, whereas *in vivo*, only treatment with the BAY Activator affected lesion area. Importantly, pVSMC growth was exclusively studied under normal conditions. The results of the FRET-based cGMP measurements and the *in vivo* approach strongly suggest that the BAY Activator has a higher efficiency under pathophysiological conditions with increased oxidative stress. A logical next step would be to assess the impact of the BAY Activator on pVSMC growth under oxidative stress conditions. Segura-Puimedon et al. have previously demonstrated that treating VSMCs with ODQ as an oxidative stress mimic inhibits growth [155]. Therefore, we hypothesize that the BAY Activator exerts a pronounced potentiating effect on pVSMC growth under such conditions.

4.4 The SMC-specific NO-GC knockout mouse model

As outlined in **Section 1.5**, interpreting the results of experiments that systematically manipulate the signaling pathway of interest becomes challenging when the observed effects are to be attributed to specific cell types. Additionally, in pharmacological approaches, such as in this study, it is challenging to distinguish between target-specific and non-specific effects as discussed in **Section 4.2.4**. While *in vitro* approaches are valuable for the investigation of isolated cellular processes, they do not capture the complexity of atherosclerosis pathogenesis. A significantly more suitable approach is provided by cell-type-specific and inducible conditional knockout mouse models, which allow for postnatal gene ablation and the attribution of effects to specific cell types. Such a genetic ablation model also offers the opportunity to evaluate the target specificity of drugs and their associated effects. To investigate the functional significance of the NO/cGMP signaling cascade specifically in VSMCs, we selectively deleted the NO-GC β1 subunit (deletion of both NO-GC1 and NO-GC2) in VSMCs using the tamoxifen-inducible Cre/loxP recombination system and compared atherosclerosis development between NO-GC^{smko} mice and control mice after 18 weeks of an atherogenic diet.

Before investigating the effects on atherosclerosis, we first validated the recombination efficiency and tissue specificity of the αSMA-CreER^{T2}-mediated NO-GC knockout. A strictly tamoxifen-dependent high recombination efficiency specific to VSMCs has already been described [169]. In line with this study, we demonstrated at the protein level that the chosen approach led to a highly efficient deletion of NO-GC expression in the aortas of NO-GC^{smko} experimental mice (**Figure 29**). Immunofluorescence analysis showed a significant reduction in NO-GC expression in the cells of the aortic media in NO-GC^{smko} mice at the single-cell level (**Figure 29 A**). This recombination efficiency was also confirmed by Western blot analyses of atherosclerotic aortas from NO-GC^{smko} and control mice (**Figure 29 B**). It is important to note that the reduction in NO-GC expression was limited to the aorta of NO-GC^{smko} mice. However, it should be considered that these analyses were performed only once as proof of principle, and therefore, it is not possible to corroborate these observations through statistical calculations. Nevertheless, the combination of results strongly suggests that the chosen approach successfully reduced NO-GC expression specifically in VSMCs.

Such a VSMC-specific genetic ablation model has also been used by Wolfsgruber et al. to investigate the pathophysiological relevance of cGKI in VSMCs for atherosclerosis [93]. As already mentioned before, this study suggested a pro-atherosclerotic role of the NO/cGMP signaling pathway mediated by cGKI. In line with this, it was reported that a global knockout of the NO-GC α1 subunit had a similar effect on atherosclerosis [155]. Consistent with this, the results of the present study on the effects of the BAY Activator also indicated a pro-atherosclerotic effect of pharmacological activation of the NO/cGMP signaling pathway (**Figure 32 A, D**). However, our results showed that despite the high recombination efficiency, the NO-GC^{smko} did not significantly affect the lesion areas in atherosclerotic aortas in both sexes (**Figure 35 A**). Instead, a possible trend toward an increased lesion area was observed. This trend may suggest an anti-atherosclerotic effect of the NO/cGMP signaling pathway in VSMCs in atherosclerosis. This would be in line with studies that have shown a reduction in lesion areas in atherosclerotic mouse models after treatment with cGMP-elevating drugs [161-164]. This would present a clear contrast to the results of the pharmacological approach in this work. However, the extent to which this trend allows such a conclusion depends significantly on the possible limitations of the study.

As highlighted in **Section 1.3.2**, the NO/cGMP signaling pathway plays a crucial role in the regulation of VSMC contractility and thus also in blood pressure regulation. Consequently, it has been reported that a global knockout of the NO-GC β1 subunit induces chronic hypertension in both male and female mice [123]. A similar increase in systolic blood pressure in male mice was also observed in the VSMC-specific NO-GC knockout mediated by SM-MHC-CreER^{T2}. Thirty days after the last tamoxifen injection, a long-term chronic increase in blood

pressure of 30 mmHg was demonstrated [94]. Given that such a significant chronic increase in blood pressure is considered as a high-risk factor for atherosclerosis, this could explain the trend toward an increased lesion area and would be a significant limiting factor of the study [1, 208]. In the present study, an increase in blood pressure was observed in both sexes of NO-GC^{smko} mice compared to their litter-matched controls, although it did not reach statistical significance (**Figure 31** (male), **Supplementary figure 12** (female)). In this context, we hypothesized that the lack of statistical significance could primarily be attributed to the limited sample size and considerable variation within the experimental groups. To explore this further, the data from male and female mice in each group were pooled after prior statistical verification. The amalgamation of the data from both sexes confirmed the trend of an increase in blood pressure in NO-GC^{smko} mice. Notably, it revealed that the NO-GC^{smko} resulted in a statistically significant increase of approximately 22 mmHg in mean blood pressure compared to the control group (**Figure 35 B**). Some studies have already shown that a comparable increase in blood pressure often correlates with an increased lesion area in atherosclerotic mouse models [208, 234-236]. It is important to note that there is a disagreement in the literature as to whether hypertension *per se* causes the increased atherosclerotic lesion area in atherosclerotic mice or if the major factor is the stimulus that also induces the hypertension [208, 237]. However, currently it cannot be ruled out that the increase in blood pressure may have influenced the results regarding the lesion area in the present study.

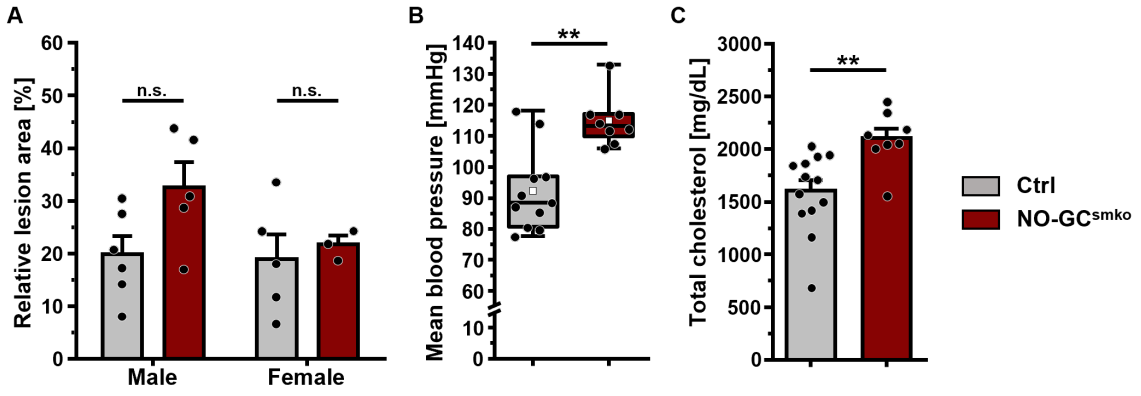

Figure 35. Overview of the main *in vivo* results of the genetic approach.
Overview of SMC-specific NO-GC knockout (NO-GC^{smko}) effects on atherosclerotic lesion area in the total aortas, blood pressure and total cholesterol plasma levels of NO-GC^{smko} and control (Ctrl) mice. The mice were bred on an ApoE-deficient background and fed with an atherogenic diet for 18 weeks. The mice were treated with tamoxifen to induce the NO-GC^{smko}. Intraperitoneal tamoxifen injections occurred in two cycles, each for five consecutive days (5 x 1 mg/mouse/day) at 8 and 10 weeks of age with a nine-day break in between and before switching to an atherogenic diet. **(A)** Analysis of relative lesion area in total aortas by Oil Red O staining of Ctrl and NO-GC^{smko} male and female mice. The atherosclerotic lesion area was determined from both sides of the aorta, averaged, and normalized to the total area of respective part. Data are represented as mean + SEM. **(B)** Mean blood pressure of Ctrl and NO-GC^{smko} mice (pooled sexes). Blood pressure measurements were performed using a tail-cuff blood pressure system at the end of the feeding period for three consecutive days. The data of the three consecutive days were averaged for each animal. Data are represented as median (horizontal line), 25% - 75% interquartile range (box), 5% - 95% range percentile (whiskers) and mean (white square). **(C)** Total cholesterol plasma levels of Ctrl and NO-GC^{smko} mice (pooled sexes). Data are represented as mean + SEM. Statistical significance is indicated by asterisk (*$p \leq 0.05$; **$p \leq 0.01$; n.s.: not significant, tested pairwise Mann-Whitney U test). Ctrl, Control, NO-GC^{smko}, SMC-specific NO-GC knockout.

As already mentioned in **Section 4.2.1**, elevated plasma lipid levels also represent a well-accepted risk factor for the development of atherosclerosis, potentially influencing the formation of atherosclerotic lesions [5, 195]. Quantification of the plasma lipid levels revealed a slight but statistically not significant difference between NO-GC^{smko} mice and their corresponding control mice of both sexes. The extent of this difference was further investigated (after prior statistical verification) by pooling the data from male and female mice, thereby increasing the sample size. It was demonstrated that, in addition to elevated blood pressure, NO-GC^{smko} mice exhibited significantly increased plasma lipid levels, e.g. total cholesterol (**Figure 35 C**). While this increase in lipid levels might have influenced the atherosclerotic lesion area in NO-GC^{smko} mice, no similar effect was observed in mice treated with the BAY Activator.

Both the increase in blood pressure and lipid levels in NO-GC^{smko} mice represent a significant limitation of the study and complicate the interpretation of the results regarding the relevance of the NO/cGMP signaling pathway in VSMCs in atherosclerosis. Furthermore, a clear limiting factor of the present study is the high variance in the experimental groups and the limited number of animals. Therefore, to avoid potential misinterpretations, the sample size for both sexes should first be increased to extract possible significances of the effects while maintaining the effect size.

In addition, it is necessary to examine the extent to which an increase in blood pressure influences the atherosclerotic lesion area. One possibility would be to treat NO-GC^{smko} mice with blood pressure-lowering drugs to avoid blood pressure effects on atherosclerosis. However, it is challenging in this context to determine to what extent the additional pharmacological treatment itself affects atherogenesis. For instance, Doran et al. demonstrated that treatment with Candesartan (angiotensin II receptor antagonist) is suitable for reducing blood pressure in atherosclerotic mouse models and thus suppressing the increase in the lesion area [238]. However, it was also shown that the effect on the lesion area occurred independently of blood pressure reduction and was primarily due to the reduction of inflammation and vascular oxidative stress. Therefore, such an approach, especially regarding the experimental setup, is challenging and requires the choice of an appropriate drug and the corresponding control groups.

In conclusion, interpretation of the observed phenotype of NO-GC^{smko} based on the current results is very complicated. At this stage, the results do not allow definitive conclusions to be drawn regarding the pathophysiological significance of the NO/cGMP pathway in VSMCs in atherosclerosis. An increase in the sample size and further experiments are needed to make an assessment.

5. Conclusion & outlook

The present study has provided new and interesting insights into the pathophysiological and pharmacological relevance of the NO/cGMP signaling pathway in VSMCs in atherosclerosis. To gain a comprehensive overview, we employed both a pharmacological and a genetic approach in this study. First, NO-GC expression was confirmed as the potential drug target under atherosclerotic conditions, highlighting the possibility of modulating the NO/cGMP signaling pathway. Next, a very detailed comparison of the effects of a NO-GC stimulator versus a NO-GC activator on atherosclerosis in male and female mice were determined. This pharmacological approach revealed that the activation of the NO/cGMP signaling axis using the NO-GC stimulator (Vericiguat) had no effect on atherosclerotic lesion area, while the NO-GC activator (BAY Activator) significantly promoted the formation of atherosclerotic lesions in male and female mice. The results of BAY Activator treatment are in accordance with previous studies that have postulated a pathophysiological role of the NO/cGMP/cGKI signaling axis in atherosclerosis based on genetic knockout models, yet they also contradict other studies conducted with similar NO-GC modulators that have demonstrated an anti-atherosclerotic effect. In our study, we were able to rule out several possible causes for this discrepancy. We detected no significant effects on blood pressure, plasma lipid levels, blood cell counts, or other physiological parameters. In addition, incorrect dosing and inadequate drug absorption were eliminated. However, it could not be ruled out that there were off-target effects of the BAY Activator.

Our initial plan was to test the compounds in a NO-GC^{smko} mouse model to validate the specificity of the effects of the respective drugs on the NO/cGMP signaling axis in VSMCs. While the NO-GC^{smko} was successfully generated within the scope of this work, the number of analyzed animals does not yet allow any clear conclusions to be drawn about the effects on atherosclerosis. The preliminary data indicated that a hypertensive phenotype and increased lipid levels induced by NO-GC^{smko} complicates the interpretation of the atherosclerosis data. Consequently, investigation of drug specificity and evaluation of the pathophysiological relevance of the NO/cGMP signaling pathway in VSMCs in atherosclerosis based on this genetic approach were initially deferred. However, *in vitro* experiments were conducted to examine the effects of the NO-GC modulators on the molecular mechanisms and the functional relevance of NO/cGMP signaling activation in VSMCs to better evaluate the specific role of VSMCs in the observed effects on atherosclerosis. The increase in cGMP generation induced by both drugs promoted VSMC growth. In accordance with their respective modes of action, the BAY Activator demonstrated higher efficacy under ODQ-induced oxidative stress conditions, while Vericiguat synergistically enhanced NO-induced cGMP generation. Based on existing literature, we hypothesized that the growth-promoting effects were associated with the role of NO-GC in the phenotypic modulation of VSMCs. Interestingly, the *in vivo* approach also revealed that the

increased atherosclerotic lesion area caused by BAY Activator treatment was accompanied by an accumulation of MAC-2-positive cells, indicating that NO/cGMP signaling activation may lead to an enrichment of macrophage-like cells derived from VSMCs within the plaque, which has to be confirmed in future fate-mapping experiments.

In conclusion, our study proposes a model in which the activation of the NO/cGMP signaling pathway in atherosclerosis promotes the phenotypic modulation of VSMCs, thereby potentially contributing to plaque growth (**Figure 36**). Notably, the BAY Activator exhibited a higher efficacy under conditions characterized by oxidative stress, potentially explaining its significant pro-atherosclerotic effect compared to Vericiguat.

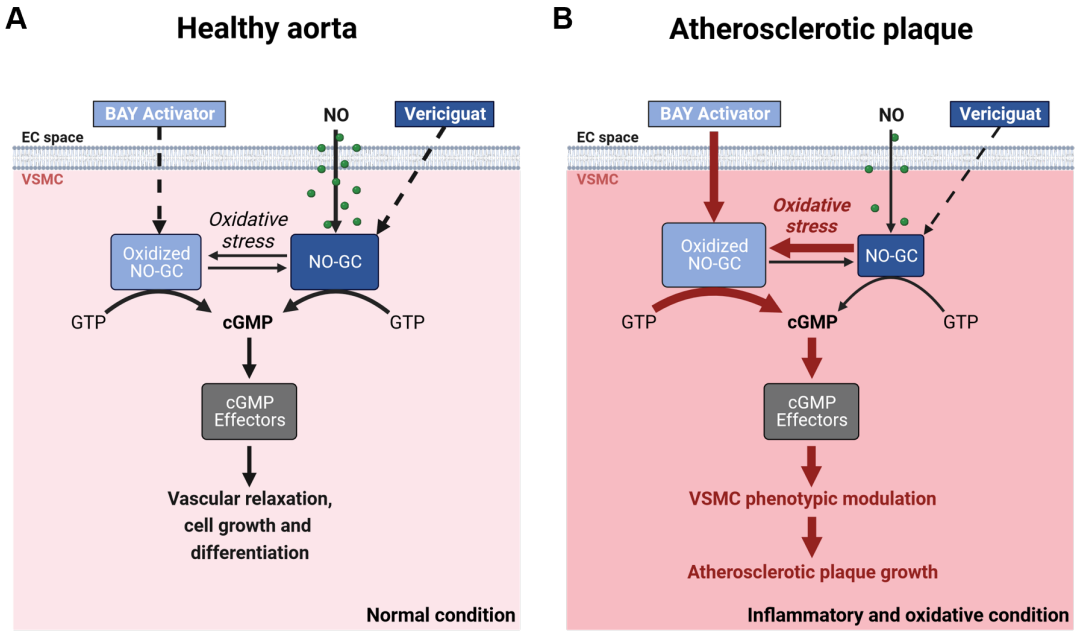

Figure 36. Proposed model of the pathophysiological and pharmacological relevance of the NO/cGMP signaling in VSMCs in atherosclerosis.
(A) In a healthy aorta, the NO/cGMP signaling pathway in vascular smooth muscle cells (VSMCs) plays an important role in regulating vascular relaxation, cell growth, and differentiation. These normal conditions are characterized by a balanced redox equilibrium between the different forms of NO-sensitive guanylyl cyclase (NO-GC): the NO-sensitive heme-containing NO-GC and the NO-insensitive oxidized, heme-free NO-GC. Under these conditions, the pathway can be activated substantially by endogenous nitric oxide (NO), BAY Activator, and Vericiguat. **(B)** We hypothesize that the NO/cGMP signaling pathway holds a significant pathophysiological relevance in the atherosclerotic plaques. Due to the highly inflammatory and oxidative conditions, there is an increased level of oxidative stress, which causes a shift in the redox equilibrium towards the NO-insensitive oxidized, heme-free NO-GC form and a reduced NO bioavailability. Under these conditions, the NO-GC activator BAY Activator exhibits a higher efficacy. Activation of the NO/cGMP signaling pathway promotes the phenotypic modulation of VSMCs, thereby facilitating plaque growth. cGMP, cyclic guanosine monophosphate; GTP, guanosine triphosphate; EC space, extracellular space; PPi, pyrophosphate. Image created using BioRender.com.

Despite our study demonstrating a strong pro-atherosclerotic effect of the BAY Activator, it is essential not to draw premature conclusions, especially in light of the substantial therapeutic benefits of NO-GC modulators in various other diseases. Our results do not question the general utility of NO-GC modulators. Moreover, other studies have pointed to therapeutic benefits in atherosclerosis, and no atherogenic effects or increased mortality rates have been reported in numerous preclinical studies or clinical applications of these drugs. Therefore, it is essential

to perform further preclinical research to thoroughly investigate the causes of the observed effects of the BAY Activator on atherosclerosis. In this context, the following aspects need to be clarified and require further research:

(1) *In vitro* cGMP imaging has provided evidence that the BAY Activator has an increased efficiency under conditions of oxidative stress induced by ODQ. However, the effect on growth was only tested under normal conditions (absence of ODQ). It would be interesting to test whether the efficacy of BAY Activator in promoting growth is also enhanced under ODQ-induced oxidative stress conditions, especially compared with the NO-GC stimulator Vericiguat.

(2) In the present study, the growth-promoting effects of the activation of the NO/cGMP signaling axis in VSMCs *in vitro* were demonstrated. In the literature, these effects have been attributed to a role in promoting phenotypic modulation. Immunohistochemical investigations or single-cell transcriptomic studies should be considered to examine whether treatment with NO-GC modulators, in addition to its growth-promoting effect, also influences the expression of marker proteins associated with contractile or phenotypically modulated VSMCs.

(3) The cellular origin of the accumulated MAC2-positive cells within the atherosclerotic plaque has not been sufficiently clarified. Inducible fate-mapping experiments are required to determine whether these cells originate from medial VSMCs or monocytes/macrophages.

(4) Furthermore, it is unclear whether the observed effects of the BAY Activator are representative for all NO-GC activators. To test such a class-wide effect, a comparative study with another NO-GC activator, such as Ataciguat or Cinaciguat, should be conducted.

(5) The chosen genetic approach in this study has not yet yielded clear results and has been unable to provide definitive conclusions about the pathophysiological relevance of the NO/cGMP signaling pathway in VSMCs in atherosclerosis. To make a more precise assessment, it will be necessary to increase the sample size. In this context, it will be important to validate the suitability of the NO-GC^{smko} mouse model for the pending verification of the specificity of the effects of BAY Activator on the NO/cGMP signaling axis in VSMCs.

References

1. Bjorkegren, J.L.M., Lusis, A.J. (2022). Atherosclerosis: Recent developments. *Cell*, *185*(10), 1630-1645. doi: 10.1016/j.cell.2022.04.004.
2. WHO. (2020). *The top 10 causes of death*. Retrieved 08.07.2023 from https://www.who.int/news-room/fact-sheets/detail/the-top-10-causes-of-death
3. Libby, P., Buring, J.E., Badimon, L., Hansson, G.K., Deanfield, J., Bittencourt, M.S., . . . Lewis, E.F. (2019). Atherosclerosis. *Nat Rev Dis Primers*, *5*(1), 56. doi: 10.1038/s41572-019-0106-z.
4. Fan, J., Watanabe, T. (2022). Atherosclerosis: Known and unknown. *Pathol Int*, *72*(3), 151-160. doi: 10.1111/pin.13202.
5. Libby, P. (2021). The changing landscape of atherosclerosis. *Nature*, *592*(7855), 524-533. doi: 10.1038/s41586-021-03392-8.
6. Basatemur, G.L., Jorgensen, H.F., Clarke, M.C.H., Bennett, M.R., Mallat, Z. (2019). Vascular smooth muscle cells in atherosclerosis. *Nat Rev Cardiol*, *16*(12), 727-744. doi: 10.1038/s41569-019-0227-9.
7. Manfredi, R., Verdoia, M., Compagnucci, P., Barbarossa, A., Stronati, G., Casella, M., . . . Ciliberti, G. (2022). Angina in 2022: Current Perspectives. *J Clin Med*, *11*(23). doi: 10.3390/jcm11236891.
8. Doenst, T., Thiele, H., Haasenritter, J., Wahlers, T., Massberg, S., Haverich, A. (2022). The Treatment of Coronary Artery Disease. *Dtsch Arztebl Int*, *119*(42), 716-723. doi: 10.3238/arztebl.m2022.0277.
9. Newman, C.B., Preiss, D., Tobert, J.A., Jacobson, T.A., Page, R.L., 2nd, Goldstein, L.B., . . . Stroke, C. (2019). Statin Safety and Associated Adverse Events: A Scientific Statement From the American Heart Association. *Arterioscler Thromb Vasc Biol*, *39*(2), e38-e81. doi: 10.1161/ATV.0000000000000073.
10. Hetherington, I., Totary-Jain, H. (2022). Anti-atherosclerotic therapies: Milestones, challenges, and emerging innovations. *Mol Ther*, *30*(10), 3106-3117. doi: 10.1016/j.ymthe.2022.08.024.
11. Tsao, C.W., Aday, A.W., Almarzooq, Z.I., Anderson, C.A.M., Arora, P., Avery, C.L., . . . Stroke Statistics, S. (2023). Heart Disease and Stroke Statistics-2023 Update: A Report From the American Heart Association. *Circulation*, *147*(8), e93-e621. doi: 10.1161/CIR.0000000000001123.
12. Wu, C., Daugherty, A., Lu, H.S. (2019). Updates on Approaches for Studying Atherosclerosis. *Arterioscler Thromb Vasc Biol*, *39*(4), e108-e117. doi: 10.1161/ATVBAHA.119.312001.
13. Daugherty, A., Tall, A.R., Daemen, M., Falk, E., Fisher, E.A., Garcia-Cardena, G., . . . Council on Basic Cardiovascular, S. (2017). Recommendation on Design, Execution, and Reporting of Animal Atherosclerosis Studies: A Scientific Statement From the American Heart Association. *Circ Res*, *121*(6), e53-e79. doi: 10.1161/RES.0000000000000169.
14. Emini Veseli, B., Perrotta, P., De Meyer, G.R.A., Roth, L., Van der Donckt, C., Martinet, W., . . . De Meyer, G.R.Y. (2017). Animal models of atherosclerosis. *Eur J Pharmacol*, *816*, 3-13. doi: 10.1016/j.ejphar.2017.05.010.
15. Meir, K.S., Leitersdorf, E. (2004). Atherosclerosis in the apolipoprotein-E-deficient mouse: a decade of progress. *Arterioscler Thromb Vasc Biol*, *24*(6), 1006-14. doi: 10.1161/01.ATV.0000128849.12617.f4.
16. Piedrahita, J.A., Zhang, S.H., Hagaman, J.R., Oliver, P.M., Maeda, N. (1992). Generation of mice carrying a mutant apolipoprotein E gene inactivated by gene targeting in embryonic stem cells. *Proc Natl Acad Sci U S A*, *89*(10), 4471-5. doi: 10.1073/pnas.89.10.4471.
17. Plump, A.S., Smith, J.D., Hayek, T., Aalto-Setala, K., Walsh, A., Verstuyft, J.G., . . . Breslow, J.L. (1992). Severe hypercholesterolemia and atherosclerosis in apolipoprotein E-deficient mice created by homologous recombination in ES cells. *Cell*, *71*(2), 343-53. doi: 10.1016/0092-8674(92)90362-g.

18. Oppi, S., Luscher, T.F., Stein, S. (2019). Mouse Models for Atherosclerosis Research-Which Is My Line? *Front Cardiovasc Med*, *6*, 46. doi: 10.3389/fcvm.2019.00046.

19. Nakashima, Y., Plump, A.S., Raines, E.W., Breslow, J.L., Ross, R. (1994). ApoE-deficient mice develop lesions of all phases of atherosclerosis throughout the arterial tree. *Arterioscler Thromb*, *14*(1), 133-40. doi: 10.1161/01.atv.14.1.133.

20. Yurdagul, A., Jr., Finney, A.C., Woolard, M.D., Orr, A.W. (2016). The arterial microenvironment: the where and why of atherosclerosis. *Biochem J*, *473*(10), 1281-95. doi: 10.1042/BJ20150844.

21. Wagenseil, J.E., Mecham, R.P. (2009). Vascular extracellular matrix and arterial mechanics. *Physiol Rev*, *89*(3), 957-89. doi: 10.1152/physrev.00041.2008.

22. Kruger-Genge, A., Blocki, A., Franke, R.P., Jung, F. (2019). Vascular Endothelial Cell Biology: An Update. *Int J Mol Sci*, *20*(18). doi: 10.3390/ijms20184411.

23. Nakashima, Y., Wight, T.N., Sueishi, K. (2008). Early atherosclerosis in humans: role of diffuse intimal thickening and extracellular matrix proteoglycans. *Cardiovasc Res*, *79*(1), 14-23. doi: 10.1093/cvr/cvn099.

24. Mazurek, R., Dave, J.M., Chandran, R.R., Misra, A., Sheikh, A.Q., Greif, D.M. (2017). Vascular Cells in Blood Vessel Wall Development and Disease. *Adv Pharmacol*, *78*, 323-350. doi: 10.1016/bs.apha.2016.08.001.

25. Ruddy, J.M., Jones, J.A., Spinale, F.G., Ikonomidis, J.S. (2008). Regional heterogeneity within the aorta: relevance to aneurysm disease. *J Thorac Cardiovasc Surg*, *136*(5), 1123-30. doi: 10.1016/j.jtcvs.2008.06.027.

26. Dobnikar, L., Taylor, A.L., Chappell, J., Oldach, P., Harman, J.L., Oerton, E., . . . Jorgensen, H.F. (2018). Disease-relevant transcriptional signatures identified in individual smooth muscle cells from healthy mouse vessels. *Nat Commun*, *9*(1), 4567. doi: 10.1038/s41467-018-06891-x.

27. Grootaert, M.O.J., Bennett, M.R. (2021). Vascular smooth muscle cells in atherosclerosis: time for a re-assessment. *Cardiovasc Res*, *117*(11), 2326-2339. doi: 10.1093/cvr/cvab046.

28. Stenmark, K.R., Yeager, M.E., El Kasmi, K.C., Nozik-Grayck, E., Gerasimovskaya, E.V., Li, M., . . . Frid, M.G. (2013). The adventitia: essential regulator of vascular wall structure and function. *Annu Rev Physiol*, *75*, 23-47. doi: 10.1146/annurev-physiol-030212-183802.

29. Warboys, C.M., Amini, N., de Luca, A., Evans, P.C. (2011). The role of blood flow in determining the sites of atherosclerotic plaques. *F1000 Med Rep*, *3*, 5. doi: 10.3410/M3-5.

30. Boren, J., Williams, K.J. (2016). The central role of arterial retention of cholesterol-rich apolipoprotein-B-containing lipoproteins in the pathogenesis of atherosclerosis: a triumph of simplicity. *Curr Opin Lipidol*, *27*(5), 473-83. doi: 10.1097/MOL.0000000000000330.

31. Gimbrone, M.A., Jr., Garcia-Cardena, G. (2016). Endothelial Cell Dysfunction and the Pathobiology of Atherosclerosis. *Circ Res*, *118*(4), 620-36. doi: 10.1161/CIRCRESAHA.115.306301.

32. Robbins, C.S., Hilgendorf, I., Weber, G.F., Theurl, I., Iwamoto, Y., Figueiredo, J.L., . . . Swirski, F.K. (2013). Local proliferation dominates lesional macrophage accumulation in atherosclerosis. *Nat Med*, *19*(9), 1166-72. doi: 10.1038/nm.3258.

33. Feil, S., Fehrenbacher, B., Lukowski, R., Essmann, F., Schulze-Osthoff, K., Schaller, M., . . . Feil, R. (2014). Transdifferentiation of vascular smooth muscle cells to macrophage-like cells during atherogenesis. *Circ Res*, *115*(7), 662-7. doi: 10.1161/CIRCRESAHA.115.304634.

34. Harman, J.L., Jorgensen, H.F. (2019). The role of smooth muscle cells in plaque stability: Therapeutic targeting potential. *Br J Pharmacol*, *176*(19), 3741-3753. doi: 10.1111/bph.14779.

35. Jebari-Benslaiman, S., Galicia-Garcia, U., Larrea-Sebal, A., Olaetxea, J.R., Alloza, I., Vandenbroeck, K., . . . Martin, C. (2022). Pathophysiology of Atherosclerosis. *Int J Mol Sci*, *23*(6). doi: 10.3390/ijms23063346.

36. Kong, P., Cui, Z.Y., Huang, X.F., Zhang, D.D., Guo, R.J., Han, M. (2022). Inflammation and atherosclerosis: signaling pathways and therapeutic intervention. *Signal Transduct Target Ther*, *7*(1), 131. doi: 10.1038/s41392-022-00955-7.

37. Doran, A.C., Yurdagul, A., Jr., Tabas, I. (2020). Efferocytosis in health and disease. *Nat Rev Immunol*, *20*(4), 254-267. doi: 10.1038/s41577-019-0240-6.

38. Galis, Z.S., Sukhova, G.K., Kranzhofer, R., Clark, S., Libby, P. (1995). Macrophage foam cells from experimental atheroma constitutively produce matrix-degrading proteinases. *Proc Natl Acad Sci U S A*, *92*(2), 402-6. doi: 10.1073/pnas.92.2.402.

39. Luo, X., Lv, Y., Bai, X., Qi, J., Weng, X., Liu, S., . . . Yu, B. (2021). Plaque Erosion: A Distinctive Pathological Mechanism of Acute Coronary Syndrome. *Front Cardiovasc Med*, *8*, 711453. doi: 10.3389/fcvm.2021.711453.

40. Owens, G.K., Kumar, M.S., Wamhoff, B.R. (2004). Molecular regulation of vascular smooth muscle cell differentiation in development and disease. *Physiol Rev*, *84*(3), 767-801. doi: 10.1152/physrev.00041.2003.

41. Owens, G.K. (1995). Regulation of differentiation of vascular smooth muscle cells. *Physiol Rev*, *75*(3), 487-517. doi: 10.1152/physrev.1995.75.3.487.

42. Babu, G.J., Warshaw, D.M., Periasamy, M. (2000). Smooth muscle myosin heavy chain isoforms and their role in muscle physiology. *Microsc Res Tech*, *50*(6), 532-40. doi: 10.1002/1097-0029(20000915)50:6<532::AID-JEMT10>3.0.CO;2-E.

43. Sweeney, H.L., Hammers, D.W. (2018). Muscle Contraction. *Cold Spring Harb Perspect Biol*, *10*(2). doi: 10.1101/cshperspect.a023200.

44. Rensen, S.S., Doevendans, P.A., van Eys, G.J. (2007). Regulation and characteristics of vascular smooth muscle cell phenotypic diversity. *Neth Heart J*, *15*(3), 100-8. doi: 10.1007/BF03085963.

45. Allahverdian, S., Chaabane, C., Boukais, K., Francis, G.A., Bochaton-Piallat, M.L. (2018). Smooth muscle cell fate and plasticity in atherosclerosis. *Cardiovasc Res*, *114*(4), 540-550. doi: 10.1093/cvr/cvy022.

46. Liu, M., Gomez, D. (2019). Smooth Muscle Cell Phenotypic Diversity. *Arterioscler Thromb Vasc Biol*, *39*(9), 1715-1723. doi: 10.1161/ATVBAHA.119.312131.

47. Jacobsen, K., Lund, M.B., Shim, J., Gunnersen, S., Fuchtbauer, E.M., Kjolby, M., . . . Bentzon, J.F. (2017). Diverse cellular architecture of atherosclerotic plaque derives from clonal expansion of a few medial SMCs. *JCI Insight*, *2*(19). doi: 10.1172/jci.insight.95890.

48. Chappell, J., Harman, J.L., Narasimhan, V.M., Yu, H., Foote, K., Simons, B.D., . . . Jorgensen, H.F. (2016). Extensive Proliferation of a Subset of Differentiated, yet Plastic, Medial Vascular Smooth Muscle Cells Contributes to Neointimal Formation in Mouse Injury and Atherosclerosis Models. *Circ Res*, *119*(12), 1313-1323. doi: 10.1161/CIRCRESAHA.116.309799.

49. Wamhoff, B.R., Hoofnagle, M.H., Burns, A., Sinha, S., McDonald, O.G., Owens, G.K. (2004). A G/C element mediates repression of the SM22alpha promoter within phenotypically modulated smooth muscle cells in experimental atherosclerosis. *Circ Res*, *95*(10), 981-8. doi: 10.1161/01.RES.0000147961.09840.fb.

50. Campbell, J.H., Campbell, G.R. (2012). Smooth muscle phenotypic modulation--a personal experience. *Arterioscler Thromb Vasc Biol*, *32*(8), 1784-9. doi: 10.1161/ATVBAHA.111.243212.

51. Chamley-Campbell, J., Campbell, G.R., Ross, R. (1979). The smooth muscle cell in culture. *Physiol Rev*, *59*(1), 1-61. doi: 10.1152/physrev.1979.59.1.1.

52. Thyberg, J., Palmberg, L., Nilsson, J., Ksiazek, T., Sjolund, M. (1983). Phenotype modulation in primary cultures of arterial smooth muscle cells. On the role of platelet-derived growth factor. *Differentiation*, *25*(2), 156-67. doi: 10.1111/j.1432-0436.1984.tb01351.x.

53. Chamley, J.H., Campbell, G.R., McConnell, J.D., Groschel-Stewart, U. (1977). Comparison of vascular smooth muscle cells from adult human, monkey and rabbit in primary culture and in subculture. *Cell Tissue Res*, *177*(4), 503-22. doi: 10.1007/BF00220611.

54. Chamley-Campbell, J.H., Campbell, G.R., Ross, R. (1981). Phenotype-dependent response of cultured aortic smooth muscle to serum mitogens. *J Cell Biol*, *89*(2), 379-83. doi: 10.1083/jcb.89.2.379.

55. Han, M., Wen, J.K., Zheng, B., Cheng, Y., Zhang, C. (2006). Serum deprivation results in redifferentiation of human umbilical vascular smooth muscle cells. *Am J Physiol Cell Physiol*, *291*(1), C50-8. doi: 10.1152/ajpcell.00524.2005.

56. Kato, M., Kyogoku, M. (1990). Competence growth factors evoke the phenotypic transition of arterial smooth muscle cells. *Ann N Y Acad Sci*, *598*, 232-7. doi: 10.1111/j.1749-6632.1990.tb42295.x.

57. Rong, J.X., Shapiro, M., Trogan, E., Fisher, E.A. (2003). Transdifferentiation of mouse aortic smooth muscle cells to a macrophage-like state after cholesterol loading. *Proc Natl Acad Sci U S A*, *100*(23), 13531-6. doi: 10.1073/pnas.1735526100.

58. Shankman, L.S., Gomez, D., Cherepanova, O.A., Salmon, M., Alencar, G.F., Haskins, R.M., . . . Owens, G.K. (2015). KLF4-dependent phenotypic modulation of smooth muscle cells has a key role in atherosclerotic plaque pathogenesis. *Nat Med*, *21*(6), 628-37. doi: 10.1038/nm.3866.

59. Wang, Y., Dubland, J.A., Allahverdian, S., Asonye, E., Sahin, B., Jaw, J.E., . . . Francis, G.A. (2019). Smooth Muscle Cells Contribute the Majority of Foam Cells in ApoE (Apolipoprotein E)-Deficient Mouse Atherosclerosis. *Arterioscler Thromb Vasc Biol*, *39*(5), 876-887. doi: 10.1161/ATVBAHA.119.312434.

60. Allahverdian, S., Chehroudi, A.C., McManus, B.M., Abraham, T., Francis, G.A. (2014). Contribution of intimal smooth muscle cells to cholesterol accumulation and macrophage-like cells in human atherosclerosis. *Circulation*, *129*(15), 1551-9. doi: 10.1161/CIRCULATIONAHA.113.005015.

61. Kim, J.B., Zhao, Q., Nguyen, T., Pjanic, M., Cheng, P., Wirka, R., . . . Quertermous, T. (2020). Environment-Sensing Aryl Hydrocarbon Receptor Inhibits the Chondrogenic Fate of Modulated Smooth Muscle Cells in Atherosclerotic Lesions. *Circulation*, *142*(6), 575-590. doi: 10.1161/CIRCULATIONAHA.120.045981.

62. Naik, V., Leaf, E.M., Hu, J.H., Yang, H.Y., Nguyen, N.B., Giachelli, C.M., . . . Speer, M.Y. (2012). Sources of cells that contribute to atherosclerotic intimal calcification: an in vivo genetic fate mapping study. *Cardiovasc Res*, *94*(3), 545-54. doi: 10.1093/cvr/cvs126.

63. Wirka, R.C., Wagh, D., Paik, D.T., Pjanic, M., Nguyen, T., Miller, C.L., . . . Quertermous, T. (2019). Atheroprotective roles of smooth muscle cell phenotypic modulation and the TCF21 disease gene as revealed by single-cell analysis. *Nat Med*, *25*(8), 1280-1289. doi: 10.1038/s41591-019-0512-5.

64. Bentzon, J.F., Majesky, M.W. (2018). Lineage tracking of origin and fate of smooth muscle cells in atherosclerosis. *Cardiovasc Res*, *114*(4), 492-500. doi: 10.1093/cvr/cvx251.

65. Pan, H., Reilly, M.P. (2019). A protective smooth muscle cell transition in atherosclerosis. *Nat Med*, *25*(8), 1194-1195. doi: 10.1038/s41591-019-0541-0.

66. Bennett, M.R., Sinha, S., Owens, G.K. (2016). Vascular Smooth Muscle Cells in Atherosclerosis. *Circ Res*, *118*(4), 692-702. doi: 10.1161/CIRCRESAHA.115.306361.

67. Hofmann, F. (2020). The cGMP system: components and function. *Biol Chem*, *401*(4), 447-469. doi: 10.1515/hsz-2019-0386.

68. Kemp-Harper, B., Feil, R. (2008). Meeting report: cGMP matters. *Sci Signal*, *1*(9), pe12. doi: 10.1126/stke.19pe12.

69. Thoonen, R., Sips, P.Y., Bloch, K.D., Buys, E.S. (2013). Pathophysiology of hypertension in the absence of nitric oxide/cyclic GMP signaling. *Curr Hypertens Rep*, *15*(1), 47-58. doi: 10.1007/s11906-012-0320-5.

70. Lehners, M., Dobrowinski, H., Feil, S., Feil, R. (2018). cGMP Signaling and Vascular Smooth Muscle Cell Plasticity. *J Cardiovasc Dev Dis*, *5*(2). doi: 10.3390/jcdd5020020.

71. Ashman, D.F., Lipton, R., Melicow, M.M., Price, T.D. (1963). Isolation of adenosine 3', 5'-monophosphate and guanosine 3', 5'-monophosphate from rat urine. *Biochem Biophys Res Commun*, *11*, 330-4. doi: 10.1016/0006-291x(63)90566-7.

72. Kuhn, M. (2016). Molecular Physiology of Membrane Guanylyl Cyclase Receptors. *Physiol Rev*, *96*(2), 751-804. doi: 10.1152/physrev.00022.2015.

73. Friebe, A., Koesling, D. (2009). The function of NO-sensitive guanylyl cyclase: what we can learn from genetic mouse models. *Nitric Oxide*, *21*(3-4), 149-56. doi: 10.1016/j.niox.2009.07.004.

74. Forstermann, U., Sessa, W.C. (2012). Nitric oxide synthases: regulation and function. *Eur Heart J*, *33*(7), 829-37, 837a-837d. doi: 10.1093/eurheartj/ehr304.

75. Biel, M., Michalakis, S. (2009). Cyclic nucleotide-gated channels. *Handb Exp Pharmacol*(191), 111-36. doi: 10.1007/978-3-540-68964-5_7.

76. Hofmann, F., Feil, R., Kleppisch, T., Schlossmann, J. (2006). Function of cGMP-dependent protein kinases as revealed by gene deletion. *Physiol Rev*, *86*(1), 1-23. doi: 10.1152/physrev.00015.2005.

77. Francis, S.H., Blount, M.A., Corbin, J.D. (2011). Mammalian cyclic nucleotide phosphodiesterases: molecular mechanisms and physiological functions. *Physiol Rev*, *91*(2), 651-90. doi: 10.1152/physrev.00030.2010.

78. Feil, R., Lehners, M., Stehle, D., Feil, S. (2022). Visualising and understanding cGMP signals in the cardiovascular system. *Br J Pharmacol*, *179*(11), 2394-2412. doi: 10.1111/bph.15500.

79. Sandner, P., Follmann, M., Becker-Pelster, E., Hahn, M.G., Meier, C., Freitas, C., . . . Stasch, J.P. (2021). Soluble GC stimulators and activators: Past, present and future. *Br J Pharmacol*. doi: 10.1111/bph.15698.

80. Ghofrani, H.A., Galie, N., Grimminger, F., Grunig, E., Humbert, M., Jing, Z.C., . . . Group, P.-S. (2013). Riociguat for the treatment of pulmonary arterial hypertension. *N Engl J Med*, *369*(4), 330-40. doi: 10.1056/NEJMoa1209655.

81. Follmann, M., Ackerstaff, J., Redlich, G., Wunder, F., Lang, D., Kern, A., . . . Stasch, J.P. (2017). Discovery of the Soluble Guanylate Cyclase Stimulator Vericiguat (BAY 1021189) for the Treatment of Chronic Heart Failure. *J Med Chem*, *60*(12), 5146-5161. doi: 10.1021/acs.jmedchem.7b00449.

82. Armstrong, P.W., Pieske, B., Anstrom, K.J., Ezekowitz, J., Hernandez, A.F., Butler, J., . . . Group, V.S. (2020). Vericiguat in Patients with Heart Failure and Reduced Ejection Fraction. *N Engl J Med*, *382*(20), 1883-1893. doi: 10.1056/NEJMoa1915928.

83. Baillie, G.S., Tejeda, G.S., Kelly, M.P. (2019). Therapeutic targeting of 3',5'-cyclic nucleotide phosphodiesterases: inhibition and beyond. *Nat Rev Drug Discov*, *18*(10), 770-796. doi: 10.1038/s41573-019-0033-4.

84. McMurray, J.J., Packer, M., Desai, A.S., Gong, J., Lefkowitz, M.P., Rizkala, A.R., . . . Committees. (2014). Angiotensin-neprilysin inhibition versus enalapril in heart failure. *N Engl J Med*, *371*(11), 993-1004. doi: 10.1056/NEJMoa1409077.

85. Solomon, S.D., Vaduganathan, M., B, L.C., Packer, M., Zile, M., Swedberg, K., . . . McMurray, J.J.V. (2020). Sacubitril/Valsartan Across the Spectrum of Ejection Fraction in Heart Failure. *Circulation*, *141*(5), 352-361. doi: 10.1161/CIRCULATIONAHA.119.044586.

86. Feygina, E.E., Katrukha, A.G., Semenov, A.G. (2019). Neutral Endopeptidase (Neprilysin) in Therapy and Diagnostics: Yin and Yang. *Biochemistry (Mosc)*, *84*(11), 1346-1358. doi: 10.1134/S0006297919110105.

87. Savarirayan, R., Irving, M., Bacino, C.A., Bostwick, B., Charrow, J., Cormier-Daire, V., . . . Hoover-Fong, J. (2019). C-Type Natriuretic Peptide Analogue Therapy in Children with Achondroplasia. *N Engl J Med*, *381*(1), 25-35. doi: 10.1056/NEJMoa1813446.

88. Savarirayan, R., Tofts, L., Irving, M., Wilcox, W., Bacino, C.A., Hoover-Fong, J., . . . Day, J. (2020). Once-daily, subcutaneous vosoritide therapy in children with achondroplasia: a randomised, double-blind, phase 3, placebo-controlled, multicentre trial. *Lancet*, *396*(10252), 684-692. doi: 10.1016/S0140-6736(20)31541-5.

89. Duggan, S. (2021). Vosoritide: First Approval. *Drugs*, *81*(17), 2057-2062. doi: 10.1007/s40265-021-01623-w.

90. Feil, R., Kemp-Harper, B. (2006). cGMP signalling: from bench to bedside. Conference on cGMP generators, effectors and therapeutic implications. *EMBO Rep*, *7*(2), 149-53. doi: 10.1038/sj.embor.7400627.

91. Ignarro, L.J., Byrns, R.E., Buga, G.M., Wood, K.S. (1987). Endothelium-derived relaxing factor from pulmonary artery and vein possesses pharmacologic and chemical properties identical to those of nitric oxide radical. *Circ Res*, *61*(6), 866-79. doi: 10.1161/01.res.61.6.866.

92. Weinmeister, P., Lukowski, R., Linder, S., Traidl-Hoffmann, C., Hengst, L., Hofmann, F., . . . Feil, R. (2008). Cyclic guanosine monophosphate-dependent protein kinase I promotes adhesion of primary vascular smooth muscle cells. *Mol Biol Cell*, *19*(10), 4434-41. doi: 10.1091/mbc.e08-04-0370.

93. Wolfsgruber, W., Feil, S., Brummer, S., Kuppinger, O., Hofmann, F., Feil, R. (2003). A proatherogenic role for cGMP-dependent protein kinase in vascular smooth muscle cells. *Proc Natl Acad Sci U S A*, *100*(23), 13519-24. doi: 10.1073/pnas.1936024100.

94. Groneberg, D., Konig, P., Wirth, A., Offermanns, S., Koesling, D., Friebe, A. (2010). Smooth muscle-specific deletion of nitric oxide-sensitive guanylyl cyclase is sufficient to induce hypertension in mice. *Circulation*, *121*(3), 401-9. doi: 10.1161/CIRCULATIONAHA.109.890962.

95. Holtwick, R., Gotthardt, M., Skryabin, B., Steinmetz, M., Potthast, R., Zetsche, B., . . . Kuhn, M. (2002). Smooth muscle-selective deletion of guanylyl cyclase-A prevents the acute but not chronic effects of ANP on blood pressure. *Proc Natl Acad Sci U S A*, *99*(10), 7142-7. doi: 10.1073/pnas.102650499.

96. Krawutschke, C., Koesling, D., Russwurm, M. (2015). Cyclic GMP in Vascular Relaxation: Export Is of Similar Importance as Degradation. *Arterioscler Thromb Vasc Biol*, *35*(9), 2011-9. doi: 10.1161/ATVBAHA.115.306133.

97. Nakao, K., Kuwahara, K., Nishikimi, T., Nakagawa, Y., Kinoshita, H., Minami, T., . . . Nakao, K. (2017). Endothelium-Derived C-Type Natriuretic Peptide Contributes to Blood Pressure Regulation by Maintaining Endothelial Integrity. *Hypertension*, *69*(2), 286-296. doi: 10.1161/HYPERTENSIONAHA.116.08219.

98. Weber, S., Bernhard, D., Lukowski, R., Weinmeister, P., Worner, R., Wegener, J.W., . . . Feil, R. (2007). Rescue of cGMP kinase I knockout mice by smooth muscle specific expression of either isozyme. *Circ Res*, *101*(11), 1096-103. doi: 10.1161/CIRCRESAHA.107.154351.

99. Lehners, M. (2022). *CNP-dependent cGMP signalling in vascular smooth muscle cells: from phenotypic plasticity to atherosclerosis* [Doctoral Thesis, University of Tubingen]. http://hdl.handle.net/10900/128603

100. Potter, L.R., Yoder, A.R., Flora, D.R., Antos, L.K., Dickey, D.M. (2009). Natriuretic peptides: their structures, receptors, physiologic functions and therapeutic applications. *Handb Exp Pharmacol*(191), 341-66. doi: 10.1007/978-3-540-68964-5_15.

101. Koller, K.J., Goeddel, D.V. (1992). Molecular biology of the natriuretic peptides and their receptors. *Circulation*, *86*(4), 1081-8. doi: 10.1161/01.cir.86.4.1081.

102. Suga, S., Nakao, K., Hosoda, K., Mukoyama, M., Ogawa, Y., Shirakami, G., . . . et al. (1992). Receptor selectivity of natriuretic peptide family, atrial natriuretic peptide, brain natriuretic peptide, and C-type natriuretic peptide. *Endocrinology*, *130*(1), 229-39. doi: 10.1210/endo.130.1.1309330.

103. Wu, C., Wu, F., Pan, J., Morser, J., Wu, Q. (2003). Furin-mediated processing of Pro-C-type natriuretic peptide. *J Biol Chem*, *278*(28), 25847-52. doi: 10.1074/jbc.M301223200.

104. Nishikimi, T., Kuwahara, K., Nakao, K. (2011). Current biochemistry, molecular biology, and clinical relevance of natriuretic peptides. *J Cardiol*, *57*(2), 131-40. doi: 10.1016/j.jjcc.2011.01.002.

105. Ogawa, T., de Bold, A.J. (2014). The heart as an endocrine organ. *Endocr Connect*, *3*(2), R31-44. doi: 10.1530/EC-14-0012.

106. Moyes, A.J., Hobbs, A.J. (2019). C-type Natriuretic Peptide: A Multifaceted Paracrine Regulator in the Heart and Vasculature. *Int J Mol Sci*, *20*(9). doi: 10.3390/ijms20092281.

107. Kelsall, C.J., Chester, A.H., Sarathchandra, P., Singer, D.R. (2006). Expression and localization of C-type natriuretic peptide in human vascular smooth muscle cells. *Vascul Pharmacol*, *45*(6), 368-73. doi: 10.1016/j.vph.2006.06.011.

108. Potter, L.R. (2011). Natriuretic peptide metabolism, clearance and degradation. *FEBS J*, *278*(11), 1808-17. doi: 10.1111/j.1742-4658.2011.08082.x.

109. Anand-Srivastava, M.B. (2005). Natriuretic peptide receptor-C signaling and regulation. *Peptides*, *26*(6), 1044-59. doi: 10.1016/j.peptides.2004.09.023.

110. Koesling, D., Mergia, E., Russwurm, M. (2016). Physiological Functions of NO-Sensitive Guanylyl Cyclase Isoforms. *Curr Med Chem*, *23*(24), 2653-2665. doi: 10.2174/0929867323666160812145050.

111. Mergia, E., Friebe, A., Dangel, O., Russwurm, M., Koesling, D. (2006). Spare guanylyl cyclase NO receptors ensure high NO sensitivity in the vascular system. *J Clin Invest*, *116*(6), 1731-7. doi: 10.1172/JCI27657.

112. Stuehr, D.J., Santolini, J., Wang, Z.Q., Wei, C.C., Adak, S. (2004). Update on mechanism and catalytic regulation in the NO synthases. *J Biol Chem*, *279*(35), 36167-70. doi: 10.1074/jbc.R400017200.

113. Geller, D.A., Billiar, T.R. (1998). Molecular biology of nitric oxide synthases. *Cancer Metastasis Rev*, *17*(1), 7-23. doi: 10.1023/a:1005940202801.

114. Hall, C.N., Garthwaite, J. (2009). What is the real physiological NO concentration in vivo? *Nitric Oxide*, *21*(2), 92-103. doi: 10.1016/j.niox.2009.07.002.

115. Friebe, A., Voussen, B., Groneberg, D. (2018). NO-GC in cells 'off the beaten track'. *Nitric Oxide*, *77*, 12-18. doi: 10.1016/j.niox.2018.03.020.

116. Horst, B.G., Marletta, M.A. (2018). Physiological activation and deactivation of soluble guanylate cyclase. *Nitric Oxide*, *77*, 65-74. doi: 10.1016/j.niox.2018.04.011.

117. Hess, D.T., Matsumoto, A., Kim, S.O., Marshall, H.E., Stamler, J.S. (2005). Protein S-nitrosylation: purview and parameters. *Nat Rev Mol Cell Biol*, *6*(2), 150-66. doi: 10.1038/nrm1569.

118. Feil, R., Lohmann, S.M., de Jonge, H., Walter, U., Hofmann, F. (2003). Cyclic GMP-dependent protein kinases and the cardiovascular system: insights from genetically modified mice. *Circ Res*, *93*(10), 907-16. doi: 10.1161/01.RES.0000100390.68771.CC.

119. Bender, A.T., Beavo, J.A. (2006). Cyclic nucleotide phosphodiesterases: molecular regulation to clinical use. *Pharmacol Rev*, *58*(3), 488-520. doi: 10.1124/pr.58.3.5.

120. Polson, J.B., Strada, S.J. (1996). Cyclic nucleotide phosphodiesterases and vascular smooth muscle. *Annu Rev Pharmacol Toxicol*, *36*, 403-27. doi: 10.1146/annurev.pa.36.040196.002155.

121. Luo, L., Cai, Y., Zhang, Y., Hsu, C.G., Korshunov, V.A., Long, X., . . . Yan, C. (2022). Role of PDE10A in vascular smooth muscle cell hyperplasia and pathological vascular remodelling. *Cardiovasc Res*, *118*(12), 2703-2717. doi: 10.1093/cvr/cvab304.

122. Zhang, L., Bouadjel, K., Manoury, B., Vandecasteele, G., Fischmeister, R., Leblais, V. (2019). Cyclic nucleotide signalling compartmentation by PDEs in cultured vascular smooth muscle cells. *Br J Pharmacol*, *176*(11), 1780-1792. doi: 10.1111/bph.14651.

123. Friebe, A., Mergia, E., Dangel, O., Lange, A., Koesling, D. (2007). Fatal gastrointestinal obstruction and hypertension in mice lacking nitric oxide-sensitive guanylyl cyclase. *Proc Natl Acad Sci U S A*, *104*(18), 7699-704. doi: 10.1073/pnas.0609778104.

124. Kang, Y., Liu, R., Wu, J.X., Chen, L. (2019). Structural insights into the mechanism of human soluble guanylate cyclase. *Nature*, *574*(7777), 206-210. doi: 10.1038/s41586-019-1584-6.

125. Horst, B.G., Yokom, A.L., Rosenberg, D.J., Morris, K.L., Hammel, M., Hurley, J.H., . . . Marletta, M.A. (2019). Allosteric activation of the nitric oxide receptor soluble guanylate cyclase mapped by cryo-electron microscopy. *Elife*, *8*. doi: 10.7554/eLife.50634.

126. Zhao, Y., Schelvis, J.P., Babcock, G.T., Marletta, M.A. (1998). Identification of histidine 105 in the beta1 subunit of soluble guanylate cyclase as the heme proximal ligand. *Biochemistry*, *37*(13), 4502-9. doi: 10.1021/bi972686m.

127. Schmidt, P.M., Schramm, M., Schroder, H., Wunder, F., Stasch, J.P. (2004). Identification of residues crucially involved in the binding of the heme moiety of soluble guanylate cyclase. *J Biol Chem*, *279*(4), 3025-32. doi: 10.1074/jbc.M310141200.

128. Wedel, B., Humbert, P., Harteneck, C., Foerster, J., Malkewitz, J., Bohme, E., . . . Koesling, D. (1994). Mutation of His-105 in the beta 1 subunit yields a nitric oxide-insensitive form of soluble guanylyl cyclase. *Proc Natl Acad Sci U S A*, *91*(7), 2592-6. doi: 10.1073/pnas.91.7.2592.

129. Friebe, A., Sandner, P., Schmidtko, A. (2020). cGMP: a unique 2nd messenger molecule - recent developments in cGMP research and development. *Naunyn Schmiedebergs Arch Pharmacol*, *393*(2), 287-302. doi: 10.1007/s00210-019-01779-z.

130. Liu, R., Kang, Y., Chen, L. (2021). Activation mechanism of human soluble guanylate cyclase by stimulators and activators. *Nat Commun*, *12*(1), 5492. doi: 10.1038/s41467-021-25617-0.

131. Russwurm, M., Koesling, D. (2004). NO activation of guanylyl cyclase. *EMBO J*, *23*(22), 4443-50. doi: 10.1038/sj.emboj.7600422.

132. Shah, R.C., Sanker, S., Wood, K.C., Durgin, B.G., Straub, A.C. (2018). Redox regulation of soluble guanylyl cyclase. *Nitric Oxide*, *76*, 97-104. doi: 10.1016/j.niox.2018.03.013.

133. Alexandre, E.C., Leiria, L.O., Silva, F.H., Mendes-Silverio, C.B., Calmasini, F.B., Davel, A.P., . . . Antunes, E. (2014). Soluble guanylyl cyclase (sGC) degradation and impairment of nitric oxide-mediated responses in urethra from obese mice: reversal by the sGC activator BAY 60-2770. *J Pharmacol Exp Ther*, *349*(1), 2-9. doi: 10.1124/jpet.113.211029.

134. Ghosh, A., Stuehr, D.J. (2012). Soluble guanylyl cyclase requires heat shock protein 90 for heme insertion during maturation of the NO-active enzyme. *Proc Natl Acad Sci U S A*, *109*(32), 12998-3003. doi: 10.1073/pnas.1205854109.

135. Rahaman, M.M., Nguyen, A.T., Miller, M.P., Hahn, S.A., Sparacino-Watkins, C., Jobbagy, S., . . . Straub, A.C. (2017). Cytochrome b5 Reductase 3 Modulates Soluble Guanylate Cyclase Redox State and cGMP Signaling. *Circ Res*, *121*(2), 137-148. doi: 10.1161/CIRCRESAHA.117.310705.

136. Sandner, P., Zimmer, D.P., Milne, G.T., Follmann, M., Hobbs, A., Stasch, J.P. (2021). Soluble Guanylate Cyclase Stimulators and Activators. *Handb Exp Pharmacol*, *264*, 355-394. doi: 10.1007/164_2018_197.

137. Forstermann, U., Xia, N., Li, H. (2017). Roles of Vascular Oxidative Stress and Nitric Oxide in the Pathogenesis of Atherosclerosis. *Circ Res*, *120*(4), 713-735. doi: 10.1161/CIRCRESAHA.116.309326.

138. Bajar, B.T., Wang, E.S., Zhang, S., Lin, M.Z., Chu, J. (2016). A Guide to Fluorescent Protein FRET Pairs. *Sensors (Basel)*, *16*(9). doi: 10.3390/s16091488.

139. Russwurm, M., Mullershausen, F., Friebe, A., Jager, R., Russwurm, C., Koesling, D. (2007). Design of fluorescence resonance energy transfer (FRET)-based cGMP indicators: a systematic approach. *Biochem J*, *407*(1), 69-77. doi: 10.1042/BJ20070348.

140. Thunemann, M., Wen, L., Hillenbrand, M., Vachaviolos, A., Feil, S., Ott, T., . . . Feil, R. (2013). Transgenic mice for cGMP imaging. *Circ Res*, *113*(4), 365-71. doi: 10.1161/CIRCRESAHA.113.301063.

141. Thunemann, M., Schmidt, K., de Wit, C., Han, X., Jain, R.K., Fukumura, D., . . . Feil, R. (2014). Correlative intravital imaging of cGMP signals and vasodilation in mice. *Front Physiol*, *5*, 394. doi: 10.3389/fphys.2014.00394.

142. Sandner, P., Vakalopoulos, A., Hahn, M.G., Stasch, J.P., Follmann, M. (2021). Soluble guanylate cyclase stimulators and their potential use: a patent review. *Expert Opin Ther Pat*, *31*(3), 203-222. doi: 10.1080/13543776.2021.1866538.

143. Murrell, W. (1879). Nitro-glycerin as a remedy for angina pectoris. *The Lancet*, *113*(2890), 80-81. doi: 10.1016/S0140-6736(02)46032-1.

144. Marsh, N., Marsh, A. (2000). A short history of nitroglycerine and nitric oxide in pharmacology and physiology. *Clin Exp Pharmacol Physiol*, *27*(4), 313-9. doi: 10.1046/j.1440-1681.2000.03240.x.

145. Stasch, J.P., Hobbs, A.J. (2009). NO-independent, haem-dependent soluble guanylate cyclase stimulators. *Handb Exp Pharmacol*(191), 277-308. doi: 10.1007/978-3-540-68964-5_13.

146. Schmidt, H.H., Schmidt, P.M., Stasch, J.P. (2009). NO- and haem-independent soluble guanylate cyclase activators. *Handb Exp Pharmacol*(191), 309-39. doi: 10.1007/978-3-540-68964-5_14.

147. Elgert, C., Ruhle, A., Sandner, P., Behrends, S. (2019). A novel soluble guanylyl cyclase activator, BR 11257, acts as a non-stabilising partial agonist of sGC. *Biochem Pharmacol*, *163*, 142-153. doi: 10.1016/j.bcp.2019.02.007.

148. Jones, A.K., Chen, H., Ng, K.J., Villalona, J., McHugh, M., Zeveleva, S., . . . Fryer, R.M. (2023). Soluble Guanylyl Cyclase Activator BI 685509 Reduces Portal Hypertension and Portosystemic Shunting in a Rat Thioacetamide-Induced Cirrhosis Model. *J Pharmacol Exp Ther*. doi: 10.1124/jpet.122.001532.

149. Cherney, D.Z.I., de Zeeuw, D., Heerspink, H.J.L., Cardona, J., Desch, M., Wenz, A., . . . Nangaku, M. (2023). Safety, tolerability, pharmacodynamics and pharmacokinetics of the soluble guanylyl cyclase activator BI 685509 in patients with diabetic kidney disease: A randomized trial. *Diabetes Obes Metab*. doi: 10.1111/dom.15099.

150. Kraehling, J.R., Benardeau, A., Schomber, T., Popp, L., Vienenkoetter, J., Ellinger-Ziegelbauer, H., . . . Sandner, P. (2023). The sGC Activator Runcaciguat Has Kidney Protective Effects and Prevents a Decline of Kidney Function in ZSF1 Rats. *Int J Mol Sci*, *24*(17). doi: 10.3390/ijms241713226.

151. Benardeau, A., Kahnert, A., Schomber, T., Meyer, J., Pavkovic, M., Kretschmer, A., . . . Sandner, P. (2021). Runcaciguat, a novel soluble guanylate cyclase activator, shows renoprotection in hypertensive, diabetic, and metabolic preclinical models of chronic kidney disease. *Naunyn Schmiedebergs Arch Pharmacol*, *394*(12), 2363-2379. doi: 10.1007/s00210-021-02149-4.

152. Lincoln, T.M., Wu, X., Sellak, H., Dey, N., Choi, C.S. (2006). Regulation of vascular smooth muscle cell phenotype by cyclic GMP and cyclic GMP-dependent protein kinase. *Front Biosci*, *11*, 356-67. doi: 10.2741/1803.

153. Tulis, D.A., Bohl Masters, K.S., Lipke, E.A., Schiesser, R.L., Evans, A.J., Peyton, K.J., . . . Schafer, A.I. (2002). YC-1-mediated vascular protection through inhibition of smooth muscle cell proliferation and platelet function. *Biochem Biophys Res Commun*, *291*(4), 1014-21. doi: 10.1006/bbrc.2002.6552.

154. Chiche, J.D., Schlutsmeyer, S.M., Bloch, D.B., de la Monte, S.M., Roberts, J.D., Jr., Filippov, G., . . . Bloch, K.D. (1998). Adenovirus-mediated gene transfer of cGMP-dependent protein kinase increases the sensitivity of cultured vascular smooth muscle cells to the antiproliferative and pro-apoptotic effects of nitric oxide/cGMP. *J Biol Chem*, *273*(51), 34263-71. doi: 10.1074/jbc.273.51.34263.

155. Segura-Puimedon, M., Mergia, E., Al-Hasani, J., Aherrahrou, R., Stoelting, S., Kremer, F., . . . Aherrahrou, Z. (2016). Proatherosclerotic Effect of the alpha1-Subunit of Soluble Guanylyl Cyclase by Promoting Smooth Muscle Phenotypic Switching. *Am J Pathol*, *186*(8), 2220-2231. doi: 10.1016/j.ajpath.2016.04.010.

156. Garg, U.C., Hassid, A. (1989). Nitric oxide-generating vasodilators and 8-bromo-cyclic guanosine monophosphate inhibit mitogenesis and proliferation of cultured rat vascular smooth muscle cells. *J Clin Invest*, *83*(5), 1774-7. doi: 10.1172/JCI114081.

157. Komalavilas, P., Shah, P.K., Jo, H., Lincoln, T.M. (1999). Activation of mitogen-activated protein kinase pathways by cyclic GMP and cyclic GMP-dependent protein kinase in contractile vascular smooth muscle cells. *J Biol Chem*, *274*(48), 34301-9. doi: 10.1074/jbc.274.48.34301.

158. Ignarro, L.J., Buga, G.M., Wei, L.H., Bauer, P.M., Wu, G., del Soldato, P. (2001). Role of the arginine-nitric oxide pathway in the regulation of vascular smooth muscle cell proliferation. *Proc Natl Acad Sci U S A*, *98*(7), 4202-8. doi: 10.1073/pnas.071054698.

159. Dobrowinski, H.G. (2019). *Influence of cGMP signaling on VSMC growth and its dependence on fibronectin in cultured VSMCs and development of atherosclerosis* [Doctoral thesis, University of Tubingen]. http://hdl.handle.net/10900/91054

160. Tsou, C.Y., Chen, C.Y., Zhao, J.F., Su, K.H., Lee, H.T., Lin, S.J., . . . Lee, T.S. (2014). Activation of soluble guanylyl cyclase prevents foam cell formation and atherosclerosis. *Acta Physiol (Oxf)*, *210*(4), 799-810. doi: 10.1111/apha.12210.

161. Mauersberger, C., Sager, H.B., Wobst, J., Dang, T.A., Lambrecht, L., Koplev, S., . . . Kessler, T. (2022). Loss of soluble guanylyl cyclase in platelets contributes to atherosclerotic plaque formation and vascular inflammation. *Nature Cardiovascular Research*, *1*(12), 1174-1186. doi: 10.1038/s44161-022-00175-w.

162. Vantler, M., Alfitian, J., Gerhardt, M., Berghausen, E.M., Zierden, M., Baldus, S., . . . Rosenkranz, S. (2018). SGC-stimulation via BAY 41-2272 exerts antiatherogenic effects in LDLR- and ApoE-deficient mice. *Eur Heart J*, *39*(803). doi: 10.1093/eurheartj/ehy563.P3789.

163. van Eickels, M., Wassmann, S., Schäfer, A., Bauersachs, J., Strobel, H., Rütten, H. (2007). Role of the sGC activator ataciguat sodium (HMR1766) in cardiovascular disease. *BMC Pharmacology*, *7*(S1). doi: 10.1186/1471-2210-7-s1-s4.

164. Balarini, C.M., Leal, M.A., Gomes, I.B., Pereira, T.M., Gava, A.L., Meyrelles, S.S., . . . Vasquez, E.C. (2013). Sildenafil restores endothelial function in the apolipoprotein E knockout mouse. *J Transl Med*, *11*, 3. doi: 10.1186/1479-5876-11-3.

165. Stehle, D. (2022). *cGMP Imaging Uncovers New Roles and Therapeutic Implications of NO/cGMP Signaling in the Kidney and in Melanoma* [Doctoral Thesis, University Tubingen]. http://hdl.handle.net/10900/128604

166. Rueden, C.T., Schindelin, J., Hiner, M.C., DeZonia, B.E., Walter, A.E., Arena, E.T., . . . Eliceiri, K.W. (2017). ImageJ2: ImageJ for the next generation of scientific image data. *BMC Bioinformatics*, *18*(1), 529. doi: 10.1186/s12859-017-1934-z.

167. Schindelin, J., Arganda-Carreras, I., Frise, E., Kaynig, V., Longair, M., Pietzsch, T., . . . Cardona, A. (2012). Fiji: an open-source platform for biological-image analysis. *Nat Methods*, *9*(7), 676-82. doi: 10.1038/nmeth.2019.

168. CharlesRiverLaboratories. (2023). *C57BL/6 Mice*. Charles River Laboratories. Retrieved 02/09/2023 from https://www.criver.com/products-services/find-model/c57bl6-mouse?region=23

169. Wendling, O., Bornert, J.M., Chambon, P., Metzger, D. (2009). Efficient temporally-controlled targeted mutagenesis in smooth muscle cells of the adult mouse. *Genesis*, *47*(1), 14-8. doi: 10.1002/dvg.20448.

170. Thunemann, M., Fomin, N., Krawutschke, C., Russwurm, M., Feil, R. (2013). Visualization of cGMP with cGi biosensors. *Methods Mol Biol*, *1020*, 89-120. doi: 10.1007/978-1-62703-459-3_6.

171. Agilent. (2023). *Real-time cell analysis (xCELLigence)*. Retrieved 27.02.2023 from https://www.agilent.com/en/product/cell-analysis/real-time-cell-analysis/rtca-analyzers

172. Lowry, O.H., Rosebrough, N.J., Farr, A.L., Randall, R.J. (1951). Protein measurement with the Folin phenol reagent. *J Biol Chem*, *193*(1), 265-75.

173. Peterson, G.L. (1977). A simplification of the protein assay method of Lowry et al. which is more generally applicable. *Anal Biochem*, *83*(2), 346-56. doi: 10.1016/0003-2697(77)90043-4.

174. Towbin, H., Staehelin, T., Gordon, J. (1979). Electrophoretic transfer of proteins from polyacrylamide gels to nitrocellulose sheets: procedure and some applications. *Proc Natl Acad Sci U S A*, *76*(9), 4350-4. doi: 10.1073/pnas.76.9.4350.

175. Laemmli, U.K. (1970). Cleavage of structural proteins during the assembly of the head of bacteriophage T4. *Nature*, *227*(5259), 680-5. doi: 10.1038/227680a0.

176. Butt, E., Abel, K., Krieger, M., Palm, D., Hoppe, V., Hoppe, J., . . . Walter, U. (1994). cAMP- and cGMP-dependent protein kinase phosphorylation sites of the focal adhesion vasodilator-stimulated phosphoprotein (VASP) in vitro and in intact human platelets. *J Biol Chem*, *269*(20), 14509-17.

177. Halbrugge, M., Friedrich, C., Eigenthaler, M., Schanzenbacher, P., Walter, U. (1990). Stoichiometric and reversible phosphorylation of a 46-kDa protein in human platelets in response to cGMP- and cAMP-elevating vasodilators. *J Biol Chem*, *265*(6), 3088-93.

178. Oelze, M., Mollnau, H., Hoffmann, N., Warnholtz, A., Bodenschatz, M., Smolenski, A., . . . Munzel, T. (2000). Vasodilator-stimulated phosphoprotein serine 239 phosphorylation as a

sensitive monitor of defective nitric oxide/cGMP signaling and endothelial dysfunction. *Circ Res*, *87*(11), 999-1005. doi: 10.1161/01.res.87.11.999.

179. Bachmanov, A.A., Reed, D.R., Beauchamp, G.K., Tordoff, M.G. (2002). Food intake, water intake, and drinking spout side preference of 28 mouse strains. *Behav Genet*, *32*(6), 435-43. doi: 10.1023/a:1020884312053.

180. Pickering, T.G., Hall, J.E., Appel, L.J., Falkner, B.E., Graves, J., Hill, M.N., . . . Roccella, E.J. (2005). Recommendations for blood pressure measurement in humans and experimental animals: part 1: blood pressure measurement in humans: a statement for professionals from the Subcommittee of Professional and Public Education of the American Heart Association Council on High Blood Pressure Research. *Circulation*, *111*(5), 697-716. doi: 10.1161/01.CIR.0000154900.76284.F6.

181. Hahn, M.G., Lampe, T., El Sheikh, S., Griebenow, N., Woltering, E., Schlemmer, K.H., . . . Stasch, J.P. (2021). Discovery of the Soluble Guanylate Cyclase Activator Runcaciguat (BAY 1101042). *J Med Chem*, *64*(9), 5323-5344. doi: 10.1021/acs.jmedchem.0c02154.

182. Mittendorf, J., Weigand, S., Alonso-Alija, C., Bischoff, E., Feurer, A., Gerisch, M., . . . Stasch, J.P. (2009). Discovery of riociguat (BAY 63-2521): a potent, oral stimulator of soluble guanylate cyclase for the treatment of pulmonary hypertension. *ChemMedChem*, *4*(5), 853-65. doi: 10.1002/cmdc.200900014.

183. Roberts, J.A., Pea, F., Lipman, J. (2013). The clinical relevance of plasma protein binding changes. *Clin Pharmacokinet*, *52*(1), 1-8. doi: 10.1007/s40262-012-0018-5.

184. Feng, M., Whitesall, S., Zhang, Y., Beibel, M., D'Alecy, L., DiPetrillo, K. (2008). Validation of volume-pressure recording tail-cuff blood pressure measurements. *Am J Hypertens*, *21*(12), 1288-91. doi: 10.1038/ajh.2008.301.

185. Corporation, K.S. (2023). Retrieved 28.02.2023 from www.kentscientific.com/products/coda-high-throughput-system/

186. Ramirez-Zacarias, J.L., Castro-Munozledo, F., Kuri-Harcuch, W. (1992). Quantitation of adipose conversion and triglycerides by staining intracytoplasmic lipids with Oil red O. *Histochemistry*, *97*(6), 493-7. doi: 10.1007/BF00316069.

187. Centa, M., Ketelhuth, D.F.J., Malin, S., Gistera, A. (2019). Quantification of Atherosclerosis in Mice. *J Vis Exp*(148). doi: 10.3791/59828.

188. ThermoFisherScientific. (2023). *Strept(avidin)–Biotin Complex Method for IHC Detection*. Retrieved 09.07.2023 from https://www.thermofisher.com/de/de/home/life-science/protein-biology/protein-biology-learning-center/protein-biology-resource-library/pierce-protein-methods/avidin-biotin-complex-method-ihc-detection.html

189. Hsu, S.M., Raine, L., Fanger, H. (1981). Use of avidin-biotin-peroxidase complex (ABC) in immunoperoxidase techniques: a comparison between ABC and unlabeled antibody (PAP) procedures. *J Histochem Cytochem*, *29*(4), 577-80. doi: 10.1177/29.4.6166661.

190. Plenz, G.A., Deng, M.C., Robenek, H., Volker, W. (2003). Vascular collagens: spotlight on the role of type VIII collagen in atherogenesis. *Atherosclerosis*, *166*(1), 1-11. doi: 10.1016/s0021-9150(01)00766-3.

191. Puchtler, H., Waldrop, F.S., Valentine, L.S. (1973). Polarization microscopic studies of connective tissue stained with picro-sirius red FBA. *Beitr Pathol*, *150*(2), 174-87. doi: 10.1016/s0005-8165(73)80016-2.

192. Junqueira, L.C., Bignolas, G., Brentani, R.R. (1979). Picrosirius staining plus polarization microscopy, a specific method for collagen detection in tissue sections. *Histochem J*, *11*(4), 447-55. doi: 10.1007/BF01002772.

193. Glassman, P.M., Muzykantov, V.R. (2019). Pharmacokinetic and Pharmacodynamic Properties of Drug Delivery Systems. *J Pharmacol Exp Ther*, *370*(3), 570-580. doi: 10.1124/jpet.119.257113.

194. Riccardi, K., Cawley, S., Yates, P.D., Chang, C., Funk, C., Niosi, M., . . . Di, L. (2015). Plasma Protein Binding of Challenging Compounds. *J Pharm Sci*, *104*(8), 2627-36. doi: 10.1002/jps.24506.

195. Bhargava, S., de la Puente-Secades, S., Schurgers, L., Jankowski, J. (2022). Lipids and lipoproteins in cardiovascular diseases: a classification. *Trends Endocrinol Metab*, *33*(6), 409-423. doi: 10.1016/j.tem.2022.02.001.

196. Ference, B.A., Ginsberg, H.N., Graham, I., Ray, K.K., Packard, C.J., Bruckert, E., . . . Catapano, A.L. (2017). Low-density lipoproteins cause atherosclerotic cardiovascular disease. 1. Evidence from genetic, epidemiologic, and clinical studies. A consensus statement from the European Atherosclerosis Society Consensus Panel. *Eur Heart J*, *38*(32), 2459-2472. doi: 10.1093/eurheartj/ehx144.

197. Boren, J., Chapman, M.J., Krauss, R.M., Packard, C.J., Bentzon, J.F., Binder, C.J., . . . Ginsberg, H.N. (2020). Low-density lipoproteins cause atherosclerotic cardiovascular disease: pathophysiological, genetic, and therapeutic insights: a consensus statement from the European Atherosclerosis Society Consensus Panel. *Eur Heart J*, *41*(24), 2313-2330. doi: 10.1093/eurheartj/ehz962.

198. Talayero, B.G., Sacks, F.M. (2011). The role of triglycerides in atherosclerosis. *Curr Cardiol Rep*, *13*(6), 544-52. doi: 10.1007/s11886-011-0220-3.

199. Davies, M.J., Richardson, P.D., Woolf, N., Katz, D.R., Mann, J. (1993). Risk of thrombosis in human atherosclerotic plaques: role of extracellular lipid, macrophage, and smooth muscle cell content. *Br Heart J*, *69*(5), 377-81. doi: 10.1136/hrt.69.5.377.

200. Yang, X., Li, Y., Li, Y., Ren, X., Zhang, X., Hu, D., . . . Shang, H. (2017). Oxidative Stress-Mediated Atherosclerosis: Mechanisms and Therapies. *Front Physiol*, *8*, 600. doi: 10.3389/fphys.2017.00600.

201. Stasch, J.P., Becker, E.M., Alonso-Alija, C., Apeler, H., Dembowsky, K., Feurer, A., . . . Schramm, M. (2001). NO-independent regulatory site on soluble guanylate cyclase. *Nature*, *410*(6825), 212-5. doi: 10.1038/35065611.

202. Arnold, W.P., Mittal, C.K., Katsuki, S., Murad, F. (1977). Nitric oxide activates guanylate cyclase and increases guanosine 3':5'-cyclic monophosphate levels in various tissue preparations. *Proc Natl Acad Sci U S A*, *74*(8), 3203-7. doi: 10.1073/pnas.74.8.3203.

203. Furchgott, R.F., Zawadzki, J.V. (1980). The obligatory role of endothelial cells in the relaxation of arterial smooth muscle by acetylcholine. *Nature*, *288*(5789), 373-6. doi: 10.1038/288373a0.

204. Melichar, V.O., Behr-Roussel, D., Zabel, U., Uttenthal, L.O., Rodrigo, J., Rupin, A., . . . Schmidt, H.H. (2004). Reduced cGMP signaling associated with neointimal proliferation and vascular dysfunction in late-stage atherosclerosis. *Proc Natl Acad Sci U S A*, *101*(47), 16671-6. doi: 10.1073/pnas.0405509101.

205. Chen, B., Li, R., Kubota, A., Alex, L., Frangogiannis, N.G. (2022). Identification of macrophages in normal and injured mouse tissues using reporter lines and antibodies. *Sci Rep*, *12*(1), 4542. doi: 10.1038/s41598-022-08278-x.

206. Krishnan, S.M., Nordlohne, J., Dietz, L., Vakalopoulos, A., Haning, P., Hartmann, E., . . . Sandner, P. (2021). Assessing the Use of the sGC Stimulator BAY-747, as a Potential Treatment for Duchenne Muscular Dystrophy. *Int J Mol Sci*, *22*(15). doi: 10.3390/ijms22158016.

207. Potoka, K.P., Wood, K.C., Baust, J.J., Bueno, M., Hahn, S.A., Vanderpool, R.R., . . . Gladwin, M.T. (2018). Nitric Oxide-Independent Soluble Guanylate Cyclase Activation Improves Vascular Function and Cardiac Remodeling in Sickle Cell Disease. *Am J Respir Cell Mol Biol*, *58*(5), 636-647. doi: 10.1165/rcmb.2017-0292OC.

208. Lu, H., Cassis, L.A., Daugherty, A. (2007). Atherosclerosis and arterial blood pressure in mice. *Curr Drug Targets*, *8*(11), 1181-9. doi: 10.2174/138945007782403829.

209. Ahluwalia, A., Foster, P., Scotland, R.S., McLean, P.G., Mathur, A., Perretti, M., . . . Hobbs, A.J. (2004). Antiinflammatory activity of soluble guanylate cyclase: cGMP-dependent down-regulation of P-selectin expression and leukocyte recruitment. *Proc Natl Acad Sci U S A*, *101*(5), 1386-91. doi: 10.1073/pnas.0304264101.

210. Nguyen, T.H., Axell, A., Turek, I., Wright, B., Meehan-Andrews, T., Irving, H.R. (2022). Modulation of Inflammatory Cytokine Production in Human Monocytes by cGMP and IRAK3. *Int J Mol Sci*, *23*(5). doi: 10.3390/ijms23052552.

211. Sandner, P., Stasch, J.P. (2017). Anti-fibrotic effects of soluble guanylate cyclase stimulators and activators: A review of the preclinical evidence. *Respir Med*, *122 Suppl 1*, S1-S9. doi: 10.1016/j.rmed.2016.08.022.

212. Tawa, M., Nakano, K., Yamashita, Y., He, Q., Masuoka, T., Okamura, T., . . . Ishibashi, T. (2021). Alteration of the soluble guanylate cyclase system in coronary arteries of high cholesterol diet-fed rabbits. *Pharmacol Res Perspect*, *9*(4), e00838. doi: 10.1002/prp2.838.

213. Reddick, R.L., Zhang, S.H., Maeda, N. (1994). Atherosclerosis in mice lacking apo E. Evaluation of lesional development and progression. *Arterioscler Thromb*, *14*(1), 141-7. doi: 10.1161/01.atv.14.1.141.

214. Moore, K.J., Sheedy, F.J., Fisher, E.A. (2013). Macrophages in atherosclerosis: a dynamic balance. *Nat Rev Immunol*, *13*(10), 709-21. doi: 10.1038/nri3520.

215. Bobryshev, Y.V., Ivanova, E.A., Chistiakov, D.A., Nikiforov, N.G., Orekhov, A.N. (2016). Macrophages and Their Role in Atherosclerosis: Pathophysiology and Transcriptome Analysis. *Biomed Res Int*, *2016*, 9582430. doi: 10.1155/2016/9582430.

216. Doring, Y., Drechsler, M., Soehnlein, O., Weber, C. (2015). Neutrophils in atherosclerosis: from mice to man. *Arterioscler Thromb Vasc Biol*, *35*(2), 288-95. doi: 10.1161/ATVBAHA.114.303564.

217. Moore, K.J., Tabas, I. (2011). Macrophages in the pathogenesis of atherosclerosis. *Cell*, *145*(3), 341-55. doi: 10.1016/j.cell.2011.04.005.

218. Evgenov, O.V., Pacher, P., Schmidt, P.M., Hasko, G., Schmidt, H.H., Stasch, J.P. (2006). NO-independent stimulators and activators of soluble guanylate cyclase: discovery and therapeutic potential. *Nat Rev Drug Discov*, *5*(9), 755-68. doi: 10.1038/nrd2038.

219. Munzel, T., Genth-Zotz, S., Hink, U. (2007). Targeting heme-oxidized soluble guanylate cyclase: solution for all cardiorenal problems in heart failure? *Hypertension*, *49*(5), 974-6. doi: 10.1161/HYPERTENSIONAHA.106.085456.

220. Stehle, D., Xu, M.Z., Schomber, T., Hahn, M.G., Schweda, F., Feil, S., . . . Benardeau, A. (2022). Novel soluble guanylyl cyclase activators increase glomerular cGMP, induce vasodilation and improve blood flow in the murine kidney. *Br J Pharmacol*, *179*(11), 2476-2489. doi: 10.1111/bph.15586.

221. Getz, G.S., Reardon, C.A. (2009). Apoprotein E as a lipid transport and signaling protein in the blood, liver, and artery wall. *J Lipid Res*, *50 Suppl*(Suppl), S156-61. doi: 10.1194/jlr.R800058-JLR200.

222. Getz, G.S., Reardon, C.A. (2012). Animal models of atherosclerosis. *Arterioscler Thromb Vasc Biol*, *32*(5), 1104-15. doi: 10.1161/ATVBAHA.111.237693.

223. Li, A.C., Brown, K.K., Silvestre, M.J., Willson, T.M., Palinski, W., Glass, C.K. (2000). Peroxisome proliferator-activated receptor gamma ligands inhibit development of atherosclerosis in LDL receptor-deficient mice. *J Clin Invest*, *106*(4), 523-31. doi: 10.1172/JCI10370.

224. Robinet, P., Milewicz, D.M., Cassis, L.A., Leeper, N.J., Lu, H.S., Smith, J.D. (2018). Consideration of Sex Differences in Design and Reporting of Experimental Arterial Pathology Studies-Statement From ATVB Council. *Arterioscler Thromb Vasc Biol*, *38*(2), 292-303. doi: 10.1161/ATVBAHA.117.309524.

225. Arnold, A.P., Cassis, L.A., Eghbali, M., Reue, K., Sandberg, K. (2017). Sex Hormones and Sex Chromosomes Cause Sex Differences in the Development of Cardiovascular Diseases. *Arterioscler Thromb Vasc Biol*, *37*(5), 746-756. doi: 10.1161/ATVBAHA.116.307301.

226. AlSiraj, Y., Chen, X., Thatcher, S.E., Temel, R.E., Cai, L., Blalock, E., . . . Cassis, L.A. (2019). XX sex chromosome complement promotes atherosclerosis in mice. *Nat Commun*, *10*(1), 2631. doi: 10.1038/s41467-019-10462-z.

227. Eales, J.M., Maan, A.A., Xu, X., Michoel, T., Hallast, P., Batini, C., . . . Tomaszewski, M. (2019). Human Y Chromosome Exerts Pleiotropic Effects on Susceptibility to Atherosclerosis. *Arterioscler Thromb Vasc Biol*, *39*(11), 2386-2401. doi: 10.1161/ATVBAHA.119.312405.

228. Buys, E.S., Sips, P., Vermeersch, P., Raher, M.J., Rogge, E., Ichinose, F., . . . Brouckaert, P. (2008). Gender-specific hypertension and responsiveness to nitric oxide in sGCalpha1 knockout mice. *Cardiovasc Res*, *79*(1), 179-86. doi: 10.1093/cvr/cvn068.

229. Vermeersch, P., Buys, E., Sips, P., Pokreisz, P., Marsboom, G., Gillijns, H., . . . Janssens, S. (2009). Gender-specific modulation of the response to arterial injury by soluble guanylate cyclase alpha1. *Open Cardiovasc Med J*, *3*, 98-104. doi: 10.2174/1874192400903010098.

230. Frey, R., Muck, W., Unger, S., Artmeier-Brandt, U., Weimann, G., Wensing, G. (2008). Pharmacokinetics, pharmacodynamics, tolerability, and safety of the soluble guanylate cyclase activator cinaciguat (BAY 58-2667) in healthy male volunteers. *J Clin Pharmacol*, *48*(12), 1400-10. doi: 10.1177/0091270008322906.

231. Stasch, J.P., Schmidt, P.M., Nedvetsky, P.I., Nedvetskaya, T.Y., H, S.A., Meurer, S., . . . Schmidt, H.H. (2006). Targeting the heme-oxidized nitric oxide receptor for selective vasodilatation of diseased blood vessels. *J Clin Invest*, *116*(9), 2552-61. doi: 10.1172/JCI28371.

232. Garthwaite, J., Southam, E., Boulton, C.L., Nielsen, E.B., Schmidt, K., Mayer, B. (1995). Potent and selective inhibition of nitric oxide-sensitive guanylyl cyclase by 1H-[1,2,4]oxadiazolo[4,3-a]quinoxalin-1-one. *Mol Pharmacol*, *48*(2), 184-8.

233. Zhao, Y., Brandish, P.E., Di Valentin, M., Schelvis, J.P., Babcock, G.T., Marletta, M.A. (2000). Inhibition of soluble guanylate cyclase by ODQ. *Biochemistry*, *39*(35), 10848-54. doi: 10.1021/bi9929296.

234. Gonzalez-Guerra, A., Roche-Molina, M., Garcia-Quintans, N., Sanchez-Ramos, C., Martin-Perez, D., Lytvyn, M., . . . Bernal, J.A. (2021). Sustained Elevated Blood Pressure Accelerates Atherosclerosis Development in a Preclinical Model of Disease. *Int J Mol Sci*, *22*(16). doi: 10.3390/ijms22168448.

235. Knowles, J.W., Reddick, R.L., Jennette, J.C., Shesely, E.G., Smithies, O., Maeda, N. (2000). Enhanced atherosclerosis and kidney dysfunction in eNOS(-/-)Apoe(-/-) mice are ameliorated by enalapril treatment. *J Clin Invest*, *105*(4), 451-8. doi: 10.1172/JCI8376.

236. Kuhlencordt, P.J., Gyurko, R., Han, F., Scherrer-Crosbie, M., Aretz, T.H., Hajjar, R., . . . Huang, P.L. (2001). Accelerated atherosclerosis, aortic aneurysm formation, and ischemic heart disease in apolipoprotein E/endothelial nitric oxide synthase double-knockout mice. *Circulation*, *104*(4), 448-54. doi: 10.1161/hc2901.091399.

237. Chen, J., Kuhlencordt, P.J., Astern, J., Gyurko, R., Huang, P.L. (2001). Hypertension does not account for the accelerated atherosclerosis and development of aneurysms in male apolipoprotein e/endothelial nitric oxide synthase double knockout mice. *Circulation*, *104*(20), 2391-4. doi: 10.1161/hc4501.099729.

238. Doran, D.E., Weiss, D., Zhang, Y., Griendling, K.K., Taylor, W.R. (2007). Differential effects of AT1 receptor and Ca2+ channel blockade on atherosclerosis, inflammatory gene expression, and production of reactive oxygen species. *Atherosclerosis*, *195*(1), 39-47. doi: 10.1016/j.atherosclerosis.2006.11.030.

Supplement

a. Supplementary figures

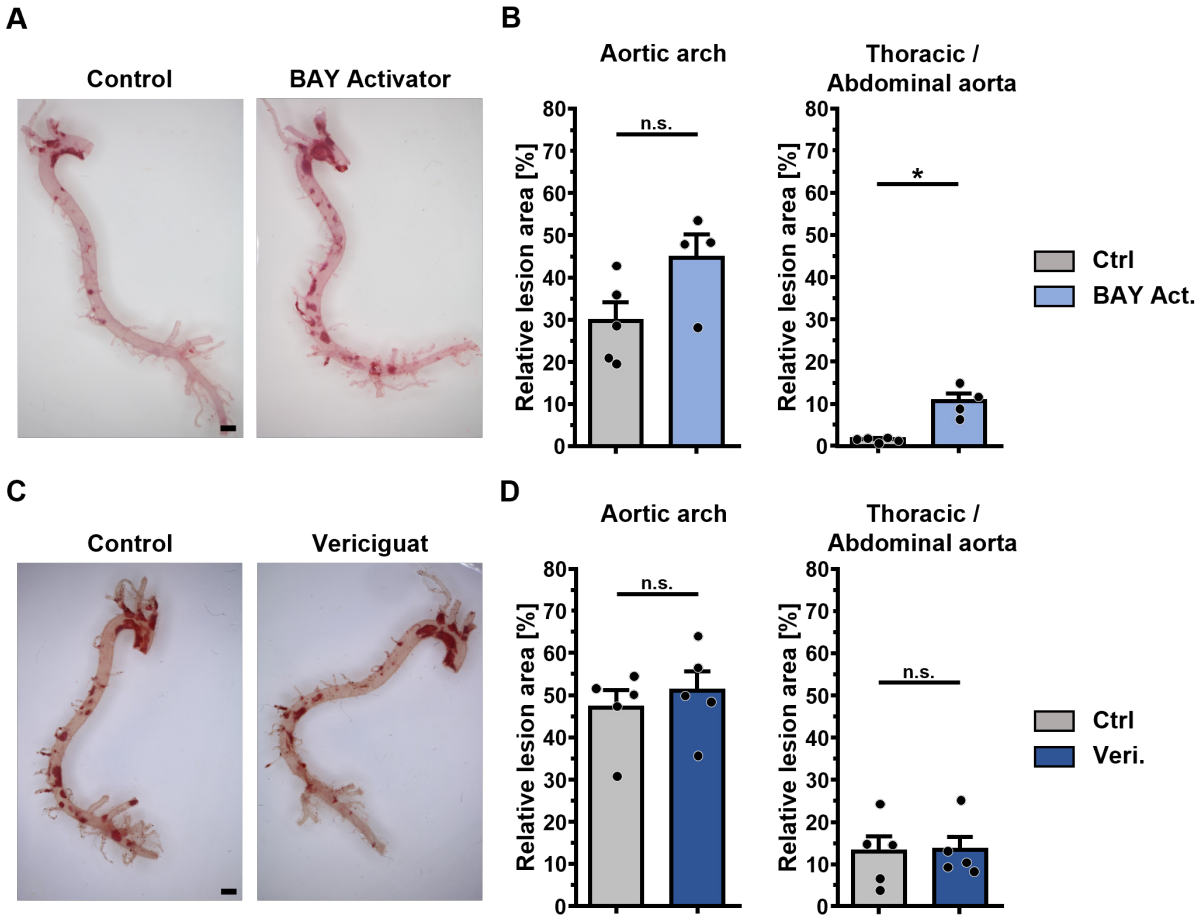

Supplementary figure 1. Atherosclerotic lesion area in female mice after treatment with BAY Activator or Vericiguat.
Analysis of atherosclerotic lesion area in aortas from ApoE^{ko} mice by Oil Red O staining after 16 weeks (Ctrl/BAY Act.) or 18 weeks (Ctrl/Veri.) treatment with BAY Activator (BAY Act.) or Vericiguat (Veri.). The drugs were supplemented at a concentration of 150 ppm into the atherosclerotic diet. **(A, C)** Representative images of Oil Red O-stained atherosclerotic aortas of control (Ctrl) and BAY Act. **(A)** or Veri. **(C)** treated female mice. Atherosclerotic lesions appear red. Scale bars are 1 mm. (**B, D)** Relative lesion area of the aortic arch or thoracic/abdominal aorta of Ctrl and BAY Act. **(B)** or Veri. **(D)** treated female mice. The atherosclerotic lesion area was determined from both sides of the aorta, averaged, and normalized to the total area of the respective part. Data are represented as mean + SEM (Ctrl BAY Act.: 5 mice, BAY Act.: 4 mice, Ctrl Veri.: 5 mice, Veri.: 5 mice.). Statistical significance is indicated by asterisk (*p ≤ 0.05; n.s.: not significant, Mann-Whitney U test). Ctrl, Control, BAY Act., BAY Activator, Veri., Vericiguat.

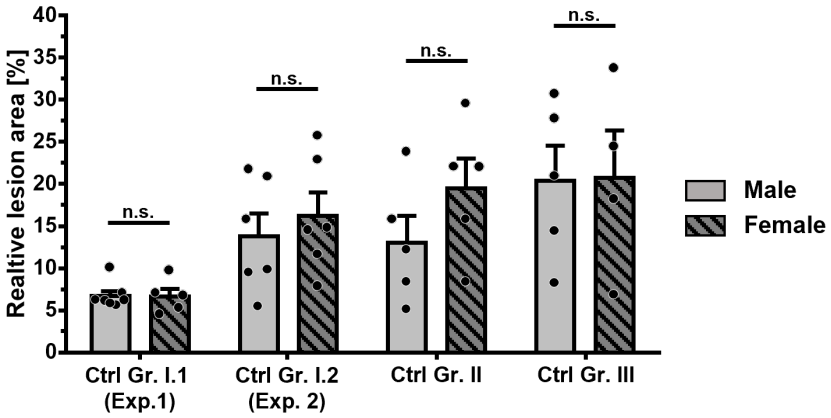

Supplementary figure 2. Effect of sex on lesion area in control mice.
Comparison of the lesion area of the total aorta between the sexes of all control groups. ApoE^{ko} mice were fed with an atherogenic diet for 16 weeks (Ctrl Gr. I.1(Exp. 1)) or 18 weeks (Ctrl Gr. I.2 (Exp. 2), Ctrl Gr. II, Ctrl Gr. III). The atherosclerotic lesion area was determined from both sides of the aorta, averaged, and normalized to the total area. Data are represented as mean + SEM (Male Ctrl Gr. I.1(Exp. 1): 7 mice, Female Ctrl Gr. I.1(Exp. 1): 5 mice, Male Ctrl Gr. I.2 (Exp. 2): 5 mice, Female Ctrl Gr. I.2 (Exp. 2): 6 mice, Male Ctrl Gr. II: 5 mice, Female Ctrl Gr. II: 5 mice, Male Ctrl Gr. III: 6 mice, Female Ctrl Gr. III: 5 mice). No statistically significant differences were found between the sexes (n.s.: not significant, tested pairwise Mann-Whitney U test). Ctrl, Control, Gr., Group; Exp., Experiment.

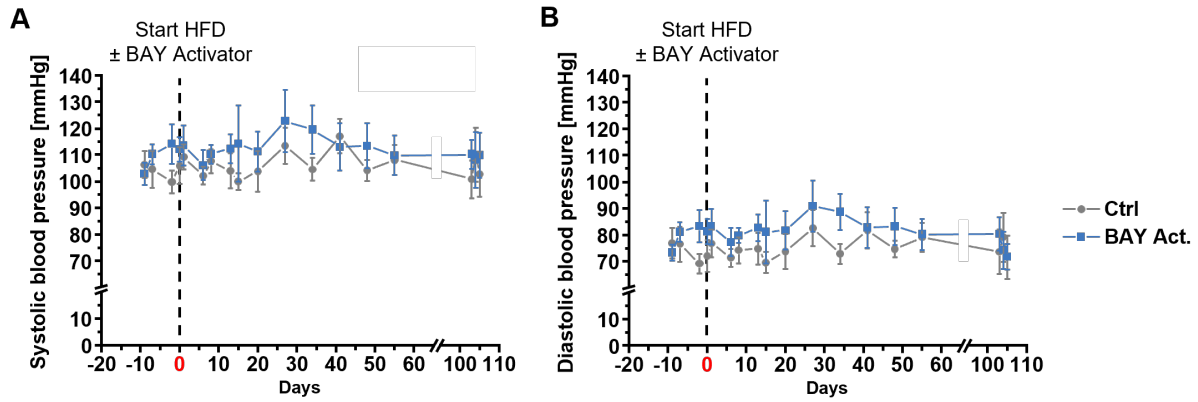

Supplementary figure 3. Effect of BAY Activator on blood pressure in male mice over the 16-week study period.
Male ApoE^{ko} mice were fed with an atherogenic diet for 16 weeks (Ctrl/BAY Act.) supplemented with BAY Activator at a concentration of 150 ppm. Time course of **(A)** Systolic and **(B)** diastolic blood pressure of Ctrl and BAY Act. treated male mice. The blood pressure was measured four times prior to the start of the treatment (dashed line) and then regularly throughout the 16-week study period. Data are represented as mean ± SEM (Ctrl BAY Act.: 7 mice, BAY Act.: 7 mice). Ctrl, Control, BAY Act., BAY Activator, HFD, high fat diet.

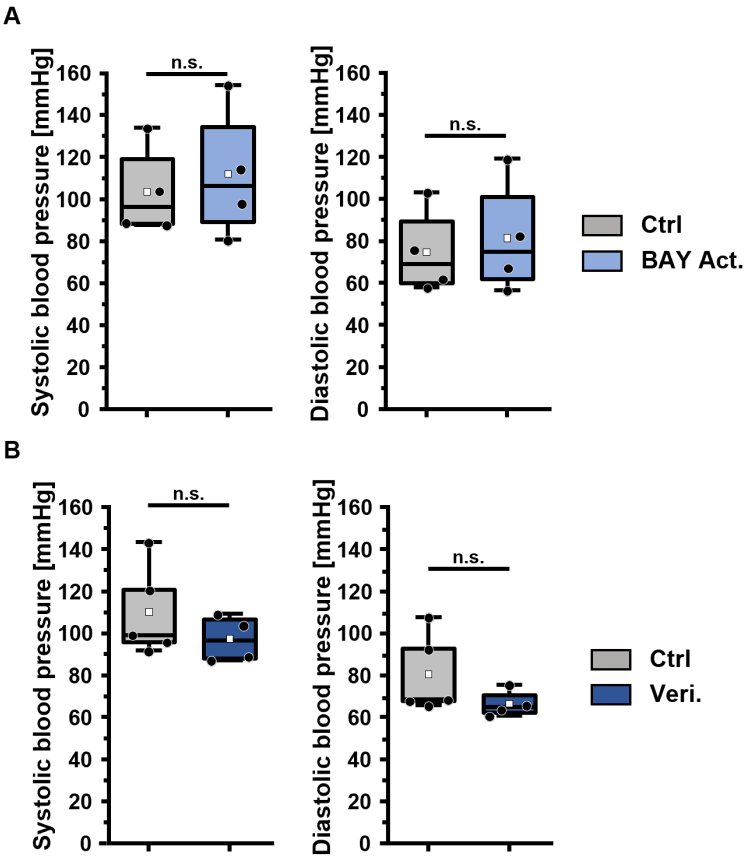

Supplementary figure 4. Blood pressure in BAY Activator- or Vericiguat-treated mice.
ApoEko mice were fed with an atherogenic diet supplemented with 150 ppm BAY Activator for 16 weeks (Ctrl/BAY Act.) or 150 ppm Vericiguat for 16 weeks 18 weeks (Ctrl/Veri.). **(A, B)** Systolic and diastolic blood pressure of Ctrl and BAY Act. **(A)** or Veri. **(B)** treated female mice. Blood pressure measurements were performed using a tail-cuff blood pressure system at the end of the feeding period for three consecutive days. The data of the three consecutive days were averaged for each animal. Data are represented as median (horizontal line), 25% - 75% interquartile range (box), 5% - 95% range percentile (whiskers) and mean (white square) (Ctrl BAY Act.: 4 mice, BAY Act.: 4 mice, Ctrl Veri.: 5 mice, Veri.: 4 mice). No statistically significant differences were found (n.s.: not significant, Mann-Whitney U test). Ctrl, Control, BAY Act., BAY Activator, Veri., Vericiguat.

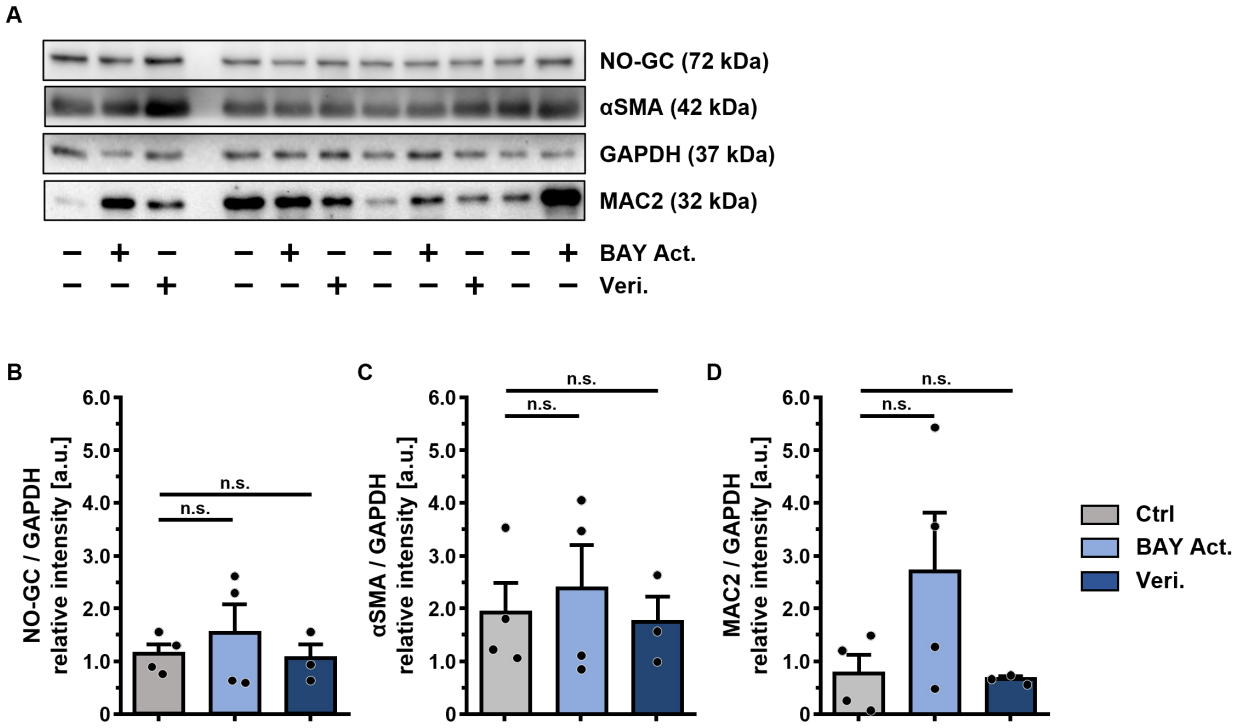

Supplementary figure 5. NO-GC, αSMA and MAC2 expression in atherosclerotic aortas of BAY Activator- and Vericiguat-treated mice.
Western blot analysis of protein expression in atherosclerotic aortas from ApoE^{ko} mice after 15 weeks of atherogenic diet. BAY Activator or Vericiguat was supplemented at a concentration of 150 ppm into the diet. **(A)** Image of Western blot analysis of NO-GC, αSMA, and MAC2 expression. GAPDH was used as loading control. **(B, C, D)** Quantification of relative band intensity of NO-GC, αSMA, and MAC2 by densitometric analysis. The band intensity was normalized to the band intensity of the loading control. Data are represented as mean + SEM (Ctrl: 4 mice, BAY Act.: 4 mice, Veri.: 3 mice). The expected molecular weights of the respective target proteins are indicated. No statistically significant differences were found (n.s.: not significant, Kruskal-Wallis ANOVA with Dunn's post hoc test). Ctrl, Control; BAY Act., BAY Activator; Veri., Vericiguat.

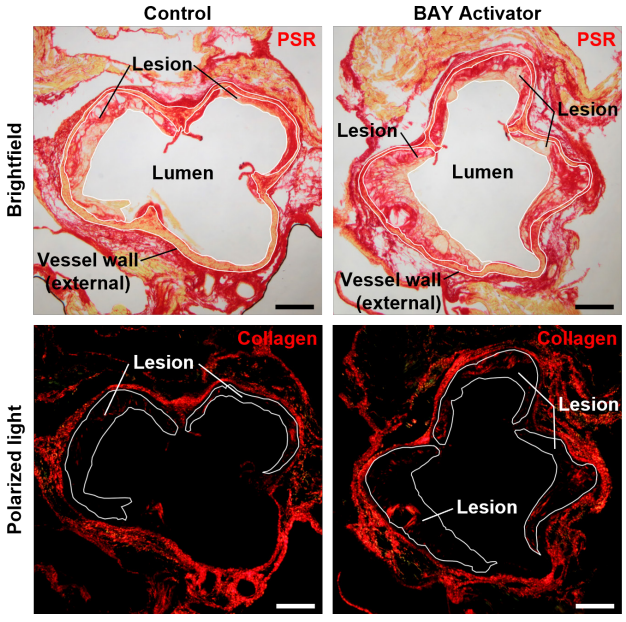

Supplementary figure 6. Effect of BAY Activator treatment on collagen content in the aortic root.
Analysis of the plaque composition in aortic root cross sections (10 µm) from ApoEko mice by Picrosirius red (PSR) after 16 weeks of atherogenic diet. BAY Activator was supplemented at a concentration of 150 ppm into the diet. Representative brightfield (top) and polarized (bottom) images of PSR-staining for collagen in aortic root sections of control (Ctrl) and BAY Activator (BAY Act.) -treated male mice. To ensure comparability, similar regions within the aortic root were selected using aortic valves as a reference. Under polarized light thick collagen fibers are displayed in red-orange and thin collagen fibers in green. Scale bars are 200 µm.

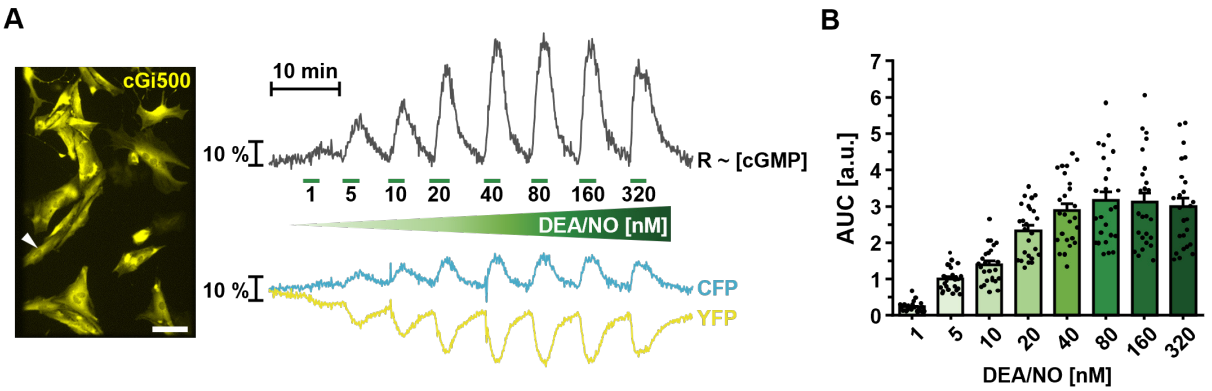

Supplementary figure 7. Real-time visualization of intracellular cGMP levels in primary VSMCs after DEA/NO treatment.
FRET-based cGMP imaging was performed in aortic pVSMCs. VSMCs were isolated from cGi-L1 mice (expressing the cGi500 biosensor globally) and cultured on coverslips for 5-6 days. **(A)** Representative cGMP measurement of VSMCs to analyze the concentration-dependent effect of DEA/NO. VSMCs were visualized by the YFP fluorescence (yellow) of cGi500 (left). The change of intracellular cGMP levels over time (grey, ratio trace "R" ~ [cGMP]) following treatment was calculated from the antiparallel change of CFP and YFP (blue, single trace CFP; yellow, single trace YFP) fluorescence intensity. The right panel depicts the cGMP response pattern of one representative VSMC. The percent change of the CFP, YFP, and ratio trace compared to the baseline ("ΔF/F" or "ΔR/R") is indicated. White arrowheads indicate the VSMC represented by the ratio trace in the right panel. Cells were treated with increasing concentrations of DEA/NO (1 nM to 320 nM) for 2 min each. (B) Statistical analysis was performed using the area under the curve (AUC) of the signals. Each dot represents an individual VSMC. Data are represented as mean + SEM (n: 25 cells). One representative measurement of two biological replicates is shown. Scale bars are 100 µm.CFP, cyan fluorescent protein; YFP, yellow fluorescent protein; AUC, area under the curve.

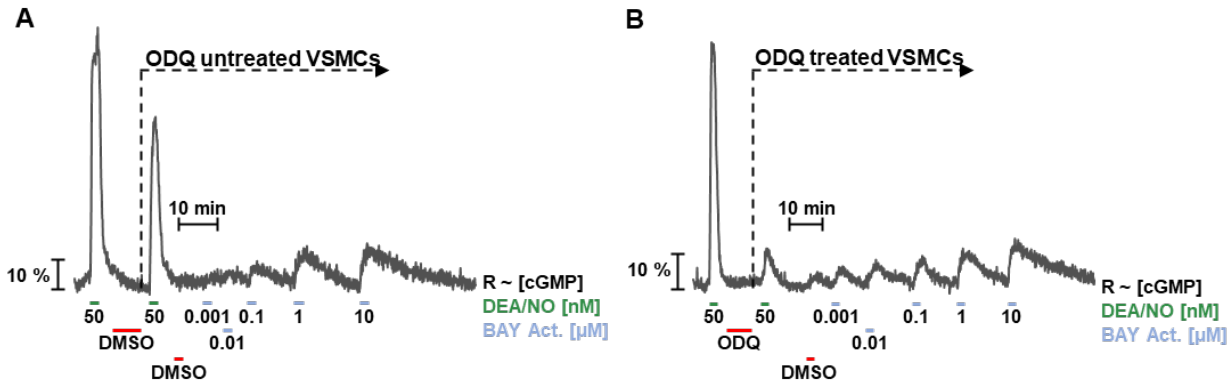

Supplementary figure 8. Effect of BAY Activator on intracellular cGMP levels in primary VSMCs.
FRET-based cGMP imaging was performed in aortic pVSMCs. VSMCs were isolated from cGi-L1 mice (expressing the cGi500 biosensor globally) and cultured on coverslips for 5-6 days. Representative cGMP measurement of VSMCs to analyze the concentration dependent effect of BAY Activator (BAY Act.) in the absence **(A)** or presence **(B)** of ODQ. The change of intracellular cGMP levels over time (grey, ratio trace "R" ~ [cGMP]) following BAY Activator treatment was determined (right, cGMP response pattern of one representative VSMC). The percent change of the ratio trace compared to the baseline ("ΔR/R") is indicated. During the measurement, cells were treated with DMSO (0.1 %, vehicle control) and increasing concentrations of BAY Act. (0.001 µM to 10 µM) for 2 min each. Cells were preincubated with ODQ (20 µM, 7min) or DMSO (0.1 %, 7 min) prior to BAY Act. treatment. The oxidation status was controlled by DEA/NO (50 nM) treatment before and after ODQ or DMSO preincubation. The dashed line indicates the ODQ treatment condition of the cells (ODQ untreated or treated). One representative measurement of three biological replicates is shown. BAY Act., BAY Activator.

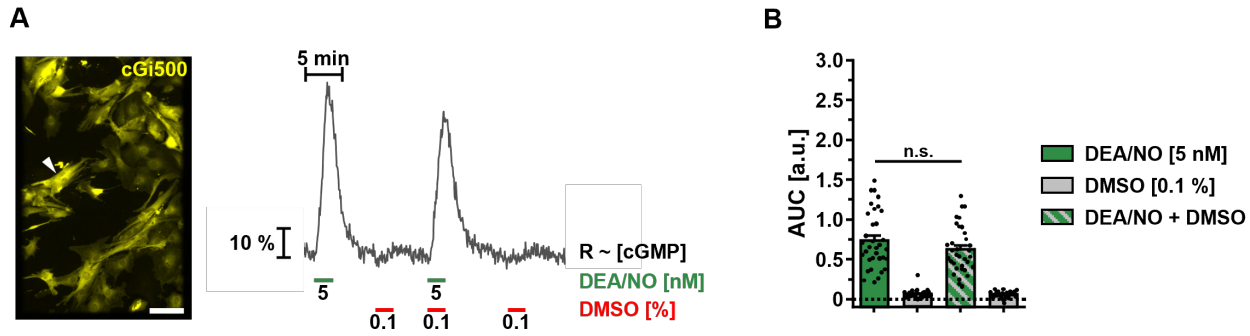

Supplementary figure 9. cGMP measurement to control potential effects of DMSO.
FRET-based cGMP imaging was performed in aortic pVSMCs. VSMCs were isolated from cGi-L1 mice (expressing the cGi500 biosensor globally) and cultured on coverslips for 5-6 days. (A) Representative cGMP measurement of VSMCs to analyze potential effects of DMSO (drug vehicle). VSMCs were visualized by the YFP fluorescence (yellow) of cGi500 (left panel). The change of intracellular cGMP levels over time (grey, ratio trace "R" ~ [cGMP]) following treatment was determined (right panel, cGMP response pattern of one representative VSMC). The percent change of the ratio trace compared to the baseline ("ΔR/R") is indicated. White arrowheads indicate the VSMC represented by the ratio trace in the right panel. Cells were treated with DEA/NO (5 nM), DMSO (0.1 %), the combination of both and DMSO (0.1 %) for 2 min each. (B) Statistical analysis was performed using the area under the curve (AUC) of the signals. Each dot represents an individual VSMC. Data are represented as mean + SEM (n: 34 cells). No statistically significant differences were found (n.s.: not significant, One-Way repeated measures ANOVA followed by post-hoc Bonferroni test). One representative measurement of three biological replicates is shown. Scale bars are 100 µm. Veri., Vericiguat; AUC, area under the curve.

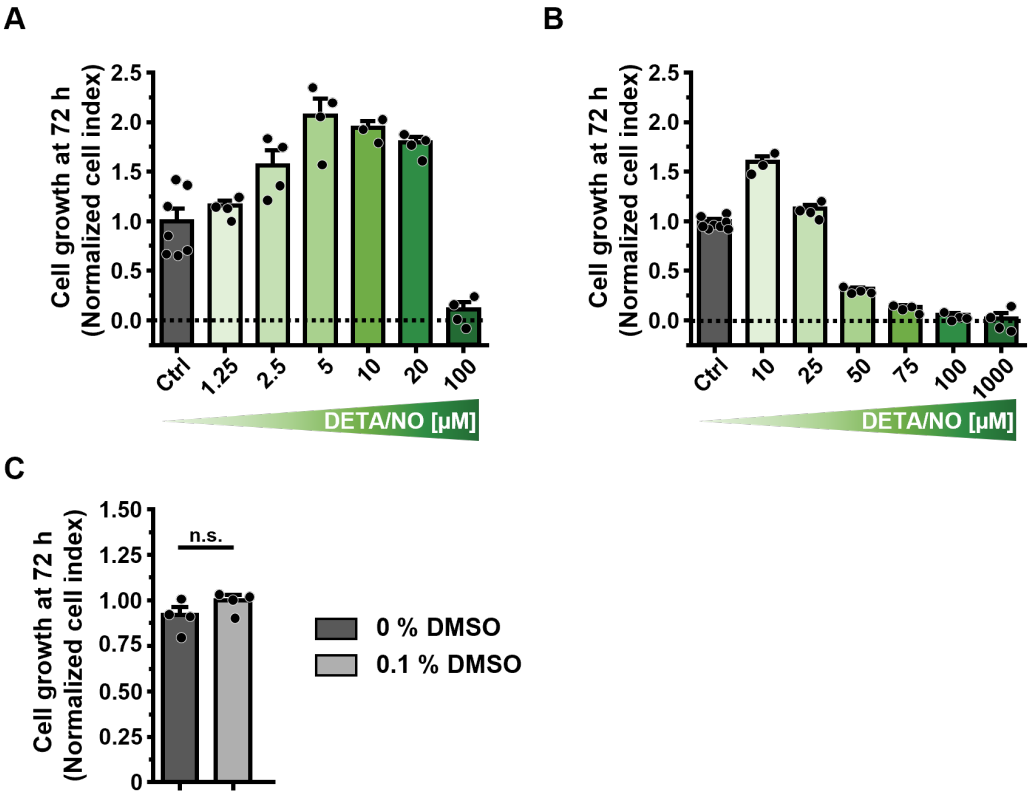

Supplementary figure 10. Impact of DETA/NO or DMSO on primary VSMC growth.
Real-time measurement of VSMC growth was performed using the xCELLigence system. pVSMCs isolated from wildtype mice were seeded in the absence (Ctrl) or presence of the NO donor DETA/NO or DMSO. The cell growth was analyzed after 72 h. **(A, B)** Analysis of VSMC growth after treatment with increasing concentration of DETA/NO (1.25 µM to 1000 µM). **(C)** Analysis of the effect of DMSO (0.1 %) on VSMC growth. Data are represented as mean + SEM (n: 3-8 wells per condition). No statistically significant differences were found (n.s.: not significant, Mann-Whitney U test). One representative measurement of three biological replicates is shown. Ctrl, Control.

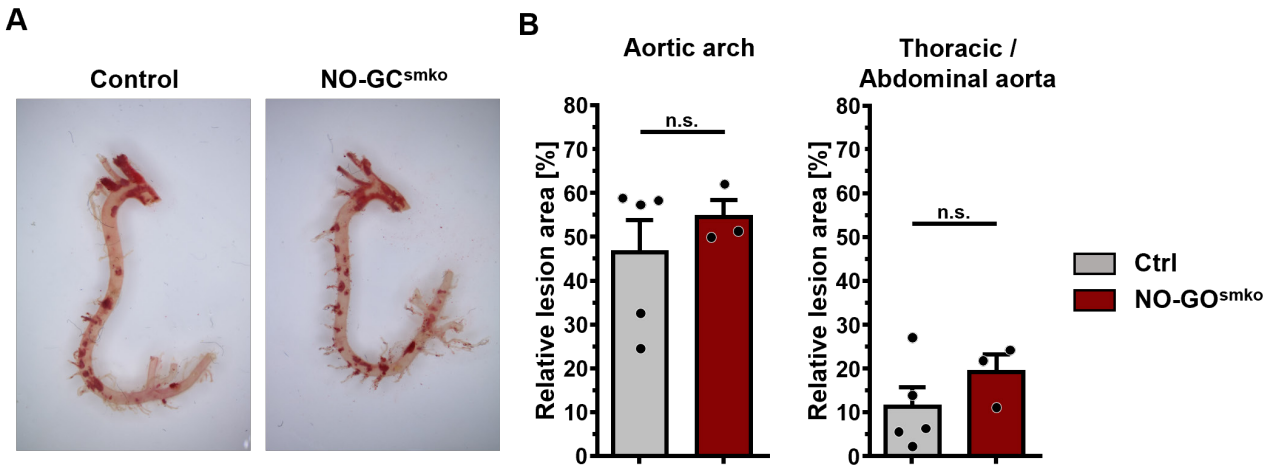

Supplementary figure 11.Effect of SMC-specific ablation of NO-GC on atherosclerotic lesion area in female mice.
Analysis of atherosclerotic lesion area in aortas from SMC-specific NO-GC knockout (NO-GC^{smko}) and control mice (Ctrl, Cre-Ctrl) mice by Oil Red O staining after 18 weeks feeding of an atherogenic diet. NO-GC^{smko} and Ctrl mice were bred on an ApoE-deficient background. The mice were treated with tamoxifen to induce the SMC-specific NO-GC knockout. Intraperitoneal tamoxifen injections occurred in two cycles, each for five consecutive days (5 x 1 mg/mouse/day) at 8 and 10 weeks of age with a nine-day break in between and before switching to an atherogenic diet. **(A)** Representative images of Oil Red O-Stained atherosclerotic aortas of control (Ctrl; Cre-ctrl and Ctrl mice were pooled) and NO-GC^{smko} female mice. Atherosclerotic lesions appeared red. Scale bars are 1 mm. (**B)** Relative lesion area of the aortic arch or thoracic/abdominal aorta of Ctrl and NO-GC^{smko} female mice. The atherosclerotic lesion area was determined from both sides of the aorta, averaged, and normalized to the total area of the respective part. Data are represented as mean + SEM (Ctrl: 5 mice, NO-GC^{smko}: 3 mice). No statistically significant differences were found (n.s.: not significant, Mann-Whitney U test). Ctrl, Control, NO-GC^{smko}, SMC-specific NO-GC knockout.

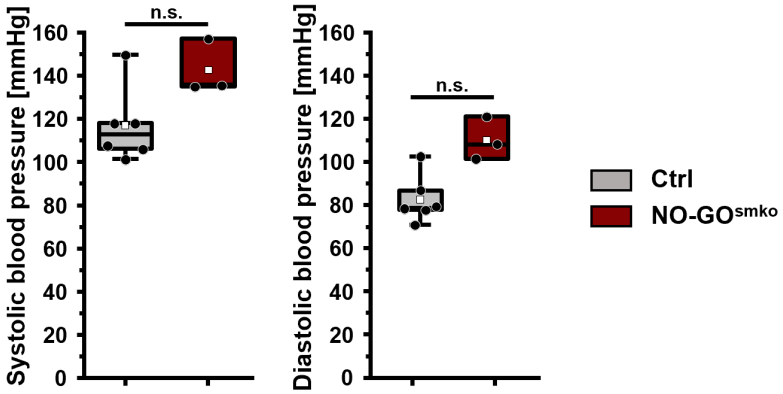

Supplementary figure 12. Impact of SMC-specific NO-GC knockout on blood pressure in female mice.
Systolic and diastolic blood pressure in SMC-specific NO-GC knockout (NO-GC^{smko}) and control (Ctrl, Cre-Ctrl) female mice. The mice were bred on an ApoE-deficient background and fed with an atherogenic diet for 18 weeks. The mice were treated with tamoxifen to induce the SMC-specific NO-GC knockout. Intraperitoneal tamoxifen injections occurred in two cycles, each for five consecutive days (5 x 1 mg/mouse/day) at 8 and 10 weeks of age with a nine-day break in between and before switching to an atherogenic diet. The blood pressure was measured at the end of the feeding period over three consecutive days using a tail-cuff blood pressure system. The data of the three consecutive days were averaged for each animal. Data are represented as median (horizontal line), 25% - 75% interquartile range (box), 5% - 95% range percentile (whiskers), and mean (white square) (Ctrl: 6 mice, NO-GC^{smko}: 3 mice). No statistically significant differences were found (n.s.: not significant, Mann-Whitney U test). Ctrl, Control, NO-GC^{smko}, SMC-specific NO-GC knockout.

b. Supplementary tables

Supplementary table 1. Overview of experimental groups to analyze the role and therapeutic potential of NO/cGMP signaling pathway in atherosclerosis.
Listed are the various experimental mouse lines that were assembled and investigated in this study. The nomenclature for the genotypes is as follows: ”wt” refers to wildtype allele, “L2” refers to a flanked targeted sequence/gen by 2 loxP sites, and “ko” refers to gene knockout. All mice were bred on C57BL/6NCrl background. Please note that all mice in experimental group III (NO-GC^{smko}, Ctrl, Cre-Ctrl) were treated with tamoxifen, although recombined cells in Ctrl mice carry one functional and one defective NO-GC allele. BAY Act.; BAY Activator; Veri., Vericiguat; BP, Blood pressure; CIH, Chromogenic immunohistochemistry; PSR, Picrosirius red; IF, Immunofluorescence.

Group	Sub-group	Drug in diet	Genotype	Tamoxifen Inj.	HFD feeding period	BP meas-urement	Performed analysis
I	BAY Act.	150 ppm	ApoE^{ko}	No	16 weeks	Kinetic + 3 final sessions	Weight gain, lipid levels and drug concentration in plasma, protein expression, Oil red O staining, IF-staining (aortic arch), CIH- and PSR-staining (aortic root),
	Ctrl	-					
II	Veri.	150 ppm	ApoE^{ko}	No	18 weeks	3 final sessions	Weight gain, lipid levels and drug concentration in plasma, protein expression, Oil red O staining
	Ctrl	-					
III	NO-GC^{smko}	-	ApoE^{ko} x NO-GC$^{L2/L2}$ x mT/cGi500-L2 x αSMA-CreERT2	Yes	18 weeks	3 final sessions	Weight gain, lipid levels in plasma, protein expression, Oil red O staining, IF-staining aorta (recombination efficiency)
	Ctrl	-	ApoE^{ko} x NO-GC$^{L2/wt}$ x mT/cGi500-L2 x αSMA-CreERT2	Yes			
	Cre-Ctrl	-	ApoE^{ko} x NO-GC$^{L2/L2}$ x mT/cGi500-L2	Yes			

Supplementary table 2. Plasma concentrations of NO-GC modulator.
Listed are the measured total and unbound plasma concentration of BAY Activator (BAY Act.) or Vericiguat (Veri.) in experimental mice. Blood was collected from mice at the end of the atherogenic diet (± 150ppm NO-GC modulator) feeding period (BAY Act.: 16 weeks, Veri.: 18 weeks) in the morning. The experimental mice were not starved before sampling. The total drug concentration and the unbound fraction in plasma were measured in collaboration with Dr. U. Hofmann (Dr. Margarete Fischer-Bosch Institute of Clinical Pharmacology) and Prof. Dr. P. Sandner (BAYER AG). For the analysis the sexes were pooled. All data are represented as mean ± SEM. *Contamination with drug; Ctrl, Control; bdl, below detection limit.

Parameter	Ctrl BAY Act.	BAY Act.	Ctrl Veri.	Veri.
Number of mice	16	8	10	10
Total drug concentration [nM]	bdl	20733.3 ± 249	2.1 ± 2.1*	2752.7 ± 304.4
Unbound fraction [nM]	bdl	16.6 ± 2	bdl	56.1 ± 8.4

Supplementary table 3. Complete blood count analysis of BAY Activator treated mice.
Listed are the values of the complete blood count analysis of mice fed a normal diet (Ctrl n.d.), atherogenic diet (Ctrl.) or atherogenic diet supplemented with 150 ppm BAY Activator. Blood was collected from mice after 16 weeks of the normal diet or atherogenic diet (± 150 ppm BAY Activator). All data are represented as mean ± SEM. Ctrl, Control; n.d., normal diet; BAY Act., BAY Activator; MCV, Mean corpuscular volume; MCH, Mean corpuscular hemoglobin; MCHC, Mean corpuscular hemoglobin concentration.

	Ctrl n.d.	Ctrl	BAY Act.
Number of mice°	3	10	4
White blood cell [/µL]	3703.4 ± 806.3	3711.5 ± 587.4	2306.4 ± 337.2
Red blood cell [/µL]	$9.7*10^6 \pm 1.69*10^5$	$8.76*10^6 \pm 6.74*10^5$	$9.96*10^6 \pm 3.71*10^5$
Hemoglobin [g/dL]	13.4 ± 0.1	13.6 ± 0.7	14.2 ± 0.7
Hematocrit [%]	44.2 ± 0.8	38.5 ± 3.6	44.8 ± 1.1
MCV [fL]	58.7 ± 1.3	64.7 ± 1.8	61.1 ± 2.9
MCH [pg]	15.7 ± 0.3	17.8 ± 0.9	16.7 ± 1.1
MCHC [g/dL]	30.4 ± 0.7	33.6 ± 1.6	31.7 ± 1.4
Platelets [/µL]	$9.18*10^6 \pm 3.61*10^5$	$1.0*10^6 \pm 1.66*10^5$	$1.04*10^6$ ±1.88 *104
Lymphocytes [%]	86.6 ± 1.9	68.7 ± 3.1	74.6 ± 5.4
Lymphocytes [/µL]	3220.2 ± 669.0	2608.8 ± 483.7	1706.6 ± 214.1
RDW SD [fL]	31.4 ± 0.9	34.7 ± 0.9	34.0 ± 0.6
RDW CV [%]	12.2 ± 0.3	12.7 ± 0.7	14.5 ± 1.8
PDW [fL]	6.9 ± 0.1	10.0 ± 0.6	9.3 ± 0.1
MPV [fL]	6.4 ± 0.2	8.2 ± 0.4	7.8 ± 0.1
PLCR [%]	2.4 ± 0.2	7.0 ± 0.8	6.1 ± 0.5

Declaration of contributions

The present work was written independently by the author without external assistance. The use of artificial intelligence (e.g., ChatGPT) was limited to proofreading some paragraphs of the thesis. All experiments were planned, conducted, and analyzed by the author, with the following exceptions:

- The analysis of plasma lipid parameters of the Vericiguat experimental group was performed by Prof. Dr. A. Peter at the University Hospital Tubingen and of the BAY Activator experimental group by Prof. Dr. P. Sandner at the pharma research center of the BAYER AG (Cardiovascular research department) in Wuppertal.
- The analysis of Vericiguat concentration in the plasma of experimental mice was performed by Dr. U. Hofmann at the Dr. Margarete Fischer-Bosch Institute of Clinical Pharmacology in Stuttgart.
- The analysis of BAY Activator concentration in the plasma of experimental mice was performed by Prof. Dr. P. Sandner at the pharma research center of the BAYER AG (Cardiovascular research department) in Wuppertal.

Acknowledgments

At this point, I would like to express my gratitude to everyone who contributed to the success of this work.

First and foremost, I would like to express my special thanks to my supervisor, Dr. Susanne Feil, for her excellent guidance and support throughout this journey. She made it possible for me to work on this exciting topic and always had time for conversations and discussions, which were very important for the preparation of this thesis.

I am grateful to Prof. Dr. Robert Feil for the opportunity to perform my doctoral research in his laboratory, for the scientific discussions, and the support.

I also acknowledge Prof. Dr. Robert Lukowski for valuable scientific exchanges and discussions over the years, as well as for reviewing this thesis.

Many thanks to Prof. Dr. Dmitriy Atochin for the opportunity to work in his laboratory in Boston and for his supervision. The international exchange allowed me to grow not only as a scientist but also as a person. I extend my gratitude to his entire team for the incredible experience.

Furthermore, I would like to thank our collaboration partners for the pleasant cooperation and support. Prof. Dr. Peter Sandner, Dr. Lisa Dietz, and the team at BAYER AG, I thank for providing animal diet and drugs, and for analyzing the plasma of the experimental animals. I also extend my gratitude to Prof. Dr. Andreas Peter and Ann Kathrin Horlacher for their support and measuring plasma lipid levels (University Hospital Tubingen). Additionally, I thank Dr. Ute Hofmann (Dr. Margarete Fischer-Bosch Institute for Clinical Pharmacology Stuttgart) for analyzing the concentration of Vericiguat in murine plasma. Special thanks to Prof. Dr. Andreas Friebe (Julius-Maximilians-University Wurzburg) for providing the NO-GC specific antibodies and NO-GC$^{L2/L2}$ mouse line.

My sincere thanks go to the entire research training group, GRK 2381, for providing an environment that facilitated the improvement of my research and skills. Gratitude is also extended to all former and current members of the Feil laboratory. A special thanks to Mariagiovanna Barresi and Barbara Birk, whose professional and personal support significantly contributed to the success of this work. I express my appreciation to Alexandra Böttcher and Dr. Maria Teresa Kristina Zaldivia for their support and friendship. I thank Dr. Moritz Lehners for his helpfulness and numerous supports. Additionally, I want to express my gratitude to Krithika Rajeeth, Daniel Pinto Quintero, and Jennifer Schulz for their assistance in the experiments. I also appreciate all the valuable contributions from the students Katrin Strobel, Anastasia Gurskaya, Heiko Olbricht, and Timo Hindenthal.

Acknowledgments

Many thanks to Dr. Anja Schmitt for the pleasant conversations, advice, and support, as well as for proofreading this work.

Finally, my deepest thanks to my family and my wife, Ann-Kristin, for their unconditional love and support during this challenging time. Despite all the difficulties, they always stood by my side and showed me the right way. Without them, this work would not have been possible. A special thanks to my cousin, Jana Hoppe, for proofreading this work.

Publications of the author

The author has contributed to the following publications:

Roessing, M., … Sandner, P., Feil, R., Feil, S. Pathophysiological and pharmacological relevance of NO/cGMP signaling in atherosclerosis. *In preparation*.

Yokomizo, S., Kopp T., **Roessing, M.**, … Feil, S., … Huang, P.L., Kahiwagi, S., Atochin, D.N. (2024). Near-infrared II photobiomodulation preconditioning ameliorates stroke injury via phosphorylation of eNOS. *Stroke*. doi: 10.1161/STROKEAHA.123.045358.

Katagiri, W., … Kopp T., **Roessing, M.**, … Feil, S., … Atochin D.N., … Kashiwagi, S. (2022). Dual near-infrared II laser modulates the cellular redox state of T cells and augments the efficacy of cancer immunotherapy. *FASEB J*; 36(10):e22521. doi: 10.1096/fj.202200033R.

Yokomizo, S.*, **Roessing, M.***, Morita, A.*, Kopp T., … Feil, S., Huang, P.L., Atochin D.N., Kashiwagi, S. (2022) Near-infrared II photobiomodulation augments nitric oxide bioavailability via phosphorylation of endothelial nitric oxide synthase. *FASEB J*, 36(9):e22490. doi: 10.1096/fj.202101890R. *Authors contributed equally.

The author has also presented his work at the following conferences:

Roessing, M., Lehners, M., Gurskaya, A., Sandner, P., Feil, R., Feil, S. (2022). Real-time analysis and therapeutic potential of NO/cGMP signaling in VSMCs and atherosclerosis. Meeting abstracts from the 10th International Conference on cGMP: Generators, Effectors and Therapeutic Implications. *J Transl Med*. 21(Suppl 1):35. doi: 10.1186/s12967-022-03800-1. Augsburg, Germany.

Roessing, M., Lehners, M., Zaldivia, M.T.K., Barresi, M., Sandner, P., Feil, R. Feil, S: (2021) Therapeutic potential of the vascular NO/cGMP signaling pathway in atherosclerosis. The 1st PhD Student Conference of the GRK 2381 on Cancer, Cardiovascular diseases & Neurological disorders. Tübingen, Germany.